The effects of processing variables on the energy absorption of composite crash structures

by Thomas A Turner, MEng

Thesis submitted to the University of Nottingham
For the degree of Doctor of Philosophy, May 2004

Contents

Abstract

Environmental pressures are driving automotive manufacturers towards light weight cost efficient structures. Composite materials have been shown to display high specific energy absorption levels thus offering opportunities for mass reduction over conventional steel structures. Whilst composites display these specific advantages, the mechanisms by which energy is absorbed are more complex and are preventing widespread acceptance of composite structures. This work aims to further scientific understanding of the crushing process and provide realistic data for a wide range of processing conditions and commonly used materials.

The main objectives of this study were to quantify the effect of industrial manufacturing conditions on the crush performance of composite structures, and to correlate the performance to a number of in-plane laminate properties. The manufacturing parameters considered are constituent material related (mould temperature, post-cure time and resin composition), interlaminar toughness related and process related (amount of binder and voidage).

The work presented in the thesis reports the results of axial crushing experiments, in-plane and inter-laminar testing performed on composite parts made from glass reinforced polyester and vinylester resins. The preforms were made from 2 fabrics; a continuous filament random mat and a 0/90° non crimp fabric. All parts were produced by resin transfer moulding (RTM) under conditions which were representative of medium volume industrial processing.

Constituent material results demonstrate clear advantages associated with the use of vinylester resin and that while relationships between all in-plane properties and the crush performance can be observed, the ultimate compressive stress is the most reliable indicator of this performance. Interlaminar toughness enhancement shows great promise for tailoring of the crush curve and increase in energy absorption of non-crimp fabrics. Results for the processing work are directly applicable to existing manufacturing and demonstrate the potential for real reductions in cycle time and increase in properties.

Acknowledgements

The author wishes to acknowledge the advice and support of his supervisors Dr N. A. Warrior and Prof. C. D. Rudd. The assistance of Dr F. Robitaille with the early stages of this work is greatly appreciated.

The following representatives of the funding companies are thanked for their help and input into this work; Nigel Keen (Reichhold UK Ltd), Nigel Fawcett (Ford Motor Company Ltd) and David Marler (Lotus Cars Ltd).

Thanks go to the technicians who have assisted with various practical parts of this work; Roger Smith and Paul Johns. Thanks also to my fellow researchers; Dr Michael Ribeaux, Dr Edward Cooper and Dr Richard Fernie.

Lastly, my thanks go to my family and friends for their support and encouragement, particularly my wife Helen.

Glossary

B-stage	Partial state of cure found in epoxy prepregs
Binder	Thermoplastic or occasionally thermosetting powder applied to fabrics during manufacture to facilitate preforming
Catalyst	Curing agent used for UP and VE resins
CFRP	Carbon Fibre Reinforced Plastic
CoFRM	Continuous Filament Random Mat (also CFRM)
CSM	Chopped Strand Mat
Cycle time	Time from start of one moulding to start of next
DCB	Double / Dual Cantilever Beam – Mode I Fracture toughness test
DSC	Differential Scanning Calorimetry
E-glass	Electrical glass – common grade of glass fibre
Exotherm	Self-perpetuating reaction caused by excess build-up of heat during cure
GRP	Glass-Reinforced Plastic
HDT	Heat Distortion Temperature – approximate measure of maximum use temperature
ILSS	Inter-Laminar Shear Stress
Isopthalic	Type of polyester resin (also orthophthalic) refers to diabasic acid used in preparation
Kevlar™	Dupont trade name for Aramid – Aromatic Polyamide
Monocoque	Unitary bodyshell construction with no separate chassis
NCF	Non-Crimp Fabric – stitched bi-, tri- or quadraxial fabric
NVH	Noise, Vibration & Harshness
PEEK	Poly Ether Ether Ketone – High performance thermoplastic matrix material
Phr	Parts-per-hundred resin – measure typically used for resin additives
Preform	Fibres in a mat formed to approximate shape of final part
Prepreg	Pre-impregnated partially cured composite
RIFT	Resin Infusion under Flexible Tooling
RTM	Resin Transfer Moulding – production process particularly suited to medium volume production of composite parts
SCRIMP™	Seeman Composites Resin Infusion Moulding Process
SCSS	Specific Sustained Crushing Stress – analogous to SEA
SEA	Specific Energy Absorption

S-glass	Trade name for High performance glass fibre, also R & T-glass
Sizing	Protective coating applied to fibres during manufacture often also serving to increase interfacial bond strength
SMC	Sheet Moulding Compound
T_g	Glass transition temperature
Thermoplastic	Polymer which softens when heated and hardens when cool
Thermoset	Polymeric resin becoming permanently hard when cured
Thresholding	Determination of black/white transition in greyscale image
TP	Thermoplastic
UD	Unidirectional
UHMWHDPE	Ultra High Molecular Weight High Density Poly-Ethylene
UP	Unsaturated Polyester (resin)
VARTM	Vacuum Assisted Resin Transfer Moulding
VE	Vinylester (resin)
Vf	Volume fraction

Nomenclature

E	Young's Modulus
G	Strain energy release rate

Subscripts

1	Longitudinal direction
F	Fibre
I	Mode I
M	Matrix
T	Tensile
C	Compressive or critical

1 Introduction

1.1 Vehicle Safety

In recent years vehicle crashworthiness has been of increasing concern. Crashworthiness has become a primary selling point for many car manufacturers. Also, the amount of legislation governing automotive safety has increased markedly, strict regulations now control car manufacturers, setting out defined targets and test types (e.g. FMVSS and EU). A number of car makers led the way by introducing test programmes aimed at meeting the new test standards. Academic research has focussed on the numerical prediction of crush performance through methods such as Finite Element Analysis and a wide range of experimental testing.

One of the major advantages of composite materials in automotive structures is the potential for increased occupant safety through more efficient absorption of crash energy. Higher efficiency in this context implies minimum mass components which can be manufactured at low cost and absorb high amounts of energy. A vehicle crash is a complex process with interactions occurring between structural and non-structural members; globally a massive amount of kinetic energy must be dissipated at any significant speed. There is a time-dependent upper limit on the deceleration tolerable by the occupants [1] see Figure 1:1.

Structural energy absorbers, designed to collapse in a predetermined and optimised manner, can be incorporated into the vehicle structure to absorb the impact energy. If high deformations are not permitted very high force levels will be transferred to the occupants, conversely if a large deformation is acceptable it is possible to significantly reduce the forces. Figure 1:2.

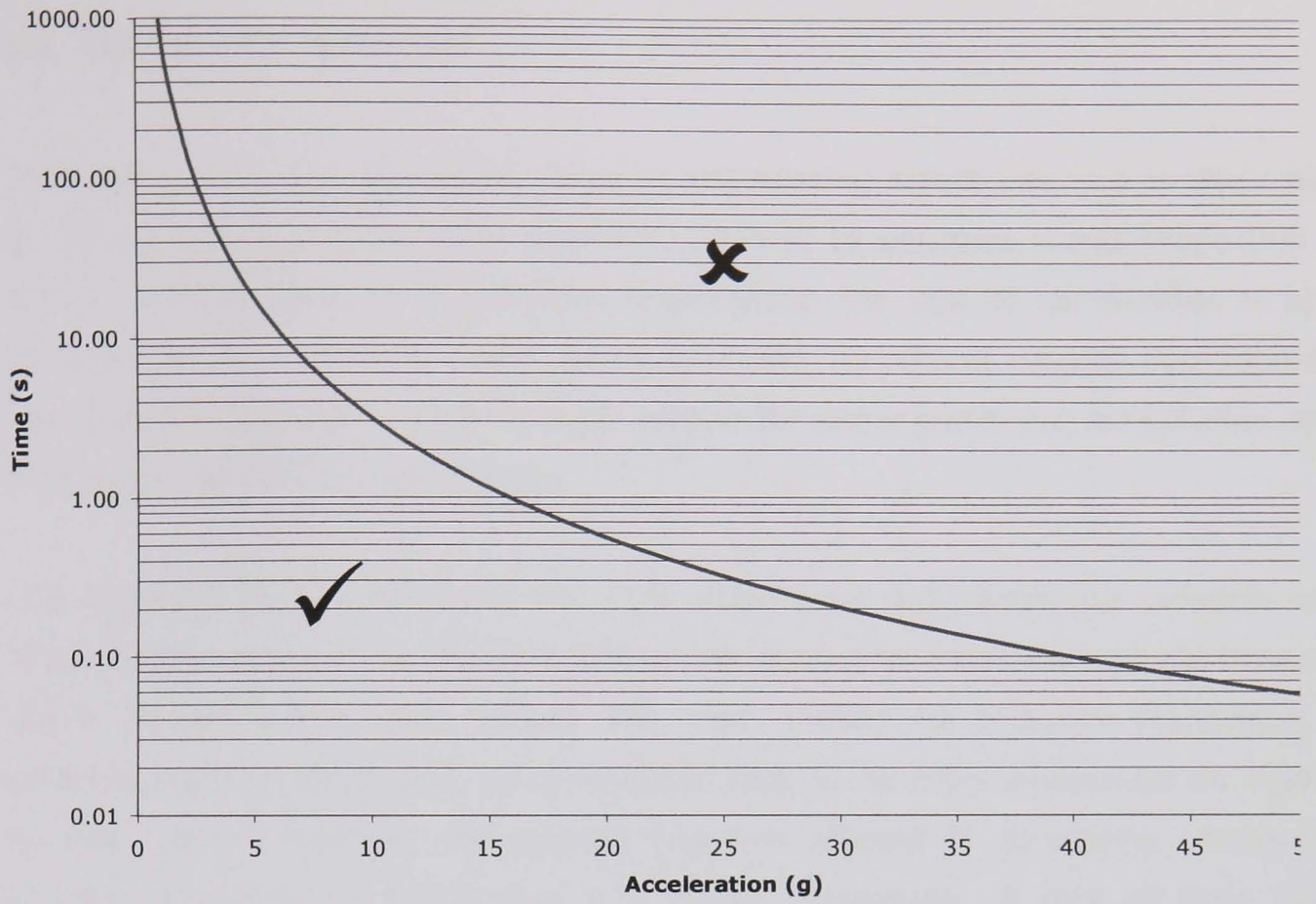

Figure 1:1 Time dependant nature of impact tolerance of typical human body

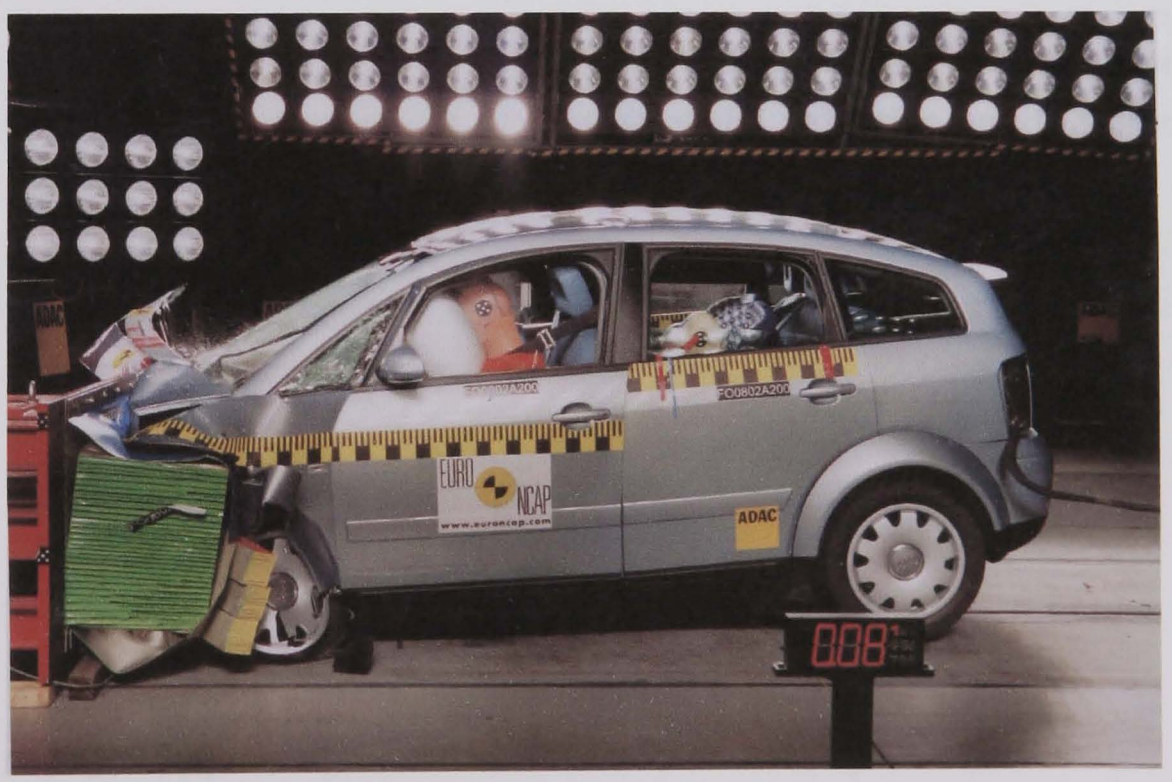

Figure 1:2 Euro NCAP frontal impact showing large deformation

1.2 Composite Materials

Composite materials are widely used in engineering structures due to their high specific mechanical properties and the potential to optimise these properties to fulfil a specific role. In automotive engineering the use of composites is split between largely cosmetic body panels and fully structural chassis components. Composites have been used for body panels for some years but acceptance as a structural material has been slow.

The transport sector accounts for 31% volume of the composite industry and 33% of the value [2]. Worldwide, the automotive and industrial vehicle industry has a market size of $26 billion. The main reason for industry resistance to composite materials is cost, as composites tend to be more expensive on a part-by-part basis. However, the design freedom offered in structural, aesthetic, acoustic and thermal properties is a major advantage. A lack of long term experience of composite materials in automotive applications also results in some reluctance [2], this is particularly true of crashworthiness applications where metals, although they may be less efficient, are well proven.

The use of composites for crash energy management gives the ability to accurately vary the fundamental properties of the part, this and the potentially low cost have both been attractive to vehicle manufacturers. As engine technology and concurrent fuel economy plateau, emphasis is shifting towards light weight, this being another area of advantage for composites. The benefits of composites in vehicle applications can be summarised as follows;

- Reduction in weight - Higher specific strength materials
- Reduction in NVH properties – Improved sound absorption
- Greater fuel economy – Reduced weight
- Reduction in emissions – Reduced weight
- Reduced cost – Low cost materials and processing
- Greater parts integration – Reduced cost

There are, however, problems associated with the design of composite energy-absorbing parts. The higher potential specific energy absorption (SEA) intrinsically suggests more emphasis on the crush mechanism. It is often true that altering one variable (e.g. loading axis) by a small amount can dramatically

change the crush performance. Factors such as these must be understood and accurately predicted if the benefits listed above are to be realised in practice. Other issues include cost, which is always of primary concern to vehicle manufacturers and processing. The processing of composites can be more involved than metals and presents a different set of safety problems.

Other benefits exist with composite materials in terms of the load-displacement response of the structure; the mode of failure for metals results in oscillation of the load displacement curve. Figure 1:3 shows an ideal load displacement curve along with typical metal and composite curves.

Figure 1:3 Ideal, metallic and composite crush curves (load vs. displacement)

Metallic structures are well understood but collapse in a crash situation is relatively inefficient due to the mode of failure. Metals fail through the formation of plastic hinges with large areas of un-yielded material between the folds, whereas composites can be made to fail in a continuous process thus absorbing significantly more energy than metals. Cost effective glass/polyester composites made by medium to high volume production processes such as RTM have been shown to be twice as efficient as steel on a specific basis [3].

The method by which metals fold is generally well understood so structures can be accurately designed to fulfil their task. Failure of composites by continuous crushing is less well understood; the large variation in possible geometries and material constituents make it difficult for designers to exploit composite materials in high specific-energy-absorbing structures. Consequently, significant efforts have been made to correlate the specific energy absorption level to the material properties of the composite, these include preform structure [4, 5], constituent material [6-8] and specimen geometry, [9-12]. Another important area of research has been to predict and model energy absorption to aid the design process. Various empirical, analytical and finite element studies by a range of authors have been largely unsuccessful in generating a unified scheme [13-17].

Many documented results are found to contradict each other, often because results are only applicable to certain other variables, e.g. fibre type or architecture. For instance, Satoh [18] and Ramakrishna [19] have shown a strong, linear relationship between interlaminar fracture toughness and SEA for high temperature thermoplastic resins with carbon fibre reinforcement, but this trend has not been observed in all composites, e.g.[20]. Unfortunately there are few generalisations which adequately describe the behaviour of composite materials in a crash situation. Composites reinforced by random mats generally exhibit higher interlaminar fracture toughness than those based on engineered or woven fabrics, and significantly higher specific energy absorptions have been reported [21] for polyester/random glass composites compared to equivalent composites based on engineered fabrics. In this case the increase in SEA is greater than the difference in fracture toughness would suggest. The higher specific in-plane strength and stiffness of engineered reinforcement fabrics are often required in structural applications and the low SEA's demonstrated by these materials can limit their potential application to crashworthy structures. This is particularly relevant for the increasing trend towards modular structures in vehicles where a crash structure may be integrated into a front end module also incorporating other features.

1.3 Moulding processes

Whilst this work is entirely concerned with resin transfer moulding (RTM) a wide variety of moulding processes are available for composite materials. Suitability of any given moulding process is dependent on production volume and required part quality. Some processes are obviously more suited to high volume and therefore automotive parts, however, many laboratory parts have been manufactured through more costly routes which are more representative of aerospace methods. There are numerous quality issues such as surface finish and void content which vary between methods.

1.3.1 Resin transfer moulding

Resin transfer moulding is a relatively new process which involves injecting resin into a fibre preform. The preform is placed in the mould before the resin is introduced which allows tight control over fibre architecture. The process is well suited to fast cycle times and automation. The fact that the mould is closed gives higher operator safety and minimal environmental issues due to lower emission of volatiles. Figure 1:4 shows a schematic of the process.

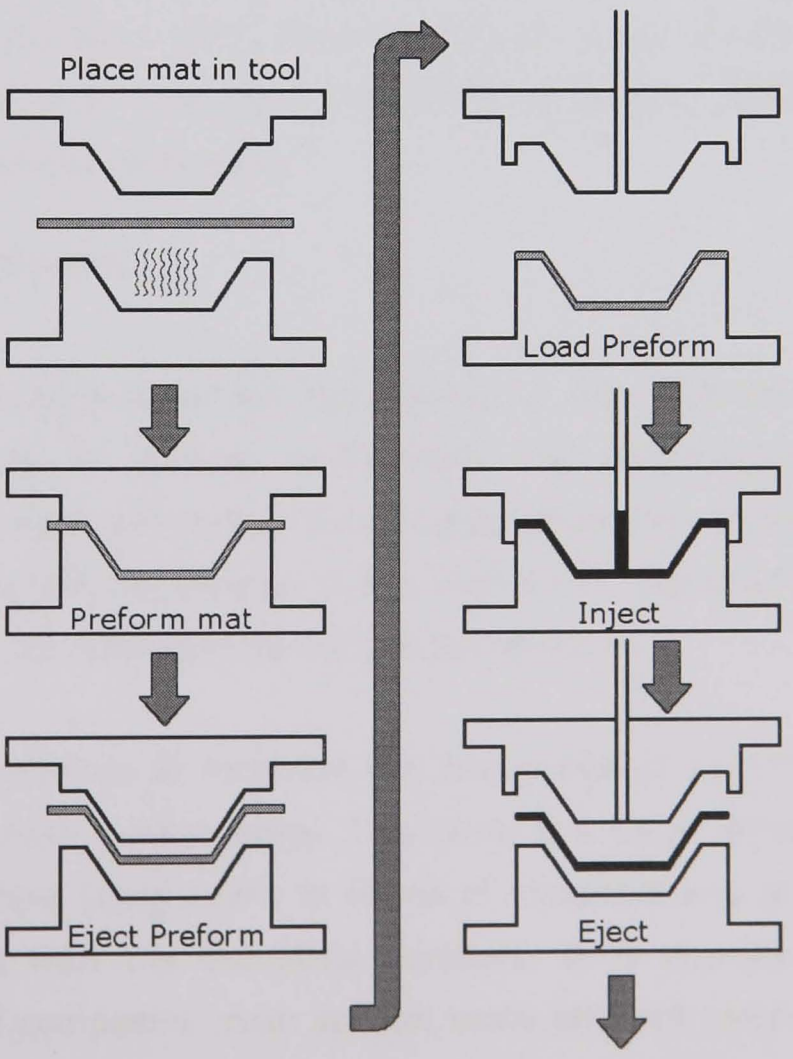

Figure 1:4 RTM schematic

RTM encompasses a range of processes. RTM in its purest sense uses a positive pressure to drive resin into the tool, variations on this approach use a vacuum to partially evacuate the tool prior to injection, this is vacuum assisted resin injection (VARI). The process is well understood with significant progress being made into computer simulation of cavity filling. There also exists a body of research into producing mouldings with minimum void content [22]. Moulding quality is highly dependent on part geometry and associated mould geometry (e.g. gating).

1.3.2 Other moulding processes

The results in this work, although produced via RTM are directly transferable to the various vacuum infusion processes. Fabrics are laid up in the same way as RTM but the tool is one sided. Often the preforming stage is omitted. The dry fibres are then vacuum bagged; often with a peel ply and a high permeability non-structural fabric. Resin is allowed into the fabric once the air has been evacuated. Large complex parts can be moulded although flow distribution can be an issue. Various terms are applied to this process as some aspects are covered by patents in some of the following cases. SCRIMP (Seeman composites resin infusion process), RIFT (Resin infusion under flexible tooling), VARI (Vacuum assisted resin injection) and VARTM (Vacuum assisted resin transfer moulding) are common processes.

1.4 Purpose of work.

The use of composites in vehicle applications is now well-established, although the vast majority of current applications are non-structural. Nevertheless composites now represent less of a psychological barrier to manufacturers. Most laboratory testing has focussed on topics such as the effect of fibre type and has often stemmed from work into aerospace applications.

The aim of this work is to increase the knowledge of the effect of processing parameters on crush performance. This work has been industrially driven and many of the choices (particularly in terms of materials and processing) resulted from discussions with the industrial partners. It is essential to increase the understanding of composite crush so that more efficient crash structures can be designed and made. Thus large sections of this work are devoted to analysis of results and possible causes for the observed phenomena. However, the primary

emphasis is on the practical aspects of the crash performance of medium volume composite parts.

Potential application areas for this work are seen primarily as demountable crash rails for either low speed or high speed impact, or for modular front end sub-assemblies. Increasingly cars are manufactured as modular units where tier one manufacturers supply large sub-assemblies for integration on the production line. It is difficult to predict the extent to which crash energy management systems will be produced in this manner as they may be incorporated into the vehicle primary structure.

Examples of demountable crash structures can be seen on cars such as the BMW M3 and Jaguar X-type where a 'bolt-on' part is used. These parts are amenable to analysis and simple testing and are close in concept to the tubes presented in this work. Design for this approach can benefit from the work presented here on resins and processing. Crash structures which are integrated into the vehicle primary structure can be more efficient as they can have multiple functions in the finished vehicle (i.e. they can be load-bearing structures) however they are more complex in terms of design and analysis. The preform work was undertaken with this type of part in mind where local changes to the preform could be made and not necessarily applied to the whole part. Additionally there are other applications in helicopter sub-floors and in commercial vehicles where impacts with smaller passenger cars are coming under legislation.

The work presented here builds upon crash energy management experience at the University of Nottingham where existing methods of specimen production have been modified to suit this work. The work also builds on a knowledge base which is documented in numerous journal papers and PhD theses [23-28]. In this work the link between fracture toughness and specific energy absorption has been of particular interest. Many important areas which greatly affect the crushing process are ignored in this work. All testing is quasi-static and so results ignore the effect of rate. Testing is performed at room temperature for a single tubular test geometry. Two fibre architectures are considered in this work but many material variations are possible, including fibre material.

The first part of this work concerns constituent materials where the objectives were to determine the effect of changing the matrix material and fibre architecture. A secondary aim was to correlate the observed effects with changes

in the more fundamental in-plane material properties. The work then moved to ways of increasing interlaminar properties at a preform level. The chosen methods were stitching and interleaving where the objectives were to determine the increase in fracture toughness given by the two methods and then determine the changes in specific energy absorption. Again there was a desire to correlate the observed changes in fracture toughness and energy absorption to further understand the crushing process. The final section of the work was purely driven by the manufacturing. The factor of interest was whether the speed of an industrial moulding process would degrade the composite properties and adversely affect the energy absorption. This was approached in two areas; binder concentration and level of porosity.

This work has been conducted under an EPSRC-funded industrial project, number GR/N 13753. The project is part of the "Materials Processing for Engineering Applications" programme. The work was undertaken between January 2001 and January 2004. 3 separate work plans of roughly equal length are presented in the results chapters. A combined review of current literature is presented, some of the work mentioned was published during the course of this work.

Chapter 1 References

1. Jones, N., *Structural impact*. 1989, Cambridge: Cambridge University Press.

2. Carreras, M., B. Forster, C. Orta, and B. Yonce, *Plastic composite materials : Industry analysis*. 2004, Michigan Business School.

3. Thornton, P., *Energy Absorption in Composite Structures.* Journal of Composite Materials, 1979. **13**: p. 247-262.

4. Thuis, H. and V. Metz, *The Influence of Trigger Configurations and Laminate Lay-up on the Failure Mode of Composite Crush Cylinders.* Composite Structures, 1993. **28**: p. 37-43 (131-137).

5. Karbhari, V. and J. Haller, *Effects of Preform Structure on Progressive Crush Characteristics of Flange-Stiffened Tubular Elements.* Composite Structures, 1997. **37**(1): p. 81-96.

6. Farley, G., *Effect of Fiber and Matrix Maximum Strain on the Energy Absorption of Composite Materials.* Journal of Composite Materials, 1986. **20**: p. 322-334.

7. Farley, G., *Energy Absorption of Composite Materials.* Journal of Composite Materials, 1983. **17**: p. 267-279.

8. Tao, W., R. Robertson, and P. Thornton, *Effects of Material Properties and Crush Conditions on the Crush Energy Absorption of Fiber Composite Rods.* Composites Science and Technology, 1993. **47**: p. 405-418.

9. Farley, G., *Effect of Specimen Geometry on the Energy Absorption Capability of Composite Materials.* Journal of Composite Materials, 1986. **20**: p. 390-400.

10. Farley, G. and R. Jones, *Crushing Characteristics of Composite Tubes with "Near-Elliptical" Cross Sections.* Journal of Composite Materials, 1992. **26**(12): p. 1741-1751.

11. Hamada, H. and S. Ramakrishna, *Scaling Effects in the Energy Absorption of Carbon-Fibre / PEEK Composite Tubes.* Composites Science and Technology, 1995. **55**: p. 211-221.

12. Fairfull, A. and D. Hull, *Effects of Specimen Dimensions on the Specific Energy Absorption of Fibre Composite Tubes.* International Conference of Composite Materials VI, 1987: p. 3.36-3.45.

13. Farley, G. and R. Jones, *Prediction of the energy-absorption capability of composite tubes.* J. Composite materials, 1992. **26**(3): p. 388-404.

14. Ramakrishna, S. and H. Hamada, *Energy Absorption Characteristics of Crash Worthy Structural Composite Materials.* Key Engineering Materials, 1998. **141**: p. 585-619.

15. Mamalis, A., M. Robinson, D. Manolakos, G. Demosthenos, M. Ioannidis, and J. Carruthers, *Review: Crashworthy capability of composite material structures.* Composite structures, 1997. **37**: p. 109-134.

16. Mamalis, A., D. Manolakos, G. Demosthenous, and M. Ioannidis, *Analytical Modelling of the static and Dynamic Axial Collapse of Thin-Walled Fiberglass Composite Conical Shells.* International Journal of Impact Engineering, 1997. **19**(5): p. 477-492.

17. Farley, G. and R. Jones, *Analogy for the Effect of Material and Geometrical Variables on Energy-Absorption Capability of Composite Tubes.* Journal of Composite Materials, 1992. **26**(1): p. 78-89.

18. Sato, H., H. Hirakawa, Z. Maekawa, H. Hamada, M. Nakamura, and D. Hull, *Comparison of Energy Absorption Among Carbon/Thermoplastic Tubes.* Proceedings of the 1993 38th International SAMPE Symposium and Exhibition, 1993. **38**(1): p. 952-966.

19. Ramakrishna, S., H. Hamada, Z. Maekawa, and H. Sato, *Energy Absorption Behaviour of Carbon-Fibre-Reinforced Thermoplastic Composite Tubes.* Journal of Thermoplastic Composite Materials, 1995. **8**: p. 323-344.

20. Thornton, P. and R. Jeryan, *Crash Energy Management in Composite Automotive Structures.* Int. Jnl. Impact Engineering, 1988. **7**(2): p. 167-180.

21. Turner, T., F. Robitaille, N. Warrior, C. Rudd, and E. Cooper, *Effect of resin formulation on crash energy absorbing composite structures made by RTM.* Plastics, Rubber and Composites, 2002. **31**(2): p. 49-57.

22. Abraham, D. and R. McIlhagger, *Investigations into various methods of liquid injection to achieve mouldings with minimum void contents and full wet out.* Composites Part A, 1998. **29A**: p. 533-539.

23. Duckett, M.J., *Rate dependent effects on the energy absorption and material properties of polymer composites*. 2001, University of Nottingham: Nottingham.

24. Cooper, E., *An elastic-plastic finite element model for composite crash structures*. 2002, University of Nottingham: Nottingham.

25. Fernie, R., *Loading rate effects on the energy absorption of lightweight tubular crash structures*. 2002, University of Nottingham: Nottingham.

26. Lourenco, N., *Predictive Finite Element Method for Axial Crush of Composite Tubes*. 2002, University of Nottingham: Nottingham.

27. Curtis, C.D., *Energy absorption and crush behaviour of composite tubes*. 2000, University of Nottingham: Nottingham.

28. Ribeaux, M., *Energy Absorption capability of damage affected composite structures*. 2003, University of Nottingham.

2 Literature Review

The following section is a review of literature related to the field of crashworthiness of composite structures. Emphasis is placed upon processing of composite materials for medium volume applications and the adjustment of various material and moulding factors to increase specific energy absorption.

The following subjects are addressed;

- Crush mechanisms
- Test piece geometry
- Composite mechanical properties
- Matrix properties
- Fibre properties
- Testing variables

The emphasis in each section and in the literature reviewed is on the effect of these properties on specific energy absorption. Where SEA values are quoted in literature it must be appreciated that there are many variables involved. Generally, only values from the same set of testing can be judged as comparable. The extent of reviewed literature is fairly broad as the work in the following chapters is based on many areas of work. The following sections on geometry, crush mechanisms and testing variables are included to allow the reader some insight into how these factors will affect the results presented in later chapters.

2.1 Crush Mechanism

The collapse of metallic tubular structures has been understood for many years with the seminal work of Alexander [1] being largely responsible for the accurate analytical modelling of energy absorption. Metal structures fail by the formation of plastic hinges about which the material buckles and folds. Although a significant amount of energy can be absorbed in this manner there exists an incomplete utilisation of the material. The collapse of composite materials can be more efficient giving potentially higher SEA levels. Analytical models are available for the calculation of energy absorption in metal tubes; these are well developed.

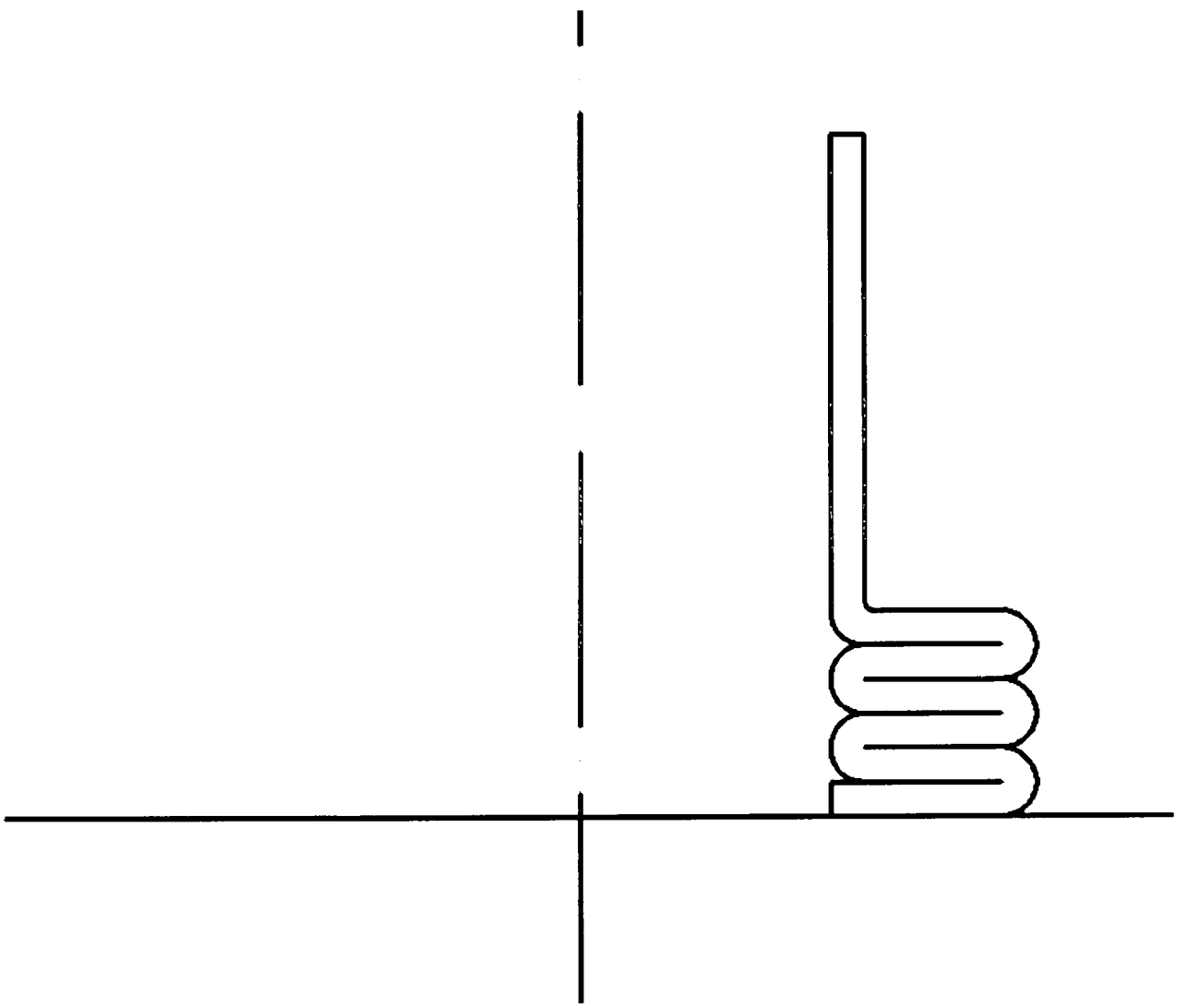

Figure 2:1 Half section through partially crushed metal tube

Figure 2:2 Aluminium tube crush showing axisymmetric (left) and diamond crush modes (right)

The majority of research on composite energy absorbing structures has been done on the axial crush of circular section tubes. Other geometries have included flat plates, frusta and rectangular section tubes. The geometry of the crush platen is also important with the most common being a flat surface, however a plug can also be used and can give very high energy absorption values (see section 2.6.3). Composites fail in a number of different modes as described below. As with metal parts the issue of global / Euler buckling is also important.

2.1.1 Failure modes

Composite tubes fail in various ways according to a variety of material and geometric factors. The worst failure mode from an energy absorption point of view is global Euler buckling where very little energy is absorbed. A similar situation occurs if the compressive load on the part causes the stress to exceed the ultimate compressive stress of the material. The main failure modes, originally identified by Farley and Jones [2] which give progressive crush are defined below.

Composite tube crush can be viewed as a balance of energy absorption mechanisms with varying contributions to the final compressive load and hence energy absorption. Further complicating the situation are interactions between the absorption mechanisms. Often there are no clear boundaries between the following failure modes and combinations can exist.

2.1.1.1 Splaying

The splaying mode is referred to as the lamina bending mode by some authors and is characterised by a centre wall crack forming with fronds splaying inside and outside the tube. Figure 2:3 shows how a stable crush is formed. There are many energy absorbing modes associated with this mode, the most important being crack growth [3]. Growth of the centre wall crack is known to be critical to this mode, although the energy dissipated in propagating the crack is not in itself the main contributor to increased energy absorption. The lamina bundles do not fragment in the splaying mode but bend around a radius (Figure 2:3 far right) which is governed in part by the length of the centre-wall crack [4]. A tighter radius causes increased energy absorption through greater fragmentation and shearing in the fronds. The interlaminar properties of the material also determine the inter-ply cracking. A triangular debris wedge is formed between the splaying fronds and acts as an additional site of frictional energy dissipation.

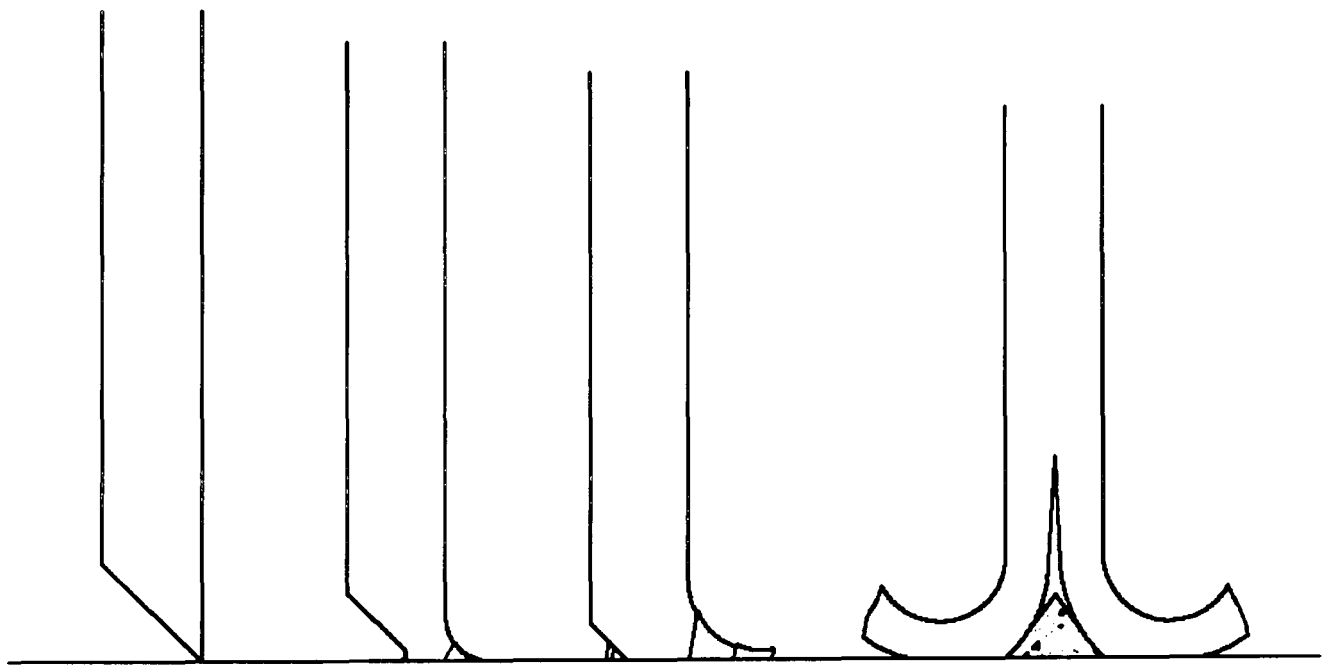

Figure 2:3 Initiation of splaying mode

2.1.1.2 Fragmentation

The fragmentation or transverse shearing mode is shown in Figure 2:4. The formation of axial and interlaminar cracks means that bundles of composite break away. These bundles act as columns that fragment upon crushing absorbing large amounts of energy. An additional energy absorption mechanism is crack propagation.

Fragmentation can occur in high strength composites where resin fracture toughness is low. As the energy absorption relies on the pulverisation of the composite, and hence fracture surface area, the size of the bundles produced is indicative of the energy absorption capability.

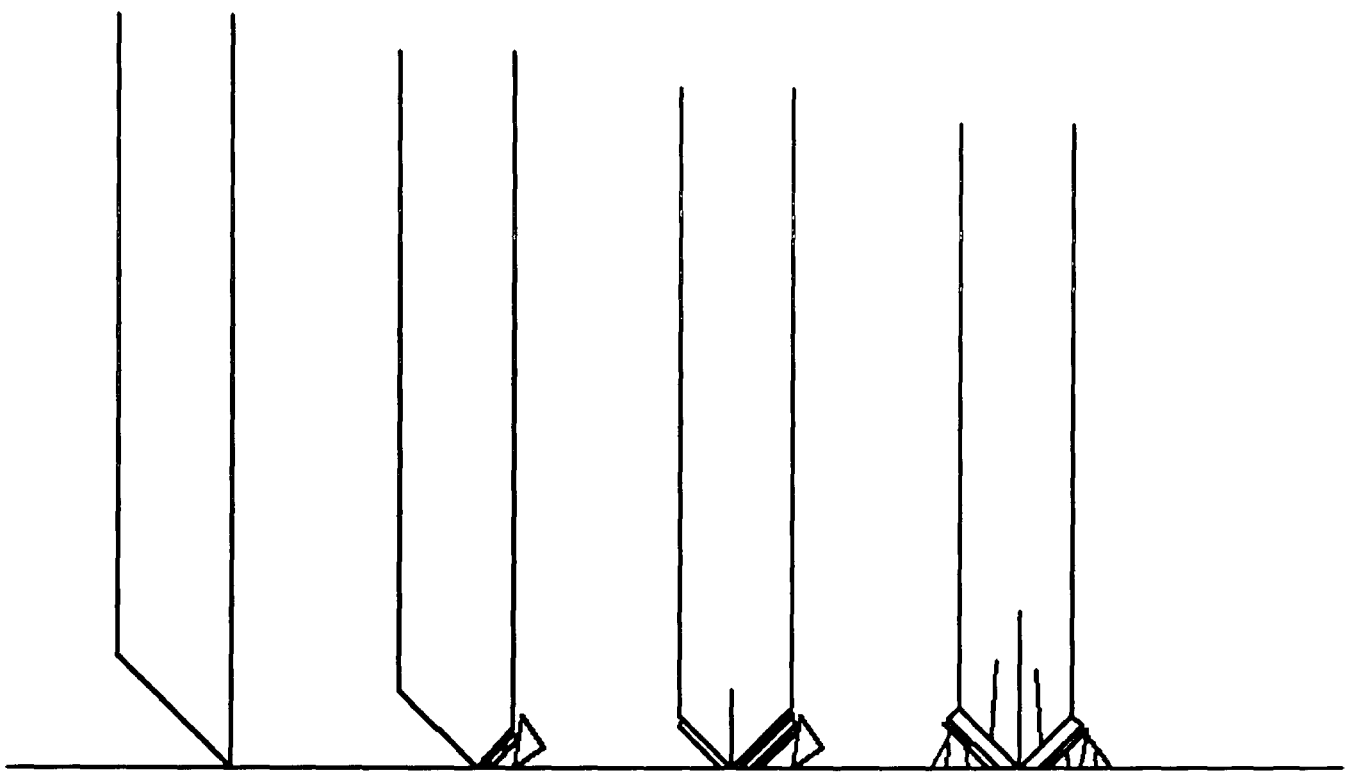

Figure 2:4 Initiation of fragmentation mode

2.1.1.3 Local buckling

The local buckling crush mode is similar to the method by which metal sections fail with the formation of plastic hinges. Aramid fibres, which are weak in compression, typically fail by this mode where the compressive strength of the composite is not high enough to sustain the type of crushing in the modes above. This behaviour is typical of a ductile composite, however it is also possible for more brittle composite materials to fail by this mode where the following conditions exist [3];

- Where low interlaminar stresses exist relative to the matrix strength
- Where the matrix failure strain is higher than that of the fibre
- Where the matrix exhibits plastic deformation under high stress

The excellent energy absorption properties of composite materials are very dependent on the crush mode. For parts to be designed for energy absorption, a given crush state must occur with certainty. Local buckling is to be avoided, as discussed above, but where there is a degree of choice in material and/or geometry it is easy to avoid. There may however be some compromise where ductile fibres are incorporated to increase damage resistance for example. The remaining failure modes are both capable of high energy absorption and are dependent on material properties. For maximum energy absorption in a structure, therefore, the sustained crushing stress must be almost at the limit defined by the material compressive strength.

The actual mechanisms by which energy is absorbed are discussed in section 2.1.3.

2.1.2 Crush Zone Morphology

Failure by the splaying mode is most common for glass-reinforced composites of relatively low volume fraction. Sectioned tubes and micrographs of typical crush zones are shown in Figure 2:5 and Figure 2:6.

Figure 2:5 Sectioned NCF tube showing inner and outer fronds

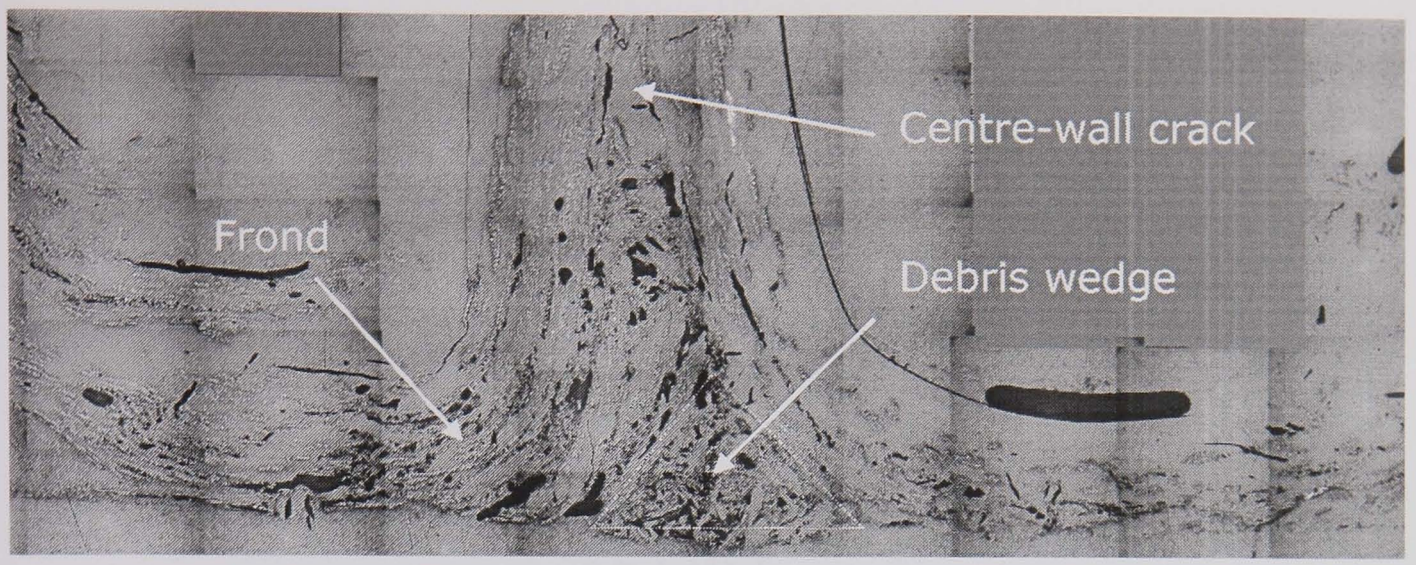

Figure 2:6 Micrograph showing frond formation and debris wedge

The splaying mode is fairly easy to visualise with the inner and outer fronds being clearly visible. The importance of the centre wall crack can be seen with its direct effect on the radius of curvature of the fronds. The debris wedge can also be seen highlighted in white.

A study of the crush zone morphology can often give greater knowledge of the crush process although it is not always easy to interpret the results. When multiple materials are involved in the crush process it can be helpful to know the interactions of them and their relative contributions to the overall energy absorption. This is especially true of stitching for instance where the exact interaction of the materials can often be determined.

2.1.3 Energy Absorbing Mechanisms

Fairfull [5], originally identified eight mechanisms by which energy was absorbed during tube crush they are as follows (see Figure 2:7);

- Mode-I centre-wall crack propagation
- Friction between debris wedge and platen
- Interlaminar frond delamination
- Flexural damage of the fronds
- Interlaminar friction between fronds after delamination
- Friction between fronds and platen
- Crack propagation / splitting between fronds
- Transverse flattening of the fronds

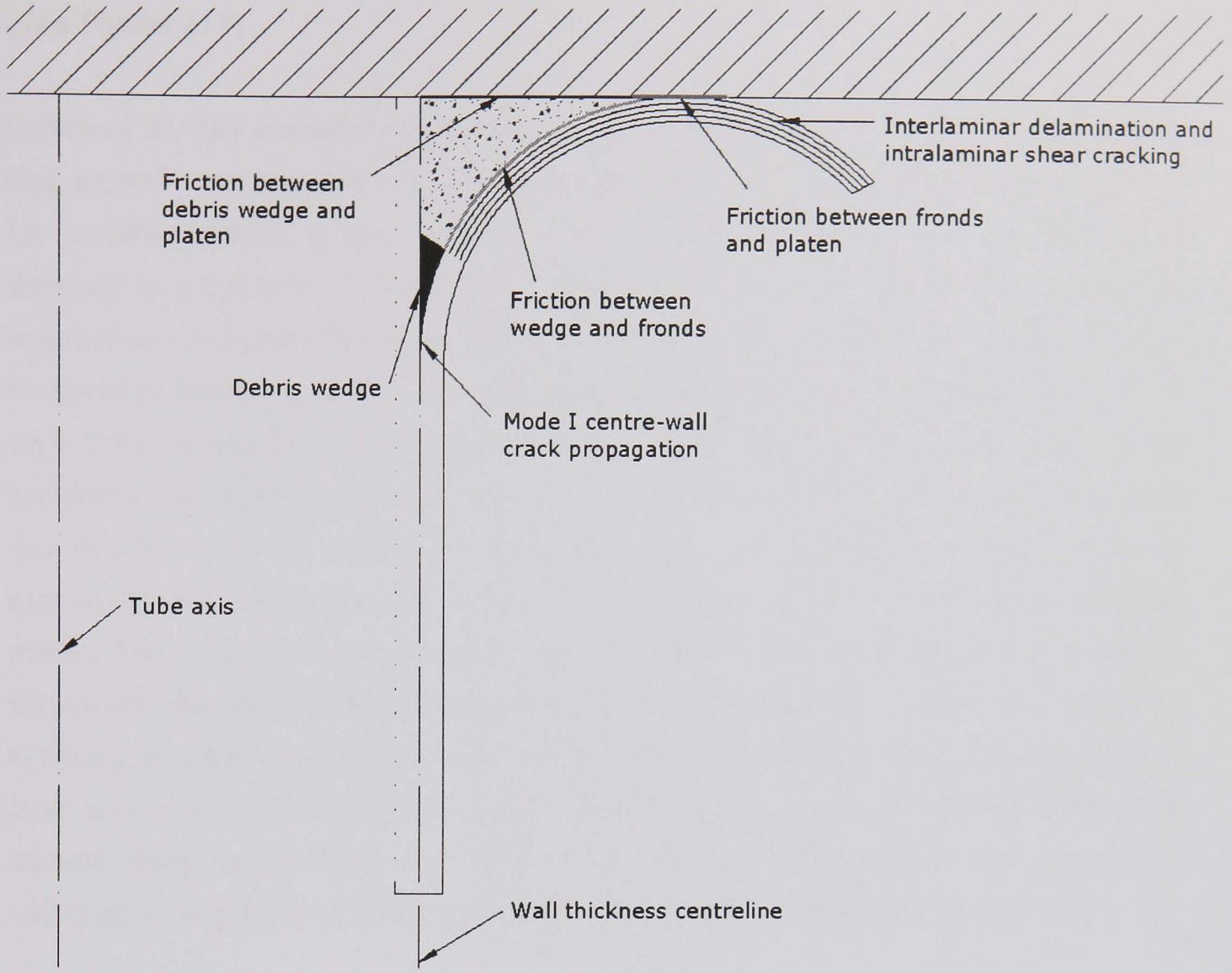

Figure 2:7 Schematic of energy absorption mechanisms

Of the list above, three are friction and five are essentially crack initiation and propagation. Various methods have been employed to isolate the energy absorbing mechanisms and calculate their effect on overall energy absorption.

Independent fracture models by Berry and Keal (in [6]) suggest that approximately one third of the energy absorption in glass cloth and filament wound tubes is accounted for in the fracture processes.

Fairfull and Hull conclude that friction is of considerable importance [7] having studied glass/epoxy tubes. Later work [6] involved an in-depth study of frictional effects using a combined torsion and compression machine. Four alternative crush platens were used ranging from fully polished through standard ground and sandblasted to a cross milled finish. Crush load levels were 7% lower than standard with the polished platen, with the sandblasted and cross-milled finishes giving marginally lower results than standard. The authors concluded that frictional effects accounted for over 50% of the total energy absorbed, they also

conclude that frictional mechanisms account for the serrations in the crush trace (See Figure 1:3)

Farley *et al.* [8] aimed to determine frictional contributions by comparing rough and smooth crushing surfaces with a wider variety of materials than that used in the original Fairfull / Hull studies. The authors conclude that it is difficult to conduct a surface roughness only comparison as it is very easy to generate interactions between the three frictional mechanisms. Tubes that crushed in the transverse shearing, brittle fracturing and local buckling modes were influenced very little by surface roughness, this is because the primary means of energy absorption for these tubes is fracturing of lamina bundles; a process which does not involve relative sliding of composite and crush platen. A wide range of responses was observed for those samples that failed by the lamina bending mode. The response was found to be a function of the relative fibre and matrix failure strains. Where fibre maximum strain exceeds matrix maximum strain an increase in SEA is observed with increasing surface roughness, the opposite is true where matrix maximum strain exceeds fibre maximum strain. Where the strains were equal there was little effect. Most of the testing was conducted using various grades of CFRP although some E-glass results are presented.

Ramakrishna tested various thermoplastic matrices with carbon fibres [9] and attributed the increased energy absorption to the higher fracture toughness levels in thermoplastics (see Table 2:1). Whilst a correlation can be seen between fracture toughness and resulting SEA, the fibre type is also shown to have an effect with an S2-glass fibre in a PEEK matrix having an SEA of 143.5kJ/kg compared to a high strength carbon fibre in the same matrix of 194.1kJ/kg.

	Carbon / Peek	**Carbon / PEI**	**Carbon / PI**	**Carbon / PAS**
SEA (kJ/kg)	194.1 ±8	155.5 ± 4.5	131.4 ± 13.7	128 ± 9.5
G_{IC} (kJ/m^2)	1.6 ~ 2.4	1.0 ~1.2	0.8 ~ 0.9	Not given

Table 2:1 SEA and fracture toughness for various thermoplastic matrices [9].

Whilst a substantial quantity of research has been undertaken, the exact contributions of each mechanism are still not known. Furthermore, it is not yet possible to predict energy absorption using an analytical approach due to the complex interactions between material properties and energy absorbing mechanisms. Some of the above mechanisms can be directly related to material properties; for instance delamination. The energy absorption levels of other modes, such as friction are more dependent on the crush load than the coefficient of friction of the material. Thus it is wrong to assume that a material with higher friction will achieve better SEA as it may not be able to sustain a high crush load. The various mechanisms above are of limited use from a design point of view but are important in terms of addressing the long-term understanding of the crush process.

2.1.4 Triggers

As suggested above the main advantage of composites in crashworthiness is their ability to crush in a progressive and more complete manner by a splaying or fragmentation mode rather than plastic buckling of a limited proportion of the material. To achieve progressive crushing the failure mode must be controlled. Thornton [10] found that a stress raiser introduced at the crush platen end served to initiate a stable, progressive crush by preventing global buckling. Later work by the same author [11] compared the benefits of two alternative trigger geometries known as tulip and bevel triggers (Figure 2:8). Glass reinforced epoxy tubes were tested with rectangular, square and cylindrical cross sections. Experiments determined that the trigger altered the SEA by generating a varying quantity of interlaminar cracking which then propagates through the composite. However, it was established that the propagation of flaws in themselves did not contribute a significant amount of energy absorption, moreover that the formation of 'kink bands' around the periphery of the tube led to the high energy absorption values. The bevel trigger was found to cause local delamination in the centre of the part wall whereas the tulip trigger did not.

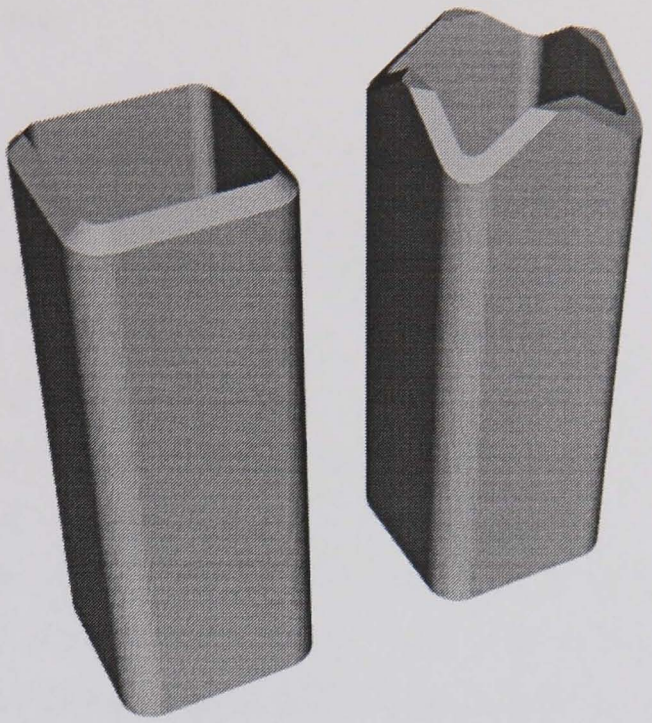

Figure 2:8 Bevel and tulip triggers applied to square tubes

The work of Sigalas *et al.* [12] provides experimental data on Tufnol (Woven glass/epoxy type RLG1) tubes. Tubes with bevel chamfers from 10 to 90° were tested. Energy absorption values of around 70kJ/kg were achieved. A thorough microscopic investigation of the chamfer zone morphology is presented. From this a detailed schematic representation of the initial crush process is given for various chamfer angles. The steady state load and crush zone morphology were found to be independent of initial chamfer angle. At high angles annular rings of material broke away and were forced towards the wall edges, whereupon crushing continued as if a lower chamfer angle had originally been used. Although different chamfer angles initiate crush differently this is a small-scale effect, which does not apply after the first few millimetres of crush.

The effect of trigger angle on crush performance of I beams and box sections has been studied by Jimenez *et al.* [13]. I beams were found to be insensitive to both trigger type and angle and gave energy absorption levels of between 37 and 39 J/g. Box sections with different trigger types and angles gave energy absorption levels between 36 and 45J/g.

Hull and Coppola [14] have tested circular section tubes and found that the steady state crush load is independent of initial chamfer angle but that the angle has a considerable effect on the load required to initiate stable crush. The testing

also included the effects of trigger angle on mandrel/plug crush and the trend was found to be similar.

Work has also been undertaken into the triggering of circular sections by varying the laminate lay-up in prepreg parts [15], the present work invariably involves post-moulding machining to form the trigger.

A review of the literature on the subject of trigger geometry shows that triggers serve the simple purpose of preventing the high initial loads that occur without them. This can be accomplished in a variety of ways, but in general, it can be seen that the trigger has little effect on the steady state crush load, providing that it has initiated a stable crush zone and efficient crush zone morphology. High trigger angles (approaching 90°) may cause more difficulties for some materials where global failure could result. When an efficient material combination and geometry has been found there may be some additional gain in SEA through experimentation with trigger angle.

2.2 Geometry

The work presented here is concerned only with prismatic sections of which there are a significant number in the literature. A substantial amount of work has also been done by authors such as Mamalis *et al.* [16-21] on the crushing characteristics of composite frusta. The most common section is circular; its ease of manufacturing and lack of discontinuities accounting for its popularity. The use of box sections for automotive applications may provide advantages in integration with existing parts but in general the energy absorption levels achieved are often 20% lower than those of circular sections [22].

2.2.1 Thickness vs. Diameter effects

Work by Thornton *et al.* [23] demonstrated that the relative density (the ratio of the volume of the tube to that of a solid with the same outer dimensions) was important in determining the stability of the crush. The t/D ratio was varied from 0.01 to 0.1. A critical density of 0.025 for carbon epoxy and 0.045 for glass epoxy was found, below which crush was unstable. Within the bounds of stable crush the SEA performance was independent of tube dimensions. Subsequent work by Fairfull and Hull [7] on glass/epoxy specimens showed that for a given value of D the SEA increased with increasing t/D ratio up to 0.2 after which it

began to decrease. No universal theory has been found for the relationship between this geometric factor and SEA.

Hamada and Ramakrishna [24] have performed a similar study for carbon fibre/ PEEK tubes and found that t/D ratios of less than 0.015 failed by brittle fracture, this is somewhat lower than that found by Thornton. For the series of tests in question, SEA was found to be dependent on the absolute value of t rather than the t/D ratio with highest specific energy absorption displayed by tubes with a wall thickness between 2 and 3mm.

Crush stability is dependent on t/D ratio as a lower boundary; as is true for conventional solid mechanics in Euler buckling. However, the absolute limit seems to depend on the material in a way which has not yet been fully identified. Beyond the broad limit of crush stability there is the issue of SEA variation which is somewhat more complex. Currently there are no analytical methods available for determination of a maximum SEA configuration. Some insight can be gained from the consideration of the energy absorption due to bending (i.e. Flexural damage and interlaminar shear of the fronds). As bending is an important factor in determining energy absorption high bending stiffness will lead to greater energy absorption; conventional beam theory suggests that thicker walled sections will give improved resistance to bending – up to the point where stiffness is too high and buckling results.

2.2.2 Length

Generally SEA has been found to be independent of length in cases where the crush occurs in a stable manner. In the case of Euler buckling, failure can be avoided by appropriate choice of length [25]. Once progressive crush is initiated the only length factor is the build up of debris within the tube interior, effective crush length is thus limited to some extent. In metal structures the concept of stroke efficiency is common which correlates somewhat with the equivalent composite response, however the load can be seen to increase fairly gradually with a composite specimen.

2.2.3 Other geometries

Other geometries less commonly used include:

- Flat plates [26-28]
- Part sections
- Stiffened beams [29]
- Sandwich structures
- Frusta [30]
- Sine webs (sinusoidal profile plates) [31, 32]

A thorough examination of these profiles is beyond the scope of this review. Flat plates and sine webs have typically found applications in helicopter sub floors whilst sandwich structures are of interest in areas where high out of plane properties are required, unfortunately, these can be seen to be even more complex to analyse than prismatic closed sections.

2.3 Composite properties

By its nature, a composite material is more complex than a homogeneous isotropic material. The choice of constituent materials has a profound effect on the outcome but this is often limited by cost and manufacturing method. The emphasis here is on mass production potential whereas most previous work has tended to focus on aerospace methods and materials. The effect of various properties of the composite is studied before examining the two main constituents of the composite; namely, the fibre and matrix, in more detail.

2.3.1 Volume Fraction

It can be seen from the rule of mixtures that as the fibres are stronger and stiffer than the matrix the composite becomes stronger and stiffer as the proportion of fibre is increased [33]. The major limitation in increasing volume fraction is the manufacturing process. Typical volume fractions range from 10% for filler loaded cosmetic parts through 20% via hand laminating to 65% via autoclave cure of prepregs.

Very little organised data is available for the effect of fibre volume fraction on SEA performance. An increase in volume fraction will lead to an increase in material density given that fibre density is always greater than resin density. If SEA is to be improved the crush load must increase by a greater extent than the material density increase. Thus an increase in volume fraction will not always

give an increase in SEA [9]. There is also a significant cost aspect which is of relevance in industrial applications.

Snowdon and Hull [34] present crush results for Sheet Moulding Compounds (SMC) at various volume fractions. Table 2:2 shows the effect of both resin system and glass content.

At low volume fractions therefore an increase in SEA is observed for SMC material, The SMC material used was hand made by impregnating 50mm CSM with the two resin systems; both of which are UP polyester based. As no filler was used the materials are essentially hand lay-up and could be expected to perform similarly to CoFRM parts manufactured by RTM.

Resin system	Glass Content (%)	SEA (kJ/kg)
40-6020	14.6	34.9
	16.4	47.0
	19.0	49.9
	21.2	51.3
40-8200	13.3	38.7
	16.0	44.2
	17.9	53.5
	25.0	56.0

Table 2:2 SEA vs. glass content for CSM SMC [34]

Farley tested prepreg tubes with 40-70% volume fraction and found that the parts suffered a 10% decrease or no change depending on the orientation of the fibres [29]. The author concluded that as the volume of matrix between the fibres decreased, the resulting loss of ILSS caused a reduction in SEA. Fibre volume fraction increases the composite density which decreases the SEA for a given crush load.

2.3.2 Interlaminar properties

Interlaminar properties describe both the fracture performance of the material and also the mechanical strength between the plies of the material. Since many of the energy absorption modes rely on fracture it can be seen that interlaminar performance is crucial to the realisation of high SEA.

The study of interlaminar properties can encompass a range of areas including;

- Resin toughening additives
- Stitching
- Fibre architecture
- Interleaving

These factors all affect the interlaminar performance of the material either by increasing fracture toughness, or by stitching, which physically ties the layers of material together. In comparison with isotropic materials, composites generally perform badly and generally sacrifice high out of plane properties for high in-plane strength and modulus.

This section deals with interleaving and the next with stitching. Resin properties and fibre architecture are discussed in sections 2.4 and 2.5.2.

Interlaminar properties do not increase energy absorption solely through increased fracture energy. Energy absorption potential is related to the length of the centre-wall crack due to the bend radius where fronds turn 90 degrees at the platen. The length of the centre-wall crack is in turn related to the mode-I fracture toughness properties of the material. If the fracture toughness can be made higher increased energy absorption can be expected. This represents a secondary effect rather than simply crack propagation energy in the centre wall crack.

Interleaf materials are thin thermoplastic plies inserted during preforming or layup between the plies of reinforcement. Interleaves are typically used in high strength prepreg carbon fibre applications to give increased interlaminar properties and hence damage resistance and impact performance.

Yuan *et al.* [35] reasoned that the known improvement given by interleaf materials in impact loading [36, 37] could be duplicated in crush performance of composite tubes. The study found that quasi-static energy absorption levels increased from 53kJ/kg to 63 kJ/kg with the addition of a tough modified interlayer. All testing was done at speeds between 7 and 10 ms^{-1}.

Hillermeier *et al.* have examined the effect of the addition of liquid and powder tackifiers for spray application to RTM laminate interlayers [38]. The liquid tackifier used consisted of 67% by weight high molecular weight epoxy and 33% polyamide-6 particles dissolved in acetone. The powder tackifier was a commercially available 3M epoxy-based material known as PT500. These materials were used in conjunction with a 6K carbon satin weave fabric and RTM6 epoxy resin from Hexcel. More consistent interlaminar morphology was obtained with the spray tackifier which gave 30% improvements in mode-II testing and a slight increase in ILSS.

Recent work at the University of Nottingham has used interleafs to increase damage tolerance of composite energy absorbers [39]. Samples were tested with and without interleaves quasi-statically and dynamically. SEA's decreased between 28.6% and 48% for quasi-static tests and between 18.2% and 29.4% for dynamic tests. The reduction was attributed to a reduction in friction in the crush zone and hence a lower compressive load, although local heating in the crush zone may also be a factor. The coefficient of friction was subsequently measured and found to reduce from 0.36 to 0.22 when an interleaf was included. Crush traces were found to be smoother implying that the interleaf reduced the normal stick-slip effect during crushing. The damage tolerance of interleaved parts was found to be up to 9 times better than standard parts.

Almost all work done on interleaves has been related to the undisputed increase in through-thickness properties – an area in which conventional composites are particularly weak. Research into RTM applications has stemmed from prior work into prepreg toughening where the use of interlayer modification is more common. Impact and out-of-plane improvements are beyond the scope of this study but there is a large quantity of work in the literature e.g. [40-42].

2.3.3 Stitching

Composites have long been known to possess poor out of plane properties, which make them particularly susceptible to interlaminar fracture. Stitching is an effective, if labour intensive method of increasing interlaminar properties. This however is often at the expense of in-plane properties [43]. A substantial amount of research exists on the effect of stitching in damage and impact situations but less is available concerning its effect on energy absorption. Many contradictions exist in terms of factors such as whether stitching degrades

certain properties, this makes prediction of the effect of stitching very difficult, largely because it is dependent on many stitching parameters.

Potential benefits from stitching are in promoting increased fragmentation in the fronds by tying the laminae together. Stitching will also slow crack growth due to greater interlaminar strength

One of the major drawbacks of stitching is the reduction of in-plane properties, although true 3D fabrics normally have lower in-plane properties due to a reduction in in-plane fibres. The reduction in properties comes partly from the damaged caused to the fibre bundles by the stitching process but also by the production of resin rich areas at the stitch knots [44]. The resultant stress concentration causes the growth of damage at low stresses. Flexural properties were shown to be substantially degraded compared to unstitched laminates.

The work of Mouritz *et al.* provides one of the most thorough investigations of Mode-I effects on a range of textile composites [43-48]. A variety of techniques for improving Mode-I interlaminar properties have been examined including braiding, knitting and stitching. These methods have been compared to more conventional methods such as toughened resins.

Daniel *et al.* [49] have used short beam shear tests to determine interlaminar shear stress (ILSS) properties of stitched and woven materials. These have then been correlated with SEA properties. A variety of materials were tested from 0/90 woven and non-crimp fabrics to quadraxial and stitched CSM. A strong link between ILSS and specific sustained crushing stress (SSCS) was found, the highest interlaminar strength being with the CSM. The authors suggested that interlaminar toughening techniques such as stitching could lead to higher SEA's.

The damage tolerance of stitched laminates has been shown to be higher than unstitched parts [50]. At ballistic speeds the carbon / epoxy laminates exhibited compressive strengths 50% higher after impact when stitched. This is of interest when parts are subjected to impact loadings, which may occur in a typical automotive application.

A comprehensive model has been proposed by Jain and Mai [51] which highlights the important parameters in stitching design and demonstrates that a high stitch

density with thin threads is an efficient format. A large number of variables are involved in the design of efficient stitching.

2.3.4 Strain to failure

Conventional laminate theory asserts the importance of fibre and matrix strain to failure and the same significance exists with tube crush. Farley has compared various carbon fibres with different moduli in epoxy matrices with different strain to failure [52]. Mechanical properties are shown in Table 2:3. The two fibres with 2 matrices led to 4 different test configurations. Six ply orientations were tested, but overall, high matrix strain to failure improved composite SEA for both fibre types by reducing interlaminar cracking. Highest SEA was achieved with the high strain to failure fibres in a high strain to failure matrix. The results also suggested that for a given fibre, the matrix should exhibit greater strain at failure for maximum SEA.

Material	Young's Modulus	Tensile failure strain
T300 (carbon fibre)	231.5	0.012
AS-4 (carbon fibre)	235.0	0.015
934 (epoxy matrix)	4.0	0.010
5245 (epoxy matrix)	3.8	0.020

Table 2:3 Mechanical properties of fibre and matrix materials (from [52])

Whilst strain to failure of the matrix is of considerable importance in determining overall SEA there is also evidence to suggest that the relative fibre/matrix strain is of importance in determining the failure mode. Farley [8] also identified the following three cases from experiments with carbon/epoxy tubes;

I Fibre failure strain exceeds matrix failure strain

II Matrix failure strain exceeds fibre failure strain

III Fibre and matrix failure strain are equal

In case I the energy absorption increased with increasing platen surface roughness whilst the opposite trend was observed for case II. The difference was attributed to the highly non-linear elastic response of the resin in case II.

2.3.5 Voidage

The detrimental effect of voids on composite materials has been understood for many years and is one of the major concerns for all liquid moulding processes. Voids are one of the most common manufacturing defects and can be caused by a variety of factors such as non-uniform velocity fields during moulding [53], injection pressure and vacuum assistance [54, 55]. These mechanisms are varying the amount of trapped air in the laminate. Voids are termed macroscopic if they exist between tows (see Figure 2:9) and microscopic if they exist within the tow. Macroscopic voids are generally affected by tooling design and preform quality but microscopic voids are produced by differences in the speed of the advancing flow front around and inside the tows. Flow within the tows is capillary driven and if the speed of this flow can be determined then the injection pressure can be adjusted to give a matched flow front velocity.

Void content can be assessed by a range of methods including density measurement, burn-off, ultrasound scanning, nuclear magnetic resonance imaging (NMRI) and acid digestion.

No data is available for the effect of voidage on specific energy absorption but voids are known to cause a major reduction in many material properties. A comprehensive review paper by Judd and Wright [56] compares 47 papers investigating the effect of void content on flexural strength, ILSS, Compressive and tensile strength, impact strength and inplane and flexural moduli. Percentage decreases between 1 and 20 are seen for 1% voidage.

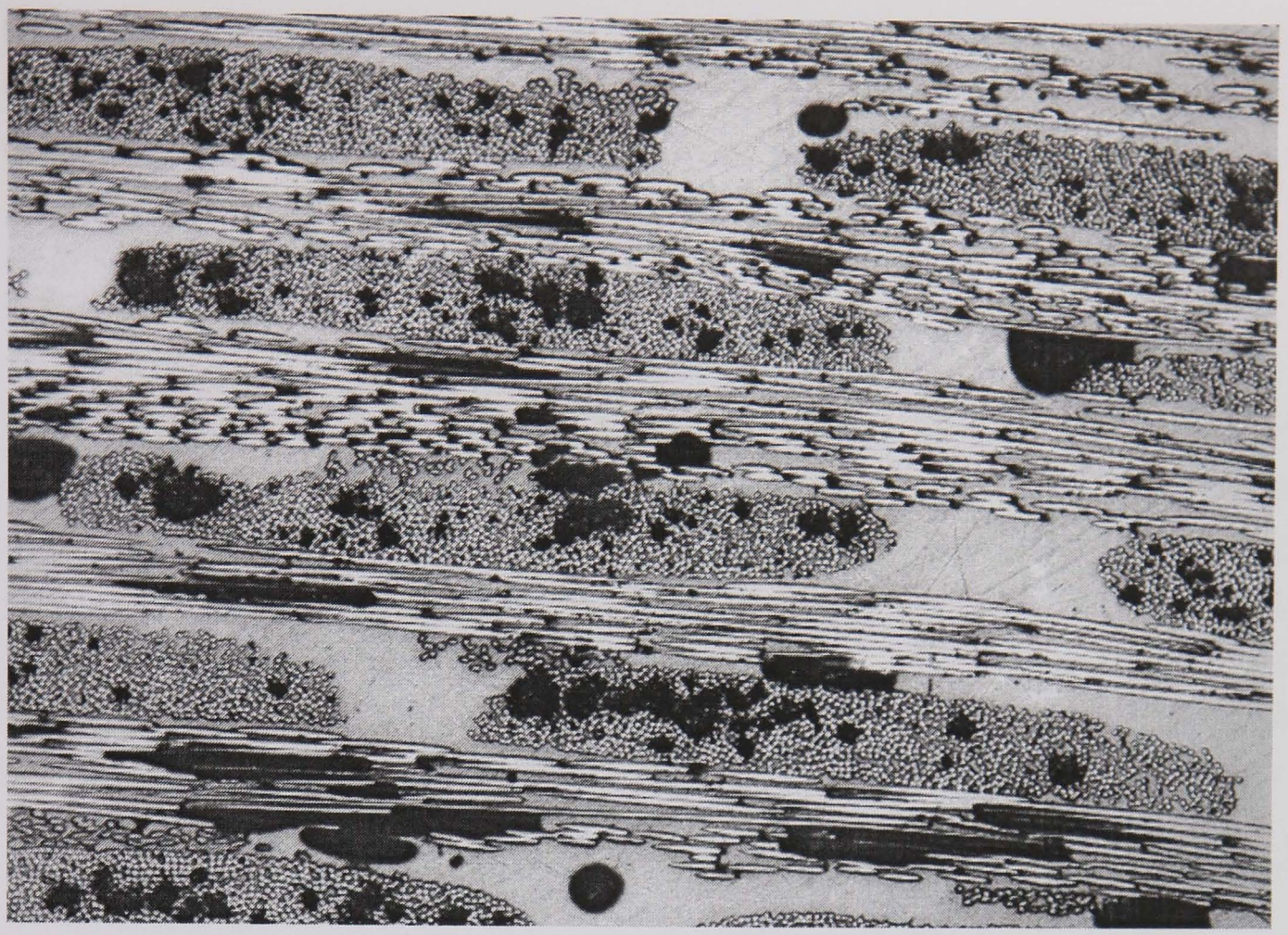

Figure 2:9 Micrograph showing both inter-tow and intra-tow voids (see Chapter 6)

Less data is available for the effect of voids on fracture toughness properties. The effect of voids on interlaminar shear properties has been investigated [57, 58] particularly with carbon/epoxy laminates; ILSS has been shown to be strongly dependant on void level. Jordan suggests that an increase in voidage (up to 6%) increases Mode-I and II fracture toughness, the latter by 55%. This is an expected result as the micro-mechanisms that lead to loss of strength and transverse modulus for carbon/epoxy systems frequently lead to an increase in toughness. Two explanations are offered, the first being that the presence of voids decreases the modulus of the resin and therefore increases its inherent toughness. The second is that voids change the stress state at the crack tip having the effect of blunting the crack tip [59].

Work continues into the prediction of mechanical properties of composites with many failure models having been developed. Some work into prediction of void effects has been based on early fracture mechanics approaches [60, 61]. Recently this approach has been developed for laminates [62], it has limited application as the size of the notches considered are far greater than the voids typically found in composites. Flow based models are available to simulate void

formation during liquid moulding e.g. Chang and Hourng [63]. Voids are one of the most common manufacturing defects and can be caused by a variety of factors such as non-uniform velocity fields during moulding [53], injection pressure and vacuum assistance [54, 55].

2.4 Matrix Properties

For a composite to work efficiently the stresses must be transferred into and between fibres. For this reason any resin system selected for use in composites must have good mechanical properties, with good toughness properties as primary aims and also good environmental resistance and adhesive properties. Cost is also an important factor in choosing a resin for industrial composites. Where high temperature operation is required it is crucial to select a resin with a high T_g.

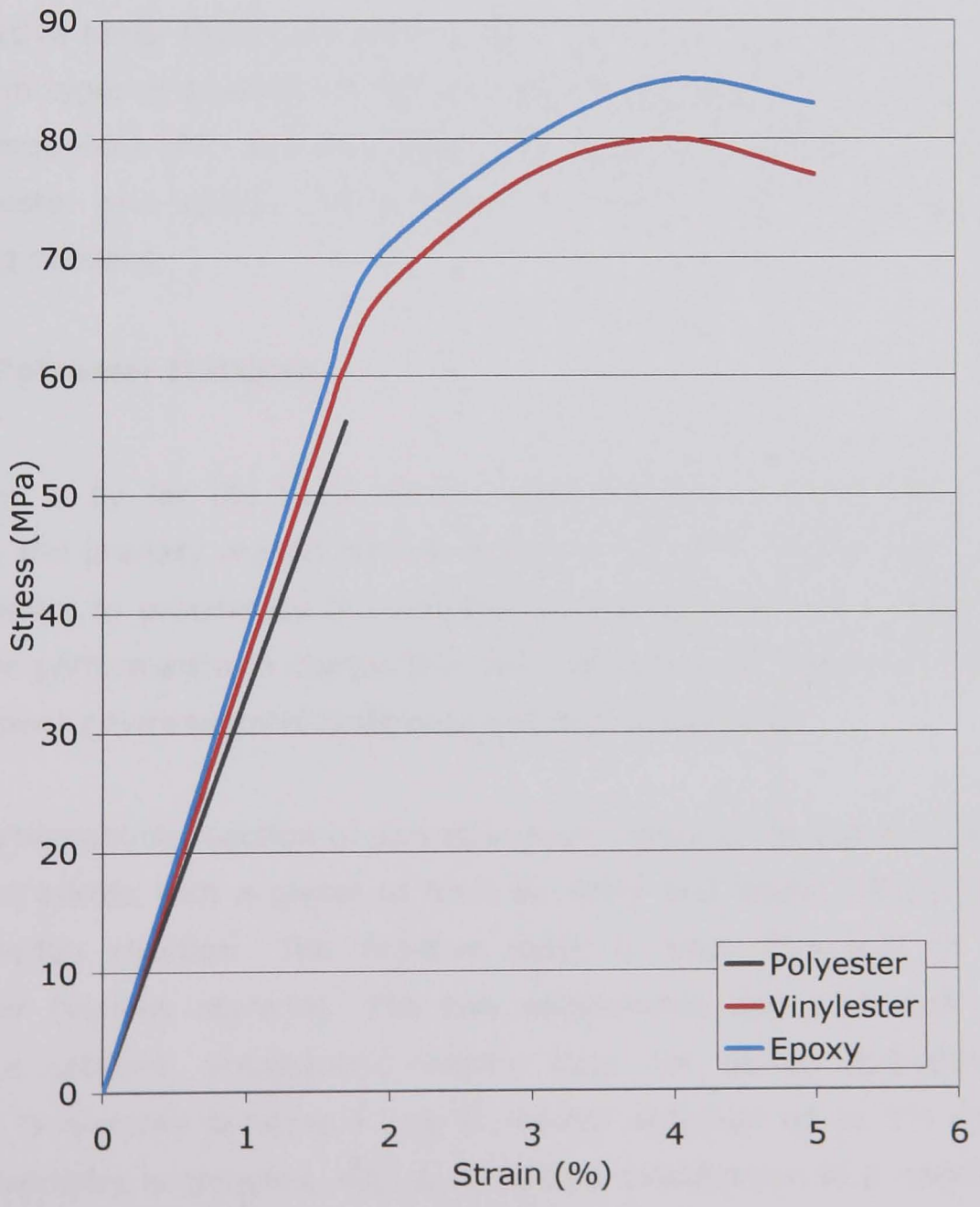

Figure 2:10 Generic stress-strain curves for thermoset resins (from various manufacturers' data)

Typical stress-strain curves are shown in Figure 2:10. Even in a simple tensile loadcase the resin must be able to deform as much as the fibre, this means that for fibres such as E-glass, high strain to failure resin is required.

	Polyester	Vinylester	Epoxy
Tensile strength (MPa)	55	80	85
Tensile modulus (MPa)	3300	3600	3800
Tensile elongation (%)	2	5	5
Volume shrinkage (%)	9	7	1.7
Relative cost	1	2	5

Table 2:4 Typical Matrix properties

The relative costs shown are approximate as epoxy costs are continuing to fall. Two main types of polymer matrix are used in composites – thermoplastics such as polypropylene (PP) and Poly Ether Ether Ketone (PEEK) and thermosets such as polyester and epoxy. The differences between these are discussed in the following sections.

2.4.1 Polyester Matrices

Polyester is by far the most widely used matrix for composites in terms of volume, the primary reason for this being its low cost, but also because it is an easy system to process by the addition of a curing agent or catalyst. Polyester has poor performance in comparison with other matrix types with low strain to failure, poor environmental resistance and high shrinkage.

The polymerisation reaction of polyester resin involves the reaction of an organic acid's anhydride with a glycol to form an ester and water. This is known as a condensation reaction. The reactive ester is then dissolved in a reactive monomer (usually styrene). The two components can cross-link using heat and/or a catalyst. Subsequent heating does not permit reshaping. Catalyst addition is typically between 1 and 3 percent although up to 5% can be used. Resin chemistry is complex, with a significant modification of properties possible by a change of glycol for instance. The rigidity is modified by the glycol and to an extent the trade-off between high strength and high stiffness can be seen in manufacturers resin selections; some being optimised for high strength and

some for high stiffness. Viscosity can also vary between 170 and 700+ mPa.s (Cone & Plate) [64]. RTM requires low viscosity resin for full wet-out and fast injection.

Choice of curing system is one of the most complex aspects for the manufacturer of composite parts. Many catalysts are suitable for a given resin, the choice depending on the processing temperature and other factors. The catalyst initiates the polymerisation by breaking down under the application of heat to form free radicals which initiate the reaction. The purpose of the accelerator is to reduce the activation energy of the catalyst allowing rapid breakdown at room temperatures. Thus high temperature moulding using catalysts such as TBPB (tert-Butylperoxy-benzoate) and TBPEH (tert-Butylperoxy-2-ethylhexanoate) do not require the addition of an accelerator.

Polyester resins as used in composites are unsaturated as opposed to saturated types which cannot be cured in the way described above.

Shrinkage is one of the primary concerns with polyester resin, a typical value being 8%. This is somewhat higher than both vinylesters (~6%) and epoxies (~1%) [65]. Problems related to the tendency of polymers to expand or contract are not confined to composites and are also an issue with processes such as injection moulding. In composites the issues are two fold; cosmetic (surface defects and flaws) and structural (induced stresses). Of these the former is typically of most concern.

Some shrinkage can be offset by the addition of a low profile additive [66-68], this can decrease shrinkage by 2-3% although to a certain extent LPA's are application specific and must be selected on the basis of molecular weight and glass transition temperature. Shrinkage causes debonding between fibres and resin and can result in lower mechanical properties as a result [65]. A common LPA is polyvinyl acetate or PVAc, this will typically be dissolved in styrene at around 30% polymer level.

A significant quantity of data exists on the effect of different LPA's on the rheology (deformation and flow), kinetics (chemistry of reactions), morphology (structure) and dilatometry (thermal expansion). A comprehensive explanation of low profile action can be found in Li and Lee [68].

Styrene is the most common comonomer for UP resins and is commonly added to reduce resin viscosity, however Sanchez *et al.* have shown that the properties of the resin are strongly influenced by the styrene concentration both in terms of thermal stability and mechanical properties [69]. The glass transition temperature of a low styrene content resin is increased from 22°C as supplied to 100°C with 58wt% styrene although mechanical properties peak at 24wt% styrene.

The effect of thermoplastic additives on mechanical properties has been studied in depth by Huang and Horng [70]. Experiments showed that in general, mechanical properties and glass transition temperature decreased for increasing LPA content.

Residual stress arises in composite laminates during elevated temperature postcures after room temperature polymerisation because through-thickness shrinkage levels tend to be higher than in-plane shrinkage [71]. This can reduce theoretical strengths significantly and must be considered at the design stage. Cowley and Beaumont have determined that under some circumstances the residual tensile stress can approach the transverse ply tensile strength [72]. Models exist to predict the volumetric changes of UP resins during cure, predictions having good agreement with experimental results [73].

2.4.2 Epoxy Matrices

Outside limited aerospace applications epoxy is the highest performance resin available for medium to high production volumes. Epoxies generally outperform polyester and vinylester resins in terms of mechanical properties and resistance to environmental attack. Epoxies also posses significantly better adhesive properties than vinylesters.

At a molecular level the basic structure of epoxy differs fundamentally from polyester. Epoxy does not rely on a catalytic cure but instead uses a hardener. The hardener is often an amine and cures the resin by an addition reaction as opposed to a condensation reaction. It is vital that the amine and epoxy molecules are present in the correct proportions as unreacted resin or hardener significantly reduces the mechanical properties.

A significant number of the reviewed papers concern epoxy parts, particularly those with an aerospace background. To date the cost of epoxy is usually prohibitive for volume production in automotive applications.

2.4.3 Vinylester Matrices

Little data exists on tube crush using vinylesters – typically work has focussed on either polyester or epoxy, however there is evidence to suggest that vinylester can perform almost as well as epoxy with a price, at the time of writing, much closer to that of polyester (see Section 3.1.1 and 4.2.1 for test data).

Vinylester matrices are broadly similar to polyester, at a molecular level the difference is in the location of the reactive sites which are only at the ends of the polymer chain. This imparts higher toughness to the matrix and makes it less prone to damage by hydrolysis. Vinylester prices are typically twice that of RTM polyesters.

Whilst there are similarities between UP and VE matrices there are important differences in the strain behaviour of the matrices. Sjögren and Berglund have investigated the transverse cracking behaviour of a variety of UP and VE matrices and observe different crack initiation modes, the fracture toughness of the matrix correlates well with the observed results but there are differences which are more difficult to explain but are attributed to pre-existing damage in the UP matrix [40].

2.4.4 Thermoplastic Matrices

The majority of work into thermoplastic matrices has been done by Ramakrishna and Hamada [4, 24, 74-78]. Thermoplastic matrices generally exhibit much higher strain to failure than thermosets and by necessity are processed through different routes. Thermoplastics vary in cost significantly with a glass/polypropylene commingled fabric being a realistic competitor to glass/polyester, however at the other end of the scale are carbon PEEK materials such as Cytec Fiberite's APC-2 with a significantly increased cost (Figure 2:11)

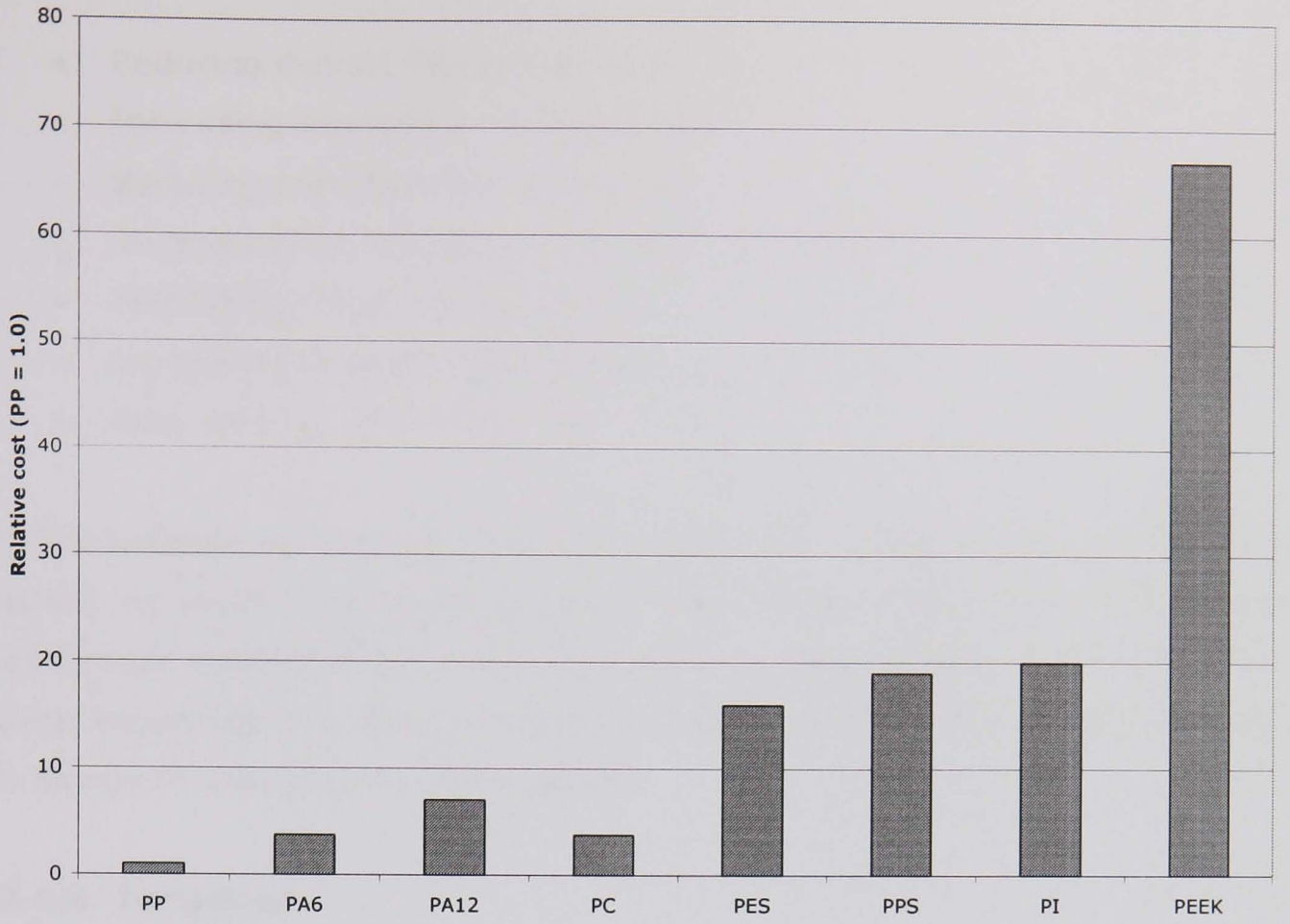

Figure 2:11 Relative costs of unreinforced thermoplastics (see [79])

Ramakrishna *et al.* [4] have compared carbon composite tubes with four different thermoplastic matrices – polyetheretherketone (PEEK), Polyetherimide (PEI), polyimide (PI) and polyacrylsulfone (PAS). The PEEK matrix displayed the highest SEA at 226kJ/kg whilst the PAS matrix displayed the lowest at 128kJ/kg. These results are significantly higher than typical glass/polyester crush results at 60kJ/kg. The high SEA achieved with carbon/PEEK is explained as follows: All tubes crushed with a splaying mode and displayed the typical features of this crush mode, however the centre-wall/longitudinal crack was significantly shorter with the PEEK matrix. Thus higher compressive forces were required to force the fronds through a tighter radius resulting in more fronds, more fragmentation and therefore higher energy absorption. The differences in matrix performance may be explained by the fact that PEEK is a semi crystalline material and the other polymers are amorphous. Ramakrishna *et al.* conclude that high mode-I fracture toughness is a very important factor in tube crush.

2.4.5 Additives

A variety of filler materials and additives have been used extensively with polyester resins. Possible reasons for their inclusion can include;

- Reducing density (Glass microspheres)
- Increasing thixotropy (Colloidal silica)
- Reducing cost (Calcium carbonate)
- Increasing fire retardance (Aluminium trihydrate)
- Facilitating mould release (Wax)
- Increasing strength (Short fibres)
- Easy sanding / finishing (Talc)

Fillers typically increase the viscosity of the resin, which can be countered to an extent by using a very low viscosity resin. Fillers reduce the temperature at which cure starts and also reduce the peak exotherm temperature – especially in thick mouldings. The effect of fillers on crush properties has not been studied but is mainly of relevance to SMC and DMC.

2.4.6 Toughness

The effect of resin toughness is of significant importance to the crush properties of composites. Tougher resins typically demonstrate higher strain to failure which can result in greater load carrying capacity by the fibres. Some of the energy absorption in a tube crush comes from the composite being forced around a tight radius, it can therefore be seen that enhanced fracture resistance may enable greater loads to be carried before separation of fibre and matrix and subsequent under-utilisation of the fibre properties.

A typical example of a toughened resin will contain rubber particles and can give an increase in fracture toughness of around 85% [80]. In the above example Stevanovic *et al.* determined that optimal particle concentration levels were 7% for mode-I and 3.5% for Mode-II.

Most literature on toughening of resins concerns epoxies where the use of liquid rubber at 10phr can increase the fracture energy of the resin by a factor of eight [81]. Newer approaches utilise core/shell particles which possess greater compatibility with the resin giving superior results to conventional liquid carboxy-terminated butadiene acrylonitrile (CTBN) [82].

Pham and Burchill [83] have shown that the fracture toughness of Dow Derakane vinylester can be improved by the addition of 5% rubber. The rubber

used was a modified low molecular weight polybutadiene, improvements in K_{IC} of two to three times and G_{IC} of ten times were experimentally determined. The blends were however found to have lower modulus and slightly changed thermal properties.

Many authors [84-86] have produced experimental data on the concept of using microvoids to toughen polymers, as rubber modification has proved to be a successful method of toughening polymers. Rubber modification works by inducing a global deformation rather than a local phenomenon. The same effect can be caused by voids instead of a rubber phase as the rubber is thought to behave as holes. Bagheri and Pearson [84] have used hollow latex microspheres to generate holes in the brittle epoxy matrix. The conclusions of this study were that the microspheres toughen the matrix in the same way as rubber particles and indeed that no superiority was displayed by rubber particles.

Jordan reports that the toughness of carbon/epoxy prepregs can be altered by changing the stacking sequence [59]. The results show that the more changes of fibre orientation in a laminate the higher the fracture toughness will be, for instance a [0(24)] laminate has a G_{IC} of 520J/m^2 whereas the same number of plies in a [45/-45(2)/45/-45/45(2)/-45/45/-45(2)/45/-45/45(2)/-45] configuration has a G_{IC} of 1333J/m^2.

No study on the effect of resin toughness on crush performance exists in the literature although some work exists on the effect of toughened interlayers (section 2.3.2). However the high performance of thermoplastic polymers can be largely attributed to increased toughness. It can therefore be surmised that increased toughness would prove beneficial for thermosetting polymers, provided that other mechanical properties (specifically modulus) are not compromised.

2.4.7 Binder

Binder is an essential part of the RTM preforming process. In large parts binder levels can reach 10% by weight of fabric to enable mechanical handling between performer and mould tool. Binder enables preform compaction and this is an important factor in determining final volume fraction, this also effects preform permeability and hence resin flow.

Tanoglu and Seyhan have investigated the effect of thermoplastic binder on compressive properties of E-glass/polyester composites with a thermoplastic polyester binder [87]. The authors tested binder levels of 0-9% by weight and found that the highest preform compaction was obtained with 3%, this leads to the highest V_f in the finished part. Further increases in binder level decreased the level of compaction. Strength and modulus values increased up to 3%wt and were also seen to decrease at higher binder levels. SEM testing showed that the failure modes of the composites were significantly altered by the presence of binder within the part and also that there was partial dissolution of the binder in the resin. A second paper by the same authors using identical materials showed that the peel strength of the preform increased with binder level up to the tested maximum of 9%wt. The flexural strength of the composite was shown to decrease by 15% and the mode-I fracture toughness by 40% at 3%wt binder [88].

2.4.8 Degree of Cure

Degree of cure has a very significant effect on polymer matrix properties. No research has been published on the effect of resin degree of cure on crush performance. Full analyses of polymer cure are available [89] but in industrial applications the onus is generally on the resin / curing system supplier to supply a product which develops a full cure level under known conditions. When rapid cycle times are used the presence of fillers and other additives may necessitate a more thorough examination of cure kinetics.

Tucker *et al.* [90] have found evidence to suggest that the effect of extended post cures can reduce the mode-I interlaminar fracture toughness of a resin. Glass/vinylester was used with post cures of 1, 4 and 24 hours at a constant temperature and as an additional variable a combination of cure temperature and post cure - 90°C/4h, 80°C/8h and 70°C/16h. The tests were performed for neat vinylester and for the composite. The results showed that post cure increased the toughness with a consistent trend between neat resin and composite, apart from the case of 24h post cure duration. The extended post cure duration was said to have weakened the fibre/matrix bond and therefore decreased the toughness.

2.5 Fibre Properties

Composites rely on high fibre mechanical properties to give high strength and stiffness. Cost is however a very important factor. E-glass is the most popular fibre by virtue of its good mechanical properties and low cost.

2.5.1 Fibre type

Fibre properties have a significant effect on in-plane properties, with carbon and aramid fibres offering significantly higher specific mechanical properties. However cost is a major factor for high volume processes. Much of the reviewed work is concerned with aerospace applications. Thornton and Edwards [91] compared glass, carbon and aramid reinforced composites and found that aramid fibres resulted in an unstable buckling failure with low energy absorption. Changes in the lay-up that increased the modulus of the tube typically increased the SEA. This work showed that hybrids with aramid also resulted in unstable collapse. Energy absorption levels for glass and carbon tubes ranged from 25 to 90kJ/kg dependant on material and lay-up, with carbon tubes having higher SEA values overall. Ramakrishna [9] has examined Dyneema SK60 UHMWHDPE fibres with carbon as a hybrid and found that the SEA could be accurately and predictably controlled by changing the ratio of the two fibres.

Farley has examined hybrid materials as a way of retaining post-crush integrity whilst having high energy absorption [92]. Composites were manufactured with both UD tape and woven hybrids of aramid and carbon. Aramid samples were the only ones to have sufficient post crush integrity although energy absorption was significantly lower than carbon. Crush performance of the hybrids was found to be representative of the materials used. Later work by Farley [52] examined the effect of fibre and matrix maximum strain on energy absorption of carbon prepreg tubes. The higher strain to failure systems showed higher SEA values. It was also suggested that to obtain high energy absorption the matrix material should have higher maximum strain than the fibre.

In general carbon fibres tend to offer higher SEA both through greater loads and lower density, in practice however the additional cost may not warrant the use of carbon; particularly as production volumes increase.

2.5.2 Fibre Architecture

All mechanical properties of composites are very sensitive to the architecture of the fibres. Typical fibre architectures include unidirectional, braided, woven and knitted. At this time no complete study exists encompassing all types, although there is a considerable amount of data available. The following section summarises some of the work undertaken but in most instances it is very difficult to view the effect of fibre orientation and architecture without also taking into account the effects of other variables; fibre volume fraction being a typical example.

Different fibres are available in a variety of architectures; woven and non-crimp, random and aligned. It is also theoretically possible to use different types of architecture in the same part.

2.5.2.1 Chopped Strand Mat

Chopped Strand Mat (CSM) is a basic form of glass mat typically consisting of 50mm glass fibres in a random orientation. A highly soluble thermoplastic powder binder is used to constrain the fibres and ease handling. These materials, whilst commonly used in hand lay-up applications have been largely superseded by the CoFRM materials described below. At similar volume fractions CSM will perform in a similar manner to CoFRM, some authors referring to CoFRM as CSM e.g. [93].

2.5.2.2 Continuous Filament Random Mat

Continuous Filament Random Mat (CoFRM or CFRM) is a commonly used material for RTM processes, it is similar in structure to CSM but the filaments are continuous and randomly laid across the surface. The advantages of CoFRM are improved mechanical properties both in terms of absolute properties repeatability and greater resistance to fibre washing. The material is somewhat easier to handle than CSM and is typically combined with a binder (at around 6% by weight) to facilitate preforming. Its low cost and ease of use make this material popular for automotive structures and have lead to interest in its crashworthiness properties. Although the material is ostensibly random, results presented in this work and by McGeehin at Nottingham [94] suggest that modulus in the warp direction is around 15% higher.

2.5.2.3 Woven textiles

Woven textiles and unidirectional materials are uncommon in automotive structures but are used extensively in aerospace structures. Aligned (non-random) materials allow significantly higher volume fractions to be obtained, typically a limit for RTM with random mat is 25% whereas aligned fabrics can reach 40% with relative ease. Higher volume fraction and more efficient geometry mean that in-plane tensile and compressive properties are much higher. This is relevant to areas of higher stress in vehicles. Little work has been done on the relative crush properties of aligned vs. random fabrics.

2.5.2.4 3D fabrics

3D reinforcements were first used in the 1960's for rocket motor nozzles where the negative coefficient of expansion of carbon fibres gave rise to problems. Nearly isotropic 3D fabric preforms were developed with 25% higher ILSS than non-interlocked fabrics, the in-plane properties in this instance were reduced by 25% [95] due to the redistribution of reinforcement. For crashworthiness the improvement in through-thickness and interlaminar properties is beneficial. 3D fabrics are more costly to make and composites constructed from them often suffer from low volume fraction and lower in-plane properties. 3D fabrics can include those made by knitting. braiding, weaving and tailored fibre placement [96]. Many configurations are possible [97] but the only fabric which has undergone systematic investigation is braid. Biaxial (2D) and triaxial (true 3D) braid has been examined extensively by Karbhari [98-100] and Chiu [101] with success. The main benefit cited is the higher interlaminar properties resulting from the mechanical interlocking of the tows, damage tolerance can also benefit greatly.

2.5.3 Sizing

The high performance of composites depends on being able to effectively transmit forces between fibres via the matrix. For this reason the interfacial bond between fibres and matrix is of great importance. Most commercial glass fibres have a size applied at the time of manufacture to protect the fibre from damage due to handling and moisture absorption. Size is typically an emulsion of coupling agents, film formers, lubricants and antistatic agents. Sjögren *et al.* [102] compared a weak (PVA) size with a methacrylsilane based size in a

glass/vinylester composite. The weak size showed substantial debonding and lower performance in transverse cracking with the first transverse crack forming at 0.2% transverse strain. The methacrylsilane coated fibres required 0.6% strain. The high toughness was attributed not only to good fibre/matrix adhesion but also to high ductility of the matrix in the immediate vicinity of the fibres. Commercially sized fibres were also tested and found to be almost as poor as the PVA sized fibres.

Hamada *et al.* [103] fabricated prepreg tubes using two different coupling agents; aminosilane and acrylsilane. The aminosilane-treated fibres bond well to the epoxy matrix and gave an SEA of 66.6kJ/kg compared to 53kJ/kg with acrylsilane. The two types gave different failure modes – aminosilane by splaying and acrylsilane by fragmentation. Improved bonding lead to failure in the matrix and hence a smoother fracture surface, meaning that lower frictional forces were developed and a splaying mode occurred. The fragmentation mode of the acrylsilane tubes is explained by shear cracking due to a reduction in compressive strength.

Tao *et al.* [104] examined the crush performance of vinylester composite rods with three different surface treatments – E-glass fibres as received, E-glass fibres with no surface treatment and E-glass fibres treated with a release agent. There was no difference in energy absorption between the sized and untreated rods but the release coated fibres exhibited significantly reduced SEA. This reduction comes not only from reduced energy absorption through fibre/matrix debonding but also through less matrix deformation.

2.5.4 Fibre Diameter

The primary advantage of glass in fibrous form is its lack of flaws and therefore a full realisation of properties over the bulk form. It may therefore be tempting to think that still smaller fibres are capable of sustaining higher stresses, this topic is generally ignored as designers are limited by commercial constraints. Glass is typically produced at between 8 and 15 μm. Tao *et al.* [104] used three fibre diameters to make composite rods. Due to the manufacturing process used the largest (23μm) fibre diameter typically gave the highest volume fraction. The specific energy absorption was also highest with the large fibre diameter. As stated above the effect of fibre diameter is not a realistic issue as factors such as cost are far more important than any potential gains in energy absorption.

2.6 Testing variables

As mentioned above it is very important to consider the effect of test conditions when comparing results. The following issues can have a massive effect on the properties of the composite. Most laboratory testing is performed at quasi-static speeds onto platens with closely controlled surface finishes and known temperatures. Composites are very sensitive to rate and temperature and the excellent performance of composite crush members is very sensitive to loading axis and frictional effects. The following sections describe the effect of different test variables on SEA.

2.6.1 Effect of test speed

The effect of test speed is an important consideration as the properties of both fibre and matrix (modulus and strain to failure) can be strain-rate sensitive. If design data is generated at quasi static speeds the true performance of the structure at impact speeds could be very different. Additionally the platen coefficient of friction can be a function of test speed [2]. This has lead Mamalis *et al.* [105] to investigate the effect of rate as the friction in the crush zone is so important in determining eventual SEA (2.1.3). The authors show good agreement between predicted and observed results for a square frusta theoretical analysis. Under dynamic conditions SEA values were between 5-15% lower than the static values, the reduction was thought to be due to a reduced coefficient of friction in the crush zone.

Karbhari and Haller tested braided E-glass, carbon and aramid tubes at high rate and observed an increase in SEA for glass, glass/aramid hybrids and triaxial glass/aramid hybrids with carbon axial tows for a splaying crush mode [106] . Some architectures showed no change with a 10x change in rate and others failing by an accordion buckling mode showed a decrease.

The effect of test speed is important yet difficult to predict due to the dependence on both materials and architecture. Results are also presented at very different strain rates making comparison problematical.

2.6.2 Temperature effects

The effect of temperature on crush characteristics is highly dependent on the matrix material. As composite crush members must be designed for high performance at elevated temperature this is an important factor. The matrix has a glass transition temperature above which the mechanical properties degrade significantly. This temperature is typically between 50°C and 110°C for polyesters but can be as high as 140°C for highly reactive systems. Epoxy prepreg materials are commonly available at 180°C. Underbonnet temperatures can be well over 100°C depending on vehicle type and operating conditions. This is an important design consideration.

Thornton has shown results for glass/epoxy and carbon/epoxy prepreg tubes where the SEA was seen to decrease rapidly with increasing temperature [10]. For the glass tubes the decrease started at -100°C but the carbon tubes retained properties to +150°C. At 0°C the two materials had equal SEA but by room temperature the glass system had already decreased significantly below carbon. An effect was also observed on the serrations of the crush curve where the curves became smoother with increasing temperature.

Extensive testing of temperature and rate effects is presented by Fontana [107]. Results for quasi-static testing of Tufnol tubes showed a slight decrease in properties from -90°C to room temperature followed by a more rapid decrease after 40°C.

2.6.3 Crush platen geometry

The most interesting alternative platen geometry is using a plug instead of a flat platen. High SEA's can be achieved but the sensitivity of the method to plug radius makes it less attractive. The bulk of research into plug crush has been undertaken by Hull [14]. Tubes crushed using a plug or internal mandrel display increasing energy absorption with decreasing plug radius up to a limiting radius whereupon debris forms a compacted autoradius upon which further crushing takes place.

2.6.4 Crush platen condition

Given that a large proportion of the energy absorbed in crush is through frictional effects at the frond / platen interface it is surmised that the condition of the platen has a major effect on SEA. The coefficient of friction has been measured by Fairfull and Hull [6]. Platens with a ground finish gave a higher crush load than a polished surface, greater levels of roughness decreased crush load as debris started to fill the grooves. A difference in crush load of 7% was observed between polished and ground. Fairfull and Hull concluded that 56% of the total energy absorbed was due to friction at the frond / platen interface.

The hardness of the platen can also have a significant effect on the crush mode. Thornton [11] found that a soft platen can reduce the effectiveness of the trigger which can lead to global buckling rather than progressive crushing.

2.6.5 Loading axis

Off-axis loading is of great concern to designers of crush elements, massive axial crush load with a low tolerance for loading angle is of limited use in real applications. Fleming and Vizzini have evaluated the effect of loading axis on truncated cones for aircraft applications and conclude that side load is an important factor in design. Small eccentricities in load are seen to increase energy absorption but further increases in eccentricity result in a significant reduction in absorption. Furthermore a tendency towards toppling is seen which results in even poorer results [108]. Later work concentrated on composite plates for helicopters [109, 110].

Han *et al.* [111] examined triaxially braided carbon tubes at 0, 5 and 10 degrees off-axis. Failure modes varied with angle and slight increases in SEA were seen with increasing angle; from 33kJ/kg at 0° to 37kJ/kg at 5° and 36kJ/kg at 10°. The authors noted that it took longer for a stable crush zone to form off-axis and attributed the slight increases in SEA to this factor and a change in crush mode.

2.7 Crush Characterisation

In order to more fully understand the crushing of composites it is important to recognise the relative importance of various material properties. A single correlation between SEA and in-plane properties will yield a definite correlation

but will not fully explain the crush properties. Complex interactions between simple mechanical properties are present and are difficult to separate. For instance it is easy to show a correlation between mode-I fracture toughness and SEA, however when mode-I fracture toughness is totally removed by inserting a layer of release film the SEA changes unpredictably. This is caused by a change in crush mode.

Many attempts have been made in the literature to quantify the effect of a single material property. Farley and Jones, for instance, have presented simple procedures for calculating the effect of variables such as ply angle using both analytical methods similar in principle to classical beam on elastic foundation theory and finite element methods [3, 112].

Much of the analytical modelling undertaken has been done by Mamalis and co-workers, including [17, 105, 113-115]. Whilst good agreement has been observed with experimental results presented, these are typically valid only for certain materials within fairly tight constraints and do not represent a unified method.

2.8 Conclusions

The reviewed work covers a wide range of factors which all affect crushing to a varying degree. Some of the factors are determined by the manufacturer of the parts (e.g. constituent materials) whereas many are determined by secondary factors (e.g. crush mode). As many of the properties as possible are fixed in this work to give consistency. All the testing factors considered in Section 2.6 are held constant. Sections 2.4 and 2.5 have demonstrated the variety of energy absorption levels available by changing material properties. The reasons for this are one of the main considerations in this work. This also applies to the interlaminar effects considered in section 2.3. Where fibre architectures are changed there are unavoidable changes in volume fraction for realistic materials e.g. changing from a random mat to a unidirectional or non-crimp fabric. This limits comparison in some areas. All geometric aspects considered in Section 2.2 are held constant. The effects of geometry are large and these are seen as outside the scope of this work. The effect of trigger geometry is not considered here but could be optimised without changing previously determined trends. The splaying crush mode is seen in all the testing in this work, although fragmentation does occur within the splaying mode.

Chapter 2 References

1. Alexander, J., *An approximate analysis of the collapse of thin cylindrical shells under axial loading.* Quarterly Journal of Mechanics and Applied Mathematics, 1960. **13**: p. 10-15.

2. Farley, G. and R. Jones, *Crush Characteristics of Continuous Fibre-Reinforced Composite Tubes.* Journal of Composite Materials, 1992. **26**(1): p. 37-50.

3. Farley, G. and R. Jones, *Analogy for the Effect of Material and Geometrical Variables on Energy-Absorption Capability of Composite Tubes.* Journal of Composite Materials, 1992. **26**(1): p. 78-89.

4. Ramakrishna, S., H. Hamada, Z. Maekawa, and H. Sato, *Energy Absorption Behaviour of Carbon-Fibre-Reinforced Thermoplastic Composite Tubes.* Journal of Thermoplastic Composite Materials, 1995. **8**: p. 323-344.

5. Fairfull, A., *Scaling effects in the energy absorption of axially crushed composite tubes*. 1986, University of Liverpool.

6. Fairfull, A.H. and D. Hull, *Energy Absorption of Polymer Matrix Composite Structures : Frictional Effects.* Symposium on Structural Failure, 1988: p. Chap 8 pp 255-279.

7. Fairfull, A. and D. Hull, *Effects of Specimen Dimensions on the Specific Energy Absorption of Fibre Composite Tubes.* International Conference of Composite Materials VI, 1987: p. 3.36-3.45.

8. Farley, G., R. Wolterman, and J. Kennedy, *The Effects of Crushing Surface Roughness on the Crushing Characteristics of Composite Tubes.* Journal of the American Helicopter Society, 1992. **37**(3): p. 53-60.

9. Ramakrishna, S., *Microstructural Design of Composite Materials for Crashworthy Structural Applications.* Materials and Design, 1997. **18**: p. 167-173.

10. Thornton, P., *Energy Absorption in Composite Structures.* Journal of Composite Materials, 1979. **13**: p. 247-262.

11. Thornton, P., *The Crush Behaviour of Glass Fiber Reinforced Plastic Sections.* Composites Science and Technology, 1986. **27**: p. 199-223.

12. Sigalas, I., M. Kumosa, and D. Hull, *Trigger Mechanisms in Energy-Absorbing Glass Cloth / Epoxy Tubes.* Composites Science and Technology, 1991. **40**: p. 265-287.

13. Jimenez, M., A. Miravete, E. Larrode, and D. Revuelta, *Effect of trigger geometry on energy absorption on composite profiles.* Composite structures, 2000. **48**: p. 107-111.

14. Hull, D. and J. Coppola, *Performance of Glass Fibre-Vinyl Ester Composite Tubes Crushed Using Internal Mandrels.* International Conference on Composite Structures, 1991: p. 129-143.

15. Thuis, H. and V. Metz, *The Influence of Trigger Configurations and Laminate Lay-up on the Failure Mode of Composite Crush Cylinders.* Composite Structures, 1993. **28**: p. 37-43 (131-137).

16. Mamalis, A., D. Manolakos, G. Viegelahn, N. Vaxevanidis, and W. Johnson, *On The Inextensional Axial Collapse of Thin PVC Conical Shells.* International Journal of Mechanical Sciences, 1986. **28**(5): p. 323-335.

17. Mamalis, A., D. Manolakos, G. Demosthenous, and M. Ioannidis, *Analytical Modelling of the static and Dynamic Axial Collapse of Thin-Walled Fiberglass Composite Conical Shells.* International Journal of Impact Engineering, 1997. **19**(5): p. 477-492.

18. Mamalis, A., D. Manolakos, G. Demosthenous, and M. Ioannidis, *Experimental Determination of Splitting in Axially Collapsed Thick-Walled Fibre-Reinforced Composite Frusta.* Thin-Walled Structures, 1997. **28**(3): p. 279-296.

19. Mamalis, A., D. Manolakos, and G. Viegelahn, *Crashworthy Characteristics of Thin Fibre-Reinforced composite Frustra under Axial Collapse.* International Journal of Vehicle Design, 1989. **10**(2): p. 165-174.

20. Mamalis, A., D. Manolakos, G. Viegelahn, G. Demosthenous, and S. Yap, *Microscopic Failure of Thin-Walled Fibre-Reinforced Composite Frustra under Static Axial Collapse.* International Journal of Vehicle Design, 1991. **12**(5): p. 557-578.

21. Mamalis, A., D. Manolakos, G. Viegelahn, S. Yap, and G. Demosthenous, *On the Axial Crumpling of Fibre-Reinforced Composite Thin-Walled Conical Shells.* International Journal of Vehicle Design, 1991. **12**(4): p. 450-467.

22. Warrior, N. and M. Ribeaux, *Effect of Damage on the Energy Absorption of Prismatic Thin-Walled Polymer Composite Structures.* Key Engineering Materials, 2003. **245-246**: p. 491-501.

23. Thornton, P., J. Harwood, and P. Beardmore, *Fibre-reinforced Plastic Composites for Energy Absorption Purposes.* Composites Science and Technology, 1985. **24**: p. 275-298.

24. Hamada, H. and S. Ramakrishna, *Scaling Effects in the Energy Absorption of Carbon-Fibre / PEEK Composite Tubes.* Composites Science and Technology, 1995. **55**: p. 211-221.

25. Hull, D., *A Unified Approach to Progressive Crushing of Fibre-Reinforced Composite Tubes.* Composites Science and Technology, 1991. **40**: p. 377-421.

26. Lavoie, J. and S. Kellas, *Dynamic Crush Tests of Energy-Absorbing Laminated Composite Plates.* Composites, 1996. **27A**: p. 467-475.

27. Lavoie, J. and J. Morton, *A Crush Test Fixture For Investigating Energy Absorption of Flat Composite Plates.* ?Experimental Techniques, 1994: p. 23-25.

28. Lavoie, J., J. Morton, and J. Jackson, *An Evaluation of the Energy Absorption of Laminated Composite Plates.* Proceedings of the IMECHE, 1995. **209**: p. 185-194.

29. Farley, G. *Energy Absorption of Composite Material and Structure*. in *Proceedings of the 43rd American Helicopter Society Annual Forum*.

30. Pafitis, D. and D. Hull, *Design of Fiber Composite Conical Components for Energy Absorbing Structures.* SAMPE Journal, 1991. **27**(3): p. 29-34.

31. Hanagud, S., J. Craig, Sriram, and W. Zhou, *Energy Absorption Behaviour of Graphite Epoxy Composite Sine Webs.* Journal of Composite Materials, 1989. **23**(5): p. 448-459.

32. Farley, G. and R. Jones, *Crushing Characteristics of Composite Tubes with "Near-Elliptical" Cross Sections.* Journal of Composite Materials, 1992. **26**(12): p. 1741-1751.

33. Voigt, W., *The rule of mixtures.* Wied. Ann., 1889. **38**: p. 373-587.

34. Snowdon, P. and D. Hull, *Energy Absorption of SMC Under Crash Conditions.* International Conference - Fibre Reinforced Composites '84, 1984. **5**: p. 1-10.

35. Yuan, Q., S. Kerth, J. Karger-Kocsis, and K. Friedrich, *Crash and energy absorption behaviour of interleaved carbon-fibre-reinforced epoxy tubes.* Journal of Materials Science Letters, 1997. **16**: p. 1793-1796.

36. Takeda, N., S. Kobayashi, S. Ogihara, and A. Kobayashi, *Effects of toughened interlaminar layers on fatigue damage progress in quasi-isotropic CFRP laminates.* International Journal of fatigue, 1999. **21**: p. 235-242.

37. Duarte, A., I. Herszberg, and R. Paton, *Impact resistance and tolerance of interleaved tape laminates.* Composite Structures, 1999. **47**: p. 753-758.

38. Hillermeier, R. and J. Seferis, *Interlayer toughening of resin transfer molding composites.* Composites Part A, 2000. **32A**: p. 721-729.

39. Ribeaux, M., *Energy Absorption capability of damage affected composite structures*. 2003, University of Nottingham.

40. Sjogren, B. and L. Berglund, *The effects of matrix and interface on damage in GRP cross-ply laminates.* Composites Science & Technology, 2000. **60**: p. 9-21.

41. Sala, G., *Impact behaviour of heat-resistant toughened composites.* Composites: Part B, 2000. **31**: p. 161-173.

42. Vickers, P., L. Boniface, A. Pricket, and J. Watts, *The effect of siloxane-type molecules on the interlaminar toughness of CFRP.* Composites Part A, 1999. **31A**: p. 559-569.

43. Mouritz, A., K. Leong, and I. Herszberg, *A review of the effect of stitching on the in-plane mechanical properties of fibre-reinforced polymer composites.* Composites: Part A, 1997. **28**: p. 979-991.

44. Mouritz, A., *Flexural properties of stitched GRP laminates.* Composites Part A, 1996. **27A**: p. 525-530.

45. Mouritz, A., *Review of applications for advanced three-dimensional fibre textile composites.* Composites Part A, 1999. **30A**: p. 1445-1461.

46. Mouritz, A. and B. Cox, *A Mechanistic approach to the properties of stitched laminates.* Composites Part A, 1999. **31A**: p. 1-27.

47. Mouritz, A., J. Gallagher, and A. Goodwin, *Flexural strength and interlaminar shear strength of stitched GRP laminates following repeated impacts.* Composites Science & Technology, 1997. **57**: p. 509-522.

48. Mouritz, A., C. Baini, and I. Herszberg, *Mode I interlaminar fracture properties of advanced textile fibreglass composites.* Composites Part A, 1998. **30A**: p. 859-870.

49. Daniel, L., P. Hogg, and P. Curtis, *The relative effects of through-thickness properties and fibre orientation on energy absorption by continuous fibre composites.* Composites part B, 1999. **30**: p. 257-266.

50. Larsson, F., *Damage tolerance of a stitched carbon/epoxy laminate.* Composites: Part A, 1997. **28**: p. 923-934.

51. Jain, L. and Y. Mai, *On the effect of stitching on Mode I delamination toughness of laminated composites.* Composites Science & Technology, 1994. **51**: p. 331-345.

52. Farley, G., *Effect of Fiber and Matrix Maximum Strain on the Energy Absorption of Composite Materials.* Journal of Composite Materials, 1986. **20**: p. 322-334.

53. Kang, M., W. Lee, and H. Hahn, *Formation of microvoids during resin-transfer molding process.* Composites Science and Technology, 2000. **60**: p. 2427-2434.

54. Young, W. and C. Tseng, J. Reinf. Plast. Compos., 1994. **13**: p. 467-.

55. Lundstrom, T., B. Gebart, and C. Lundemo, J. Reinf. Plast. Compos., 1993. **12**: p. 1339-.

56. Judd, N.C.W. and W.W. Wright, *Voids and their effects on the mechanical properties of composites - an appraisal.* SAMPE Journal, 1978. **14**: p. 10-14.

57. Bowles, K. and S. Frimpong, *Void Effects on the Interlaminar Shear Strength of Unidirectional Graphite-Fiber-Reinforced Composites.* J Comp. Mater., 1992. **26**(10): p. 1487-1509.

58. Costa, M., S. Almeida, and M. Rezende, *The influence of porosity on the interlaminar shear strength of carbon/epoxy and carbon/bismaleimide fabric laminates.* Composites Science & Technology, 2001. **61**: p. 2101-2108.

59. Jordan, W., *Changing the toughness of graphite fiber/resin based composites by changing their internal structure.* Composites Part B, 1999. **31**: p. 245-252.

60. Waddoups, M., J. Eisenmann, and B. Kaminski, *Microscopic Fracture Mechanics of Advanced Composite Materials.* J. Composite materials, 1971. **5**: p. 446-454.

61. Whitney, J.M. and R.J. Nuismer, *Stress fracture criteria for laminated composites containing stress concentrations.* J. Composite materials, 1974. **5**: p. 253-265.

62. Chen, P., Z. Shen, and J. Wang, *Prediction of the strength of notched fiber-dominated composite laminates.* Composites Science & Technology, 2001. **61**: p. 1311-1321.

63. Chang, C. and L. Hourng, *Study on Void Formation in Resin Transfer Moulding.* Polymer Engineering and science, 1998. **38**(5): p. 809-818.

64. Reichhold UK Ltd., *Norpol International Product range*.

65. Schubel, P., *Classification of automotive "Class A" panels via RTM*, in *School of Mechanical, Materials, Manufacturing and Management*. 2004, University of Nottingham: Nottingham.

66. Kinkelaar, M., S. Muzumdar, and J. Lee, *Dilatometric Study of Low Profile Unsaturated Polyester Resins.* Polymer Engineering and science, 1995. **35**(10): p. 823-836.

67. Huang, Y. and C. Liang, *Volume shrinkage characteristics in the cure of low-shrink unsaturated polyester resins.* Polymer, 1996. **37**(3): p. 401-412.

68. Li, W. and J. Lee, *Shinkage control of low-profile unsaturated polyester resins cured at low temperature.* Polymer, 1998. **39**(23): p. 5677-5687.

69. Sanchez, E., C. Zavaglia, and M. Felisberti, *Unsaturated polyester resins: Influence of the styrene concentration on the miscibility and mechanical properties.* Polymer, 2000. **41**: p. 765-769.

70. Huang, Y. and J. Horng, *Effects of thermoplastic additives on mechanical properties and glass transition temperatures for styrene-crosslinked low-shrink polyester matrices.* Polymer, 1998. **39**(16): p. 3683-3695.

71. Stone, M., I. Schwartz, and H. Chandler, *Residual stresses associated with post-cure shrinkage in GRP tubes.* Composites Science & Technology, 1997. **57**: p. 47-54.

72. Cowley, K. and P. Beaumont, *The measurement and prediction of residual stresses in carbon-fibre/polymer composites.* Composites Science & Technology, 1997. **57**: p. 1445-1455.

73. Hill, R., S. Muzumdar, and L. Lee, *Analysis of volumetric changes of unsaturated polyester resins during curing.* Polymer Engineering and science, 1995. **35**(10): p. 852-859.

74. Hamada, H., J. Coppola, D. Hull, Z. Maekawa, and H. Sato, *Comparison of Energy Absorption of Carbon / Epoxy and Carbon / PEEK Composite Tubes.* Composites, 1992. **23**(4): p. 245-252.

75. Hamada, H., S. Ramakrishna, and H. Sato, *Crushing Mechanism of Carbon Fibre / PEEK composite Tubes.* Composites, 1995. **26**(11): p. 749-755.

76. Hamada, H., S. Ramakrishna, and Z. Maekawa, *Effect of Cooling Rate on the Energy Absorption Capability of Carbon Fibre/PEEK Composite Tubes.* Polymers & Polymer Composites, 1995. **3**(2): p. 99-104.

77. Hamada, H., S. Ramakrishna, and H. Sato, *Effect of Fibre Orientation on the Energy absorption Capability of Carbon Fibre / PEEK Composite Tubes.* Journal of Composite Materials, 1996. **30**(8): p. 947-963.

78. Hamada, H., S. Ramakrishna, and H. Sato, *Effect of Testing Temperature on the Energy Absorption Behavior of Carbon Fiber/PEEK Composite Tubes.* Journal of Reinforced Plastics and Composites, 1996. **15**(1): p. 30-47.

79. Maxwell, J., *Plastics in the automotive industry*. 1994: Woodhead publishing.

80. Stevanovic, D., P. Ben Jar, A. Lowe, and S. Kalyanasundaram. *The influence of rubber particle concentration on fracture toughness of interlayer-toughened vinyl-ester/glass fibre composite*. in *ICCM 12*.1999

81. Sultan, J. and F. McGarry, *Effect of rubber particle size on deformation mechanisms in glassy epoxy*. Polymer Engineering and science, 1973. **13**(1): p. 29.

82. Day, R., P. Lovell, and A. Wazzan, *Toughened carbon/epoxy composites made by using core/shell particles.* Composites science & Technology, 2000. **61**: p. 41-56.

83. Pham, S. and P. Burchill, *Toughening of vinyl ester resins with modified polybutadienes.* Polymer, 1995. **36**(17): p. 3279-3285.

84. Bagheri, R. and R. Pearson, *The use of microvoids to toughen polymers.* Polymer, 1995. **36**(25): p. 4883-4885.

85. Bagheri, R. and R. Pearson, *Role of particle cavitation in rubber-toughened epoxies: 1. Microvoid toughening.* Polymer, 1996. **37**(20): p. 4529-4538.

86. Zhang, Z. and S. Zhu, *Microvoids in unsaturated polyester resins containing poly(vinyl acetate) and composite with calcium carbonate and glass fibres.* Polymer, 2000. **41**: p. 3861-3870.

87. Tanoglu, M. and A. Seyhan, *Compressive mechanical behaviour of E-glass/polyester composite laminates tailored with a thermoplastic preforming binder.* Materials Science and Engineering, 2003. **A363**: p. 335-344.

88. Tanoglu, M. and A. Seyhan, *Investigating the effects of a polyester preforming binder on the mechanical and ballistic performance of E-glass fiber reinforced polyester composites.* International Journal of Adhesion & Adhesives, 2003. **23**: p. 1-8.

89. Lu, M., M. Shim, and S. Kim, *Curing behaviour of an unsaturated polyester system analyzed by Avrami equation.* Thermochimica Acta, 1998. **323**: p. 37-42.

90. Tucker, R., P. Compston, and P. Jar, *The effect of postcure duration on the mode 1 interlaminar fracture toughness of glass-fibre reinforced vinylester.* Composites Part A, 2001. **32**: p. 129-134.

91. Thornton, P. and P. Edwards, *Energy Absorption in Composite Tubes.* Journal of Composite Materials, 1982. **16**: p. 521-545.

92. Farley, G., *Energy Absorption of Composite Materials*. Journal of Composite Materials, 1983. **17**: p. 267-279.

93. Quek, S., A. Wass, J. Horrman, and V. Agaram, *The crushing response of braided and CSM glass reinforced composite tubes.* Composite Structures, 2001. **52**: p. 103-112.

94. McGeehin, P., *Preform manufacture for liquid moulding processes*. 1994, University of Nottingham.

95. Murphy, J., *Reinforced plastics handbook*. 1994: Elsevier Advanced Technology.

96. Mattheij, P., K. Gliesche, and D. Feltin, *3D reinforced stitched carbon/epoxy laminates made by tailored fibre placement.* Composites Part A, 2000. **31A**: p. 571-581.

97. Kamiya, R., B. Cheesman, P. Popper, and T. Chou, *Some recent advances in the fabrication and design of three-dimensional textile preforms : a review.* Composites science & Technology, 2000. **60**: p. 33-47.

98. Karbhari, V., P. Falzon, and I. Herzberg. *Effect of Braid Architecture on Progressive Crush of Composite Tubes*. in *41st International SAMPE Symposium*. 1996.

99. Karbhari, V., P. Falzon, and I. Herzberg, *Energy Absorption Characteristics of Hybrid Braided Composite Tubes.* Journal of Composite Materials, 1997. **31**(12): p. 1164-1186.

100. Karbhari, V. and J. Haller, *Progressive Crush of Hybrid Composite Components.* Automotive Composites Consortium Conference ???, 1997: p. 1-10.

101. Chiu, C.H., C.K. Lu, and C.M. Wu, *Crushing Characteristics of 3-D Braided Composite Square Tubes.* Journal of Composite Materials, 1997. **31**(22): p. 2309-2327.

102. Sjogren, B., R. Joffe, L. Berglund, and E. Mader, *Effects of fibre coating (size) on properties of glassfibre/vinylester composites.* Composites Part A, 1999. **30**: p. 1009-1015.

103. Hamada, H., S. Ramakrishna, M. Nakamura, Z. Maekawa, and D. Hull, *Progressive Crushing Behaviour of Glass/Epoxy Composite Tubes with Different Surface Treatment.* Composite Interfaces, 1994. **2**(2): p. 127-142.

104. Tao, W., R. Robertson, and P. Thornton, *Effects of Material Properties and Crush Conditions on the Crush Energy Absorption of Fiber Composite Rods.* Composites Science and Technology, 1993. **47**: p. 405-418.

105. Mamalis, A., D. Manolakos, G. Demosthenous, and M. Ioannidis, *Energy Absorption Capability of Fiberglass Composite Square Frusta Subjected to Static and Dynamic Axial Loading.* Thin-Walled Structures, 1996. **25**(4): p. 269-295.

106. Karbhari, V. and J. Haller, *Rate and architecture effects on progressive crush of braided tubes.* Composite Structures, 1998. **43**: p. 93-108.

107. Fontana, Q., *Speed and Temperature Effects in the Energy Absorption of Axially Crushed Composite Tubes*. 1990, University of Cambridge.

108. Fleming, D. and A. Vizzini, *The Effect of Side Loads on the Energy Absorption of Composite Structures.* Journal of Composite Materials, 1992. **26**(4): p. 486-499.

109. Fleming, D. and A. Vizzini, *Energy Absorption of Composite Plates under Off-Axis Loads.* Journal of Composite Materials, 1996. **30**(18): p. 1977-1995.

110. Fleming, D. and A. Vizzini, *Off-Axis Energy Absorption Characterization of Composites for Crashworthy Rotorcraft Design.* Journal of the American Helicopter Society, 1996. **41**(3): p. 239-246.

111. Han, Y., A. Yee, V. Li, H. Wang, N. Kikuchi, H. Wu, V. Agaram, and G. Nusholtz. *Axial and off-axis static crushing of triaxially braided carbon FRP composite square tubes*. in *American Society for Composites 15th Technical Conference*. 2000. Texas.

112. Farley, G. and R. Jones, *Prediction of the energy-absorption capability of composite tubes.* J. Composite materials, 1992. **26**(3): p. 388-404.

113. Mamalis, A.G., D.E. Manolakos, G.A. Demosthenous, and M.B. Ioannidis, *The static and dynamic axial collapse of fibreglass composite automotive frame rails.* Composite Structures, 1996. **34**: p. 77-90.

114. Mamalis, A., D. Manolakos, G. Demosthenous, and M. Ioannidis, *The Static and Dynamic Axial Crumbling of Thin-Walled Fibreglass Composite Square Tubes.* Composites Part B : Engineering, 1997. **28B**(4): p. 439-451.

115. Mamalis, A., D. Manolakos, G. Demosthenous, and M. Ioannidis, *The deformation mechanism of thin-walled non-circular composite tubes subjected to bending.* Composite structures, 1995. **30**: p. 131-146.

3 Experimental Methods

The following text describes the methodology used in preparing and testing specimens. Details of calculations undertaken to process results and relevant international standards are also included. The chosen fabrics were selected as they were already in use for automotive applications. Reasoning behind the resin choices is given in Chapter 4.

The primary means for evaluation of crush properties is the quasi-static axial tube crush, but other test methods used include in-plane coupon testing and Double cantilever beam (Mode I fracture toughness). Tertiary methods of examination used include measurement of void levels, volume fraction and crush zone morphology.

3.1 Materials

3.1.1 Resins

A variety of resins are used in testing. Manufacturers data is presented in this chapter, some additional resin testing is presented in chapter 4.

The main resin used for crush testing is Reichhold Norpol 631-610, this is an isophthalic polyester resin developed for RTM applications. The resin is pre-accelerated. A high HDT of 105°C makes it suitable for vehicle applications where fairly high temperatures may be encountered – e.g. Under-bonnet areas.

A vinylester resin was also used for crush testing, Reichhold DION 9500 was selected primarily because of its very high strain to failure of around 9%. The 9500 is a rubber modified resin not specifically intended for RTM and having a significantly higher viscosity (see Table 3:1 and Figures 3:1 and 3:2). The chemical structure of vinylester resin allows higher bond strengths and slightly lower shrinkage. The table below shows the manufacturers data for the two resins above and a standard RTM resin (420-100) for comparison.

Resin	Type	Tensile UTS (MPa)	Tensile Modulus (MPa)	Elongation (%)	HDT (°C)	Viscosity (mPa.s)
420-100	PE	65	3700	3.5	67	180-210
631-610	PE	76	3300	3.7	105	290-330
DION 9500	VE	70	3100	9	80	500-750

Table 3:1 Resin property data

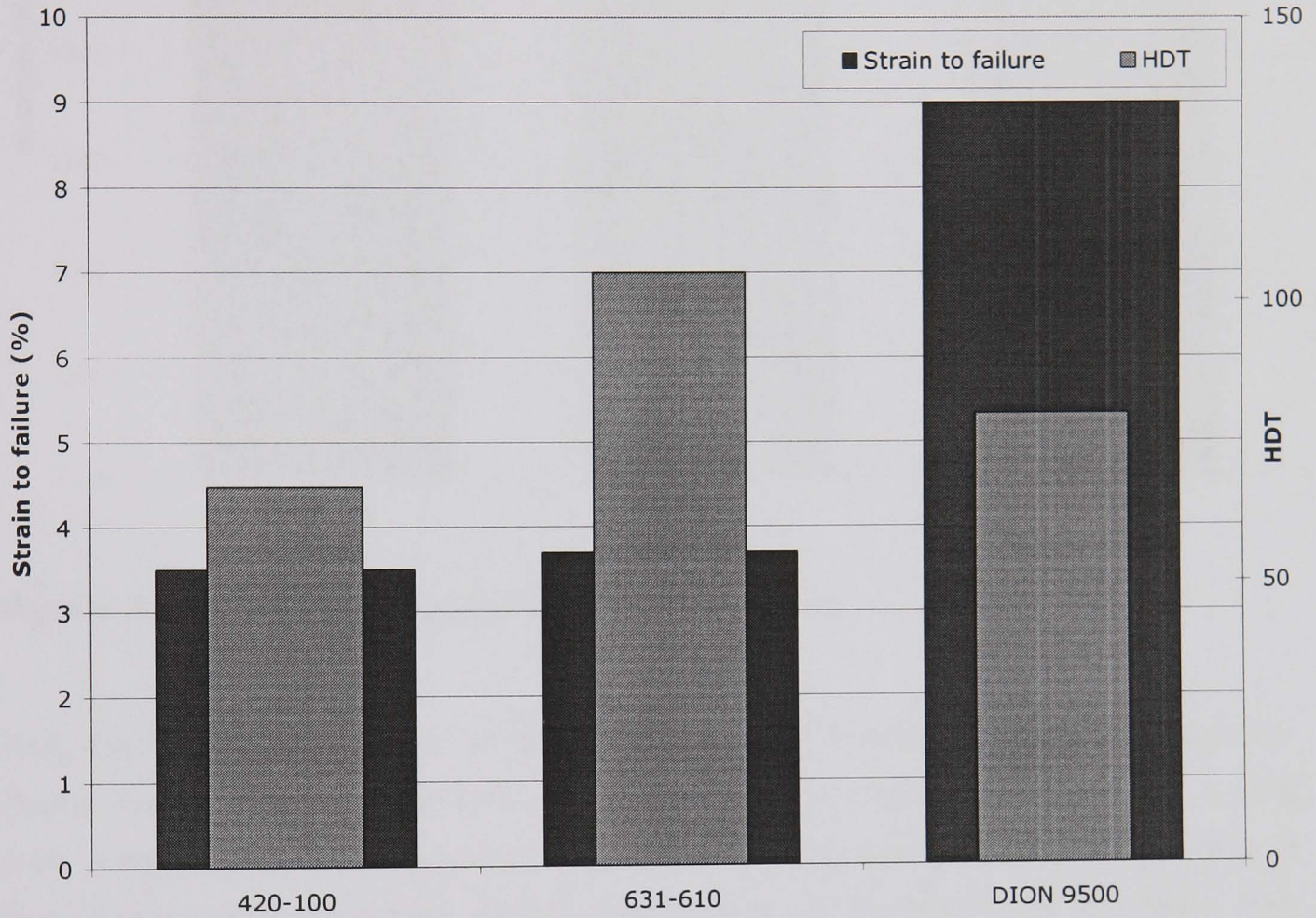

Figure 3:1 Strain to failure and HDT of resins (data from manufacturer)

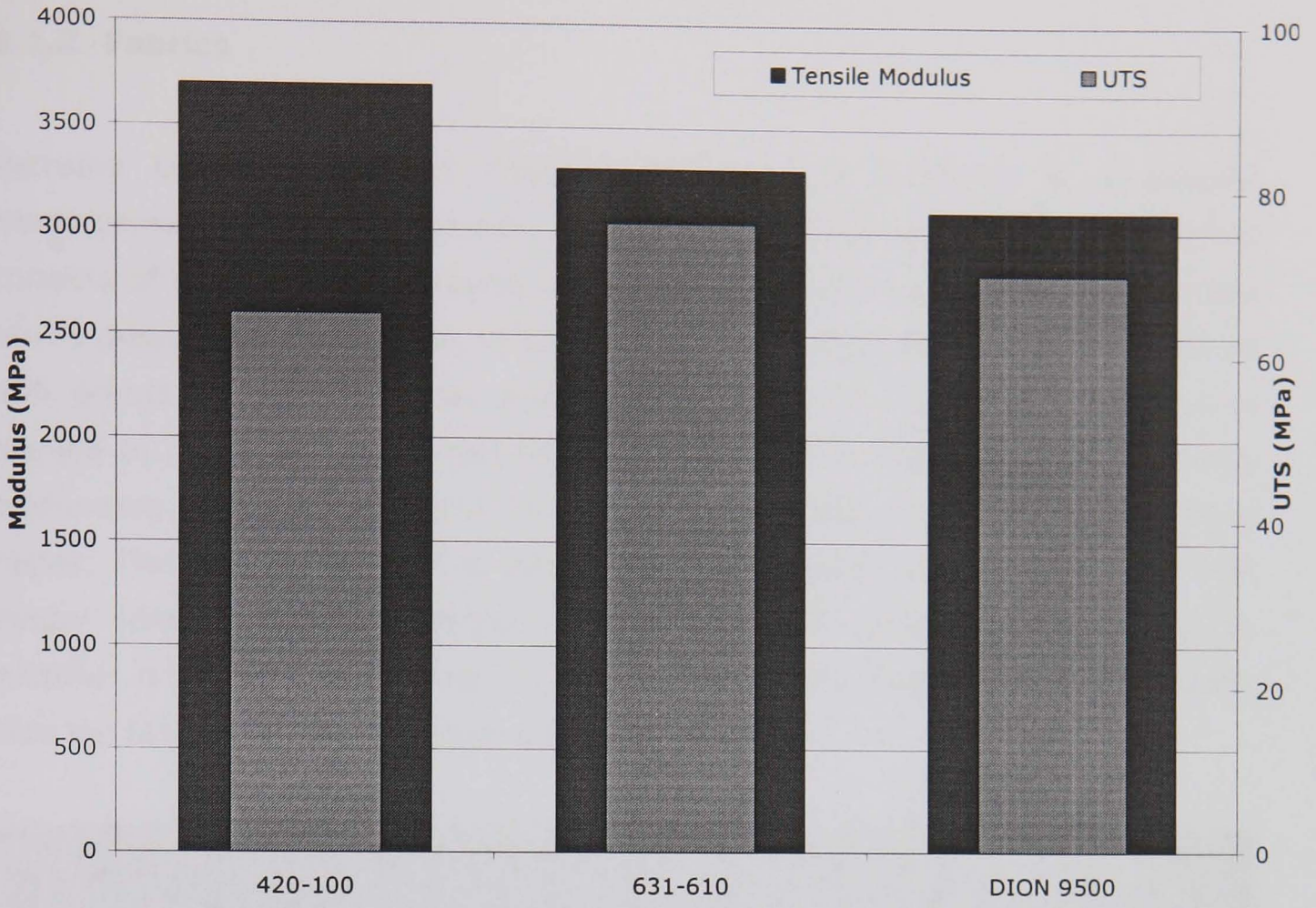

Figure 3:2 Tensile modulus and UTS of resins

The mechanical properties of the polyester and rubber toughened vinylester resins do not differ significantly but the reduced shrinkage of vinylester during cure means that lower residual stresses are built into the matrix resulting in higher composite properties. Additionally higher matrix/fibre bond strengths may be realised.

Resins were supplied in 20Kg drums and removed using a drum mounted pump.

3.1.2 Fabrics

Vetrotex Unifilo Continuous Filament Random Mat (CoFRM) is a popular reinforcement for RTM processes, in particular vehicle applications. The fabric consists of a 50 tex tow randomly orientated in a swirling pattern on the surface of the glass (See Figure 3:3). U750-450(127) was used, this is product U750 at 450 grams per square meter and 1270mm width. A standard silane size is applied to the fibres and a medium solubility binder is incorporated to facilitate preforming. The 50 tex strand gives high permeability allowing use with filled resins. The loss on ignition is quoted by the manufacturer as 8%. This high binder content can be expected to vary composite properties depending on whether resin flushing is used. The fabric has a high natural loft which means that the fabric must be compacted whilst preforming.

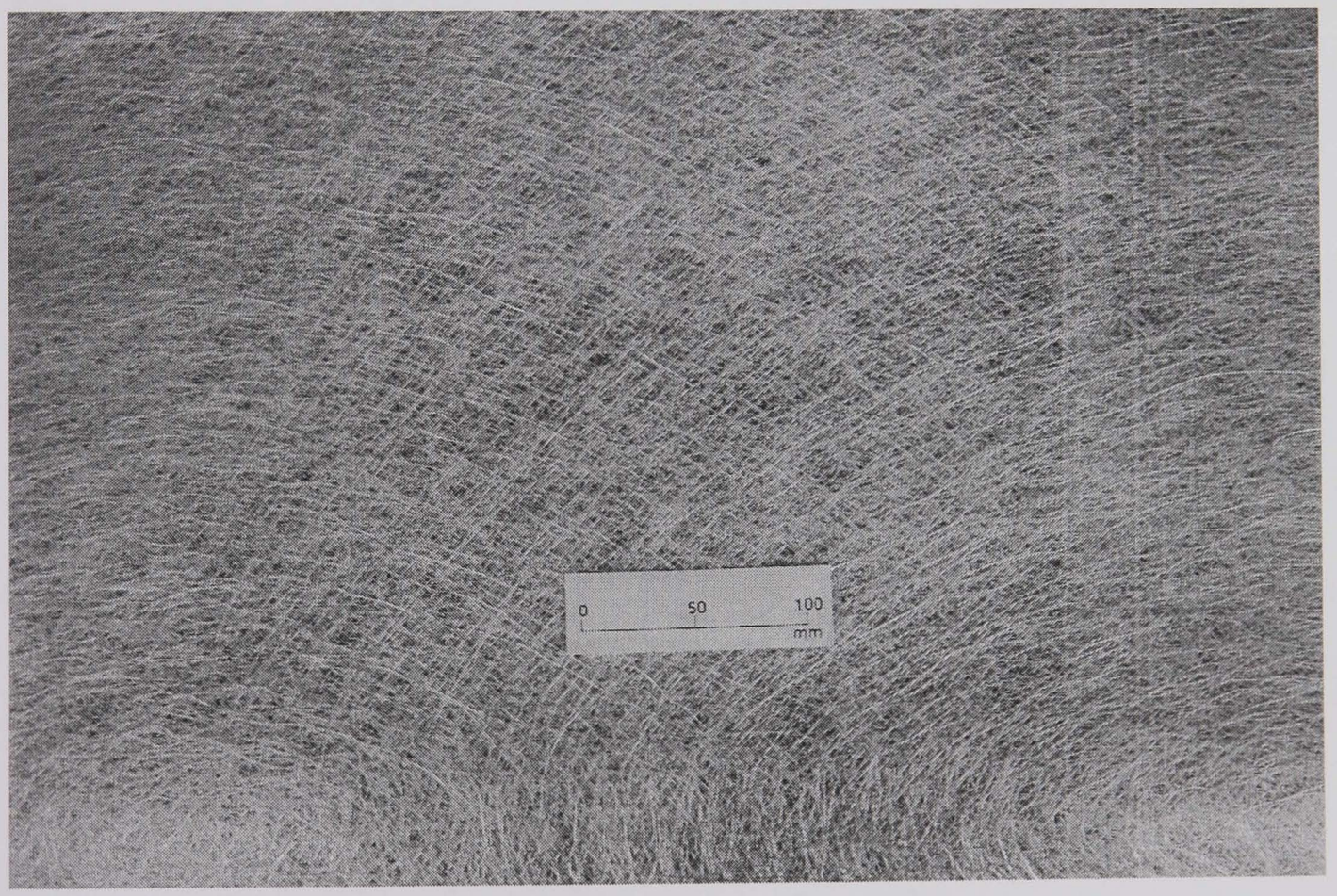

Figure 3:3 Structure of Unifilo

A non-crimp stitched E-glass fabric was also used. Supplied by Vetrotex / Brunswick Technologies international (BTi) this is designated as ELT566 and is 566gsm in a 0/90° architecture as shown in Figure 3:4. The width supplied is 1270mm.

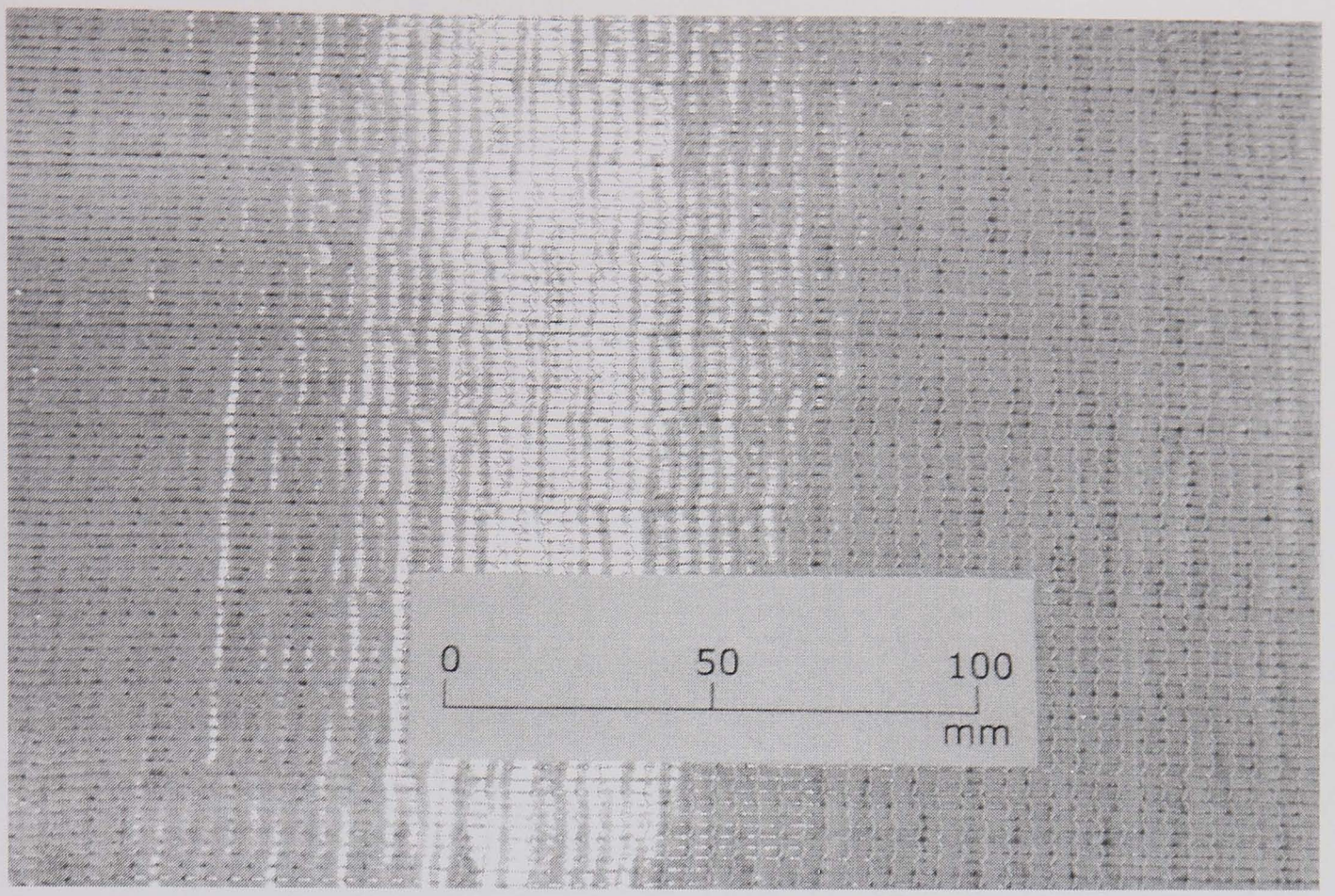

Figure 3:4 Structure of NCF

3.1.3 Curing systems

Curing systems were supplied by Akzo Nobel chemicals, quantities used were based on recommendations from the resin supplier. Different catalysts were used according to the moulding temperature with exact quantities depending on required gel time. The exact nature of the catalysts used is given below.

Trigonox 44B	Acetylacetone peroxide in solvents (AAP)
Butanox LPT	Methyl ethyl ketone peroxide in dimethyl phthalate (MEKP)
Trigonox K-80	Cumyl hydroperoxide 80% in aromatic solvents
Trigonox 141	2,5-Dimethyl-2,5-di(2-ethylhexanolperoxy)hexane

Catalysts were chosen to prevent the foaming which can sometimes occur with vinylester resins and also to enable use with mixtures of the two resins.

Akzo NL51-P accelerator (6% cobalt) was used with the vinylester resin. As stated above, the polyester resin was pre-accelerated

3.1.4 Ancillary materials

3.1.4.1 Release Agent

The release agent selected was Chem-trend Chemlease PMR-90 which is a high slip, high gloss release agent suited to RTM applications. The tubular parts made are particularly difficult to release and effective application is essential. The release agent was applied by wiping a thin even layer on to the mould, waiting until the solvent has almost totally evaporated (up to 60 seconds dependent on room temperature) wiping / spreading with a clean piece of lint-free cloth. This process was repeated at least 5 times at 15 minute intervals. PMR-90 is a semi-permanent release material meaning that multiple pulls should be possible, however occasional tool cleaning can remove the release layer necessitating re-application. Approximate number of releases therefore varied in production from 1-6.

3.1.4.2 Powder binder

A powder binder was used on the non-crimp fabric at approx. 6% addition by weight. This allowed preforming in the same manner as the CoFRM material. Even binder distribution was achieved by using a shaker to apply a given quantity to the preform. Where necessary the powdered binder was melted onto the glass fabric by using a hot domestic iron with a layer of release paper between it and the glass. After the binder was melted onto the fabric a hot air gun could be used to re-melt the binder. The binder selected was DSM Resins Neoxil 940, a high molecular weight bisphenolic polyester powder. Solubility in styrene is very high, the specific gravity is 1.1g/cm^3.

Where binder was dissolved in resin prior to moulding, the binder was stirred into un-catalysed resin and left covered for 24 hours

3.1.4.3 Interleaf materials

All interleaf materials are manufactured by Sarna Xiro (now Collano Xiro) and supplied by Cornelius Chemical Co. UK. The two interleaves used for this study are as detailed in Table 3:2. Also shown is the interleaf used in preliminary work. All interleaves used are described as compatible with the other materials in use.

Designation	Preliminary	Interleaf 1	Interleaf 2
Product code	Puro H	XAF23.401	Puro X
Material	TPU	PP	TPU
Melt temperature	65-85	140-150	100-130
Heat resistance	75°C	130°C	90°C
Density	1.16	1.24	1.18
Weight	50gsm	40gsm	100gsm

Table 3:2 Interleaf film properties

The interleaves were selected from a very large range, primarily for their higher heat resistance as the resin was also chosen for this purpose. This makes the resulting material more suitable for underbonnet applications. The required melt temperature can easily be achieved during preforming as a hot air gun is used to melt the binder. The two interleaves were chosen to provide different properties; the thin PP having a high modulus bondline and the thick TPU having a lower modulus.

3.1.4.4 Stitching materials

Stitching materials for preliminary testing included

16% PTFE coated E-glass (Polux ST600)

- 11tex x 12 construction
- 0.28mm diameter
- ~54N tensile strength

Reverse twist lubricated polyester (Somac TKT30)

- High abrasion resistance
- 280/3 construction
- ~49N tensile strength
- 21% elongation

Reverse twist bonded Nylon (Somac TKT40)

- 253/3 construction
- ~44N tensile strength
- 18% elongation

Reverse twist long staple spun Kevlar (Somac TKT50)

50/3 construction – 460 turns per meter

~72N tensile strength

5% elongation

Technical specifications were supplied by the respective manufacturers.

3.2 Test Methods

3.2.1 Axial crush testing

Axial crushing is the main method by which SEA is determined. No official standard exists for this type of testing but the method used is one that has been employed at the University of Nottingham for many years. The method was designed to be compatible with testing performed by other researchers to allow comparison of results.

Axial crush testing is undertaken on the 1000kN servo-hydraulic Instron 8500 testing machine running at 10mm/min, this is deemed to be quasi-static operation. A flat finish-ground steel crush platen is used to crush onto. Data acquisition and machine control is done via a dedicated PC.

Figure 3:5 Tube undergoing testing in Instron 8500

Specific Energy Absorption (SEA) is the term used in this work and can be taken as directly comparable (see over) with 'Specific sustained crushing stress' (SSCS) used by authors such as Gary Farley and 'Specific crushing stress' employed by Derek Hull. SEA takes into account the density of the material and is thus more applicable when designing to a minimum weight.

The crush calculations use the data from 5mm to 50mm, thus avoiding the crushing of the chamfer and the compression of inner fronds (Figure 3:6). SEA is calculated by summing the area under the load-displacement curve to give total energy and then dividing by mass per unit length.

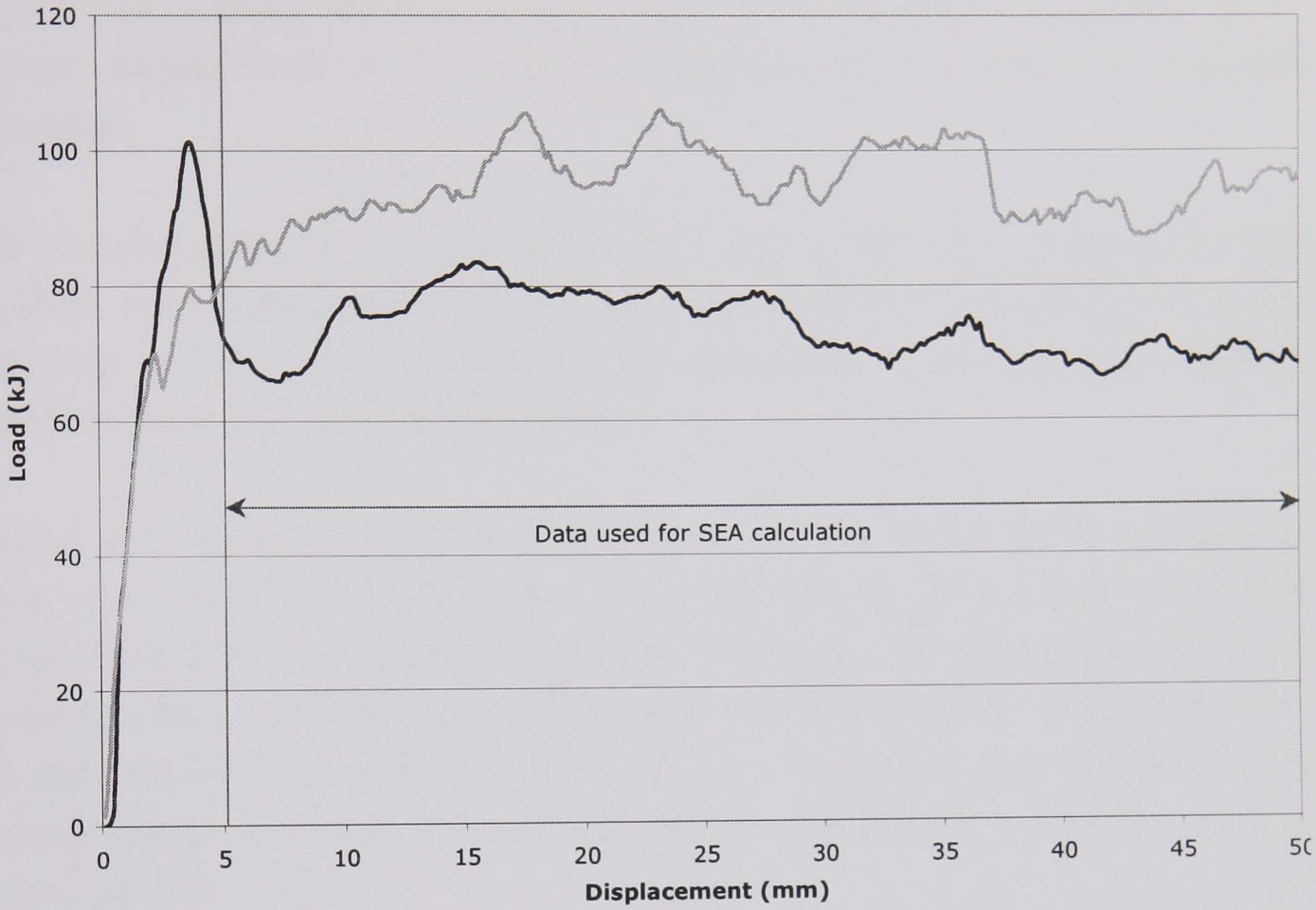

Figure 3:6 Data used for SEA calculations: 5 to 50 mm

SEA is calculated as follows:

- The trapezium rule is used to calculate the area under the curve for each value of displacement (~0.17mm)
- This data is summed for all data points between 5 and 50mm
- SEA is then Total Energy / Mass per unit length / crush length

This value is identical to SSCS or specific crushing stress although this calculation could be approached in the following manner:

- Mean load can be calculated by averaging the loads from 5 to 50mm of crush.
- Mean stress is then Mean load / Cross-section area
- SSCS = Mean stress / Density

3.2.2 In-plane testing

In-plane coupon testing is employed to characterise the contribution of the principal in-plane factors to the overall crush response. Axial crush performance is dependent on a large number of material properties, most of which have an associated in-plane test standard. To ensure the validity of this approach the in-plane samples must be made under exactly the same conditions as the tube samples.

All in-plane testing was performed at 25 ± 2 °C to ASTM standards D3410 and D3039. Tensile and compressive testing was performed at 0.5 mm/min on a 100 kN Instron 1195 electro-mechanical testing machine. Each test was repeated three times in two material directions.

Strain was measured using an extensometer for the tensile tests connected to the controlling PC. For compressive and shear testing strain gauges were used connected to an InstruNet 100 datalogger, the tests were manually synchronised and data was copied as described below. Shear strain gauges were Kyowa KFG-3-120-D16 and compressive KFG-5-120-C1. Specimens were cleaned using acetone and marked to show gauge position. Gauges were attached using a cyanoacrylate adhesive.

Results are copied from the Instron testing PC and converted to metric units in Microsoft Excel. Three measurements of the coupons are taken in two directions and inputted into the spreadsheet. Averages are taken and stress is calculated by dividing maximum load by the cross-sectional area.

3.2.3 DCB testing

The Double Cantilever Beam (DCB) test is used to determine Mode I fracture toughness of a sample. The relevant standard used for geometry and sample preparation is ASTM 5528. The geometry is as shown in Figure 3:7.

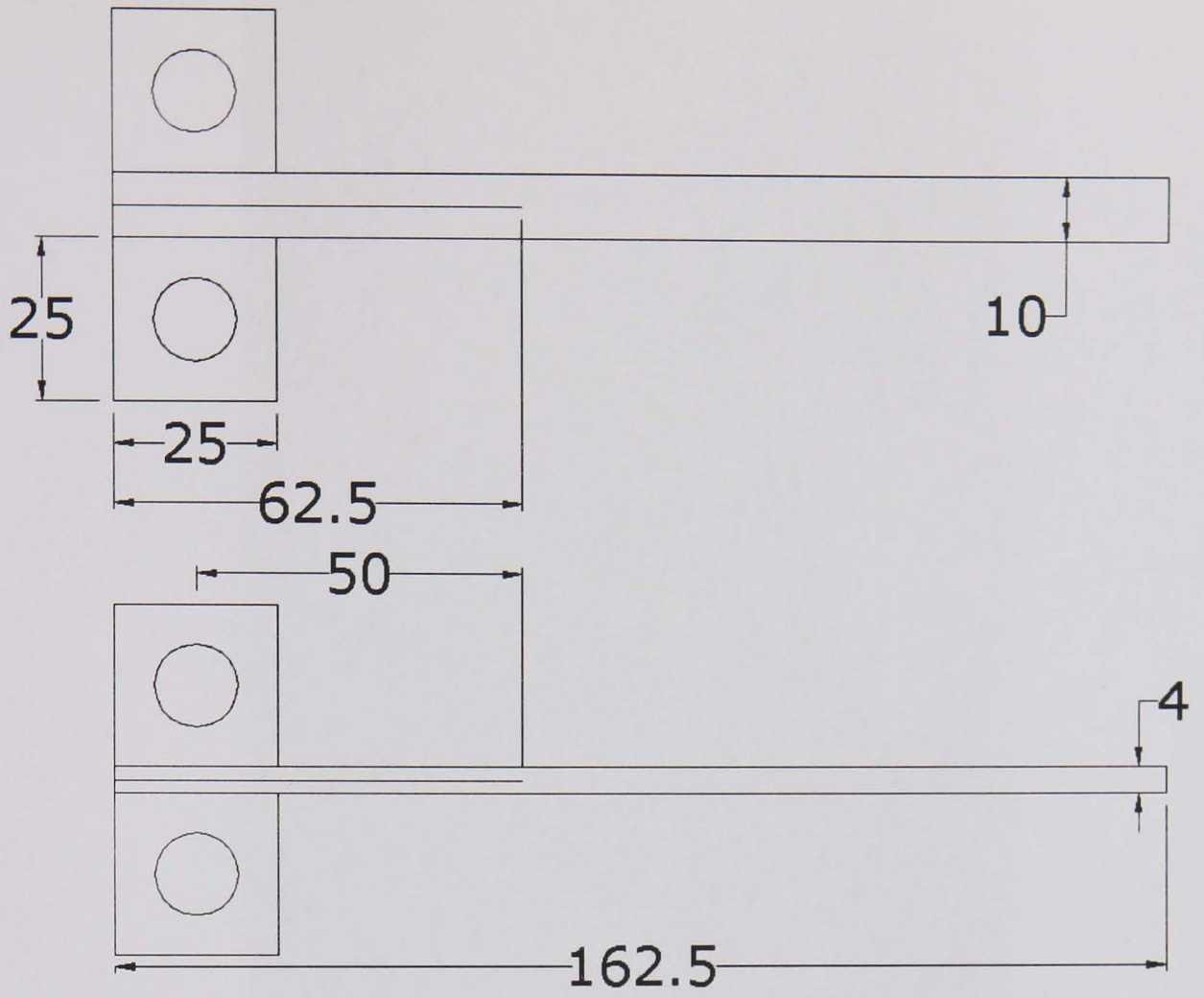

Figure 3:7 Thick and thin DCB geometry

Two thicknesses have been used in the present work. The thin specimen is the standard size but did not have sufficient beam stiffness for stitched samples. In preference to bonding reinforcing strips of a different material to the beams the parts were moulded thicker with reinforcing composite manufactured-in. Where the samples are stitched only the inner 4mm of sample is stitched through such that the stitch length is comparable. The 10mm specimens are 12 layers thick for CoFRM and 18 layers thick for NCF. This provides volume fractions and interlaminar properties equivalent to the tube samples. Figures 3:8 and 3:9 show a DCB test in progress with the standard and thick geometry respectively.

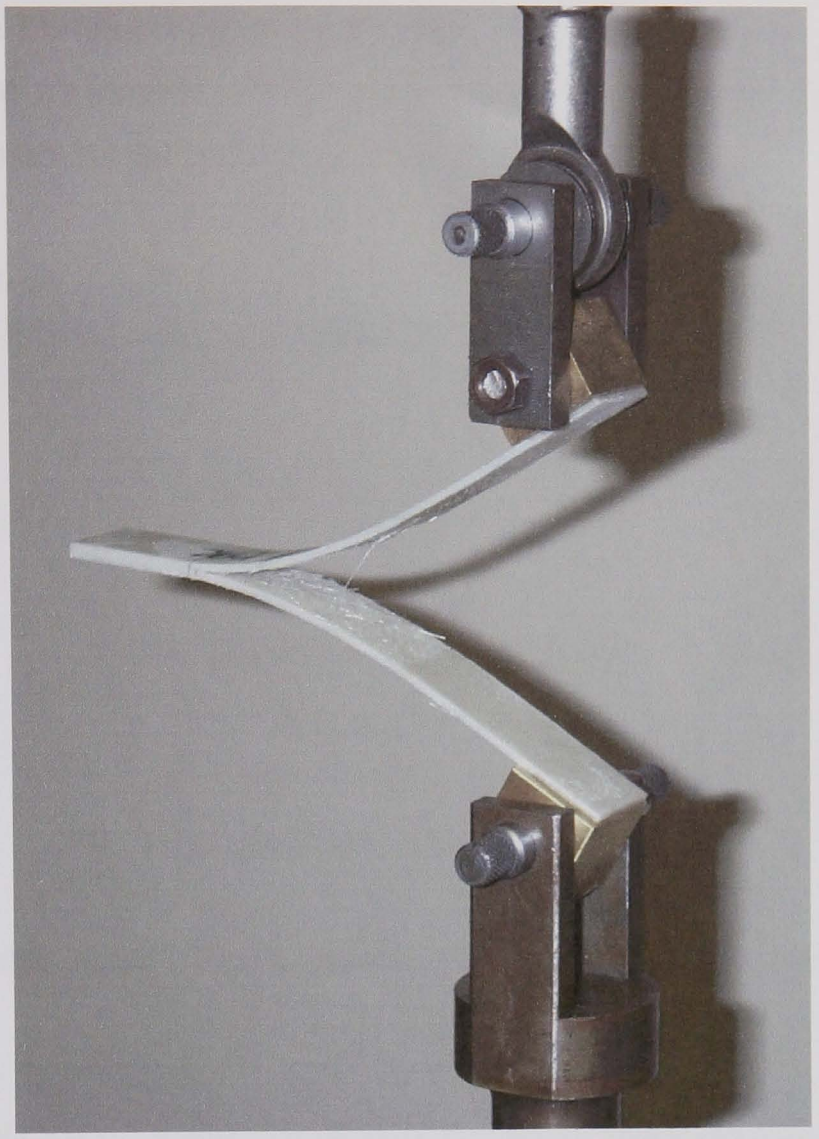

Figure 3:8 DCB test on thin specimen

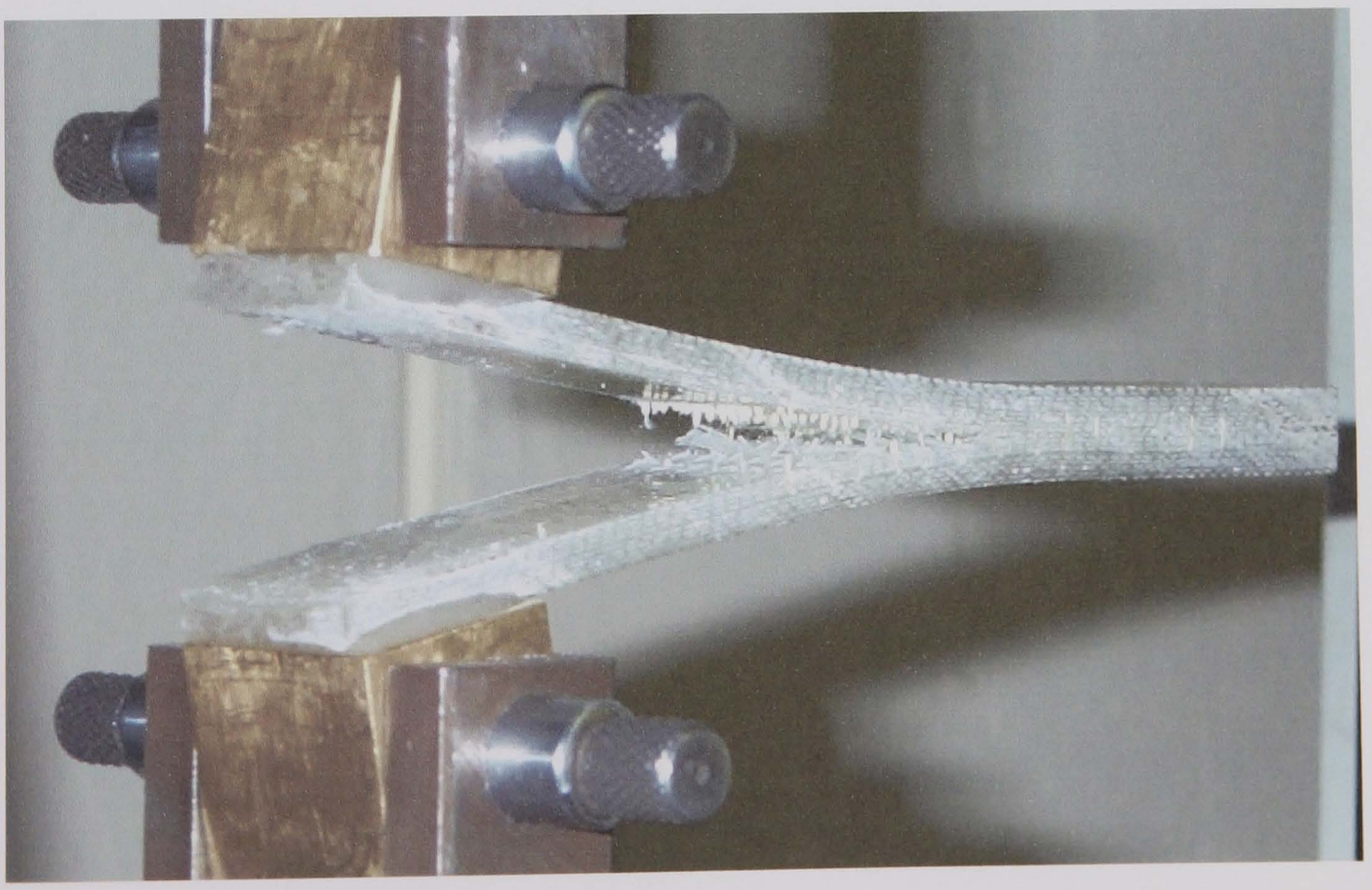

Figure 3:9 DCB test on thick stitched specimen showing stitch pull-out

Brass blocks are bonded to the specimen ends using a cyanoacrylate adhesive in a jig to ensure alignment. PTFE inserts are used between blocks and loading pins. The test speed for all tests was 5mm/min.

The Mode I fracture toughness (critical strain energy release rate) G_{IC} value was calculated using the following equation:

$$G_{Ic}(J/m^2) = \frac{E}{A \times B}$$

Where
- E = Area under load-deflection curve between the initial and final position (N/m)
- A = Crack length corresponding to E (m)
- B = Specimen width (m)

The area under the curve is calculated using the trapezium rule in a spreadsheet (see 3.2.1)

G_{Ic} is related to fracture toughness K_{Ic} by the following equation:

$$G_{Ic} = (1-\nu^2)\frac{K_{Ic}^2}{E}$$

Where
- ν = Poisson's ratio
- E = Young's modulus

3.2.4 Tertiary test methods

A variety of additional test methods have been used in various parts of the work; the methods used are detailed below.

3.2.4.1 Degree of cure

Degree of cure was evaluated on a Perkin-Elmer DSC 1 Differential Scanning Calorimeter running two consecutive thermal analyses on each cured resin sample. Resin cure is completed in the first run; the second run generates the baseline, which is subtracted from the first run. The resultant area is compared to the curve obtained by analysing uncured resin, allowing the cure level to be obtained. Testing was done at 10°C/min from 20°C to 220°C. Moulded parts were stored in a freezer at -25°C prior to DSC testing in order to prevent further room-temperature cure until the test was performed. Parts were allowed to reach room temperature before testing took place.

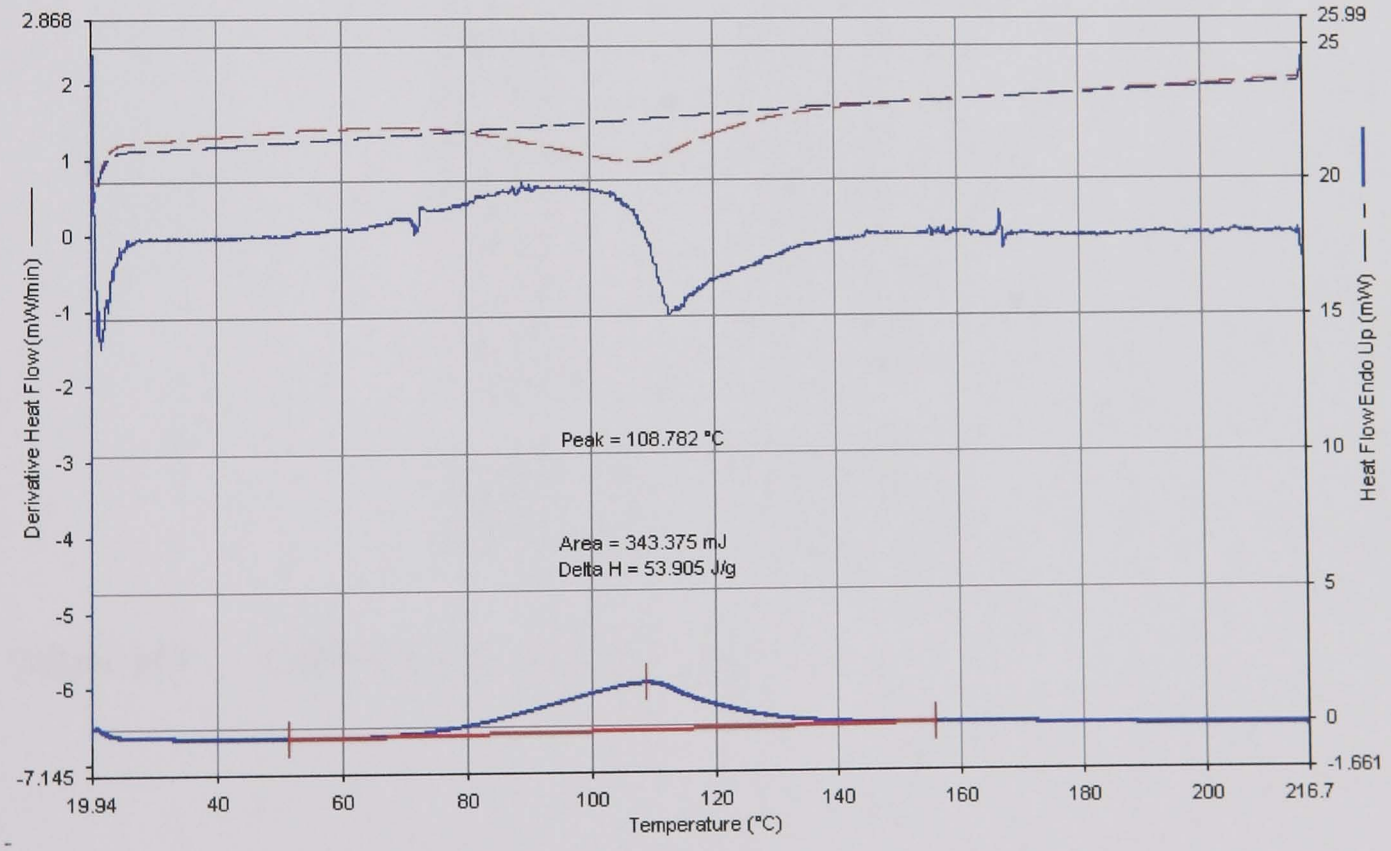

Figure 3:10 Screen shot from DSC program showing area representing uncured resin (lower curve)

3.2.4.2 Volume Fraction determination

Fibre volume fraction is determined in accordance with BS ISO 1172 [2]. Samples are cut to fit in steel trays in groups of 6-8 and weigh around 5g. Samples are accurately weighed in the tray and the weight of the tray is also noted. Samples are then placed in a furnace at 625°C for 30 minutes ensuring total loss of resin. The samples are then re-weighed to determine weight of fibre. Fibre volume fraction is then easily calculated using the following formula;

Fibre volume fraction = Volume of glass / Volume of specimen

Volumes are calculated using manufacturers supplied density measurements.

The results obtained are shown below;

Density of Fibres	2560	kg/m3
Density of resin	1120	kg/m3
Sample 1	21.0	%
Sample 2	23.8	%
Sample 3	21.8	%
Sample 4	20.5	%
Sample 5	21.3	%
Sample 6	21.4	%
Sample 7	23.5	%
Sample 8	21.2	%
Average Vf	**21.8**	**%**
St Dev.	1.08	

Table 3:3 CoFRM burn-off test results

Density of Fibres	2560	kg/m3
Density of resin	1120	kg/m3
Sample 1	39.0	%
Sample 2	38.5	%
Sample 3	38.7	%
Sample 4	39.3	%
Sample 5	40.4	%
Sample 6	39.4	%
Sample 7	39.1	%
Sample 8	39.9	%
Average Vf	**39.3**	**%**
St Dev.	0.63	

Table 3:4 NCF burn-off test results

3.2.4.3 Viscosity determination

Where quoted , viscosity measurements are performed using a Brookfield DV-II viscometer with a number 2 spindle. The spindle was cleaned in acetone between measurements. All measurements were determined at laboratory temperature which was 25°C.

3.3 Tooling

The following section describes the tooling and process control used to manufacture specimens for testing.

3.3.1 Tube specimens

Tube specimens are manufactured in a closed mould consisting of inner and outer steel mandrels with steel end-caps. Injection occurs through the lower end cap into a peripheral gate. The resulting flow front is perpendicular to the axis of the tube. Tool geometry is shown in Figure 3:11.

Closed loop heating is used to ensure rapid and consistent heating of the mould. The inner and outer mandrels have separate heaters and control systems (Figure 3:12). K type thermocouples are used to monitor the temperature. Warm up time is about 30 minutes.

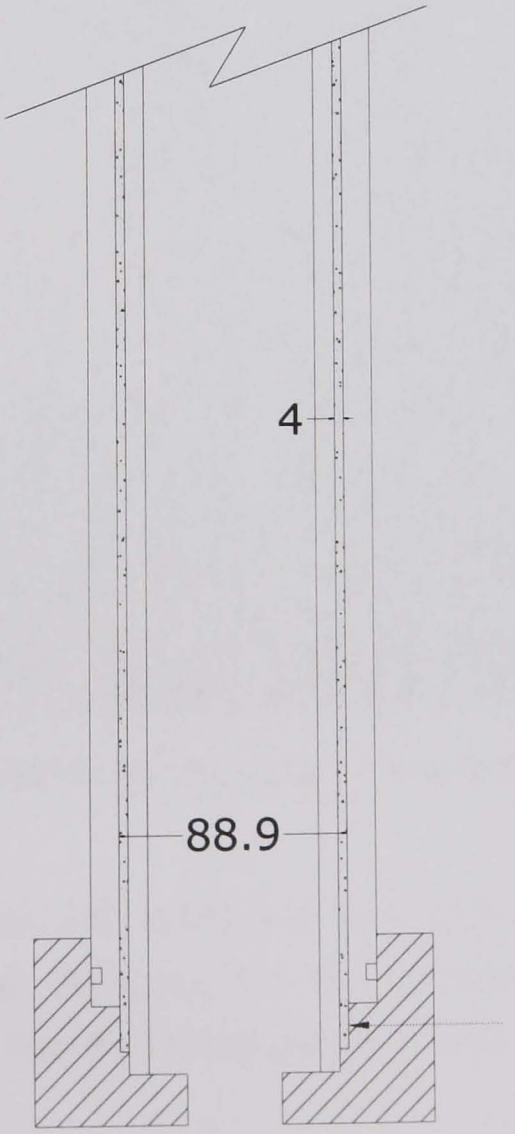

Figure 3:11 Schematic of RTM tube mould

Figure 3:12 Tube mould showing external band heaters

Parts produced are 3.7mm wall thickness with 88.9mm outer diameter and length 450mm. Shrinkage accounts for the difference between the cavity thickness of 4mm and the final part thickness of 3.7mm.

3.3.2 In-plane specimens

In-plane mouldings are performed in a 518 x 537 x 4mm aluminium tool installed in a 20 ton Fox & Offord hydraulic press (Figure 3:13). A similar heating system exists.

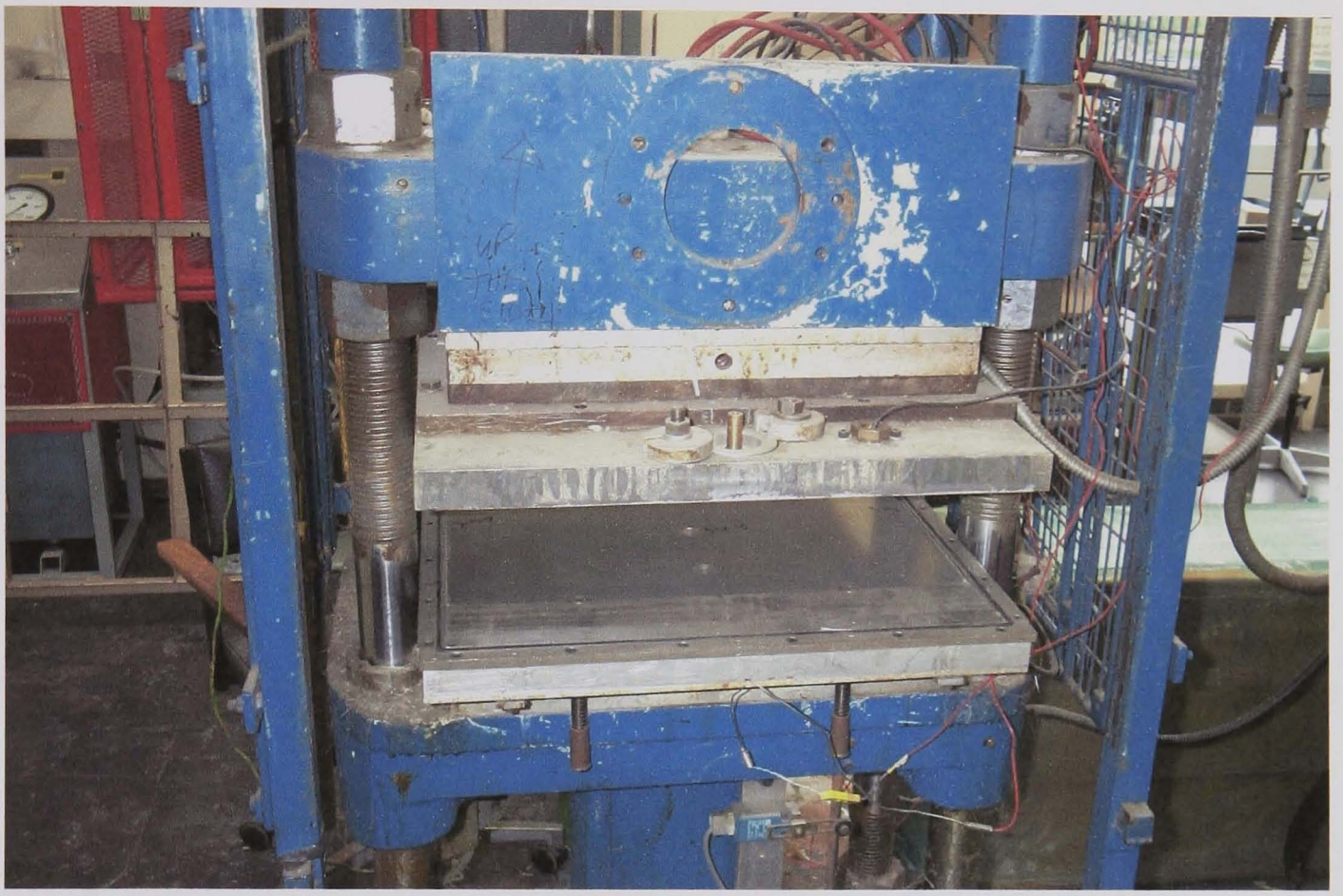

Figure 3:13 Tooling used to manufacture in-plane specimens

All in-plane parts are produced to support the crush testing so wherever possible identical moulding parameters are used, there are however inevitable differences due e.g. to the geometry of the tooling: The width of the tool at 518mm is somewhat larger than the circumference of the tube mould at 283mm.

3.3.3 DCB specimens

DCB specimen dimensions are shown in section 3.2.3 above, the tool dimensions are as follows;

Thin tool : 90 x 250 x 4mm
Thick tool : 120 x 200 x 10mm

4 samples can be extracted from each moulding.

3.4 Specimen Manufacture

3.4.1 Tube specimens

The RTM process requires the two distinct stages; those of preforming and moulding. The list and accompanying figures below show the main steps:

- Cut glass from roll approx 500mm x 2000mm
- Spread binder onto glass if necessary (for NCF mouldings)
- Place end of glass sheet into preformer (Figure 3:14)
- Tighten preformer loading bolts
- Wind preformer whilst applying heat and tension to sheet
- Trim glass to length to give correct number of layers
- Remove glass preform

- Apply release agent to all tool surfaces
- Place preform on inner mandrel
- Assemble tool and tighten
- Preheat
- Connect tubing
- Inject resin (Figure 3:15)
- Cure
- Demould

The resulting tube is allowed to reach room temperature naturally. Parts are placed in a cold oven and heated to the required postcure temperature for the prescribed time. During moulding efforts are taken to ensure consistency of parts and minimise manufacturing errors. Moulding temperatures are closely monitored and closed-loop controlled. Preform tightening and winding tension is consistently maintained. Winding tension is relatively low as volume fractions are low. Injection pressures are monitored using a digital display and accurately set.

When postcure is completed the tubes are removed from the oven and cut on a diamond wheel saw. 4 samples are obtained at 100mm each. At this time parts can also be cut for void and volume fraction determination. Tubes are chamfered at 45 degrees on one end of each part in a jig using a disc sander. Parts are identified and numbered according to their position in the mould (Figure 3:16).

One part for each type of moulding configuration (e.g. resin or fibre type) is weighed and measured to determine the mass per unit length.

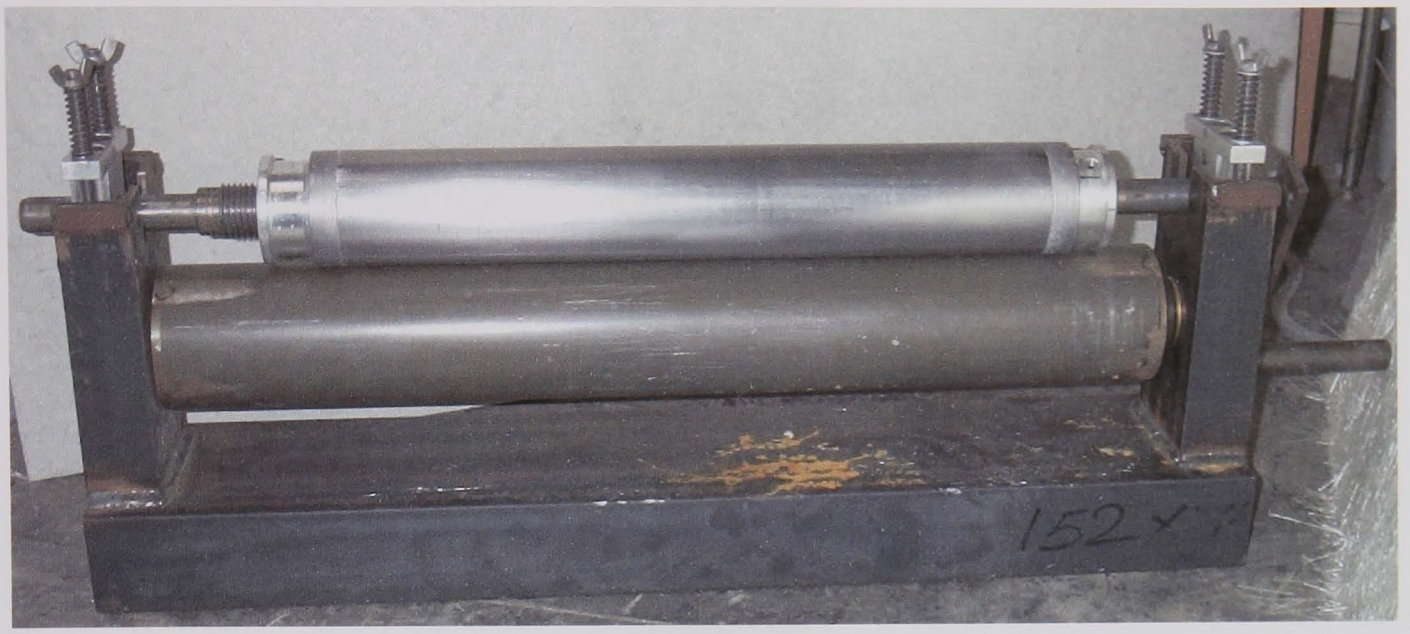

Figure 3:14 Preformer used to manufacture tube specimens (inner mandrel of mould shown at top)

Figure 3:15 Pressure pot used for RTM injection

Figure 3:16 Identification of cut samples with location of chamfer and direction of injection.

3.4.2 Wall thickness deviation

Accurate SEA calculations rely on the correct determination of the specimen mass per unit length which is easily measured before chamfering of the parts. Once determined for a particular set of testing an average value was adhered to for all samples. Stress calculations rely on the accurate determination of wall thickness. As part of the characterisation of the tooling a series of wall thickness measurements were taken of the parts produced. Four wall thickness measurements were taken on each of the four samples produced in a moulding. The results of this study appear in Figure 3:17. The relatively high spread is caused by the random nature of the reinforcement where surface volume fraction is variable and shrinkage is lower for higher local volume fractions. Shrinkage can be seen to depend on temperature as the 70°C mouldings have a thinner section than the 50°C mouldings (see Chapter 4 for moulding details).

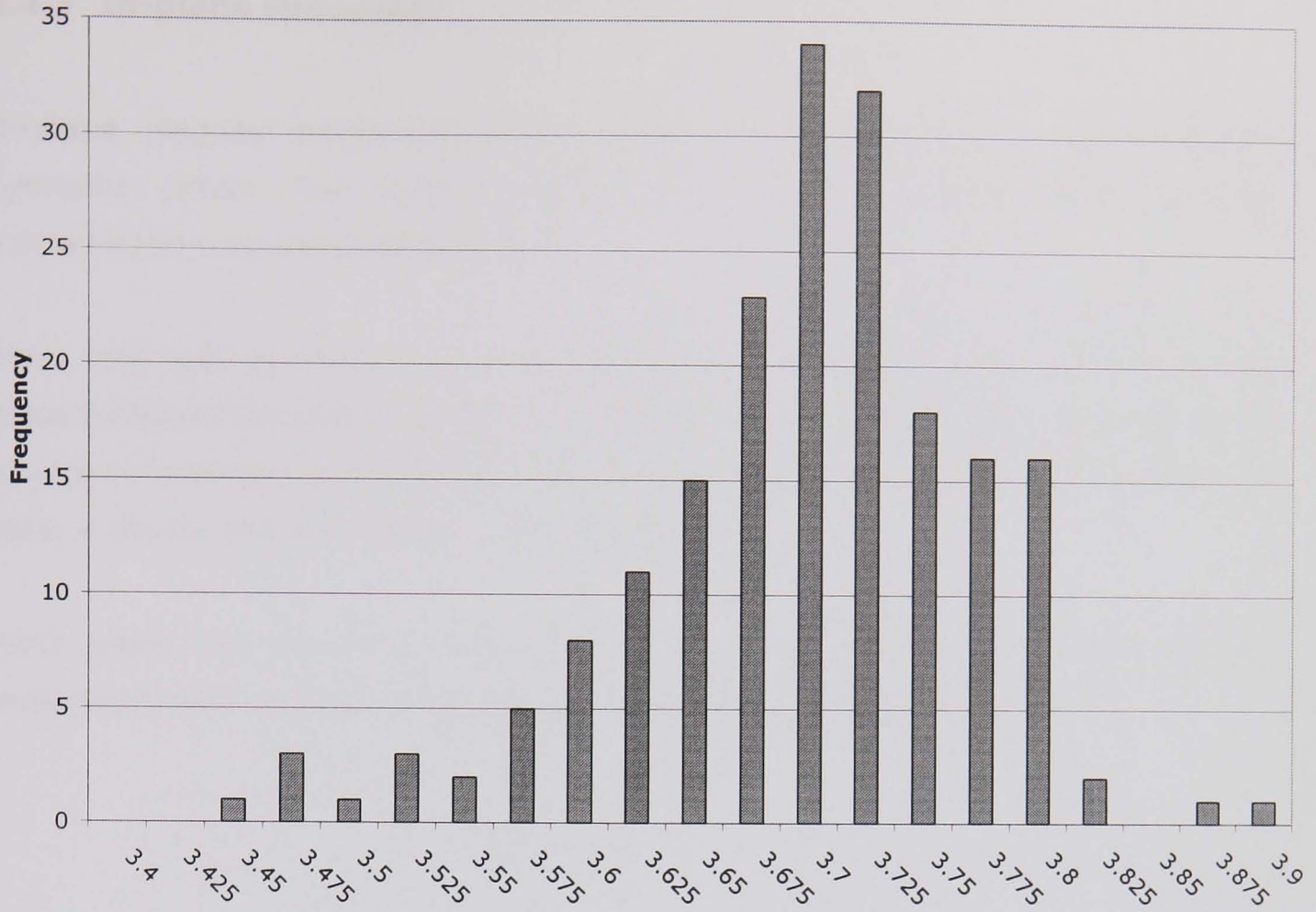

Figure 3:17 Frequency distribution of wall thickness

Moulding	Average(mm)
R1a	3.726
R1b	3.718
R1c	3.736
R2a	3.719
R2b	3.709
R2c	3.726
R3a	3.656
R3b	3.632
R3c	3.669
R4a	3.662
R4b	3.671
R4c	3.671

Table 3:5 Wall thickness averages

3.4.3 In-plane specimens

In-plane plaques measuring 518 x 537mm were made in a Fox & Offord hydraulic press. The same heating and material configurations as the concomitant tube samples were used.

Glass mat was cut from the same roll as tube samples and preformed in the press between two plates at 80°C for 30 minutes. Final trimming then took place to ensure accurate fitting in the tool. Cavity thickness is 4mm which results in parts a similar thickness to the tube mouldings.

Parts were cut on an abrasive waterjet cutter at 50mm/min to ensure consistency and accuracy. The plaque geometry is shown below.

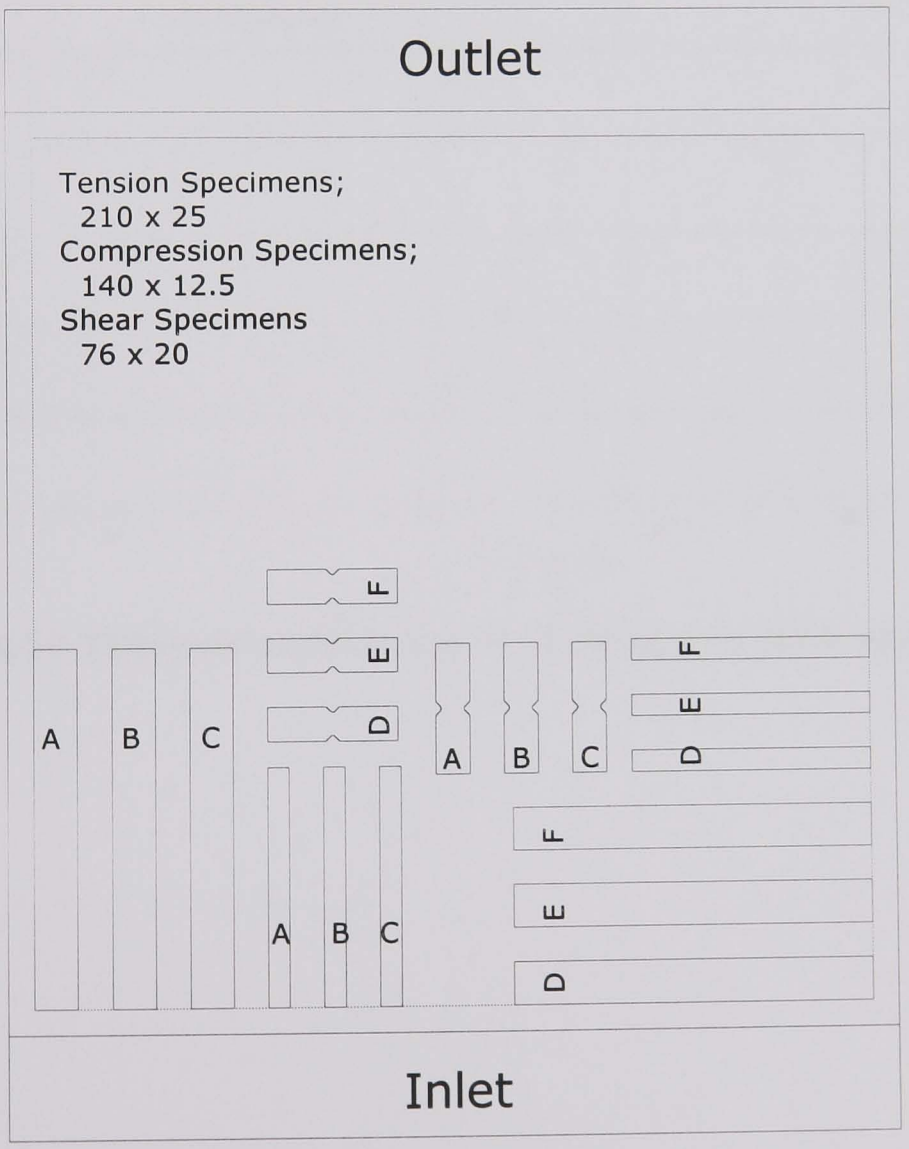

Figure 3:18 Waterjet cutting plan for in-plane testing showing 0/90 tests

3.4.4 Postcure

All parts are postcured for 2 hours in a hot air oven set to 80°C for 2 hours. Parts are placed in a cold oven to minimise thermal shock. Parts were removed from the oven and allowed to cool to room temperature. Testing showed that parts in the oven underwent the thermal profile shown in Figure 3:19.

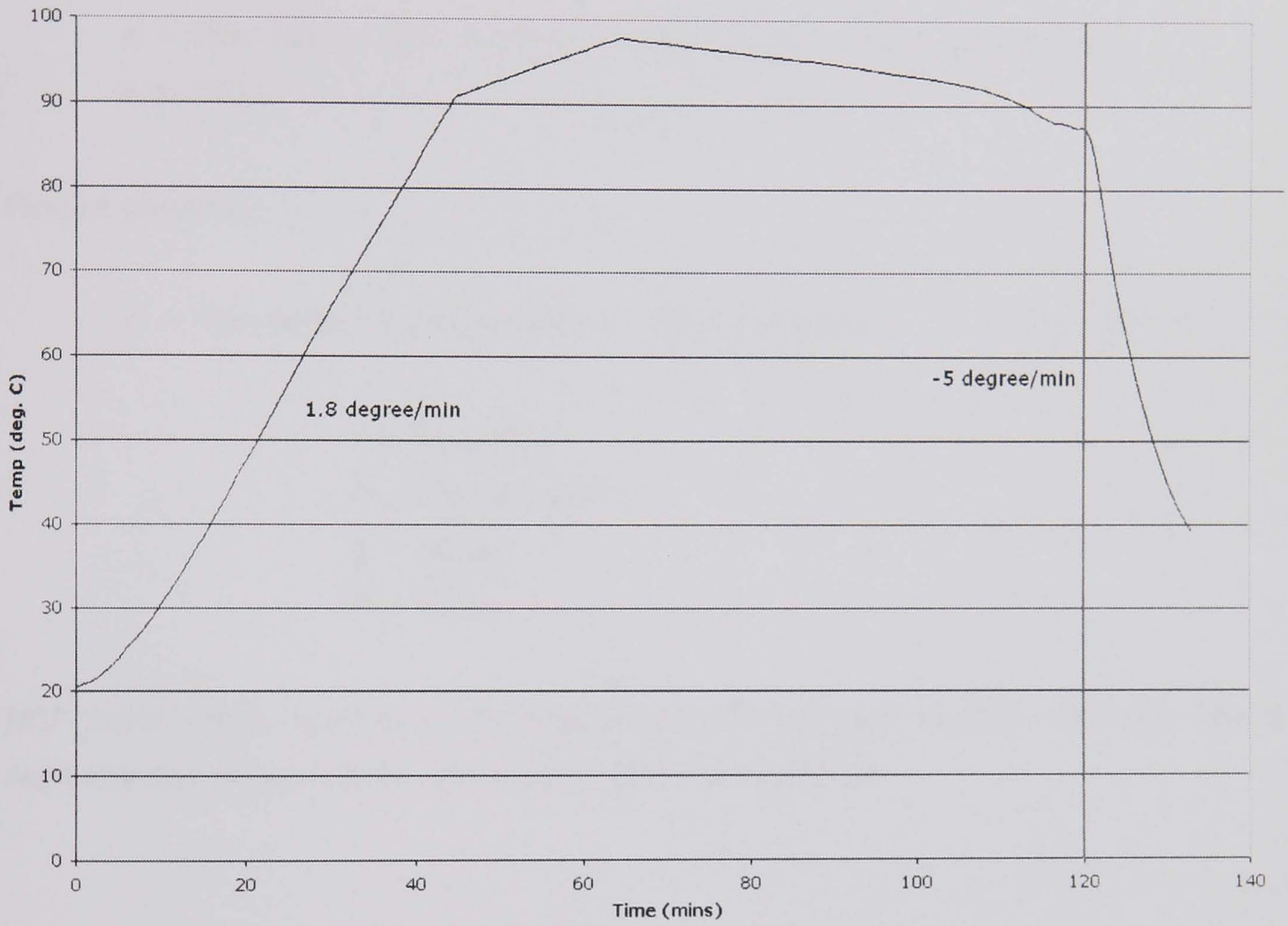

Figure 3:19 Thermal profile of part undergoing postcure

3.5 Part designation

Parts are designated according to the section of work, position in tube and repeat number.

Tube samples;

= Plan letter, (Ref. Letter), Configuration, repeat, cut position
e.g. PS2C

Plaque sample;

= Plan letter, Configuration #, type, cut letter e.g. R3TF

T = Tension
C = Compression
S = Shear
D = DCB

NCF tubes often have only one repeat and are designated R1S, R2S etc. The S replaces the repeat letter, cut identification is as above.

3.6 Material costs

This section aims to quantify the economic aspects of the materials discussed in this work. The costs at the time of writing are as follows:

- UP resin £ 1.38/kg
- VE resin £ 2.80/kg
- CoFRM glass £ 2.15/kg
- NCF glass £ 4.00/kg estimated

Therefore in terms of raw materials the two fibre architectures have costs as follows:

- 22%V_f CoFRM/UP £ 1.55/kg
- 22%V_f CoFRM/VE £ 2.66/kg
- 38%V_f NCF/UP £ 2.38/kg
- 38%V_f NCF/VE £ 3.26/kg
- Glass SMC £ 1.80/kg
- Steel £ 0.51/kg
- Aluminium £ 2.20/kg

These values are based on raw materials only and do not include wastage. Providing that the materials are moulded in the same manner the above results can be taken as a fairly good comparison between the parts. A comparison between composite and metallic structure is less valid due to the differences in production method.

4 Influence of Constituent materials

4.1 Introduction

The objective of the first study was to identify the effect of the resin system on the energy absorption potential of composite tubes. A review of available literature showed that whilst there is some data for different resin types, there is no systematic study showing results for different matrices with a common fibre architecture. Isolation of resin properties is important in understanding the crush mechanism and in volume production a change of resin represents a fairly easy modification.

Parts were made with two resins – a polyester and a vinylester, at different processing temperatures. The cost of epoxy resins was too high for the intended production volumes. The objective was to isolate the resin properties from the composite and determine their effect. Although only two resins are used, a variety of cure temperatures and postcure times gave nine different degrees of cure and hence nine different resin properties. Conversely while there are nine configurations it is possible to consider the differences between the matrices under similar moulding conditions and therefore compare 'generic' polyester and vinylester results.

A subsidiary aim was to investigate how processing speed affects the end properties; if the parts are to be representative of industrial parts then cycle times must be low. Low cycle time typically means high processing temperatures, typically this makes the process more sensitive to manufacturing tolerances such as injection pressure and catalyst selection. During this work the resin supplier assisted by helping to select curing systems that were appropriate for the resin and moulding temperature. This was particularly important at the higher moulding temperatures and with the vinylester resin which can suffer from foaming and production of excess polystyrene products.

It was also hoped that as well as providing valuable experimental data for production parts that this testing would give some insight into the contribution of resin properties on the crush response. For instance is high matrix toughness important to maximise crush properties? Previous work has suggested that this is the case. Before embarking on a major programme of testing some preliminary work was undertaken with a wide range of resin systems.

4.2 Rationale

The preliminary work undertaken involved investigation into the properties of the neat resin and also the effect of resin modifications on tube crush. The work resulted from a review of literature on the effect of resin properties on tube crush and comprised a series of speculations as to which chemical modifications would increase resin properties.

4.2.1 Preliminary resin testing

Neat resin testing was undertaken in order to quantify the improvement of the vinylester matrix over a polyester one without considering the effect of the fibres. The tests shown here are simple in-plane tests, other potential benefits may exist which are not identified by these tests. The plaques were moulded at a low (~0.5bar) injection pressure but otherwise cured and postcured as the others. Cure levels of almost 100% were achieved. The results fall slightly short of the manufacturers test results as they are moulded in a large plaque and do have a small but significant void content. Shrinkage is also a major factor in neat resin testing at it can impart a large pre-stress into the part thus reducing ultimate stresses.

4.2.1.1 In-plane properties

Neat resin testing of large plaques is fraught with difficulties due to the high level of shrinkage during cure. Due to time constraints the parts detailed below were full size plaques moulded in the Fox and Offord tool used for the production of all in-plane samples. The 631-610 plaque suffered from extensive cracking due to shrinkage and as a result fewer samples were obtained. It is unlikely that the samples tested were free of flaws or porosity and the results from this section should be taken as questionable.

Figure 4:1 shows average stress-strain curves for the two resins. The area under each curve shows the total strain energy for the specimens. Calculating the area for each specimen gives a value of 1.02 for the UP resin and 2.51 for the VE. This represents the difference in toughness in the two resins.

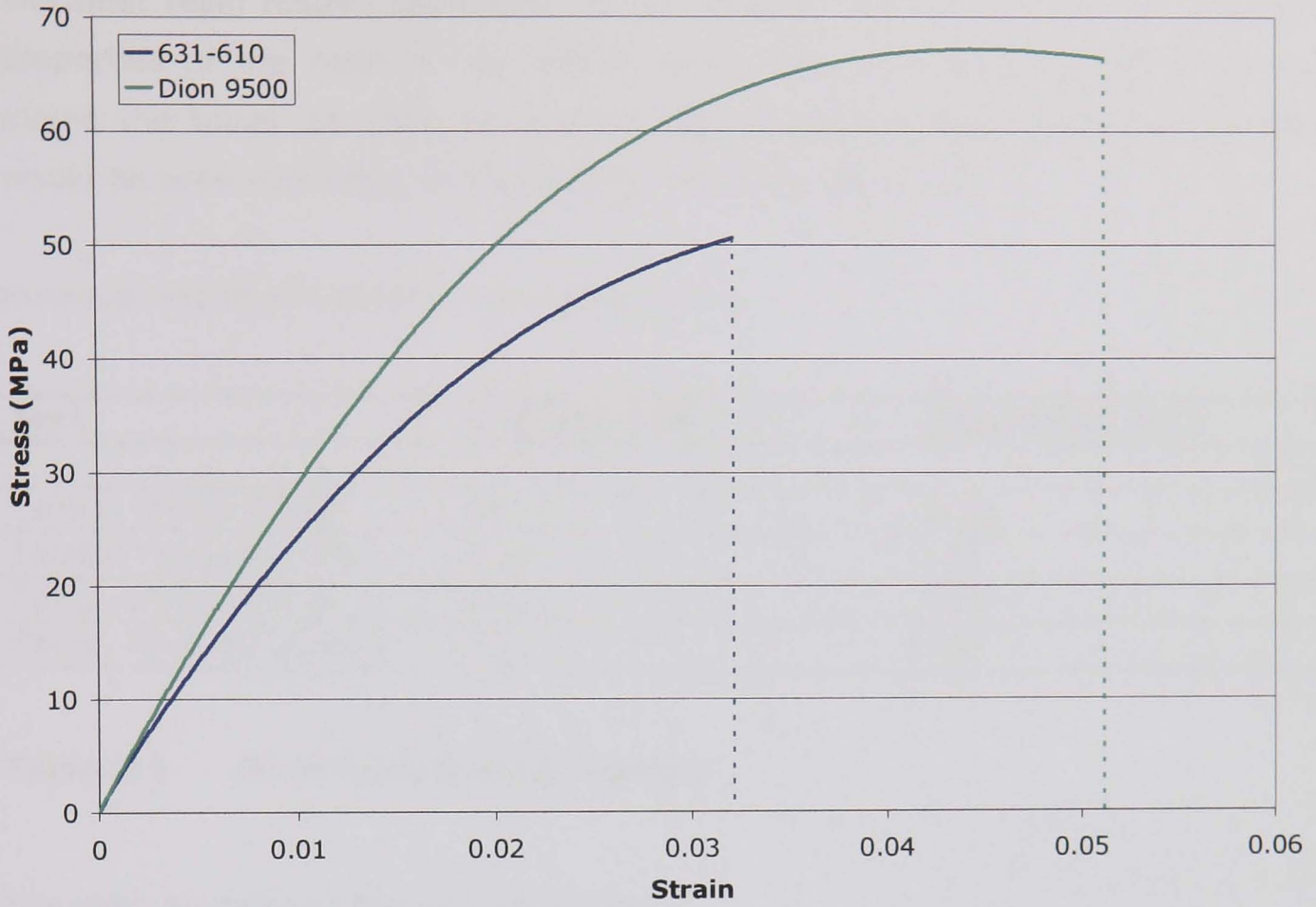

Figure 4:1 In-plane tensile testing results

Compression testing was also undertaken and showed slightly better results for the UP resin (Table 4:1). Specimen bending can affect compressive testing results as seen in Figure 4:2.

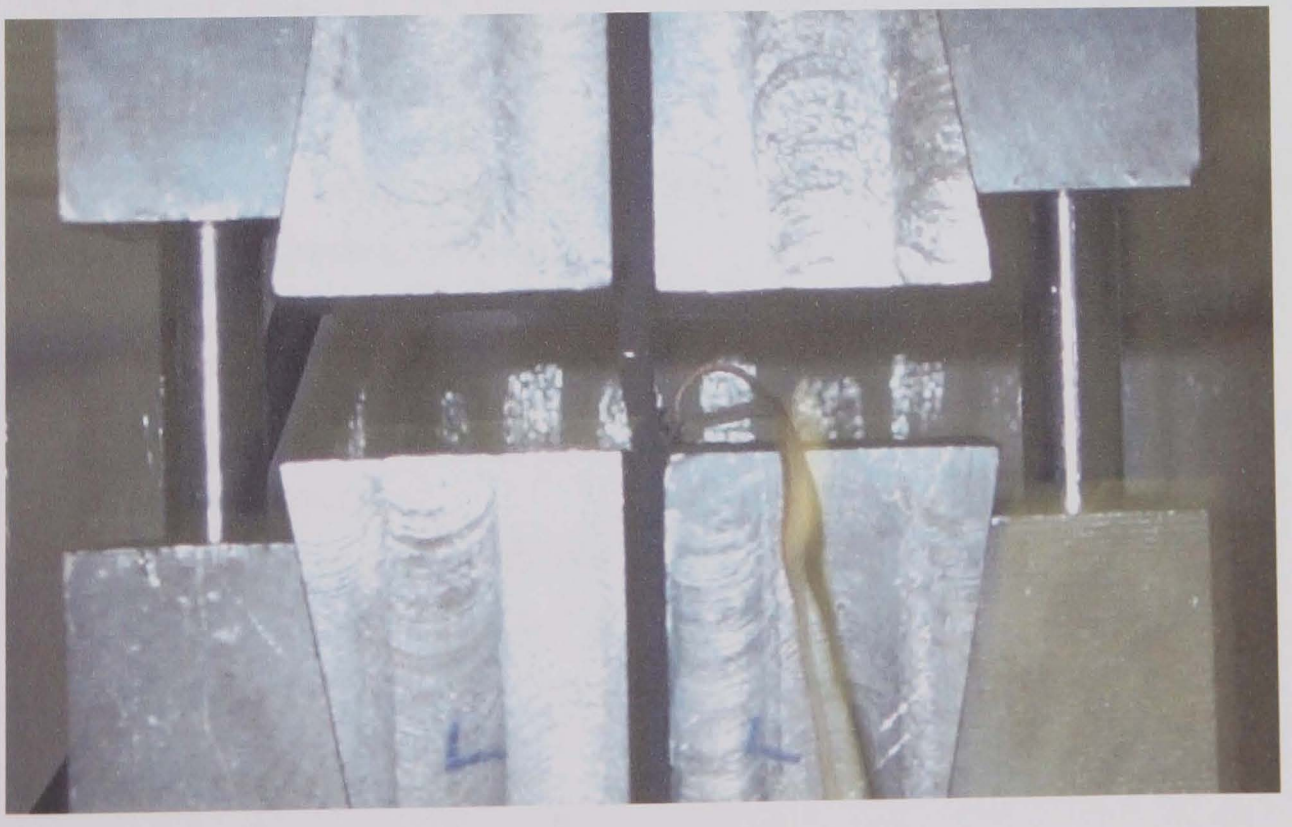

Figure 4:2 Bending level of compressive specimen before failure

The neat resin results show that we are unable to fully replicate the optimum properties of the resin in our tooling using the same process with which we mould the tubes. In order to improve these results proper casting of samples would be used according to the relevant standard (BS 2782)

Average results are shown in the table below.

Test	631-610 (UP)	DION 9500 (VE)
Tensile stress (MPa)	51.13	63.25
Tensile Modulus (GPa)	2.63	2.75
Comp. Stress (MPa)	74.13	71.67
Comp. Modulus (GPa)	3.17	3.39

Table 4:1 Neat resin testing results

The main benefits of the vinylester are;

- Higher tensile and compressive moduli
- Higher Strain to failure

Note that compressive stress in the composite cannot be directly compared to compressive stress in the resin. Good composite compressive properties rely on the prevention of fibre buckling.

There are also other potential benefits to using vinylester not necessarily reflected in this testing such as;

- Improved interfacial adhesion
- Lower residual stresses through lower volume shrinkage (6-7% vs. 9%)
- Lower density
- Low water induced degradation
- Improved fatigue properties

4.2.2 Preliminary crush testing

A tougher matrix was seen as a potential improver of properties and this was accomplished by a variety of means – both in terms of off the shelf resins and the addition of chemicals into the resin mixture. Composite crush testing was used with the CoFRM fibre.

The following resins were tested:

1 420-100 Control (standard polyester RTM resin)
- 1.1 420-100 + 15% low profile additive (PVA) to reduce shrinkage
- 1.2 420-100 + 5% Polycaprolactone – to alter toughness
- 1.3 420-100 + 20% styrene – to alter toughness
- 1.4 420-100 + 20% 420-000 (UP resin) – to alter toughness
- 1.5 420-100 + 20% vinylester (DION 9500) – to alter toughness

2 631-610 control (high T_g polyester RTM resin)
- 2.1 631-610 + 20% vinylester (DION 9500)
- 2.2 631-610 + 5% Dimer acid (Diglycidyl ester) – flexibiliser

3 DION 9500 vinylester (High toughness resin)

4 Epoxy (Scott Bader Crystic epoxy D5316 / D5130)

The conventional polyester resins were used as a benchmark for modifications to the base resins and for the vinylester and epoxy resins. All modifications were done with a view to giving a range of toughness. Guidance on which materials to test came from a variety of sources.

Figures 4:3 to 4:5 show the results of the testing. Average results are shown for 4 specimens from 1 moulding. The vinylester resin can be seen to give increased SEA over the standard UP resin, the epoxy gives even higher SEA. The effect of the additions (1.1 to 1.5 above) was significant with most giving a reduced SEA over the standard resin.

The two UP resins are compared in Figure 4:5. The high T_g 631-610 showed reduced SEA but was necessary for automotive applications. The addition of 20% vinylester increased SEA for both resins.

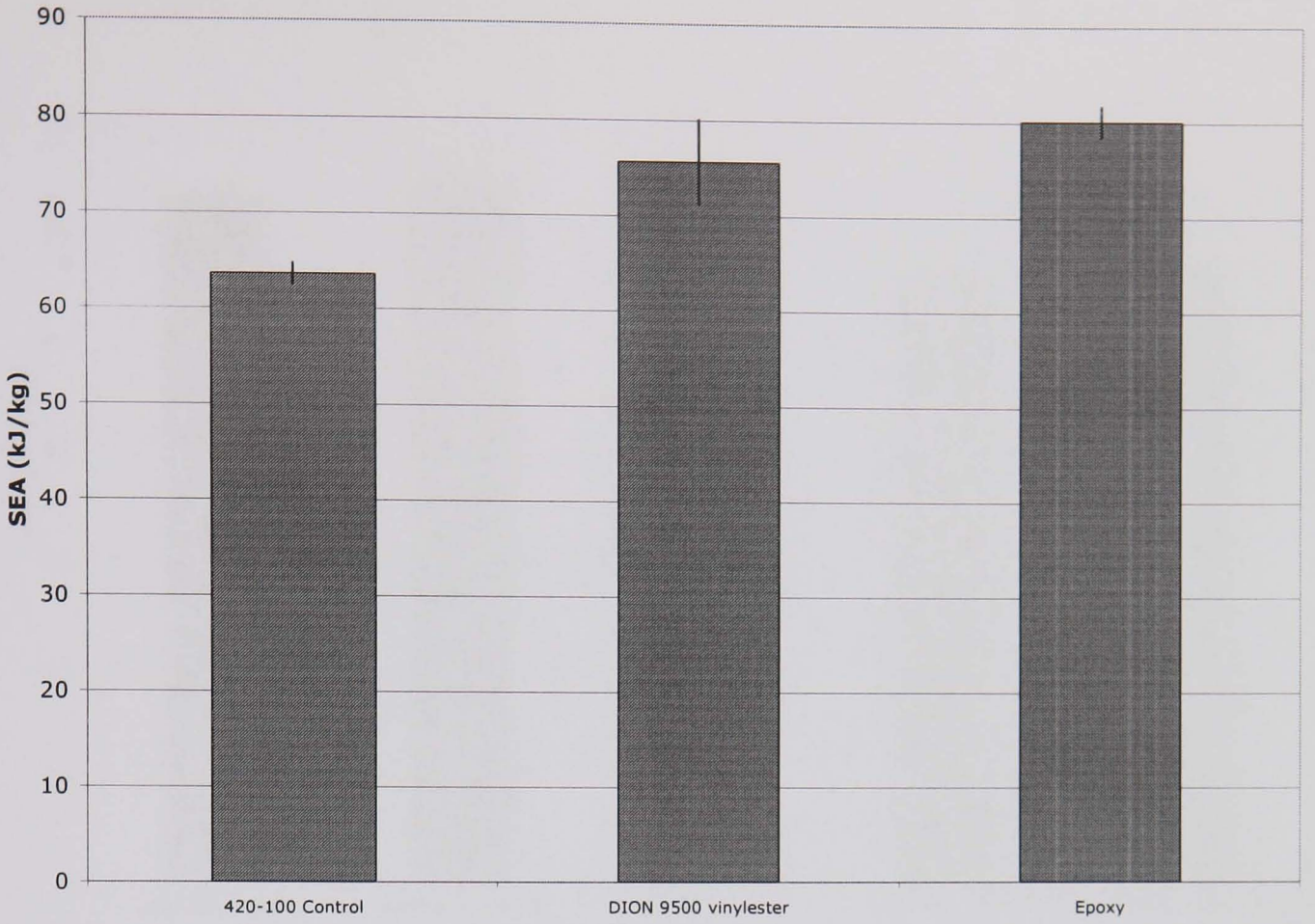

Figure 4:3 Comparison of standard UP, VE and EP resin (specific energy absorption)

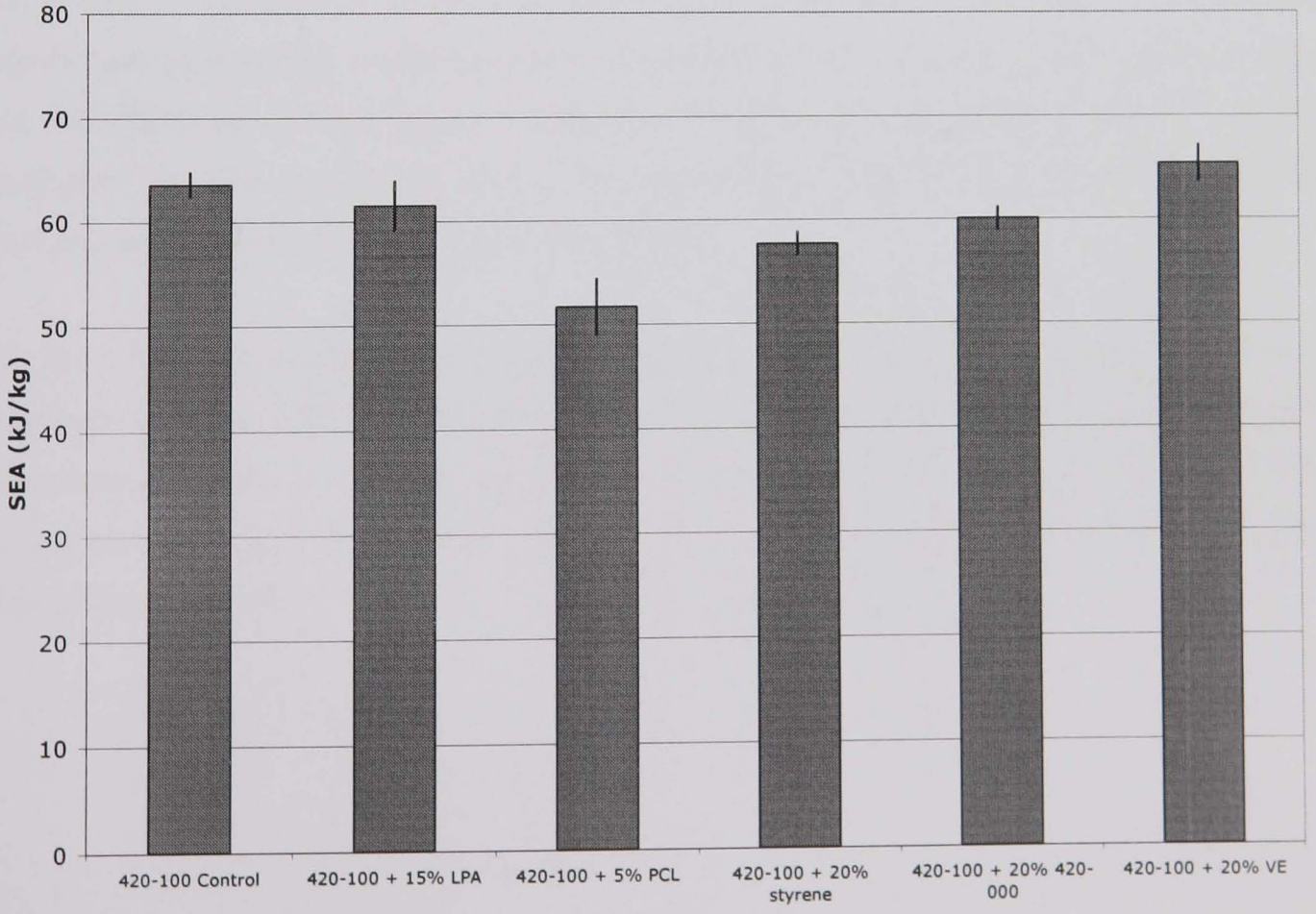

Figure 4:4 Effect on UP control resin of various additions (SEA)

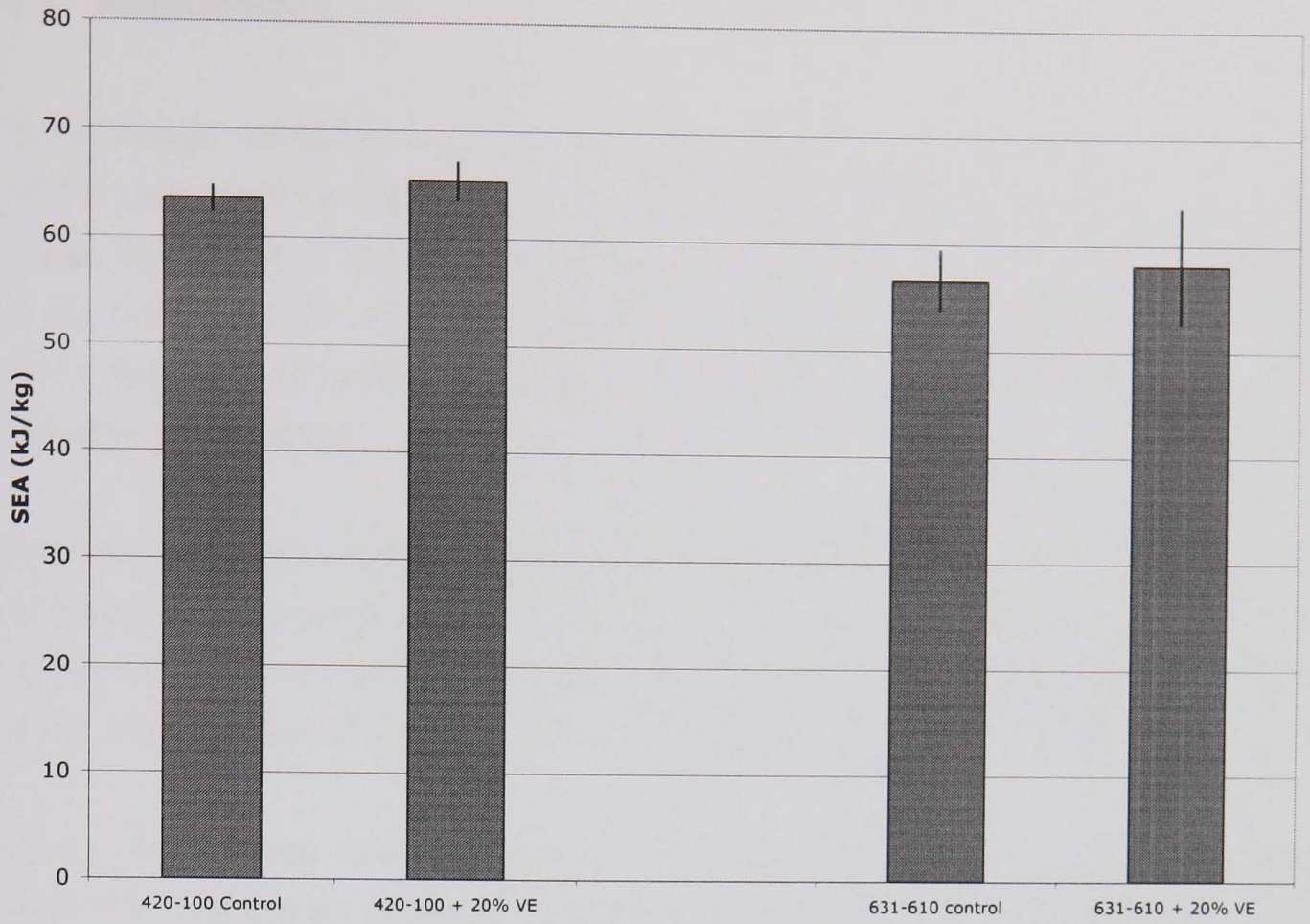

Figure 4:5 Comparison of two UP resins and effect of addition of 20% VE resin

The main conclusions from this work were that the increases given by the vinylester and epoxy matrices were in excess of those which could be expected via modification of existing UP matrices. The main disadvantage of the VE and EP matrices is the increased cost. The increase in SEA was attributed to the increased failure strain energy of the matrix.

At the time of testing the price of epoxy was thought to be prohibitive for medium volume RTM so this was discounted from the main testing. Vinylester was also thought to be too expensive but was included in case such high SEA's could be developed that lower volumes of material could be used, thus offsetting the price increase.

4.3 Methodology

Three design variables were chosen and the resulting experimental design is simple, the variables were chosen to give a range of final properties but also to assess the effect of representative processing conditions on the final properties of the composite. To assess the degree of cure differential scanning calorimetry (DSC) testing was undertaken. The variables were resin type, cure temperature and postcure duration.

The two resins used are compatible and can be mixed together as required. The optimum curing agents are different however as special attention must be given to the minimisation of foaming with the vinylester resin. The objective was to attain a wide range of resin properties using the two resins and a mix.

Figure 4:6 shows the experimental matrix. The effects of the moulding parameters and their effect on the variability of the results were analysed using standard Taguchi techniques [1]. Taguchi analysis is typically used to assess the relative effect of a number of parameters on a response. The technique assumes that the variation of the response with the input parameters is linear. In order to assess the reliability of this assumption with regard to the experimental data it is customary to conduct one test at the centre of the experimental domain. If the response is a linear function of the input parameters the value measured at the centre will be equal to the average of the values obtained at the corners. Configuration R9 (See section 4:4) was used for this purpose; its moulding temperature (60 °C), post-cure time (30 minutes) and resin content (50:50) correspond to the centre of the experimental domain for all parameters (50 ~ 70°C, 0 ~ 60 minutes, 100:0 ~ 0:100 polyester/vinylester content)

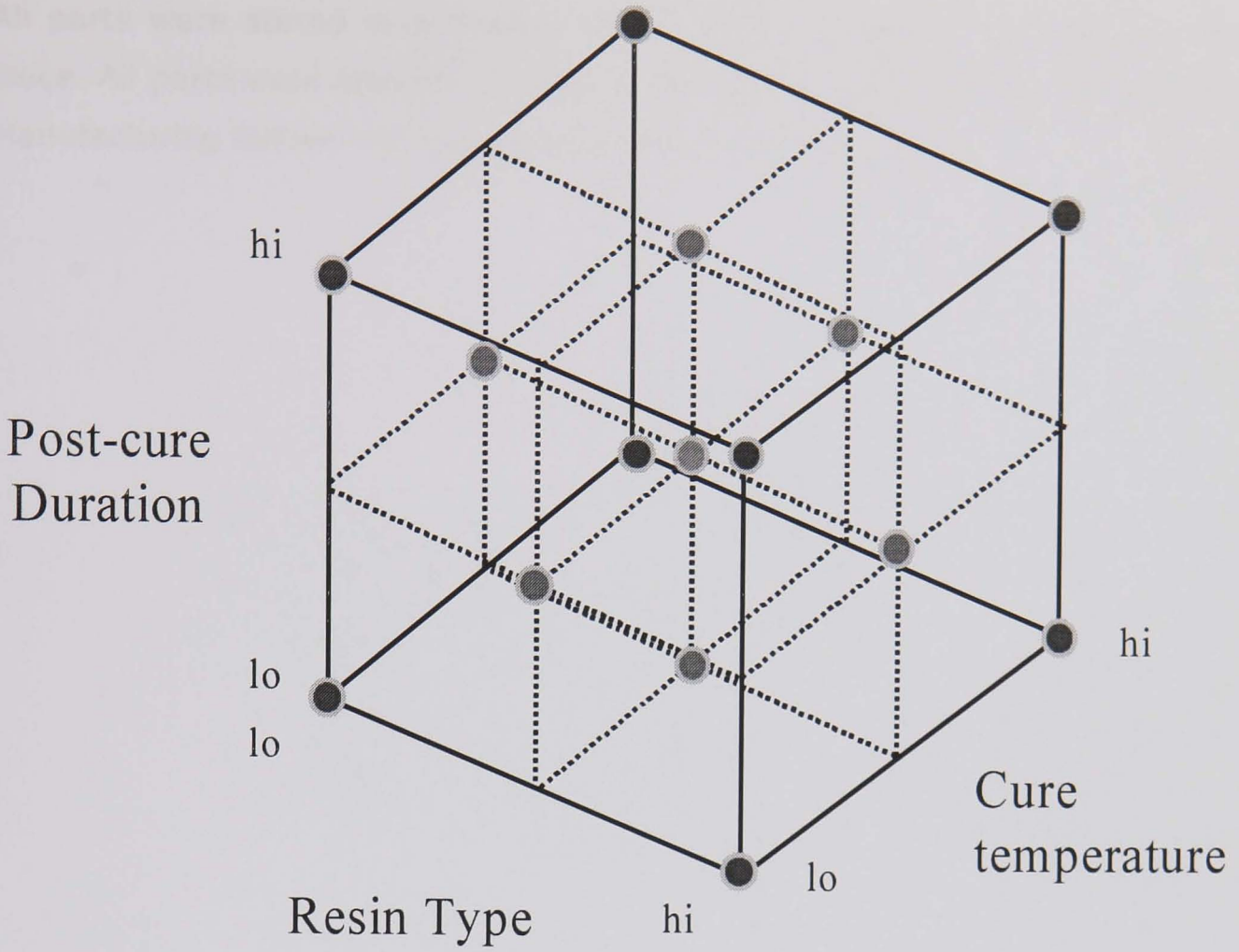

Figure 4:6 Experimental matrix (see also Table 4:2)

The first resin used (631-610) was selected as it is already in use in an automotive crashworthiness application. The vinylester resin was selected as it had very high toughness, which was thought to be beneficial to crush properties. These values were chosen to attain very low cures at one extreme and fully cured parts at the other. The cure temperature was also thought to have an effect on the final degree of cure but also on the processing speed. Higher processing temperatures allow faster manufacturing thus providing cost savings. Cure temperatures of 50 to 70°C were selected based on industrial experience. Postcure duration was chosen to vary between no postcure and 1 hour at 80°C.

Experiments were performed at the extremes of the variable limits giving 8 scenarios plus an additional test with each variable having a central value. Statistical theory shows that if all possible combinations of the variables are tested, as here, the interactions of the variables can also be studied. An interaction is the synergistic effect observed when two parameters are modulated simultaneously, that is, additional change beyond what is expected of the two parameters individually.

All parts were stored in a freezer below −25°C to prevent further cure taking place. All parts were allowed to reach room temperature (25±2°C) before testing. Manufacturing follows the regime documented in Chapter 3.

4.4 Moulding configurations

The moulding configurations were designated R1 to R9 where R9 is the processing condition located at the centre of the experimental domain.

Designation	Cure Temp. (°C)	Postcure Duration (min)	Resin System
R1	50	0	631-610
R2	50	60	631-610
R3	70	0	631-610
R4	70	60	631-610
R5	50	0	DION 9500
R6	50	60	DION 9500
R7	70	0	DION 9500
R8	70	60	DION 9500
R9	60	30	50:50 mix

Table 4:2 Moulding configurations

Tube Crush

- 9 configurations
- 3 moulding repeats (3 separate tube mouldings)
- 4 crush samples cut from each moulding
- 108 tests

In-plane Tension, Compression and Shear

- 11 configurations (including 2 neat resin)
- 1 plaque per configuration
- samples per plaque (3x0°, 3x90°)
- 198 tests

DCB Testing

- 9 Configurations
- 1 small plaque moulding (90 x 250mm)
- 3 samples per plaque
- 27 tests

DSC Testing

- 9 Configurations

- 3 tube repeats
- samples per tube (3 repeats each end)
- 162 tests

The following table shows the catalyst and accelerator levels used for each resin system at the different temperatures. The values are based entirely on data supplied by Reichhold UK. The 631-610 system is pre-accelerated and does not require the addition of cobalt.

Resin System	Cure Temperature	Catalyst	Catalyst % wt.	Cobalt /phr.
631-610	All (R1-R4)	Trigonox 44B	1	N/A
631-610	50 deg C	Butanox LPT	2	0
DION 9500	50 deg C	Butanox LPT	1.5	0.5
631-610/9500	50 deg C	Butanox LPT	1.5	0.25
631-610	60 deg C	Trigonox K-80	2.5	0.2
DION 9500	60 deg C	Trigonox K-80	1.5	0.5
631-610/9500	60 deg C	Trigonox K-80	2	0.25
631-610	70 deg C	Trigonox 141	2	0
DION 9500	70 deg C	Trigonox 141	1	0.5
631-610/9500	70 deg C	Trigonox 141	2	0.25

Table 4:3 Curing systems used for tested resins at all moulding temperatures

4.5 Axial tube crush results

Overall crush results for the CoFRM fibre architecture appear in Table 4:4 below, repeats a, b & c occupy separate rows and the different samples along the length of the tube appear in the four columns. Average SEA's for each moulding are given along with the standard deviation.

Tube ref.	SEA A	SEA B	SEA C	SEA D	Av. SEA	st. dev.
R1a	21.91	18.71	29.41	31.47	25.37	6.1
R1b	33.87	37.32	26.46	35.01	33.17	4.7
R1c	36.52	30.98	37.55	42.76	36.95	4.8
R2a	63.40	61.17	56.78	62.69	61.01	3.0
R2b	62.52	62.36	N/A	59.61	61.50	1.6
R2c	51.98	46.64	51.90	56.28	51.70	3.9
R3a	38.01	21.40	15.83	25.79	25.26	9.4
R3b	40.07	18.93	12.21	21.47	23.17	11.9
R3c	34.24	22.79	21.01	23.25	25.32	6.0
R4a	54.93	47.67	33.64	55.41	47.91	10.2
R4b	58.41	49.61	36.87	52.06	49.24	9.0
R4c	57.62	28.06	11.90	26.23	30.95	19.2
R5a	24.08	39.43	37.54	27.50	32.14	7.5
R5b	43.13	48.72	45.58	34.35	42.94	6.2
R5c	36.39	39.81	39.07	33.42	37.17	2.9
R6a	77.36	79.16	77.36	76.01	77.47	1.3
R6b	76.12	78.50	76.08	74.30	76.25	1.7
R6c	78.61	76.20	77.52	76.90	77.31	1.0
R7a	76.84	78.65	83.46	76.27	78.80	3.3
R7b	67.53	81.90	76.32	76.92	75.67	6.0
R7c	59.09	78.33	77.63	78.40	73.36	9.5
R8a	80.65	81.48	79.35	73.49	78.74	3.6
R8b	80.28	83.08	77.47	76.34	79.29	3.0
R8c	75.26	77.54	77.63	72.84	75.82	2.3
R9a	76.23	73.43	65.51	69.51	71.17	4.7
R9b	70.79	72.48	70.63	68.48	70.59	1.6
R9c	72.15	70.58	67.42	67.48	69.41	2.3

Table 4:4 Overall SEA results

Figure 4:7 and Table 4:5 below show the repeat averages for R1 to R9. Error bars denote the range of values obtained for each moulding configuration (3 tubes and 4 samples per tube). The variations are high as there are significant differences between mouldings as well as between configurations. Inter- and Intra- moulding variations are higher in under-cured samples.

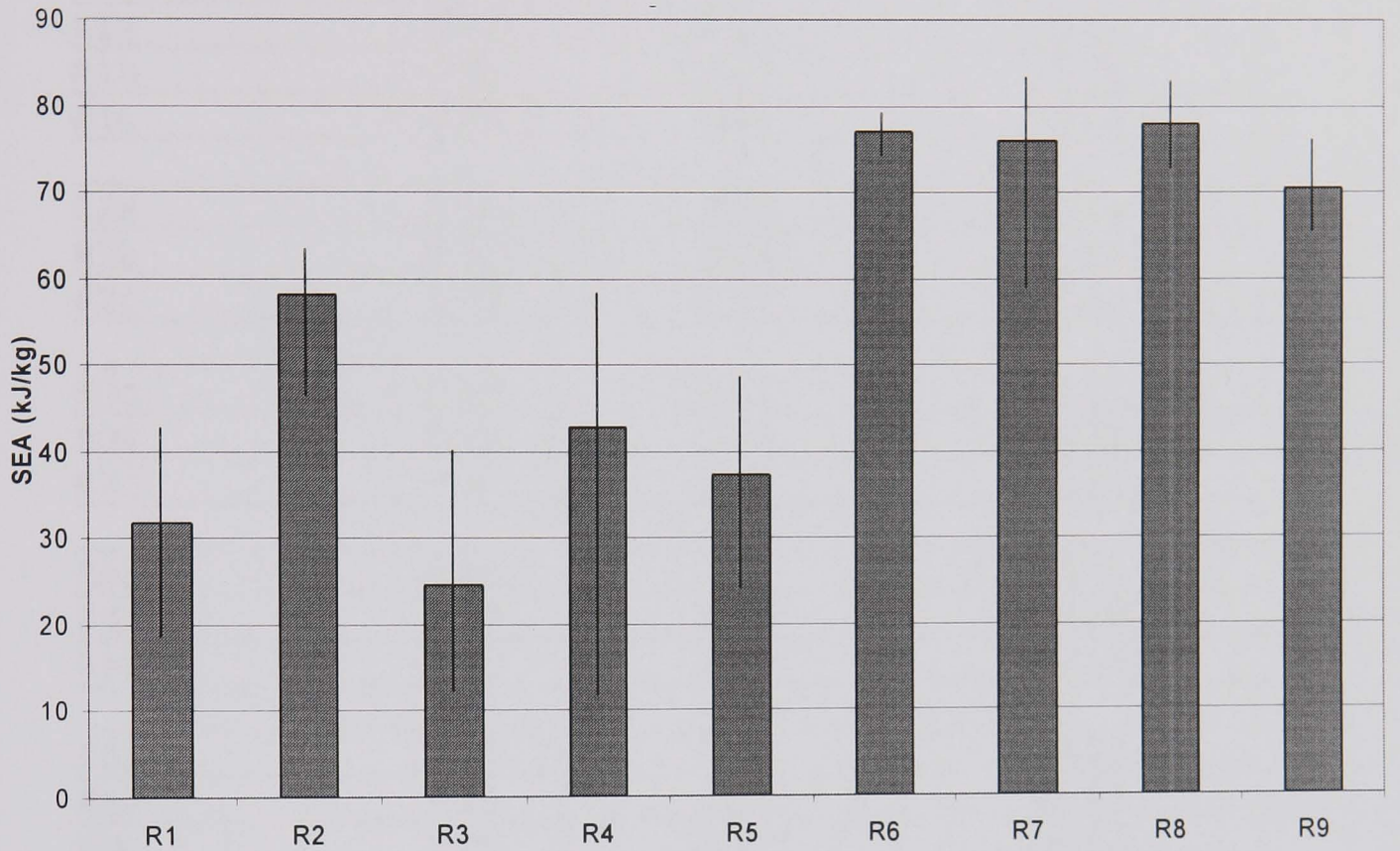

Figure 4:7 Overall average SEA values (error bars show range)

	SEA	st dev
R1	31.8	5.9
R2	58.1	5.5
R3	24.6	1.2
R4	42.7	10.2
R5	37.4	5.4
R6	77.0	0.7
R7	75.9	2.7
R8	77.9	1.9
R9	70.4	0.9

Table 4:5 Average SEA values

In general, vinylester tubes (R5 to R8) show significantly better performance in crush than polyester tubes (R1 to R4); this is best demonstrated by comparing the optimal configurations R2 and R8. The average SEA for configuration R9,

where the two resins were mixed at 50:50, falls approximately midway between the optimal results obtained with the two resins.

Tube designation	Av-to-peak ratio	Steady-state crush variability	Onset stiffness
	Dimensionless	st dev	kN/mm
R1a	0.83	3.05	12.91
R1b	0.75	3.23	16.35
R1c	0.90	2.24	19.07
R2a	0.90	3.85	28.88
R2b	0.92	3.26	25.69
R2c	0.91	2.85	23.12
R3a	0.89	2.12	10.79
R3b	0.33	2.38	12.68
R3c	0.91	1.31	15.22
R4a	0.89	3.81	19.66
R4b	0.92	1.95	20.98
R4c	0.78	4.87	15.12
R5a	0.77	0.97	16.28
R5b	0.91	2.35	21.83
R5c	0.88	1.22	16.69
R6a	0.93	3.78	29.00
R6b	0.92	3.60	29.04
R6c	0.94	3.26	30.89
R7a	0.93	3.49	31.08
R7b	0.89	6.47	37.70
R7c	0.83	13.35	34.26
R8a	0.92	4.09	31.90
R8b	0.92	4.06	31.34
R8c	0.92	3.82	34.06
R9a	0.92	4.24	30.49
R9b	0.92	3.95	31.23
R9c	0.94	2.76	31.41

Table 4:6 Load displacement curve features

In general the variability is much higher where the mouldings are not subjected to a postcure as small differences in the moulding time lead to large differences in cure level. These differences are normally mitigated by the postcure. R4 is the

exception to this rule, the difference being caused by catalyst breakdown at the high moulding temperature.

Table 4:6 shows the results of efforts made to analyse the actual curve to see if any major differences between the various configurations can be found. The SEA calculation averages the load-displacement curve and may therefore miss important points of interest. Figure 4:8 displays the factors of interest. The following factors were studied:

- Curve average to peak ratio (Mean load / Peak load)
- Steady state crush variability (Standard deviation of load points from 10mm to 50mm of crush)
- Initial / onset stiffness (The effective stiffness whilst the trigger is crushing)

The last of these relies on a degree of interpretation of the data as it is the inclination of the line from the origin to the top of the initial peak. On occasion the origin does not coincide with the base of the line and has been adjusted to show the true modulus. This analysis fails to give any real new information and is subject to considerable errors. All three factors follow the same trend which closely approximates the SEA results.

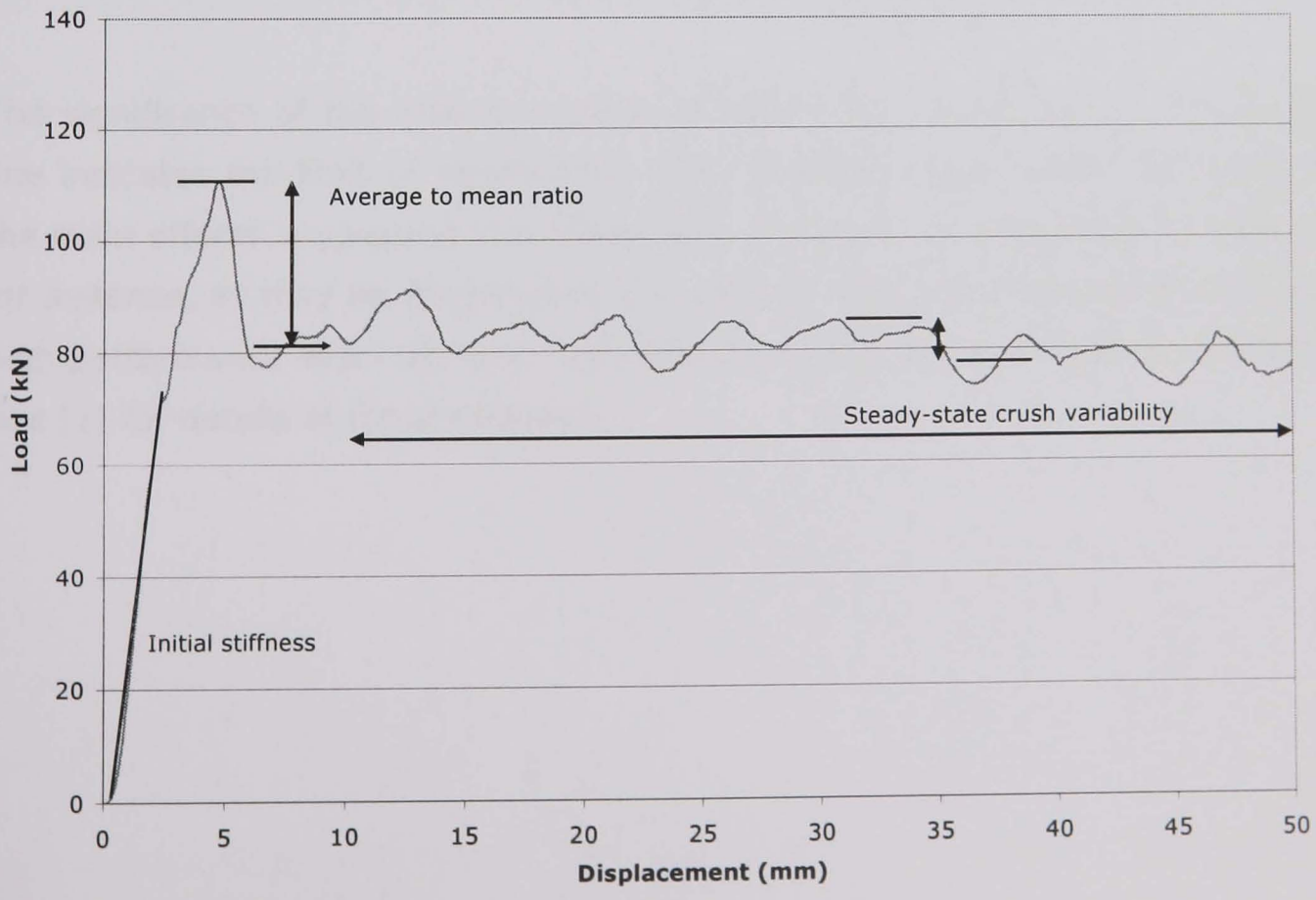

Figure 4:8 Crush curve features

4.5.1 Statistical analysis

The analysis below is performed for the first 8 samples (i.e. excluding R9) to reduce the problem to a simple 2-level full factorial design. Initially the 96 data points (Four samples from each of three mouldings for 8 configurations) were analysed for main effects to show where the differences in SEA come from. This is shown below in Figure 4:9. The graph shows that the resin choice is the most significant factor closely followed by postcure. Temperature is much less significant.

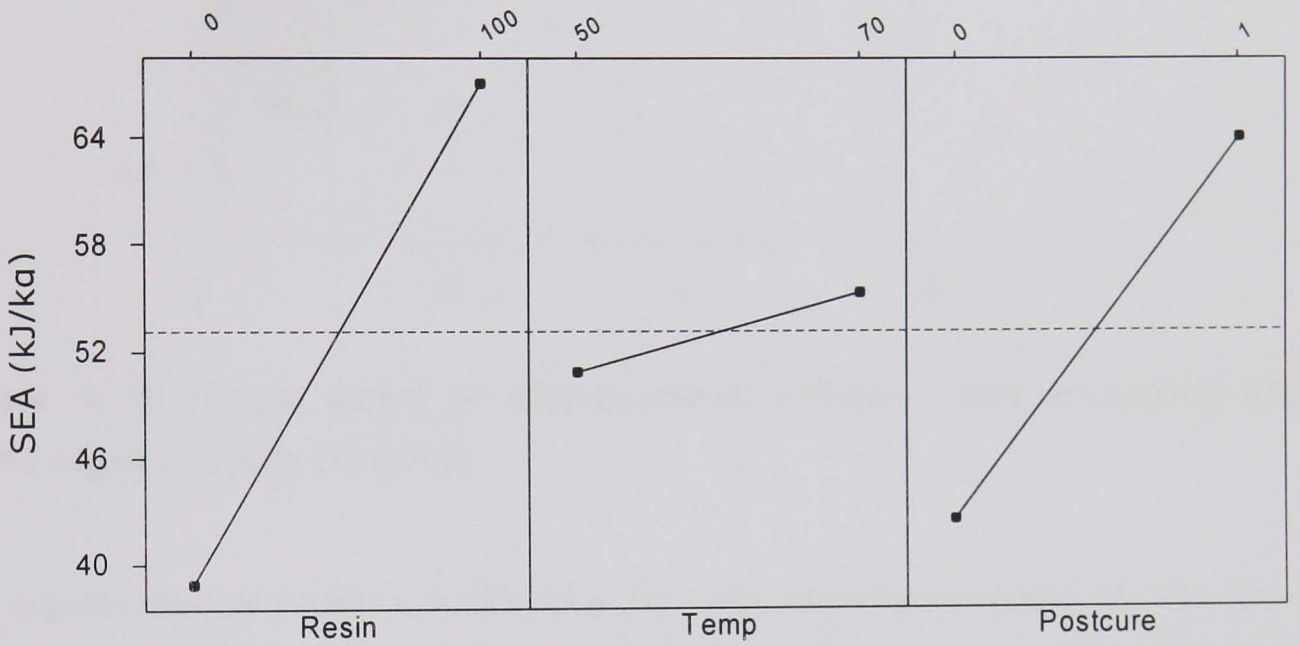

Figure 4:9 Main Effects plot – Data means for SEA (CoFRM)

The significance of the effects is shown in the Pareto chart below. The dashed line indicates the limit of significance. The interactions are almost as strong as the main effects suggesting that single factors cannot be considered in isolation, for instance, as may be conjectured it is unlikely that a high temperature curing high performance resin will give high SEA if it is not cured at high temperature. See [1] for details of these methods.

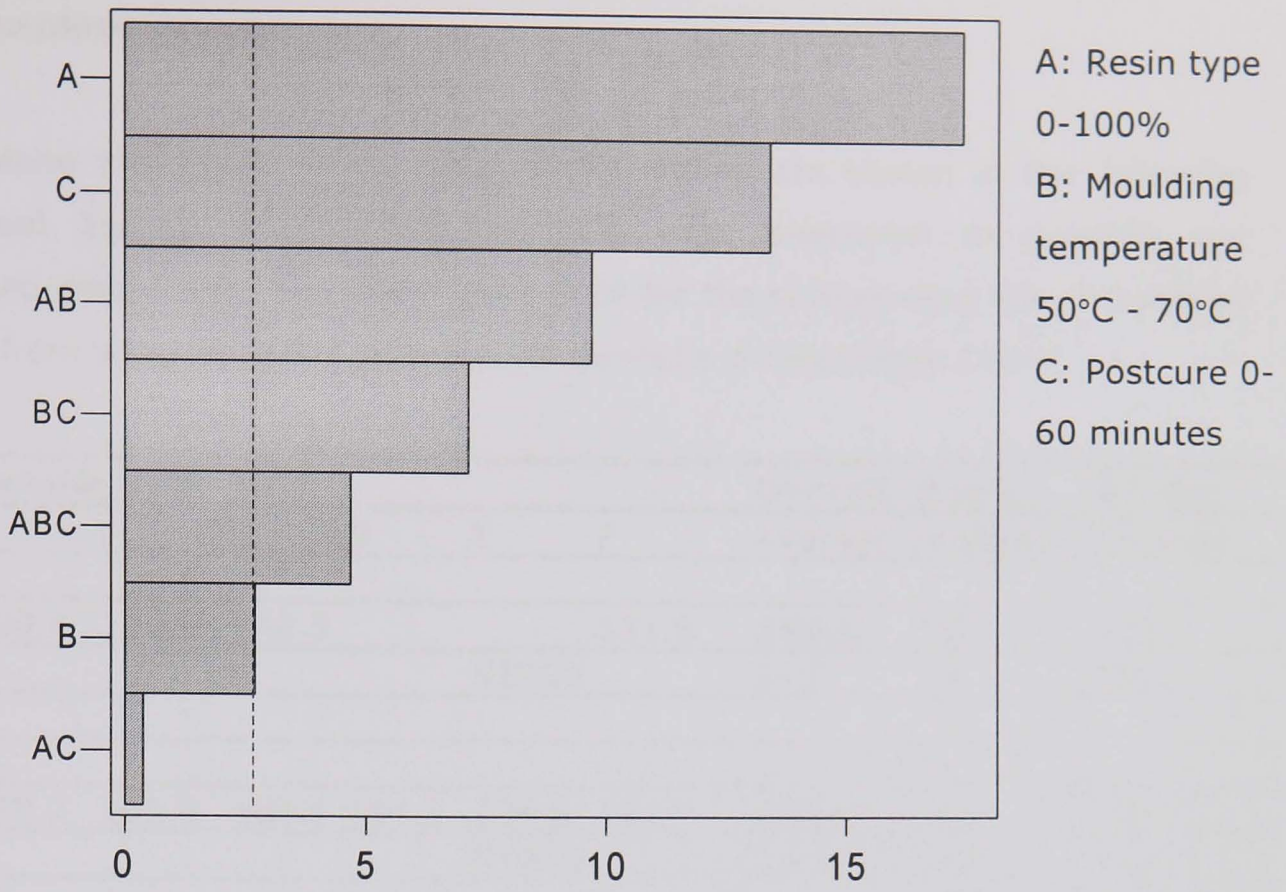

Figure 4:10 Pareto chart of standardised effects : SEA at alpha=0.01 (99% significance) (CoFRM)

The significance of location in the tool has also been investigated for the same set of samples. The effect of both repeat and position is low compared to the parameters of interest. On average a slight decrease in SEA along the length of the tube can be seen although the significance is low.

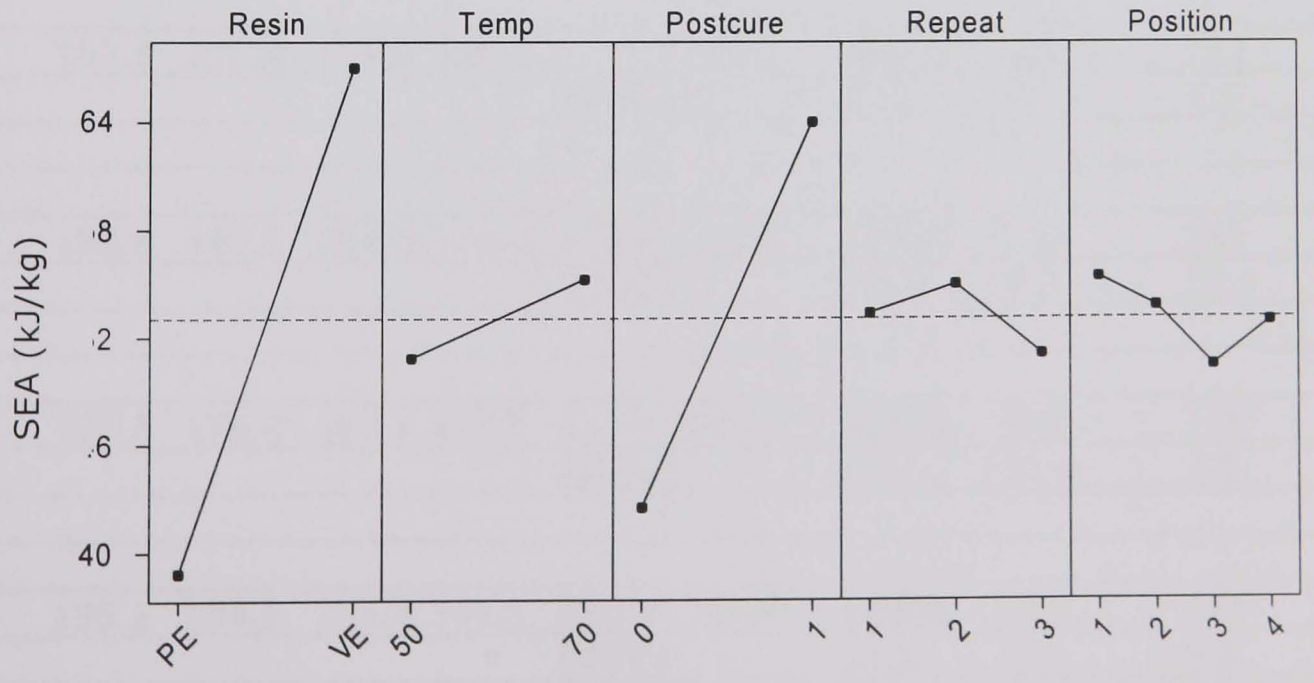

Figure 4:11 Main Effects plot including effect of moulding repeat and position in tool (CoFRM)

4.5.2 In-plane results

The in-plane properties of the nine configurations are shown in the following tables and figures. 0 and 90° directions were measured to quantify any anticipated differences. See also Figure 3:18 for the cutting diagram. 0° average is taken from samples A to C and the 90° average is taken from D to F

	Tensile UTS MPa						**Overall**	**0 deg.**	**90 deg.**
	A	B	C	D	E	F	Average	Average	Average
R1	160.4	162.0	148.5			131.6	**150.6**	157	132
					STDEV		14.0	7.4	n/a
R2	138.7	161.9	154.6	124.3	136.5	121.7	**139.6**	152	128
					STDEV		16.0	11.8	7.9
R3	94.8	104.8	101.1	81.0	79.8	79.0	**90.1**	100	80
					STDEV		11.6	5.1	1.0
R4	161.8	174.8	191.3	139.7	129.5	143.0	**156.7**	176	137
					STDEV		23.5	14.8	7.0
R5	161.7	153.9	174.1	134.9	119.2	137.3	**146.8**	163	130
					STDEV		20.1	10.2	9.8
R6	183.3	217.6	194.6	161.9		162.3	**183.9**	198	162
					STDEV		23.5	17.5	0.3
R7	188.8	199.5	204.5	174.3	156.8	154.9	**179.8**	198	162
					STDEV		21.2	8.0	10.7
R8	193.3	170.4	183.1	179.0	173.5	180.3	**180.0**	182	178
					STDEV		8.0	11.4	3.6
R9	195.1	184.6	185.3	149.5	155.6	142.4	**168.8**	188	149
					STDEV		22.2	5.9	6.6

Table 4:7 CoFRM in-plane Tensile UTS

	Tensile Modulus			GPa			Overall	0 deg.	90 deg
	A	B	C	D	E	F	Average	Average	Average
R1	9.5	8.4	7.8			6.8	**8.1**	8.6	6.8
					STDEV		1.1	0.6	n/a
R2	11.2	11.0	11.4	8.1	9.4	8.8	**10.0**	11.2	8.8
					STDEV		1.4	0.2	0.2
R3	6.4	7.6	7.5	4.9	5.7	5.7	**6.3**	7.2	5.4
					STDEV		1.1	0.7	0.5
R4	9.7	11.0	11.5	7.9	7.9	8.3	**9.4**	10.7	8.0
					STDEV		1.6	0.9	0.2
R5	8.3	8.5	9.6	7.0	6.5	7.8	**7.9**	8.8	7.1
					STDEV		1.1	0.7	0.6
R6	10.9	11.6	12.3	9.0		9.7	**10.7**	11.6	9.4
					STDEV		1.3	0.7	0.5
R7	10.7	10.7	10.8	8.9	9.2	8.6	**9.8**	10.7	8.9
					STDEV		1.0	0.0	0.3
R8	11.2	11.0	10.7	10.0	10.1	11.2	**10.7**	11.0	10.4
					STDEV		0.5	0.3	0.7
R9	10.3	9.9	8.6	11.0	8.9	9.1	**9.6**	10.4	8.9
					STDEV		0.9	0.6	0.2

Table 4:8 CoFRM in-plane tensile modulus

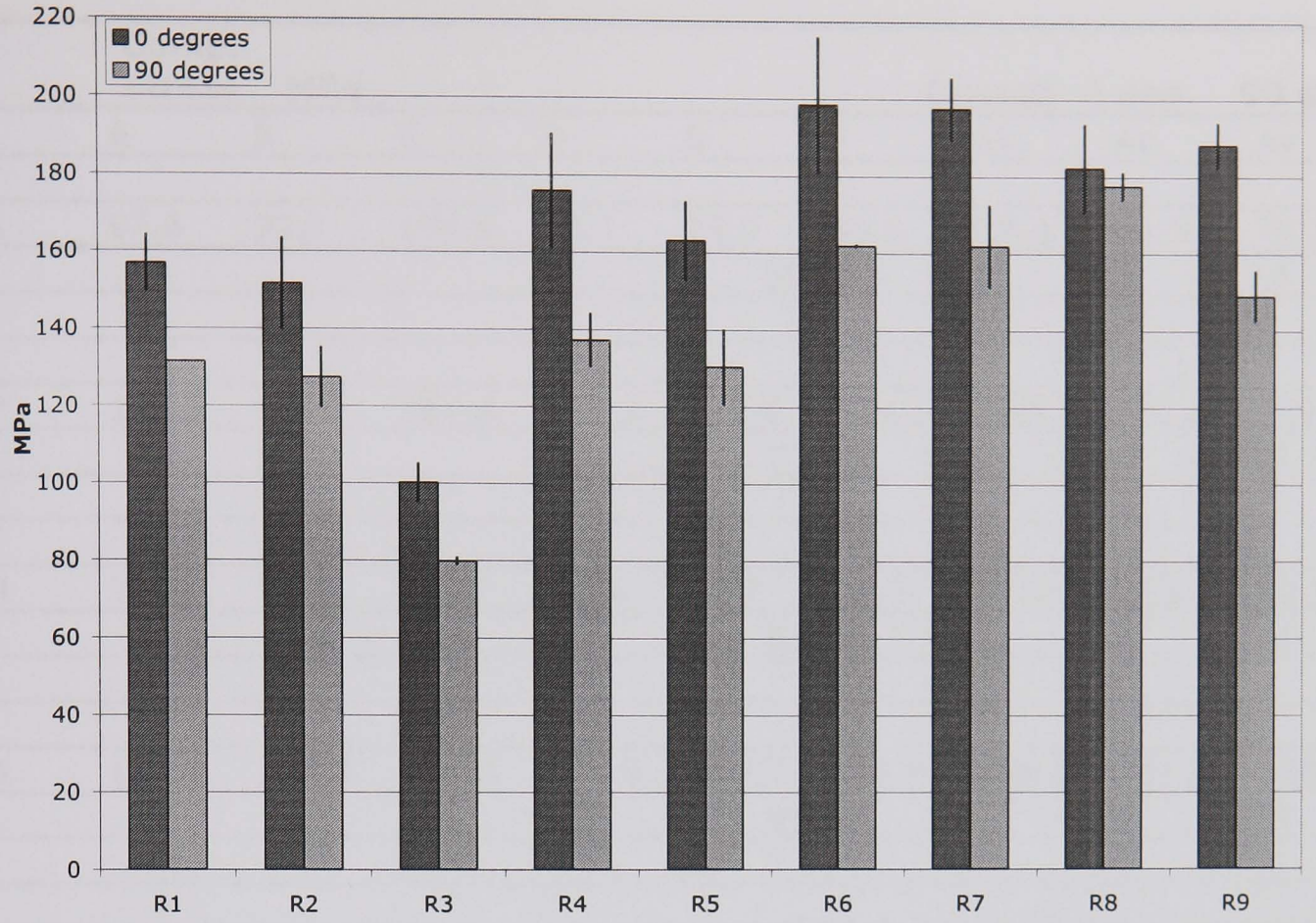

Figure 4:12 CoFRM in-plane ultimate tensile stress

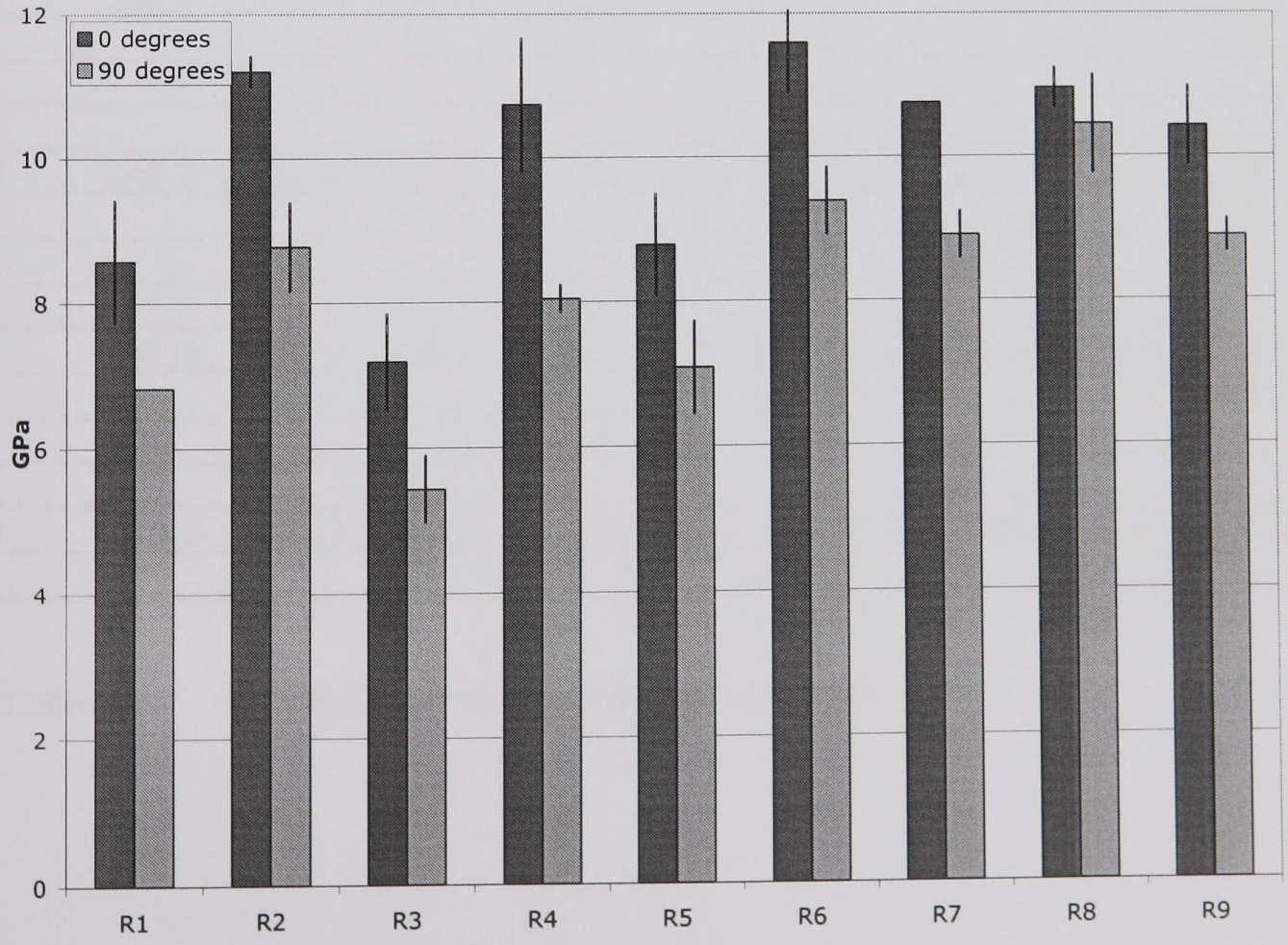

Figure 4:13 CoFRM in-plane tensile modulus

	Comp. Stress MPa						Overall	0 deg.	90 deg.
	A	B	C	D	E	F	Av.	Av.	Av.
R1	97.6	92.1	108.8	81.1	76.0	80.6	**89.4**	99.5	79.3
						STDEV	14.0	8.6	3.6
R2	173.0	195.7	167.8	166.3	158.6	153.3	**169.1**	178.8	159.4
						STDEV	8.7	8.3	4.1
R3	36.6	31.1	34.0	31.9	31.7	28.0	**32.2**	33.9	30.5
						STDEV	9.0	8.0	7.3
R4	151.9	150.3	131.5	128.5	130.5	126.5	**136.5**	144.5	128.5
						STDEV	8.4	7.8	1.5
R5	85.9	90.9	78.2	73.8	72.5	69.7	**78.5**	85.0	72.0
						STDEV	10.5	7.5	2.9
R6	186.0	190.9	192.0	173.2	164.3	182.2	**181.4**	189.6	173.2
						STDEV	6.0	1.7	5.2
R7	148.0	166.4	176.1	157.2	167.6	168.5	**164.0**	163.5	164.4
						STDEV	6.0	8.7	3.8
R8	181.0	174.3	182.7	191.1	169.8	184.3	**180.5**	179.3	181.7
						STDEV	4.2	2.5	6.0
R9	158.3	160.9	168.2	151.2	164.5	158.9	**160.3**	162.5	158.2
						STDEV	3.6	3.2	4.2

Table 4:9 CoFRM in-plane compressive stress

	Comp. Modulus GPa						Overall	0 deg.	90 deg
	A	B	C	D	E	F	Av.	Av.	Av.
R1	8.6	6.9	8.7	7.8	10.0	10.0	**8.7**	8.1	9.3
						STDEV	13.8	12.1	13.4
R2	12.0	13.3	13.5	11.0	10.1	11.7	**11.9**	12.9	10.9
						STDEV	11.0	6.6	7.1
R3	7.2	11.7	10.2	8.5	7.8	6.4	**8.6**	9.7	7.6
						STDEV	23.1	23.6	14.3
R4	11.0	14.3	13.8	11.5	9.7	13.2	**12.2**	13.0	11.5
						STDEV	14.7	13.7	15.3
R5	9.9	8.5	8.5	6.4	7.0	6.7	**7.8**	9.0	6.7
						STDEV	17.5	9.1	4.5
R6	11.2	12.0	12.8	10.1	9.8	9.6	**10.9**	12.0	9.8
						STDEV	11.9	7.0	2.5
R7	10.9	12.1	11.9	9.7	9.3	9.0	**10.5**	11.6	9.3
						STDEV	12.7	5.4	4.0
R8	13.7	12.5	12.0	10.9	12.5	12.6	**12.4**	12.7	12.0
						STDEV	7.4	6.7	8.2
R9	12.4	11.7	11.9	11.1	11.7	12.8	**11.9**	12.0	11.9
						STDEV	4.9	2.9	7.2

Table 4:10 CoFRM in-plane compressive modulus

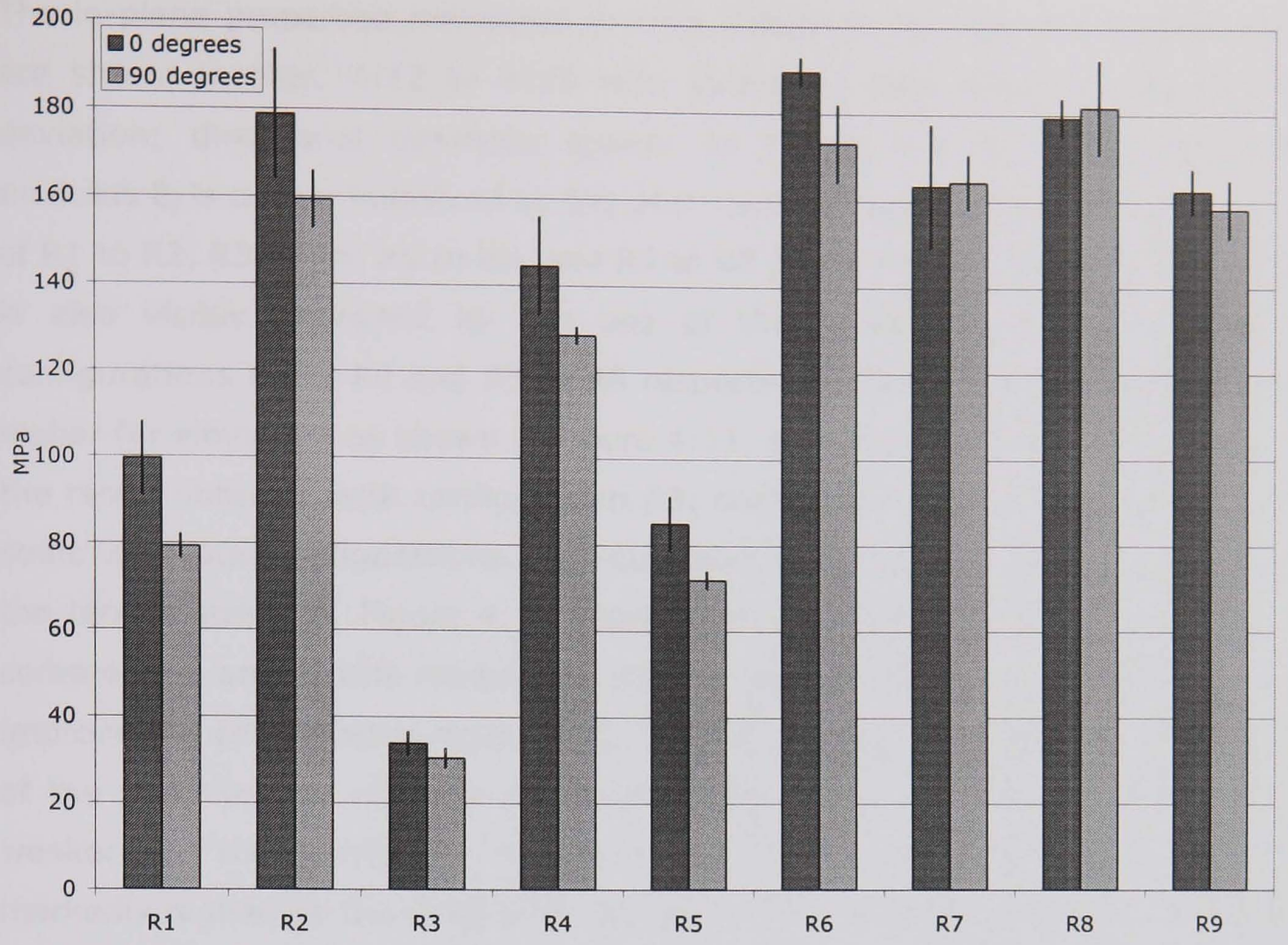

Figure 4:14 Ultimate Compressive Stress

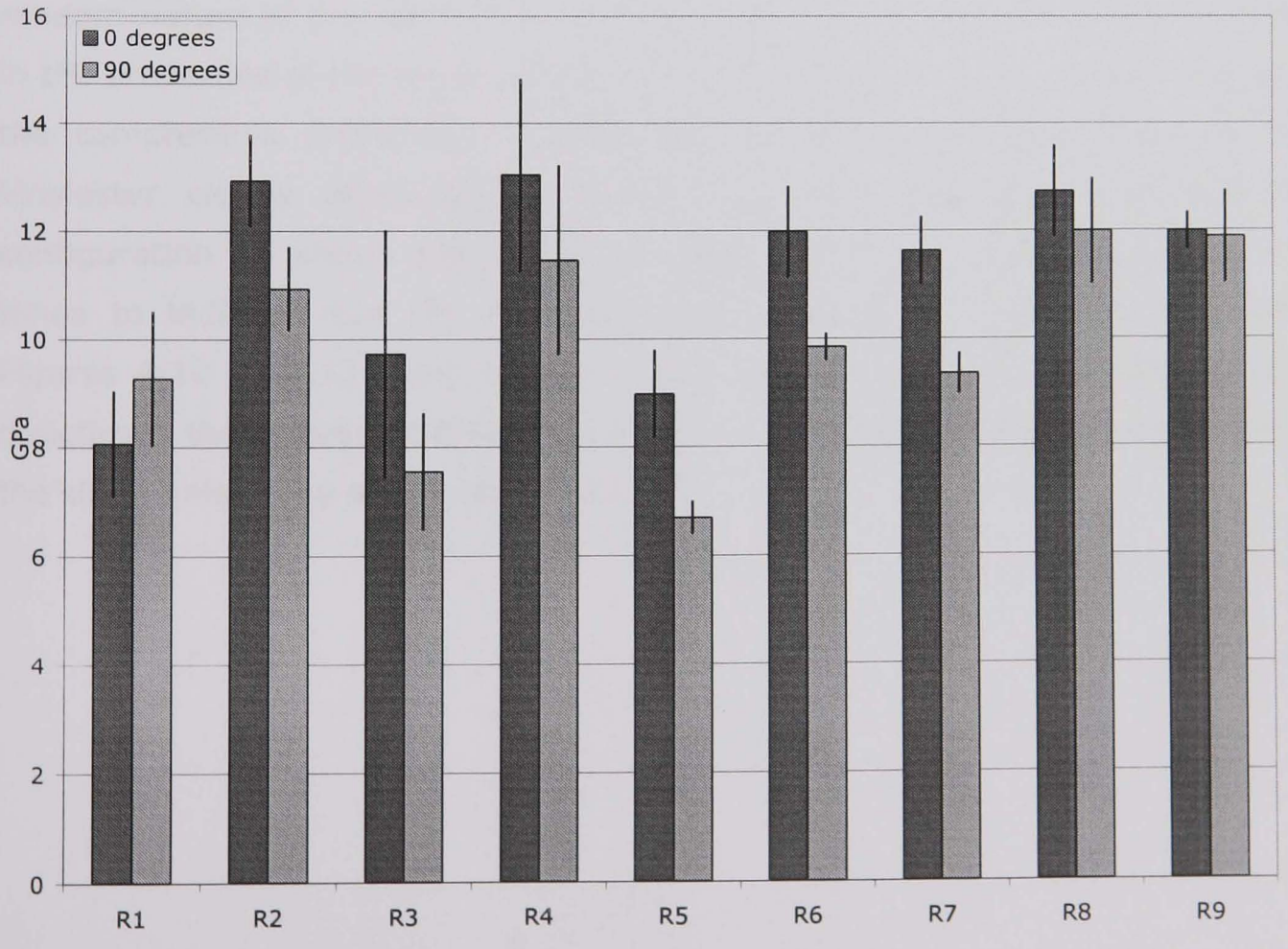

Figure 4:15 Compressive Modulus

The in-plane properties measured in both directions for the nine configurations are shown in Figs. 4:12 to 4:15 with variability bars denoting the standard deviation; directional averages appear in Tables 4:7 to 4:10. The tensile modulus E_t is clearly improved by the post-cure as seen by comparing the results of R1 to R2, R3 to R4, R5 to R6, and R7 to R8 (Figure 4:13). The tensile modulus is also visibly improved by the use of the vinylester resin as shown by configurations R1 to R4 and R5 to R8 respectively. The ultimate tensile stress is higher for vinylester as shown in Figure 4:11, although this trend is partly due to the result obtained with configuration R3; configuration R4 actually outperforms some vinylester configurations. Post-cure also has a generally beneficial effect on the tensile strength. Figure 4:15 shows that the effect of the post-cure on the compressive and tensile moduli are similar; however a change in resin does not improve the compressive modulus E_c. Finally, Figure 4:14 shows a strong effect of the post-cure on ultimate compressive strength UCS although this effect is weaker for the vinylester moulded at 70°C. The compressive strength is markedly higher for the vinylester. Temperature effects are present in individual cases but even out overall.

Tensile properties are affected by the properties of the resin because of the random nature of the reinforcement. However, Figure 4:25 shows that changes in the properties of the resin, especially through post-cure, have more impact on the compressive properties, notably the ultimate compressive strength. The vinylester clearly offers higher tensile stress and modulus. The fact that configuration R4 shows high tensile properties but poor SEA (See Figure 4:7) tends to indicate that the relationship between these properties is weaker. Figures 4:10 to 4:13 show that the above trends are similar in both material directions; the consistent difference observed for both directions is explained by the slight anisotropy of the reinforcement.

4.5.3 Interlaminar Mode-I testing results

The curves for R1 and R5 were not used to generate G_{Ic} data (see below). R6 had the highest stiffness and equal highest fracture toughness with R9. The vinylester samples all perform significantly better than the polyester ones, it would also appear that the 50:50 mix retains vinylester's good fracture toughness properties.

As the table shows, the lowest cure level specimens failed to test due to insufficient bending strength in the beams. The picture over shows the effect (Figure 4:17). The modulus is so low in the beams that they bend before any crack growth occurs, when this happens it can no longer be considered a valid test. The R1DC sample was tested after overnight room temperature cure.

The average improvement through using the vinylester is around 30 to 40%. This is roughly the same improvement percentage seen in SEA values (See Figure 4:7).

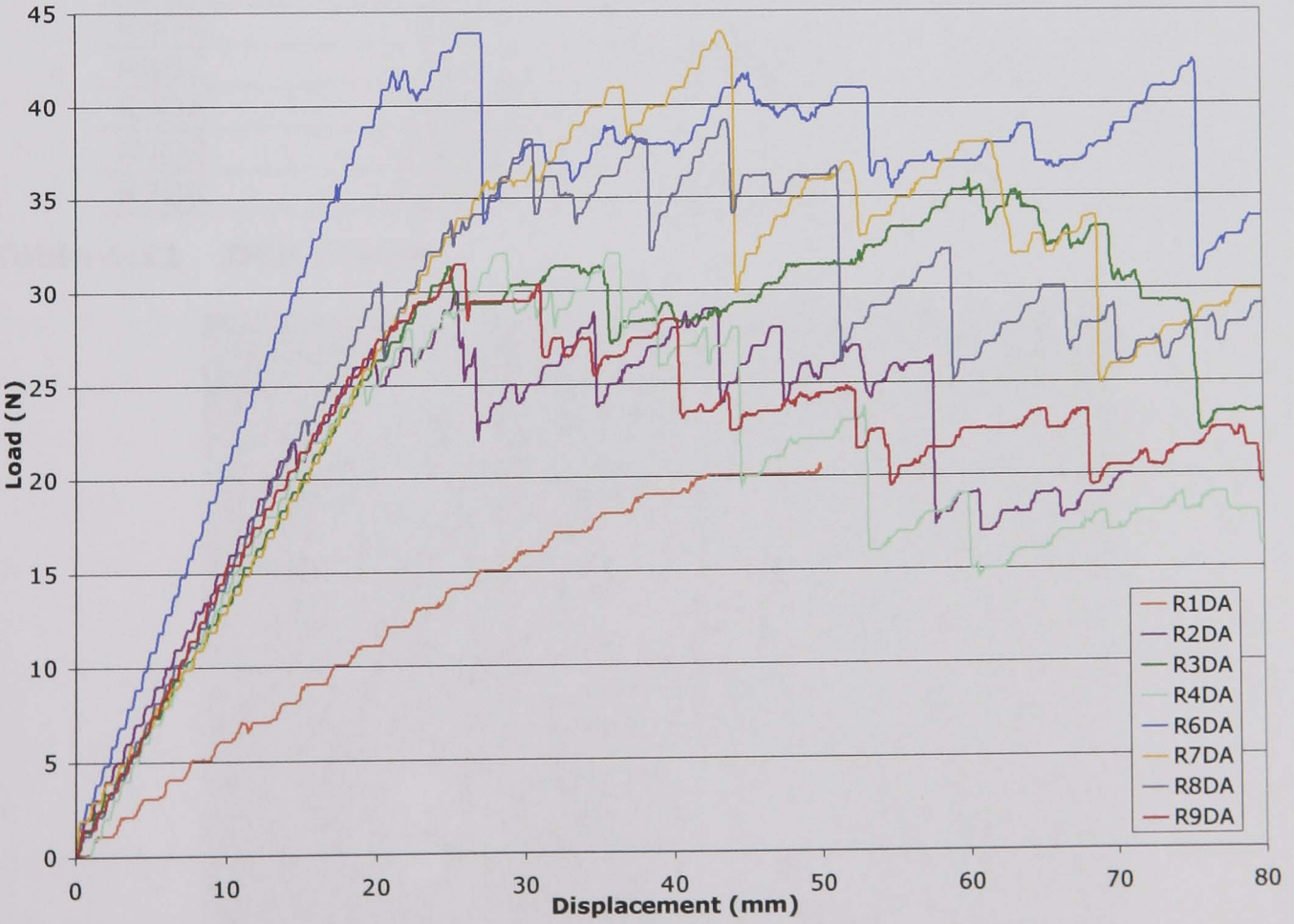

Figure 4:16 DCB results for R1 to R9 (R1 test invalid)

The overall results are shown below.

Sample	G_{Ic} (J/m^2)	Average	St Dev
R1DA	N/A		
R1DB	N/A		
R1DC	837.8	**N/A**	N/A
R2DA	747.4		
R2DB	743.1		
R2DC	883.1	**791.2**	10.1
R3DA	1024.2		
R3DB	879.3		
R3DC	959.3	**954.3**	7.6
R4DA	658.8		
R4DB	587.7		
R4DC	705.6	**650.7**	9.1
R5DA	N/A		
R5DB	N/A		
R5DC	N/A	**N/A**	N/A
R6DA	1464.3		
R6DB	1304.0		
R6DC	924.6	**1231.0**	22.5
R7DA	993.8		
R7DB	1145.5		
R7DC	926.1	**1021.8**	11.0
R8DA	997.5		
R8DB	1284.2		
R8DC	1206.5	**1162.7**	12.8
R9DA	1155.5		
R9DB	1284.1		
R9DC	1288.8	**1242.8**	6.1

Table 4:11 DCB results

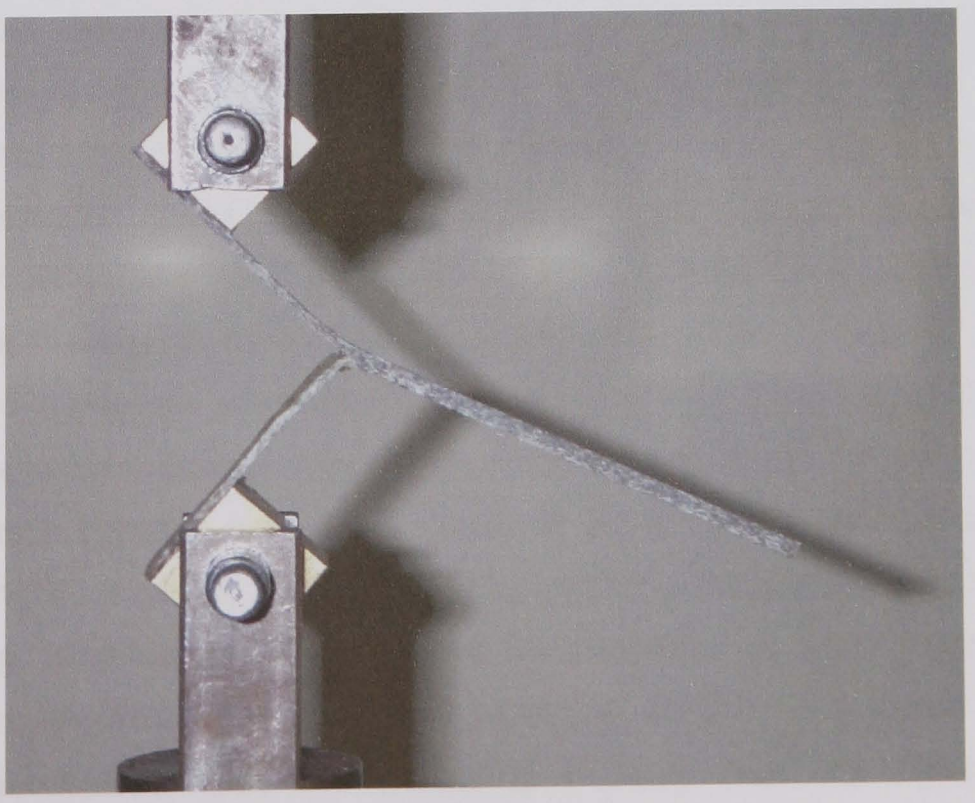

Figure 4:17 Bending of DCB specimen (e.g. sample R1)

4.5.4 Degree of cure results

Differential scanning calorimetry (DSC) testing has been carried out as previously described (section 3.2.4.1). The results are tabulated below. SEA has been correlated with percentage conversion. It has been problematical to produce consistently undercured samples as the results show.

Average degree of cure for the nine configurations appears in Figure 4:18 and Table 4:12. Each bar represents the average of 18 results generated from samples taken at each end of the 3 tubes moulded for each configuration; 3 samples were collected at each location. As expected the post-cure has the strongest effect on the degree of cure as seen by comparing R1, R3, R5 and R7 to R2, R4, R6 and R8; the variability decreases accordingly. The results show that the cure is virtually unaffected by a change in resin; identical conditions lead to similar results for both resins. The temperature also has an effect that only appears for samples that are not post-cured (R1 to R3 and R5 to R7).

The high variability observed with R7 is indicative of the moulding difficulties presented by this configuration. The corresponding moulding parameters seem to represent the limit of what is feasible with the geometry and tools selected for this work; however, post-curing tubes produced under these conditions leads to excellent results. Configuration R9 produced very high conversion despite the lower injection temperature and post-cure time.

The standard deviations presented in Figure 4:18 include the variability generated by collecting three samples at both ends of the tube, from three different tubes. An inter-group study was performed in order to see which variable ('sample', 'end', 'tube') induces most variability. An average was obtained for all values of the degree of cure that fall in a certain group; for example one average was obtained for each group 'tube 1', 'tube 2' and 'tube 3'. The standard deviation of these three averages was then calculated. A higher standard deviation indicates that the average values associated with the variable 'tube' are more spread; hence, the variable 'tube' induces some variability. For configurations R1 and R5, most variability can be associated with the position in the tube (e.g. inlet/outlet). These tubes were injected at lower temperature and were not post-cured. For high temperature and/or post-cured tubes, the variability associated with the moulding ('tube') was the most important; however as the cure exotherm is 342 J/g the variabilities observed are low,

indicating good repeatability of material and process. Again, the limitations in repeatability associated with configuration R7 clearly appear.

Taguchi analysis was performed on the above data; results appear in Table 4:13. As expected, post-cure has the strongest effect on cure, however the effect of all other parameters on the response is limited. The moulding temperature does not have a major effect on the degree of cure. The higher temperature caused moulding difficulties with the selected curing systems as seen for configurations R4 and R7. The viscosity of the resin is sufficiently low to inject at the selected pressure; hence, no benefit resulted from injecting at high temperature. Whilst not affecting the degree of cure, changes in moulding parameters may affect other properties. This would indicate that the performance in crush is not fully determined by the degree of cure.

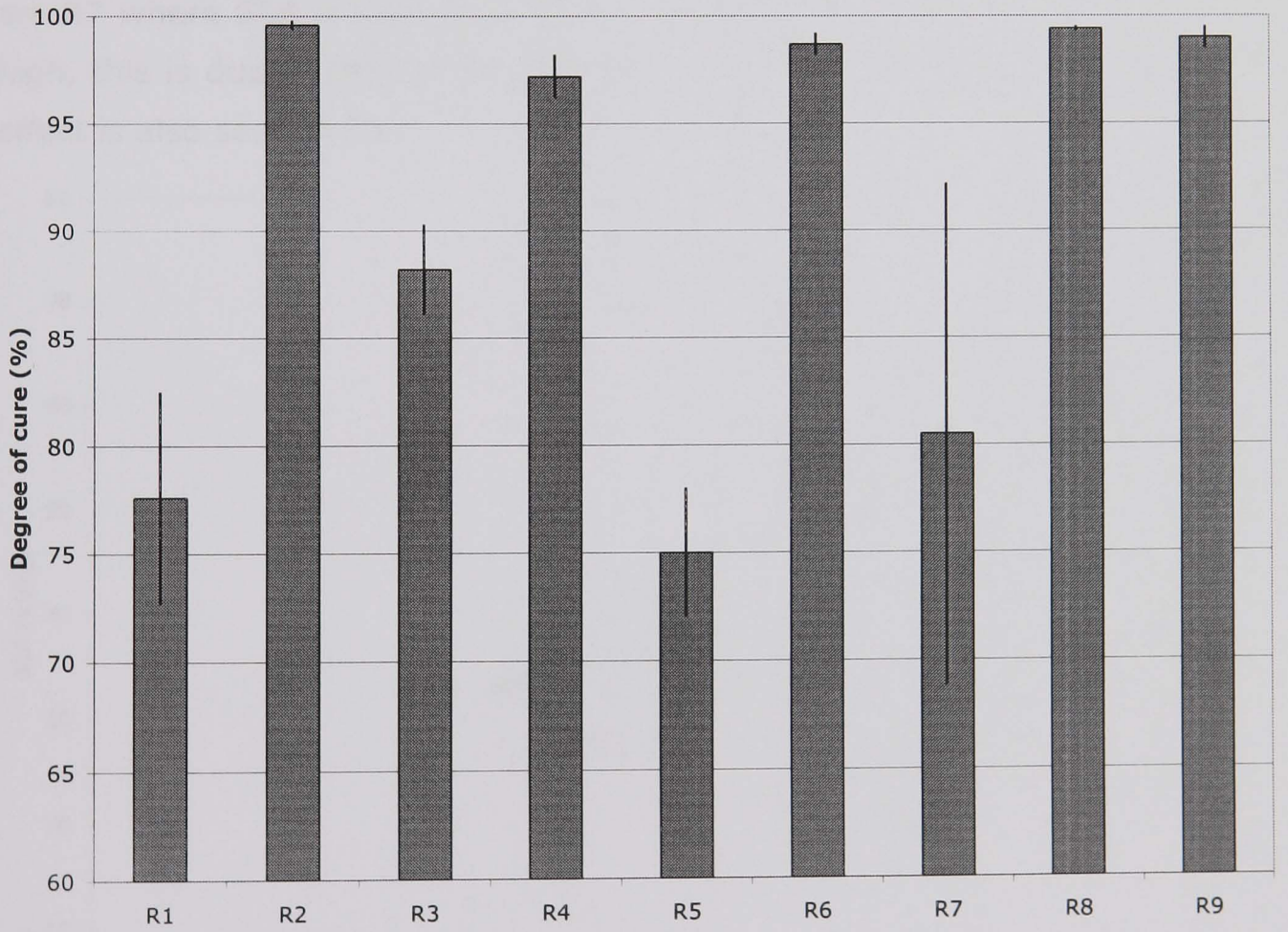

Figure 4:18 Average degree of cure values from DSC testing

Configuration	DSC %	st dev
R1	**77.6**	4.9
R2	**99.6**	0.2
R3	**88.2**	2.1
R4	**97.2**	1.0
R5	**75.0**	3.0
R6	**98.7**	0.5
R7	**80.5**	11.7
R8	**99.4**	0.1
R9	**99.0**	0.5

Table 4:12 DSC results

A very weak correlation between SEA and degree of cure can be seen in Figure 4:19. Generally high degree of cure is linked with high SEA, the two exceptions are R7 where SEA is high and cure is low, and R4 where SEA is low but cure is high, this is due to catalyst breakdown at the high moulding temperatures. This effect is also seen in R3.

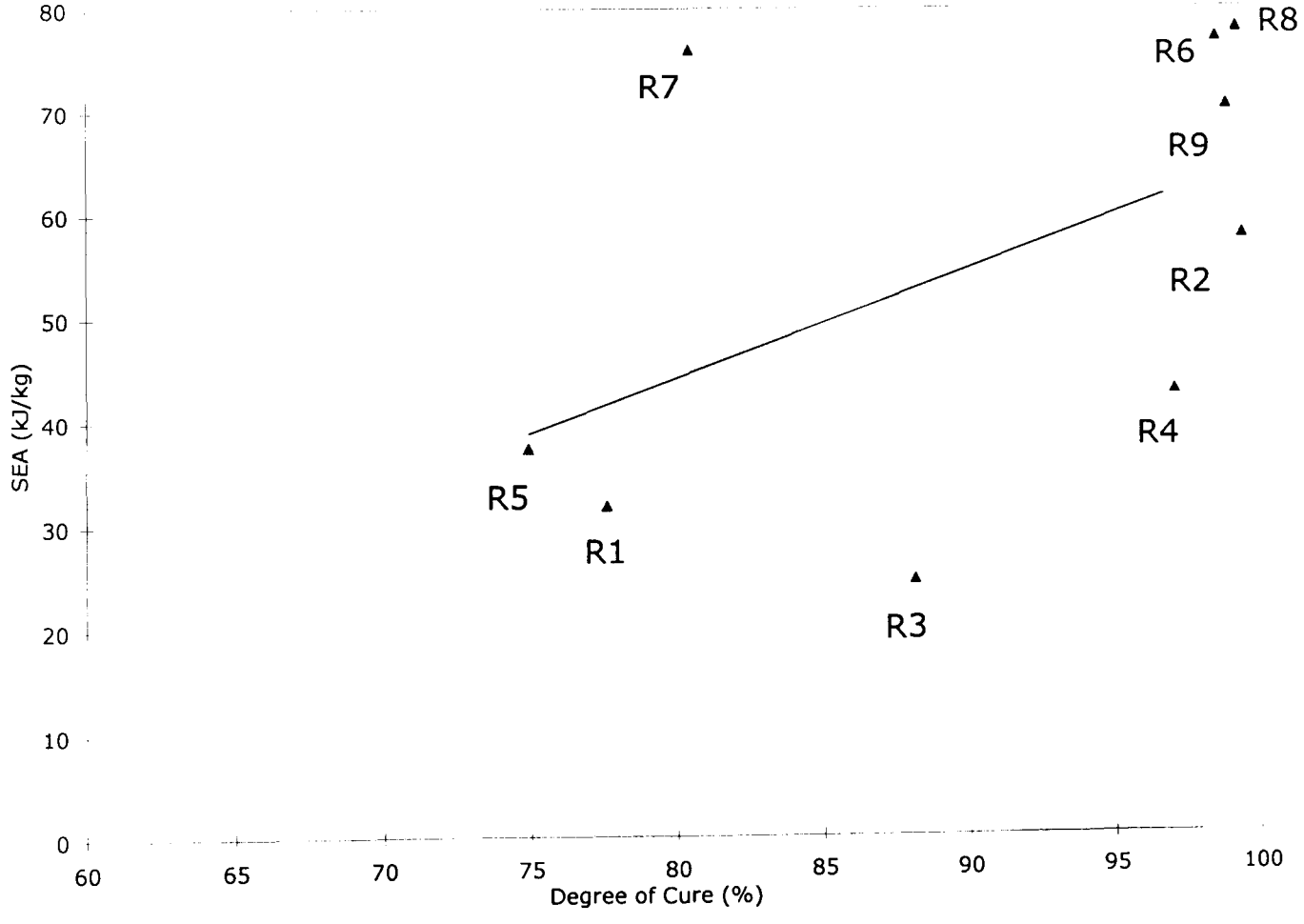

Figure 4:19 Correlation between SEA & degree of cure (Least squares fitted line)

Parameter	Effect
Resin	-0.03983
Post-cure	0.233665
Temp	0.020354
Resin + Post-cure	0.04994
Resin + Temperature	-0.03088
Post-cure+ Temperature	-0.03046
All	0.052065

Table 4:13 Taguchi analysis : DSC results

4.5.5 Statistical correlation

The aim of the following analysis is to establish the degree of correlation between the final specific energy absorption of a part and the in-plane testing results from the same configuration. Analysis has been performed for R1-R9 for. the following;

- SEA vs. Tensile Stress
- SEA vs. Tensile Modulus
- SEA vs. Compressive Stress
- SEA vs. Compressive Modulus

Analysis has been performed using the data analysis function in Microsoft Excel which employs standard statistical techniques. Regression analysis was used and an F-test applied [1]. For a given data set, a value of f is calculated from the error and regression sums of squares. The calculated value of f is compared to tabulated values of F. The latter values represent the probability that a true hypothesis is rejected for a significance level α. Generally speaking, higher F values correspond to better correlations; these values depend on the sample size and chosen confidence level α. A smaller value of α corresponds to a more stringent test.

The R square value is equivalent to the r-value from a least-squares correlation test and shows how closely the parameters X and Y are related. By taking the square of the r-value, all values of r^2 are positive and fall between 0 (no correlation) and 1 (perfect correlation). R^2 can only give a guide to the accuracy of fit and does not indicate whether an association between the variables is statistically significant (Unlike the F-value).

As well as trying to correlate the whole series, regression analysis was also conducted on only fully cured (R2,R4,R6,R8) and only vinylester (R5,R6,R7,R8). Although these represent lower sample sizes a variable is removed which may make analysis easier.

Standard tables give us the value of F required for acceptance at 95% & 99% significance level, these are as follows;

α=0.05	$F_{1,7}$	$F_{1,17}$
F-value	5.59	4.45

α=0.01	$F_{1,7}$	$F_{1,17}$
F-value	12.25	8.40

Table 4:14 Values of F needed for acceptance of hypothesis at 95% and 99% significance

Overall Results	Tensile stress (MPa)	Compressive stress (MPa)	Tensile Mod. (GPa)	Compressive modulus (GPa)
r2 - All	**0.54**	**0.83**	**0.56**	**0.36**
r2 - vinylester only	0.47	0.97	0.58	0.62
r2 - fully cured only	0.31	0.78	0.18	0.06
F- all	19.13	79.39	20.47	8.86
F- vinylester only	5.35	182.75	8.39	9.87
F- fully cured only	2.73	20.77	1.30	0.35

Table 4:15 Statistical analysis results

The results in the table above show that there is significant correlation between all four in-plane results (i.e. the F-tests are all higher than the value needed for acceptance at alpha = 0.05). Increasing the strictness of the test by reducing alpha does result in rejection of compressive modulus. The smaller tests using only some of the samples gave no new information.

For the fracture toughness results the correlation is relatively poor (Figure 4:24). The r^2 value found was 0.4 which is similar to that found for compressive modulus. The F-test was not passed at 95%, this means that there are no statistical grounds for acceptance

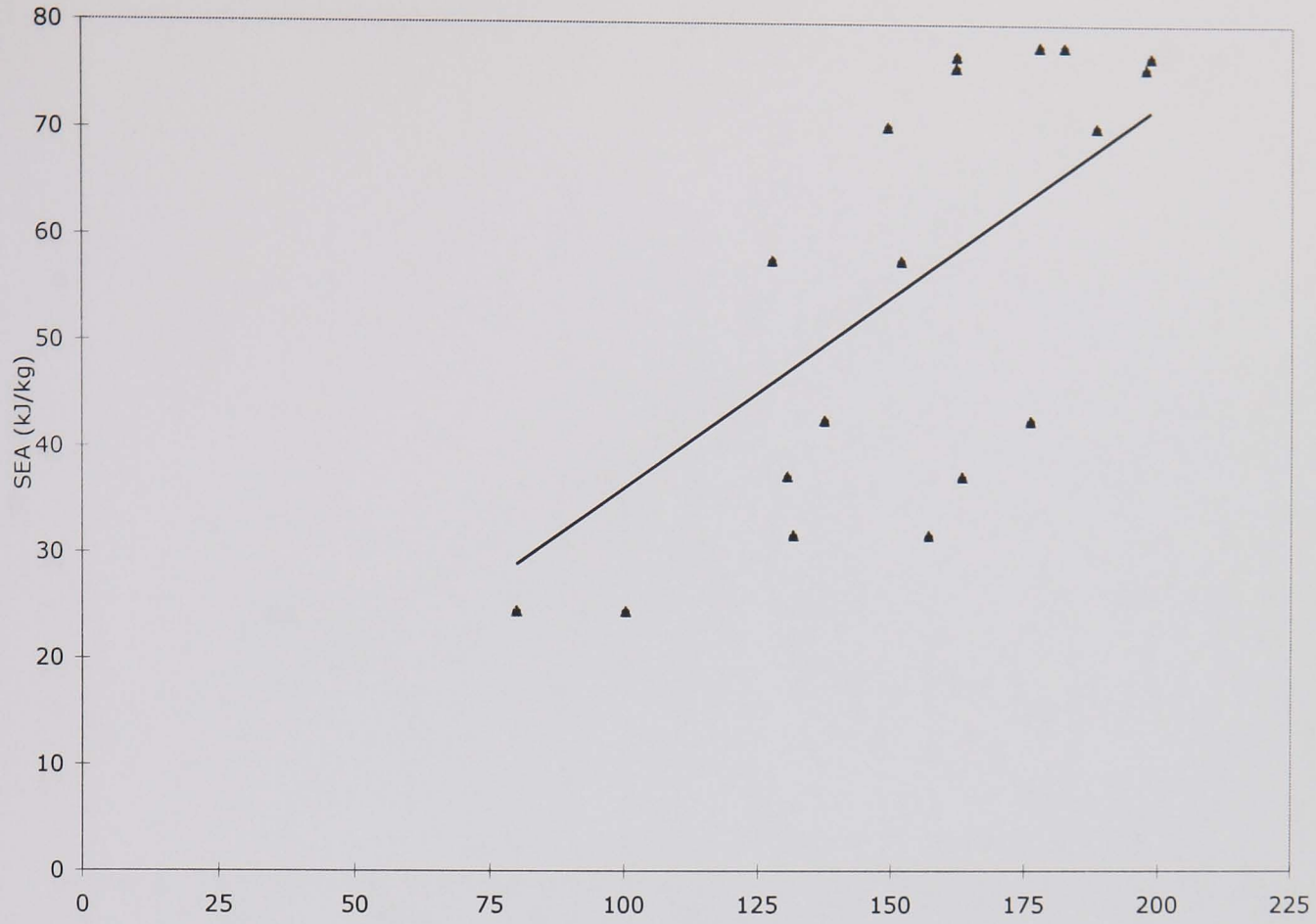

Figure 4:20 Ultimate Tensile stress (MPa) vs. SEA

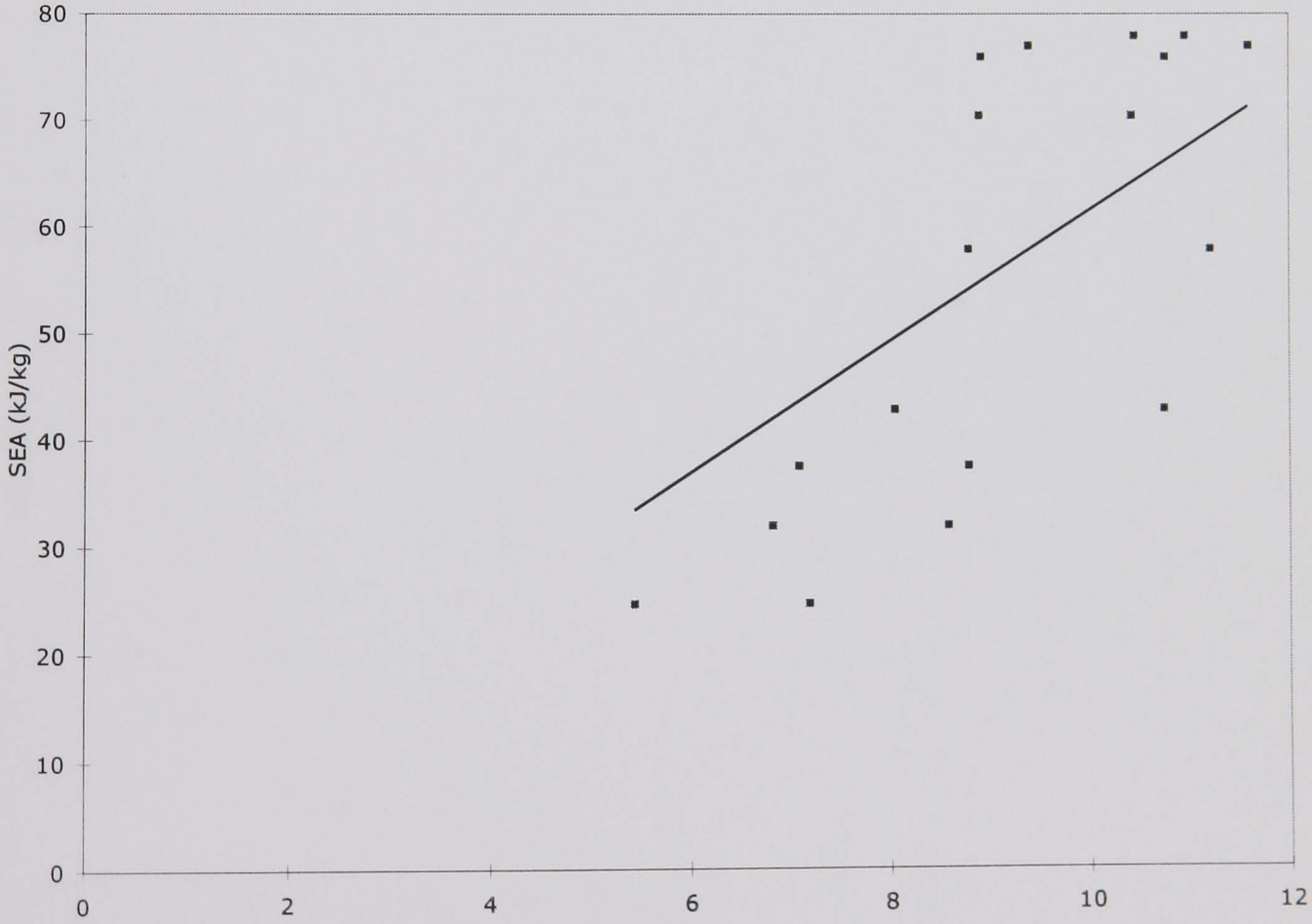

Figure 4:21 Tensile modulus (GPa) vs. SEA

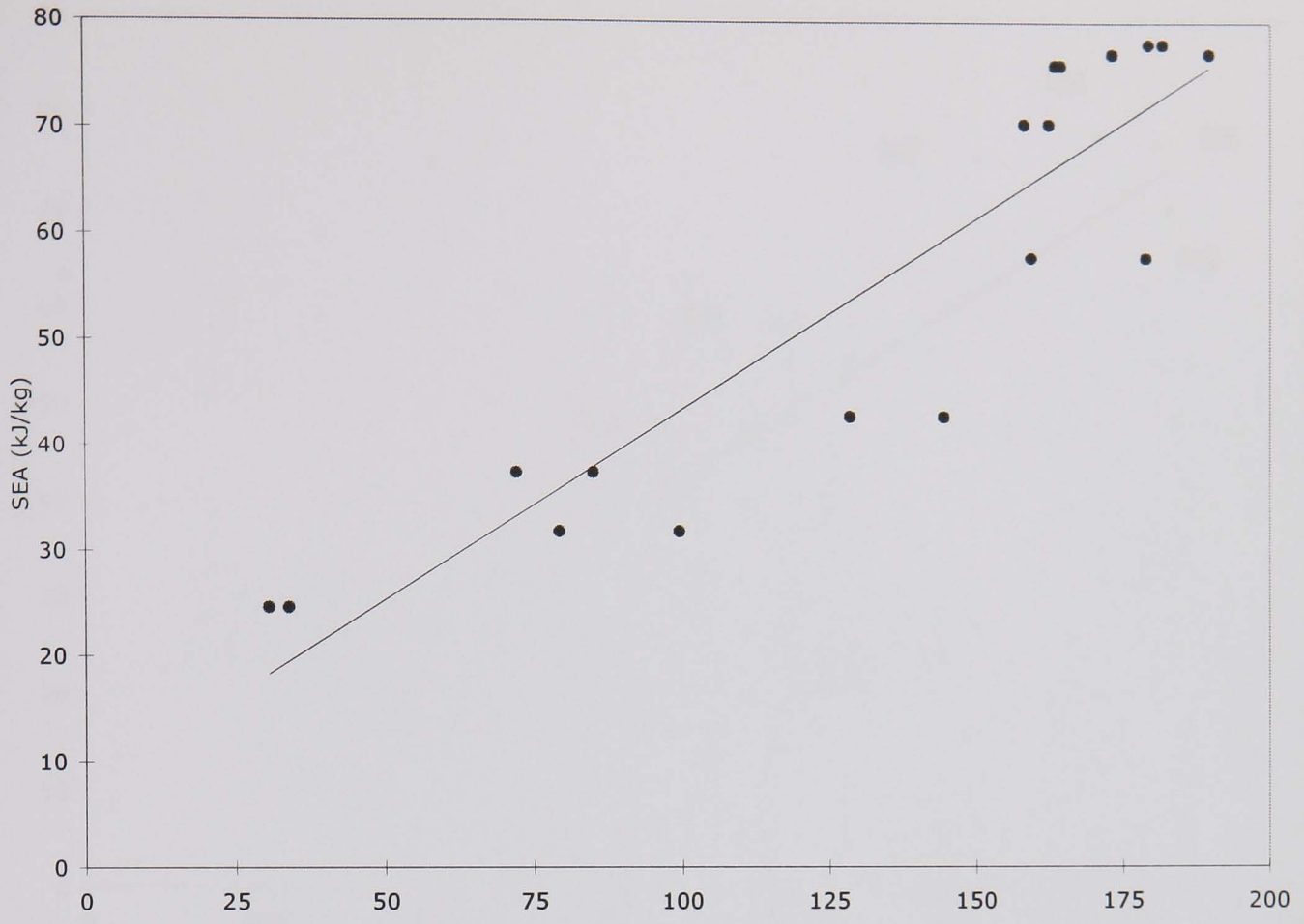

Figure 4:22 Compressive stress (MPa) vs. SEA

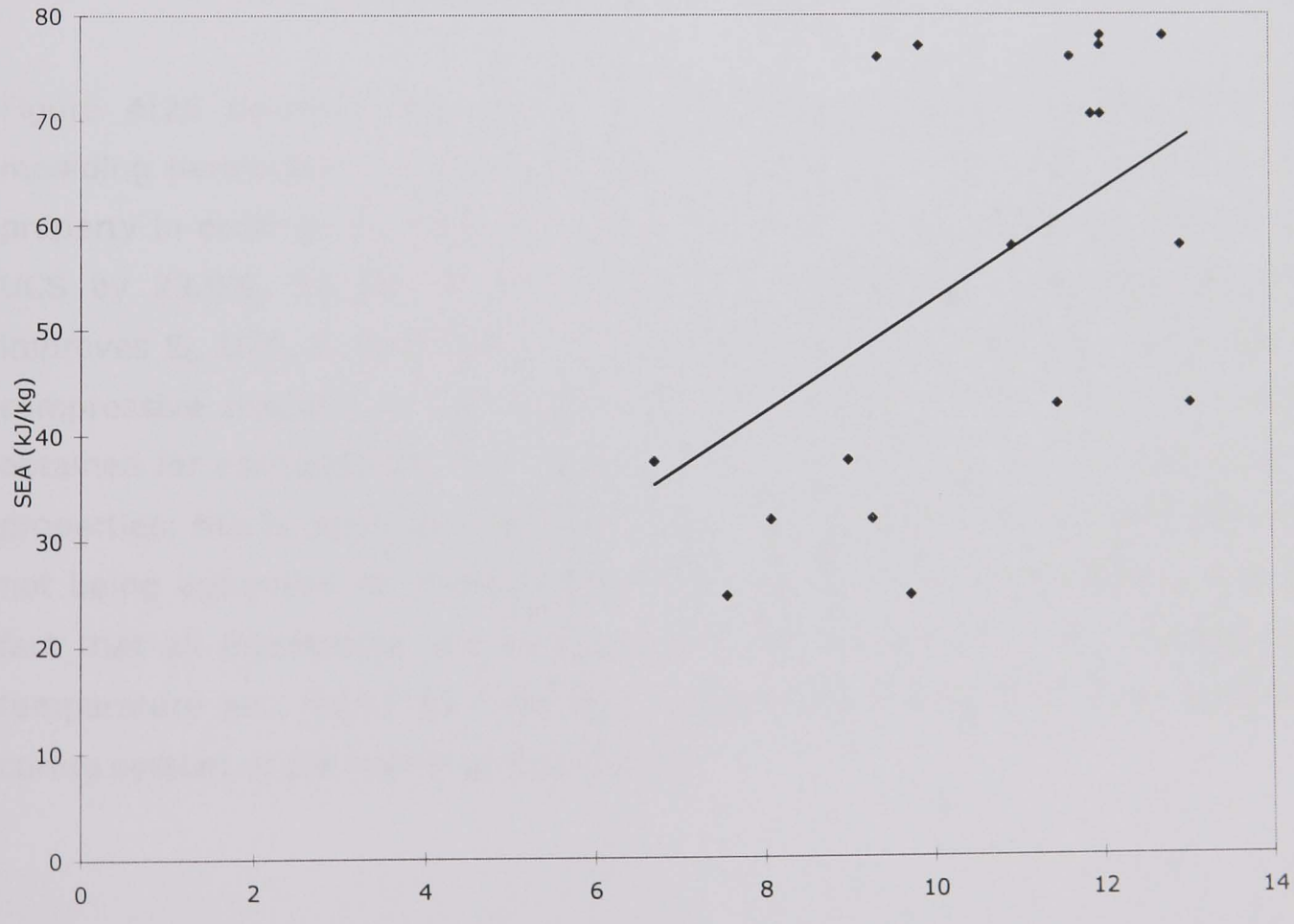

Figure 4:23 Compressive modulus (GPa) vs. SEA

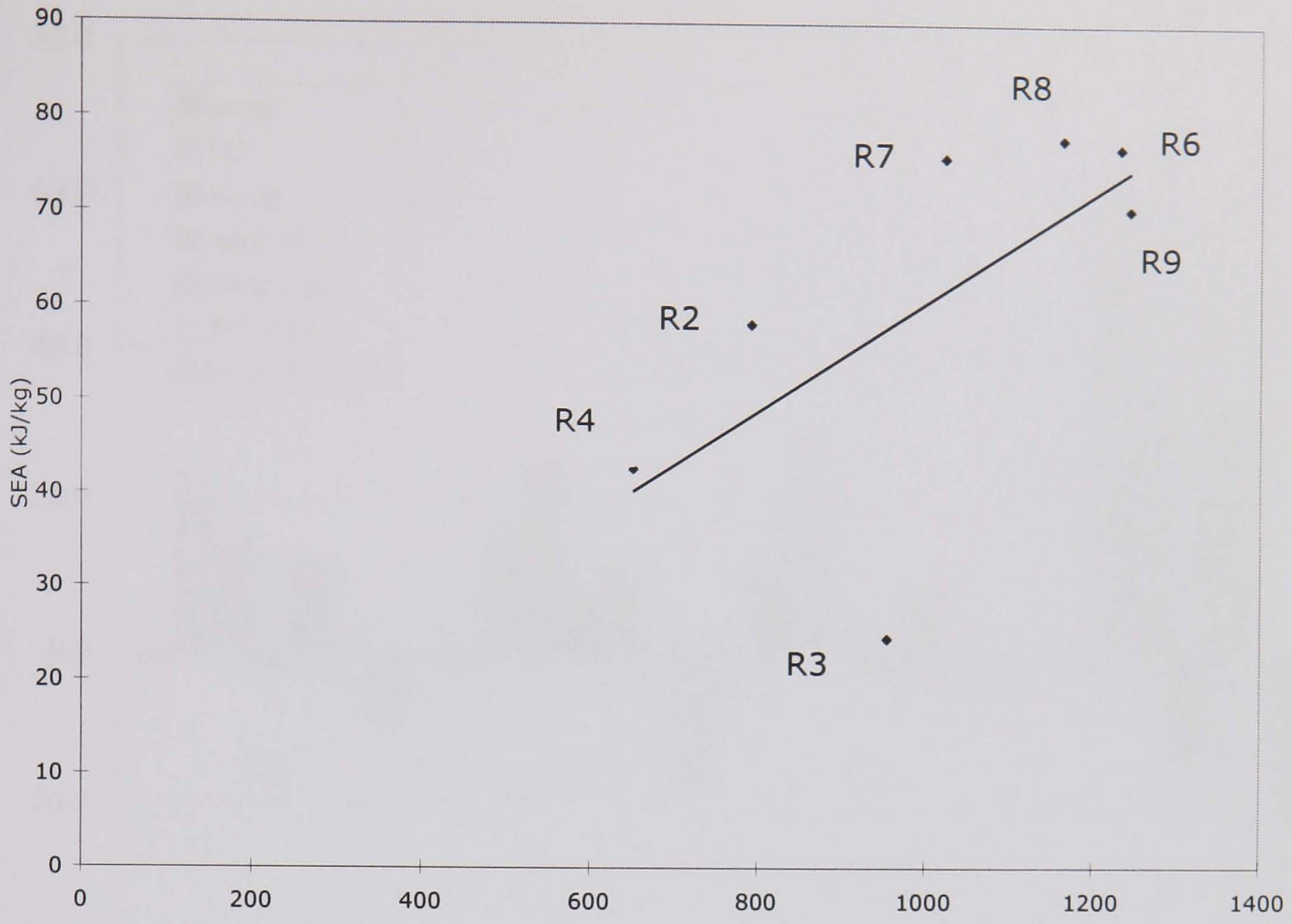

Figure 4:24 Fracture toughness (J/m^2) vs. SEA

Figure 4:25 presents the results of a Taguchi analysis. The effects of the moulding parameters on the properties are shown as percentage values of each property in order to normalize the data. The post cure improves E_t, UTS, E_c and UCS by 23.9%, 15.1%, 28.4% and 58.8% respectively. Changing the resin improves E_t, UTS, E_c and UCS by 14.5%, 25%, 0.5% and 34.4%. The effect on compressive modulus is very small; this is essentially due to the low results obtained for configuration R5. The direct effect of temperature is minimal for all properties; this is partly due to the curing system selected for the polyester resin not being optimised for configurations R3 and R4. This is also reflected in the fact that all interactions are negative with the exception of the interaction of temperature and resin; the vinylester configurations benefit from an optimised curing system at the higher temperature.

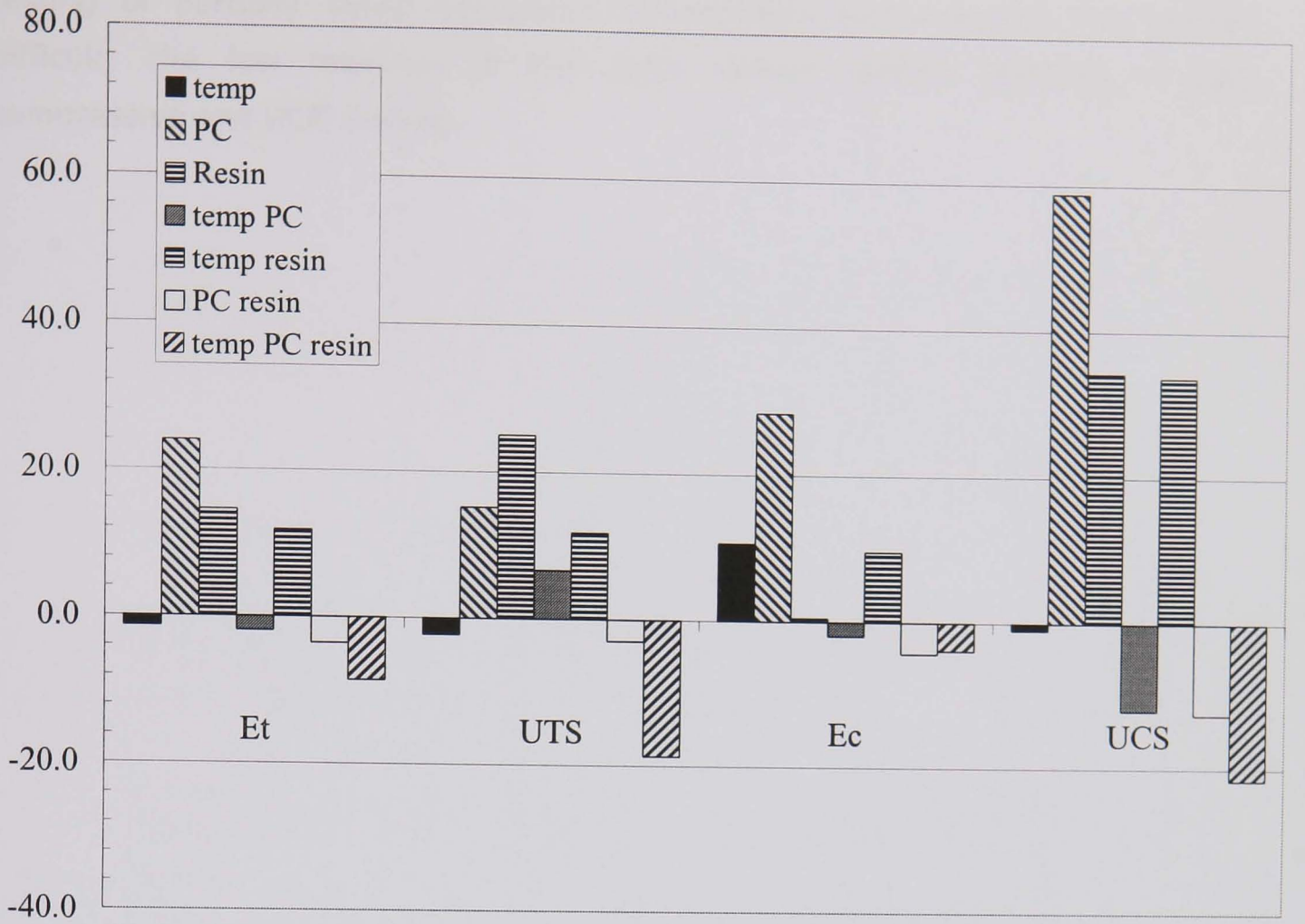

Figure 4:25 Taguchi Analysis – correlation between in-plane tests and SEA (percentage variation in property)

All the results show that the benefit of postcure is seen in all configurations. Postcure cannot be said to have improved the variability in the way it does with crush results. From the compressive modulus graph (Figure 4:15), it can be seen that the polyester has greater compressive modulus than the vinylester and closely matches vinylester on compressive strength when processed as R2. It is clear that there is no configuration that gives the best properties for all tests although it could be argued that R6 comes closest. The in-plane results show that there is a compromise with processing speed and in-plane properties although further optimisation of the catalyst would doubtless improve this.

Good crush performance depends upon interactions between many properties including those listed here. The analysis presented here provides a partial view of the crush situation. Furthermore, correlations must be considered with caution; whilst an increase in a particular in-plane property may not translate into better crush performance a reduction in the same in-plane property might lead to poor performance due to a change in crush mode, for example. The

testing of partially cured specimens by standard test methods has proven difficult; the low modulus of the parts caused sample bending in both compressive and DCB testing.

4.6 Effect of fibre architecture

4.6.1 Introduction

In order to determine the effect of the fibre architecture the above testing was repeated for to 0/90 non-crimp fabric. The testing was on a smaller scale using one moulding repeat instead of three.

4.6.2 Axial tube crush results (NCF)

Crush test results for the NCF appear in Table 4:16. As stated above, only one repeat was moulded for each of the configurations R1-R9.

Tube ref.	SEA A	SEA B	SEA C	SEA D	Av. SEA	st. dev.
R1S	33.67	31.86	25.98	29.31	**30.21**	3.3
R2S	38.39	42.37	40.28	39.50	**40.13**	1.7
R3S	30.18	32.44			**31.31**	1.6
R4S	35.53				**35.53**	0.0
R5S	30.39	29.51	31.81	27.18	**29.72**	1.9
R6S	47.88	43.32	45.41	46.37	**45.74**	1.9
R7S	46.15	45.14	45.97	46.58	**45.96**	0.6
R8S	54.07	47.32	48.67	45.74	**48.95**	3.6
R9S	39.63	41.42	36.13	40.43	**39.40**	2.3

Table 4:16 NCF crush results

Note that most samples from R4S failed to crush in the same way that the CoFRM samples collapsed. This also accounts for the missing data from R3S positions C and D.

The NCF results follow the same trend as the CoFRM results (see Figure 4:26). Scatter within the moulding is lower than for CoFRM. Differences between

configurations e.g. R1-R2 are greater with CoFRM. The NCF material has a more ordered structure particularly in terms of the interlaminar geometry and this may explain the lower scatter. The polyester NCF tubes range between 69% and 127% of the CoFRM tubes whereas the vinylester and mixed tubes (R5-R9) range between 59% and 79%. Differences between the fabrics are reduced when the cure level is lower. Crush variability cannot be directly compared due to the reduced number of moulding repeats and hence samples with the NCF tubes.

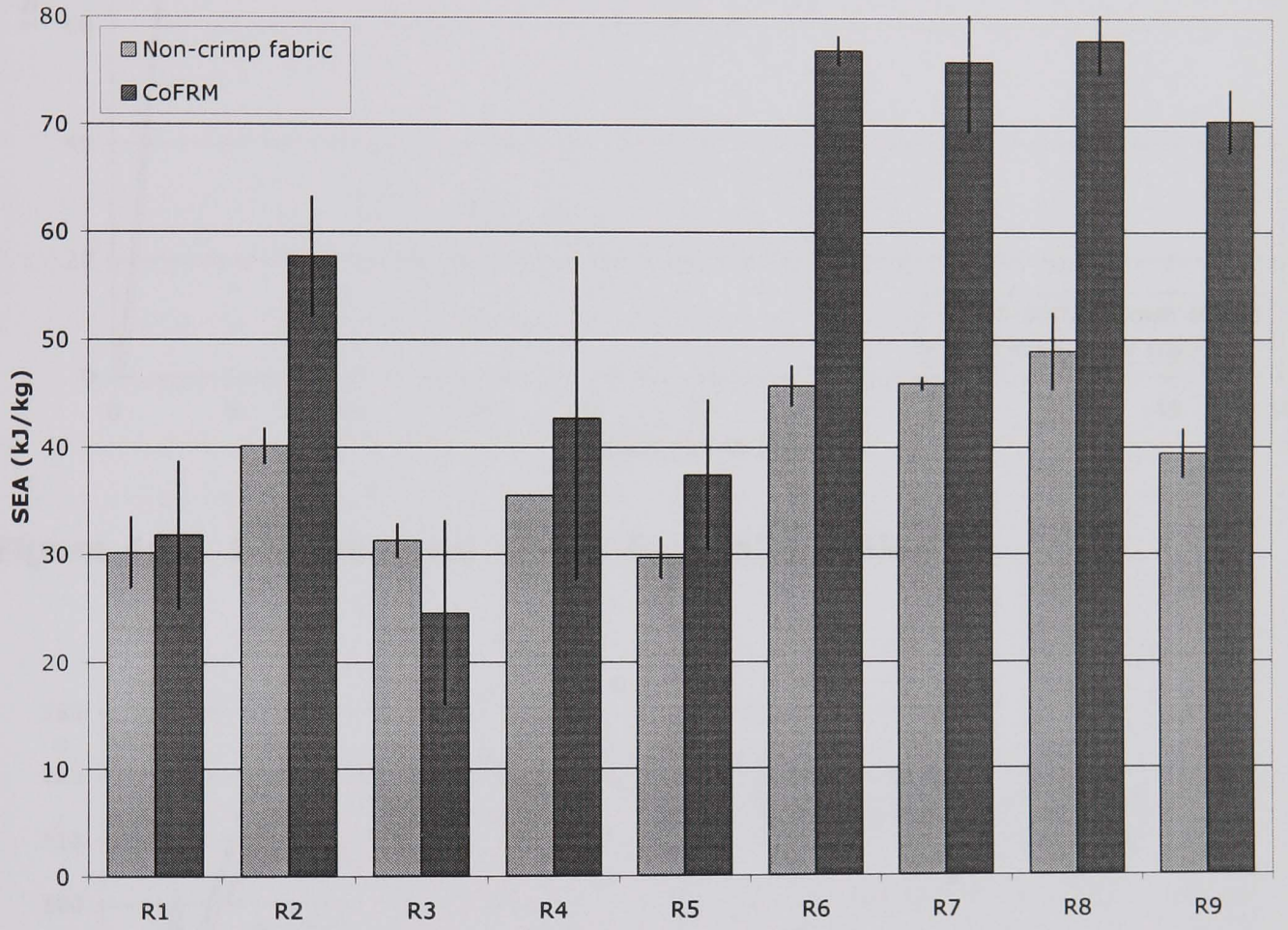

Figure 4:26 Crush results for NCF and CoFRM

The difference in load-displacement characteristics can be seen below. The NCF has a similar initial stiffness but has a first peak which the CoFRM does not exhibit. Steady state crush variation is similar for the two fabrics. The decrease in load with length occurs for a significant proportion (~5/8ths) of the crush curves to a varying degree. The curve shown represents a worst case. The reason for this is not known but is probably due to a build-up of debris at the crush zone.

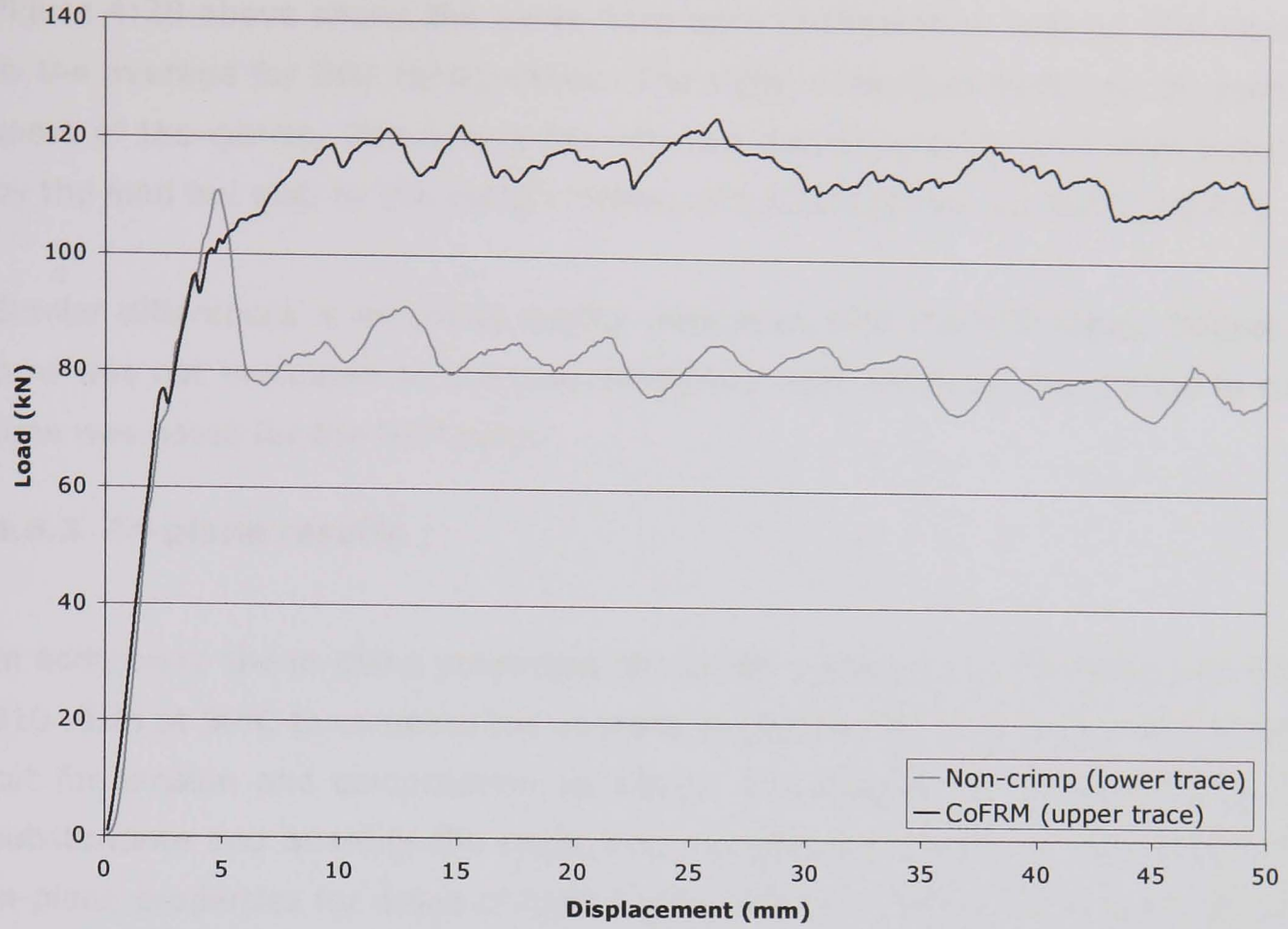

Figure 4:27 Sample crush curves for configuration R6

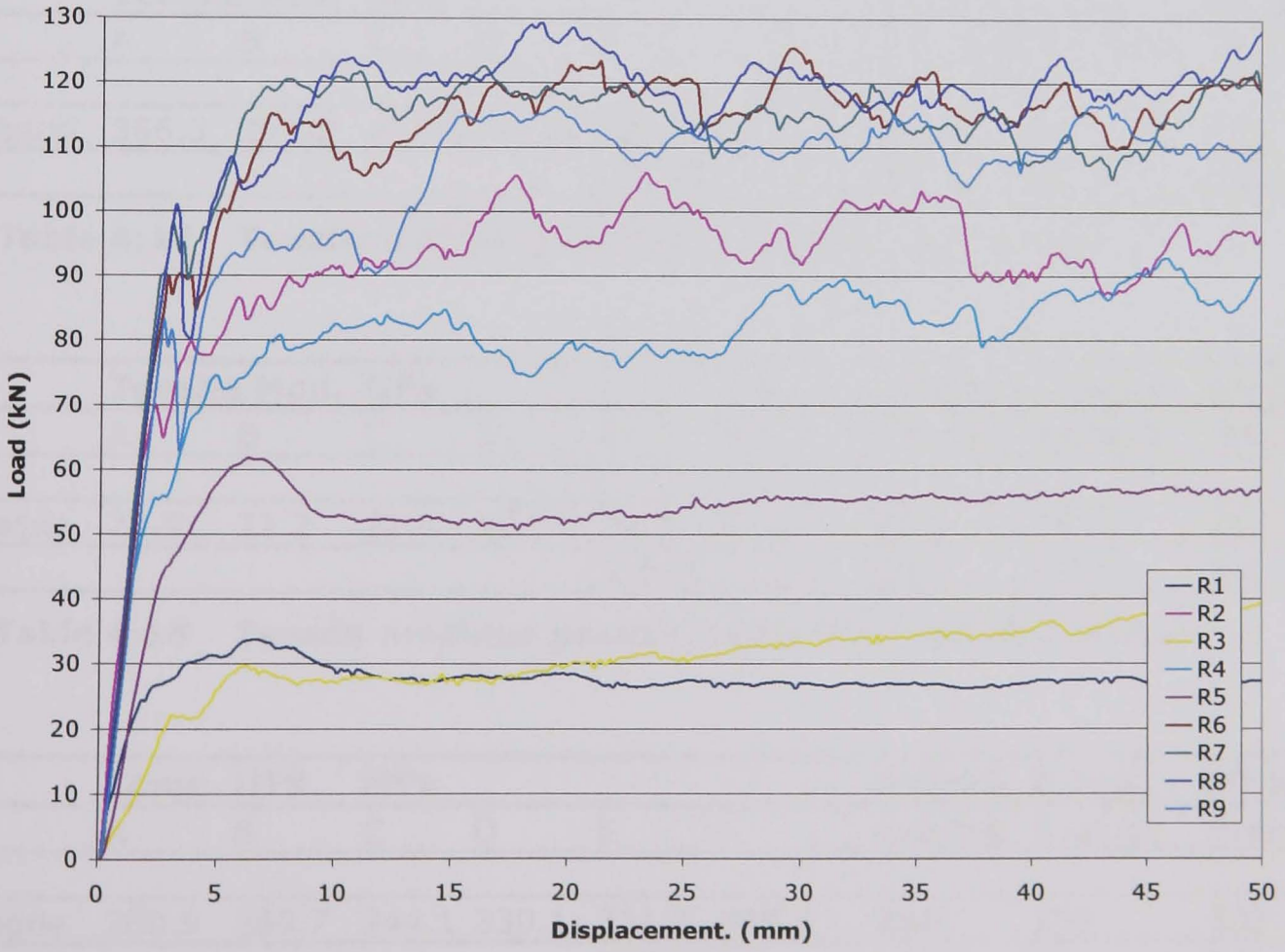

Figure 4:28 Average crush curve comparison (CoFRM)

Figure 4:28 above shows the curve from each configuration with an SEA closest to the average for that configuration. The slight downward trend can be seen in some of the curves. The curves fall into two distinct groups, best differentiated by the load but also by the initial stiffness (R1,R3,R4,R5 vs. R2,R6,R7,R8,R9).

Similar differences is moulding quality were seen with the NCF tubes. Degree of cure was not evaluated as the cure conditions were identical. No change in cure time was noted for the NCF parts.

4.6.3 In-plane results

In addition to the in-plane properties for CoFRM a plaque was moulded with 631-610 resin at 50°C to compare the in-plane properties of the NCF. 6 samples were cut for tension and compression as before. The purpose of this testing was to substantiate and quantify the claim that the NCF material would provide higher in-plane properties for areas of high stress. Again, modulus measurements were taken from the load-displacement curve according to ASTM standards from 0.001 to 0.003 strain.

	Tensile UTS MPa						**Overall**	**0 deg.**	**90 deg.**
	A	B	C	D	E	F	Average	Average	Average
Plaque	366.3	399.8	407.0	350.1	391.9	382.7	**383**	391	375
					STDEV		21.4	21.7	22.0

Table 4:17 Tensile UTS properties for 631-610 NCF plaque

	Tensile Mod. GPa						**Overall**	**0 deg.**	**90 deg.**
	A	B	C	D	E	F	Average	Average	Average
Plaque	20.0	22.2	21.4	22.1	21.4	21.3	**21.4**	21.2	21.6
					STDEV		0.8	1.1	0.4

Table 4:18 Tensile modulus properties for 631-610 NCF plaque

	Comp. UTS MPa						**Overall**	**0 deg.**	**90 deg.**
	A	B	C	D	E	F	Average	Average	Average
Plaque	260.9	269.7	244.1	330.1	331.9	335.8	**296**	258	333
					STDEV		41.6	13	2.9

Table 4:19 Compressive UTS properties for 631-610 NCF plaque

	Comp. Mod GPa						Overall	0 deg.	90 deg.
	A	B	C	D	E	F	Average	Average	Average
Plaque	24.1	24.8	24.4	30.1	23.3	20.7	**24.6**	24.4	24.6
					STDEV		3.1	0.4	4.0

Table 4:20 Compressive modulus properties for 631-610 NCF plaque

Table 4:21 below shows a comparison between the average properties obtained from CoFRM plaque R2 and the equivalent NCF plaque. The results show that the NCF is roughly twice as strong and twice as stiff as CoFRM.

Property	CoFRM	NCF	Difference
Tensile UTS	140	383	2.74x
Tensile Modulus	10.0	21.4	2.14x
Compressive UTS	169	296	1.75x
Compressive Modulus	11.9	24.6	2.07x

Table 4:21 Comparison of in-plane properties for CoFRM and NCF

4.6.4 Statistical analysis

The effects are similar to the CoFRM results shown in section 4.5.1. There are slight differences for the non-crimp fabric tests. There are no repeats for the NCF testing so the sample size is 3 times smaller.

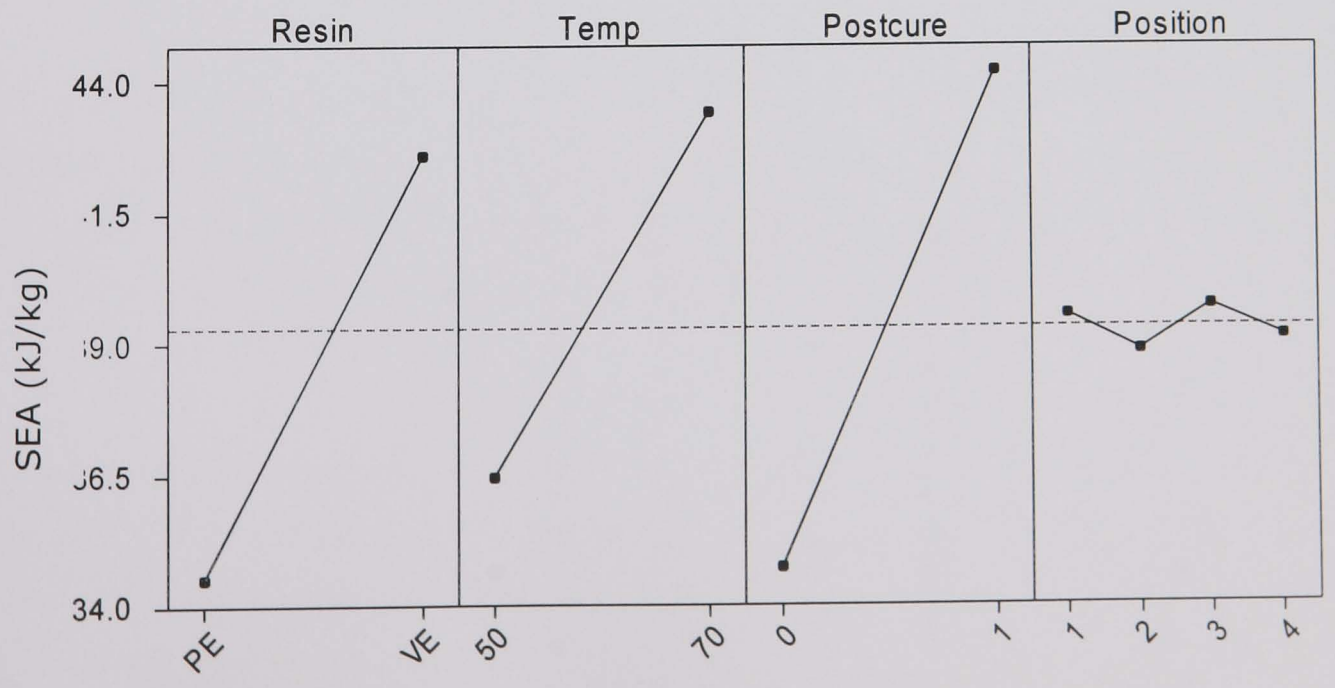

Figure 4:29 Main effects plot – data means for SEA (NCF)

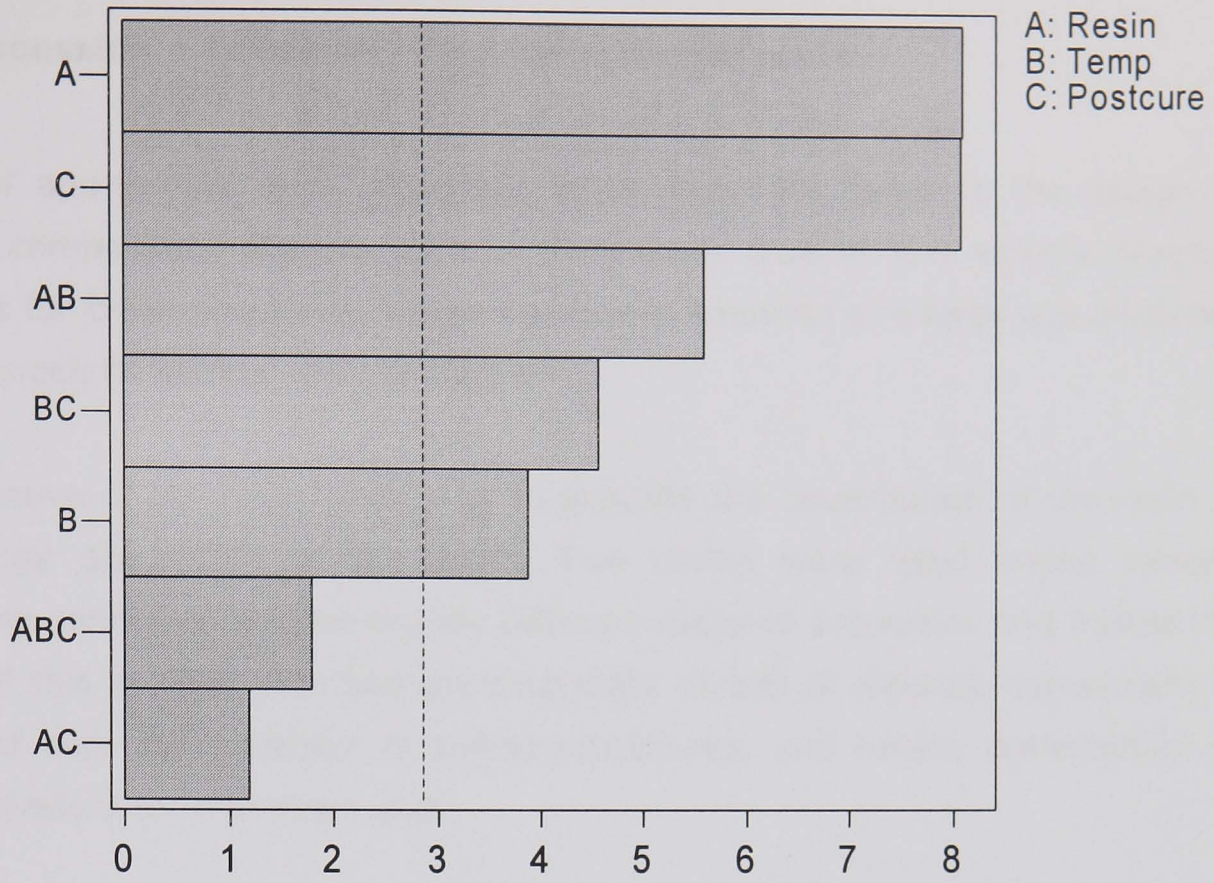

Figure 4:30 Pareto chart of standardised effects : SEA at alpha=0.01 (NCF)

The results all have slightly lower significance (compare Figure 4:10 with Figure 4:30) but resin and postcure are still the most important factors. The order of the effects is almost the same but position in the tool has no effect and temperature shows as having a greater effect.

4.7 Discussion – Influence of material constituents

Choice of appropriate resin properties is an important factor in the design of efficient composite materials; this is particularly true of low volume fraction materials for crash structures where significant amounts of energy are absorbed through crack formation and propagation.

The objective of the resin study was to quantify the contribution of the resin to the energy absorption of the parts. Two resins were used under varying processing conditions to give slightly different material properties and assess the impact of this on SEA. This had the secondary benefit of allowing assessment of degree of cure for a variety of curing procedures, and hence, optimisation of curing schedule for minimum cost.

The crush testing is complemented by a full range of in-plane and fracture toughness testing. This was done for a variety of reasons:

- To compare the effect of resin type on in-plane properties and fracture toughness
- To generate baseline in-plane property data
- To allow correlation of in-plane results with SEA results
- To allow correlation of degree of cure and fracture toughness results with SEA
- To assess the impact of cure level on in-plane and fracture toughness results

Cost is a primary factor in deciding which material to use so it was envisaged that cost would be correlated against benefit in moving from a low cost polyester to a higher cost vinylester. The benefits of vinylester and epoxy materials were shown in the preliminary work, but the ultimate aim was to achieve similar results with a low cost resin.

The relevance of this work is obvious as little work on the effect of matrix material in high volume parts is available in the literature. Much of the available data concerns thermoplastic matrices. This work also provides valuable data for the prediction of crush response as in-plane and crush data is available for 2 architectures under nine resin conditions. The statistical methods employed in

this chapter are basic but serve to demonstrate the main influencing factors to the overall SEA and also the correlations between SEA and in-plane and fracture toughness properties.

4.7.1 Preliminary work

Neat resin testing showed that the modulus and UCS of the resins were similar but that the vinylester had a higher UTS (+20%) and total strain energy (see Figure 4:1) . The lower volume shrinkage of the vinylester resin was obvious in the mouldings. In depth resin testing was not undertaken as comprehensive manufacturers data was available. The testing undertaken was important in showing both the advantages of the vinylester but also the similarities with the UP resin in most other main areas.

The preliminary work gave a valuable insight into the effect of resin type on crush properties, the main conclusion being that there were significant gains to be made in SEA performance by improving the toughness of the resin. Less clear was how to improve the performance of a low cost polymer. Limited success was obtained with the addition of various thermoplastics and the help of the resin supplier was enlisted to provide some solutions, of these the modified vinylester was carried forward to the main experimental study with the polyester.

4.7.2 Tube crush results

The crush results show that the average SEA for UP CoFRM is 60kJ/kg for case R2 in this geometry, which is the baseline case most closely related to industrial mouldings. Moving to the vinylester resin increases the average to approximately 80kJ/kg. The results gained from the 50:50 mixture (R9) suggest that the trend between vinylester content and SEA is linear, as the material gave an SEA of 70kJ/kg. In the NCF case where R2 and R9 both gave 40kJ/kg, pure vinylester gave 45kJ/kg (Figure 4:26).

Crush zone micrographs for the two fibre architectures are shown below in figures 4:29 and 4:30. The figures show extensive intralaminar fracturing of the CoFRM sample whereas the NCF sample delaminates during crush allowing unhindered shearing between the fibre layers. This effect is shown in Figure 4:33 where the polyester stitching has failed yet the laminæ are intact. This explains the significant reduction in SEA observed with the NCF architecture.

Figure 4:31 CoFRM crush zone micrograph

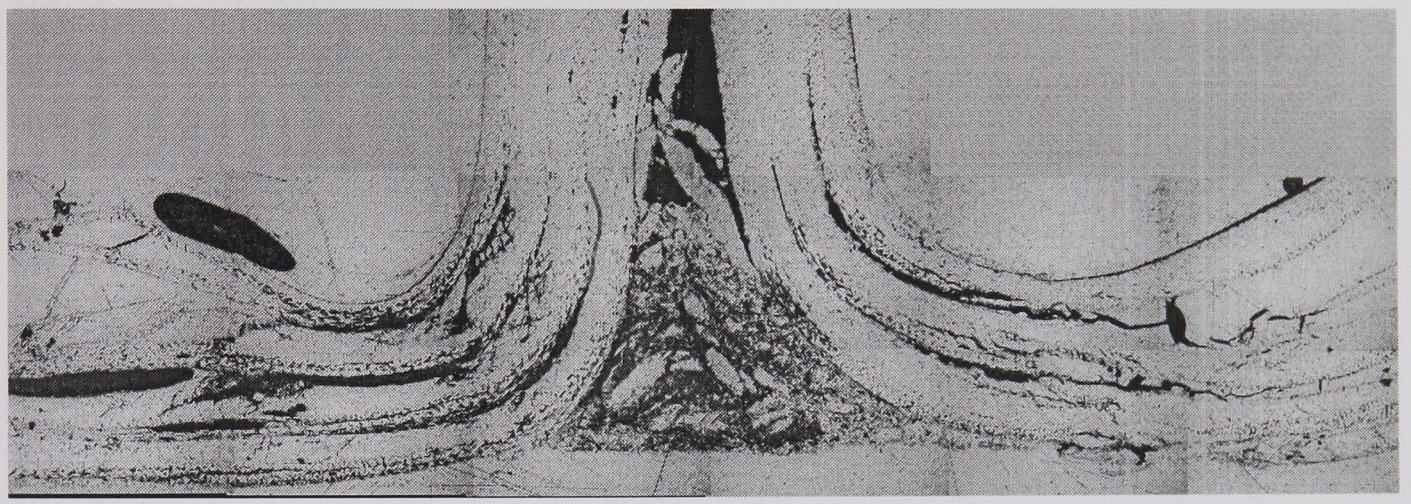

Figure 4:32 NCF crush zone micrograph

Figure 4:33 Delamination of NCF fronds

The importance of the matrix is highlighted by the fact that the results achieved for the undercured samples were much lower than those for ultimate cure. Higher cure also has the benefit of decreasing the variability seen in the SEA values – this is probably due to the difficulties in producing undercured specimens. Variability between mouldings is greater but cure levels are also more likely to vary along the length of the tube.

NCF and CoFRM results follow a very similar trend for SEA except where the cure level is very low when the difference between the two architectures is less apparent. Examination of the crush trace gives little new information. All adequately cured samples have high average to peak ratios and low variability. The onset stiffness is of interest as high stiffness approaches the optimum crush curve (see Introduction). The vinylester tubes have higher stiffness as the initial stages of crush are dependant on the compressive strength of the composite.

4.7.3 In-plane and fracture toughness results

In-plane results in general show lower variability between the 9 moulding configurations than the crush testing. The exception to this is the compressive stress which shows large variations (probably due to the test geometry). The in-plane results for the fully cured specimens match the neat resin testing results well. The vinylester resin offers little benefit in terms of tensile properties; particularly tensile modulus where no great difference is seen between R2/4 and R6/7/8 (see Figure 4:1). Compressive modulus for the polyester resin is 10% higher than that for vinylester. This cannot be explained purely by the matrix compressive modulus as it is similar for the two matrices. Compressive properties in the composite are dependent on the ability of the resin to maintain fibre alignment not directly on matrix modulus.

The limited in-plane testing performed on the NCF material showed the increase in in-plane properties given by this material over CoFRM. The tensile properties are over twice as high and the compressive properties are around two times higher. It is assumed that the tensile properties for the nine configurations would vary in a similar manner to the CoFRM, but presumably with lower variation due to the increased volume fraction and more ordered fibre architecture.

The DCB testing was subject to difficulties at low cure levels as the material will not fracture; this is the effect of the interlaminar toughness exceeding the flexural strength for this test geometry. The main conclusion is that the vinylester resin improves fracture toughness by 66% (comparing the average of R2 and R4 with the average of R6 and R8 – see Figure 4:7). The hybrid mixed resin shows a high toughness which cannot be easily explained, it is also unclear whether this effect would be apparent in other fibre architectures. Sample R3 (UP, 70deg. cure, no postcure) is unusual in that it has higher apparent fracture toughness than R2 or R4 yet is under-cured. The three repeats are from one moulding which may have had a higher cure level than the R3 tube specimens, although this may not fully explain the result. Figure 4:34 shows the correlation between the proportion of vinylester resin in the mixture and the fracture toughness and SEA.

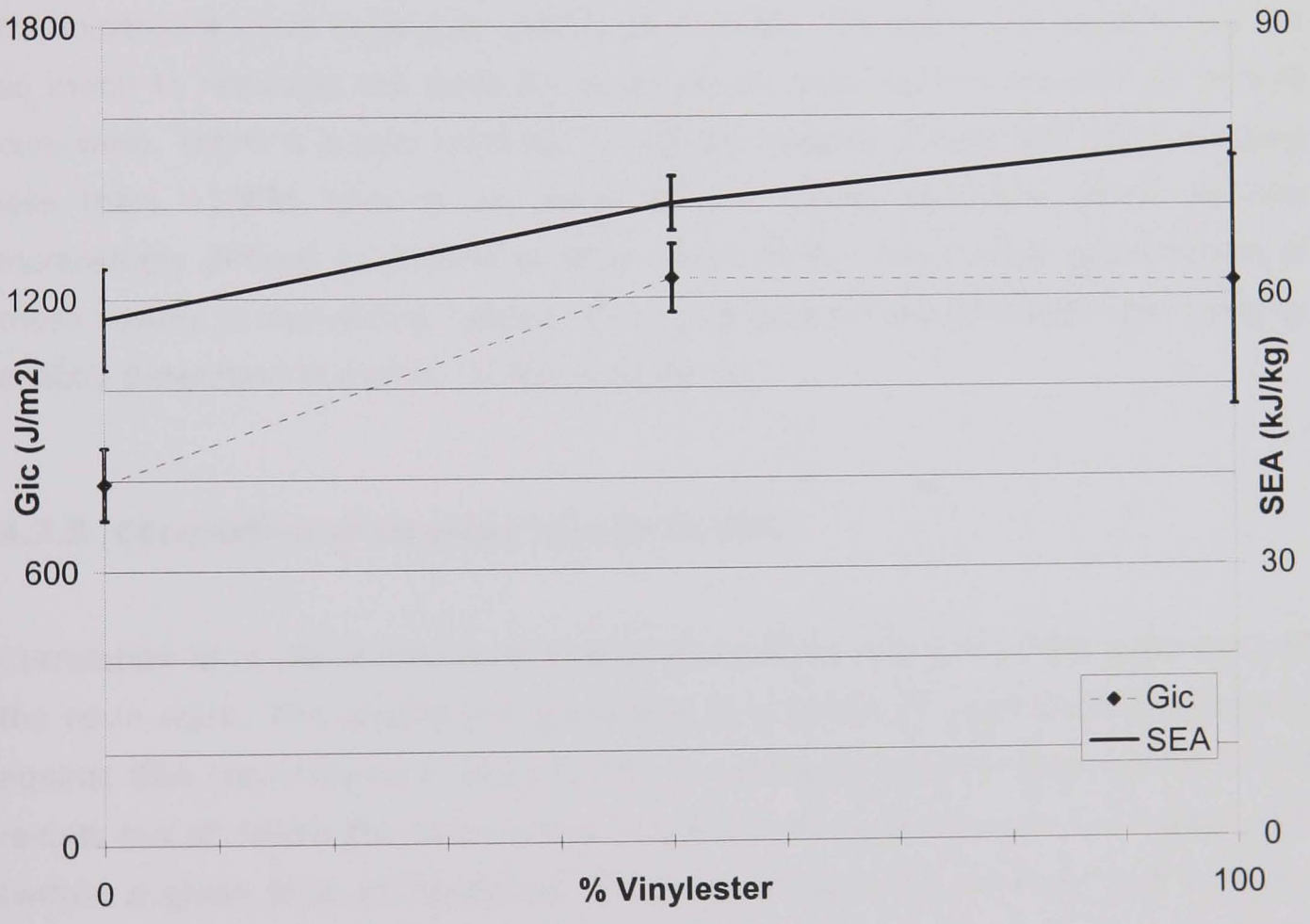

Figure 4:34 Fracture toughness and energy absorption vs. resin mix (CoFRM)

4.7.4 Degree of cure results

DSC data is presented in Figure 4:18. The cure data serves two purposes in this work. The first is to validate the cure level obtained in the crush testing to ensure accuracy and repeatability. The second is to see whether cure level has a direct effect on the SEA.

The results showed that the resin is fully cured by the chosen method independent of resin type. The postcure is essential in providing full cure although there is evidence to suggest that R7 (high temperature cure, no postcure) approaches full cure. Optimisation of processing could give full cure in the mould. However there are other reasons for providing a postcure. Safety is an important factor in an industrial process and a postcure ensures that under-cured parts do not leave the production line. It is also more cost effective to use the expensive main tooling as quickly as possible. Therefore the benefits are not so much in reducing the need for postcure as reducing the original 30 minute cure time. There is a poor correlation between degree of cure and SEA, anything less than ~100% cure is not commercially viable and cure levels become increasingly difficult to determine after about 95%. Any further examination of these results is impossible without neat resin data for the different cure levels to exactly determine the effect of low cure levels.

4.7.5 Correlation of in-plane results to SEA

Correlation of in-plane results to energy absorption was one of the main aims of the resin work. The results are presented as a graph of each in-plane property against SEA (see Figures 4:19 to 4:23). In general there is a large spread in the results but all follow the same trend; Higher in-plane properties give higher SEA (within a given fibre architecture). The only property to correlate well with the SEA was ultimate compressive stress. Two tests were applied to the data, the r^2 value providing an easily interpreted result. The results range from 0.36 for E_c through ~0.55 for tensile properties to 0.83 for UCS. The r^2 value indicates the proximity of the experimental data to the regression line where a value of 1 indicates perfect correlation.

The fact that in general the correlation is poor implies that the SEA is dependent either on a combination of properties or on properties not tested. As it is

impossible to isolate one material property it is very difficult to determine the exact contribution of each. Crushing performance is dependent both on material properties and crush zone morphology, these two are of course interlinked. For instance, fracture toughness affects centre wall crack length which in turn affects the energy absorption through tighter bending of the fronds.

Vinylester resin appears to improve crush performance through a combination of higher composite ultimate compressive stress and increased fracture toughness. The inability to fully isolate one property is seen as a major obstacle to full understanding in this area.

Chapter 4 References

1. Hicks, C.R. and K.V. Turner, *Fundamental Concepts in the Design of Experiments*. 1999: Oxford University Press.

5 Effect of interlaminar toughening methods

The work documented in Chapter 4 suggested the importance of Mode I fracture toughness in controlling mode of failure and consequent energy absorption properties. The toughness of the composite can be increased by modifying the preform structure. Dramatic gains are cited in the literature for both stitching and interleaving. The aim of the investigation was therefore to quantify the effect of various methods of increasing Mode I fracture toughness on SEA. This involved testing both the SEA of the composites and the Mode I fracture toughness to quantify any gains. The two methods chosen were interleaving, where a thin polymer film is inserted on the centreline of the composite to limit interlaminar crack growth, and through stitching, where (in this case) aramid threads reinforce the composite in the Z-direction.

Two different interleaves were chosen on the basis of their service temperature and differing properties and were both deemed to be compatible with glass fabrics by the manufacturers. A range of through thickness stitch materials were considered but it proved impossible to reliably sew with any material other than Kevlar 49 so stitch density is the only variable.

Double cantilever beam tests were performed to measure the effect of the methods for enhancing through-thickness properties and to allow assessment of any correlation between SEA and fracture toughness. In-plane testing was also conducted to determine the effect of stitching on in-plane strength and modulus.

5.1 Methodology

A wide range of interleaf films was available in many different polymers and with many film thicknesses. Initial testing showed that a basic polyurethane film increased the strength of the bond between the glass plies significantly, further discussions with the supplier lead to the choice of two films with a high melt temperature – one a thin polypropylene film with high modulus and the other a thicker polyurethane with much lower modulus. As only two films could be tested due to time constraints the aim was to encompass a wide range of properties by having a stiff bondline and a lower modulus bondline with two different polymers. The high melt temperature gave some problems with processing and made the task of rolling a preform much more time-consuming. Tests were conducted to ensure that the film was melting by peeling back the edge of the preform which was then cut and discarded after rolling.

The use of stitching to toughen composites is thoroughly covered in the literature, the primary advantage being a substantial increase in out-of-plane properties. Unfortunately stitching can lead to damage in the composite as a result of the impact of the needle and the displacement of the fibres causing local kinks in the fibre path Figure 5:1. Micrographs from this work did not show any visible damage (See Figures 5:18 and 5:19). Needle speeds were kept deliberately low and preforms were made fairly soft to allow flexing during stitching.

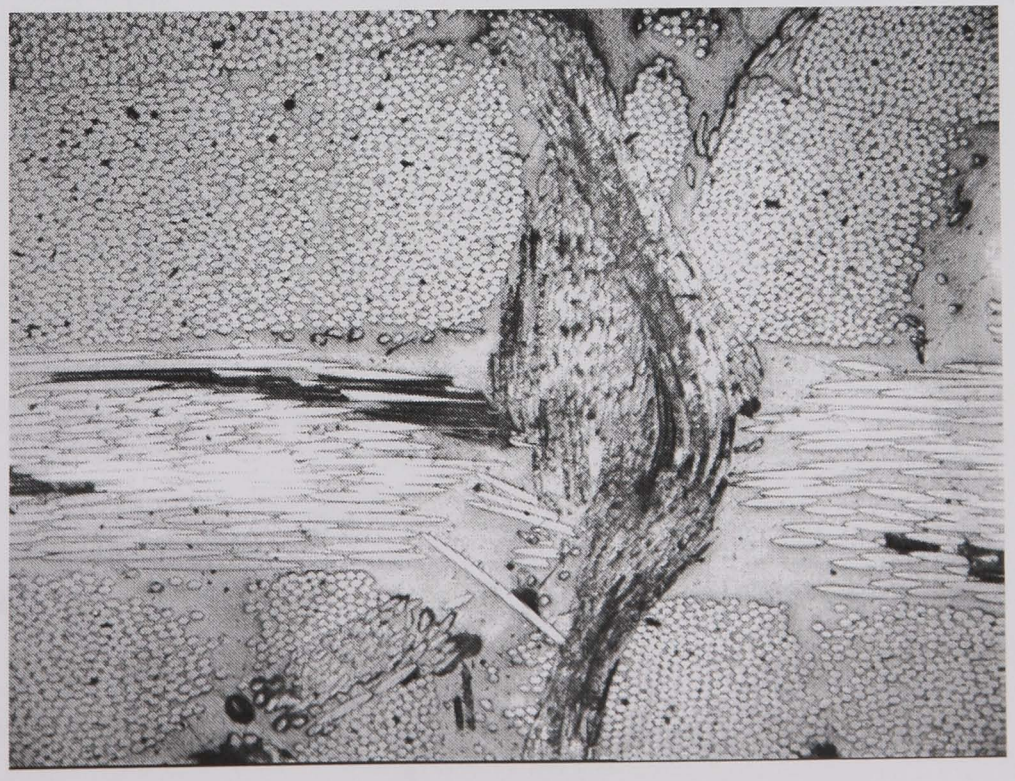

Figure 5:1 Micrograph showing potential damage caused by stitching [1]

5.1.1 Specimen manufacture - Interleaved specimens

Interleaf materials were included at the preforming stage and heated to the required melt temperature window with a hot air gun. In some cases DCB specimens were made by stacking the layers of glass fabric and interleaf material in a hot air oven and compressing in a screw press. In tubular preforms the interleaf material was introduced to give the correct position in the final part. Interleaves were inserted either side of the mid plane of the moulded parts. Figures 5:2 and 5:3 show the position of the interleaf film in CoFRM and NCF preforms.

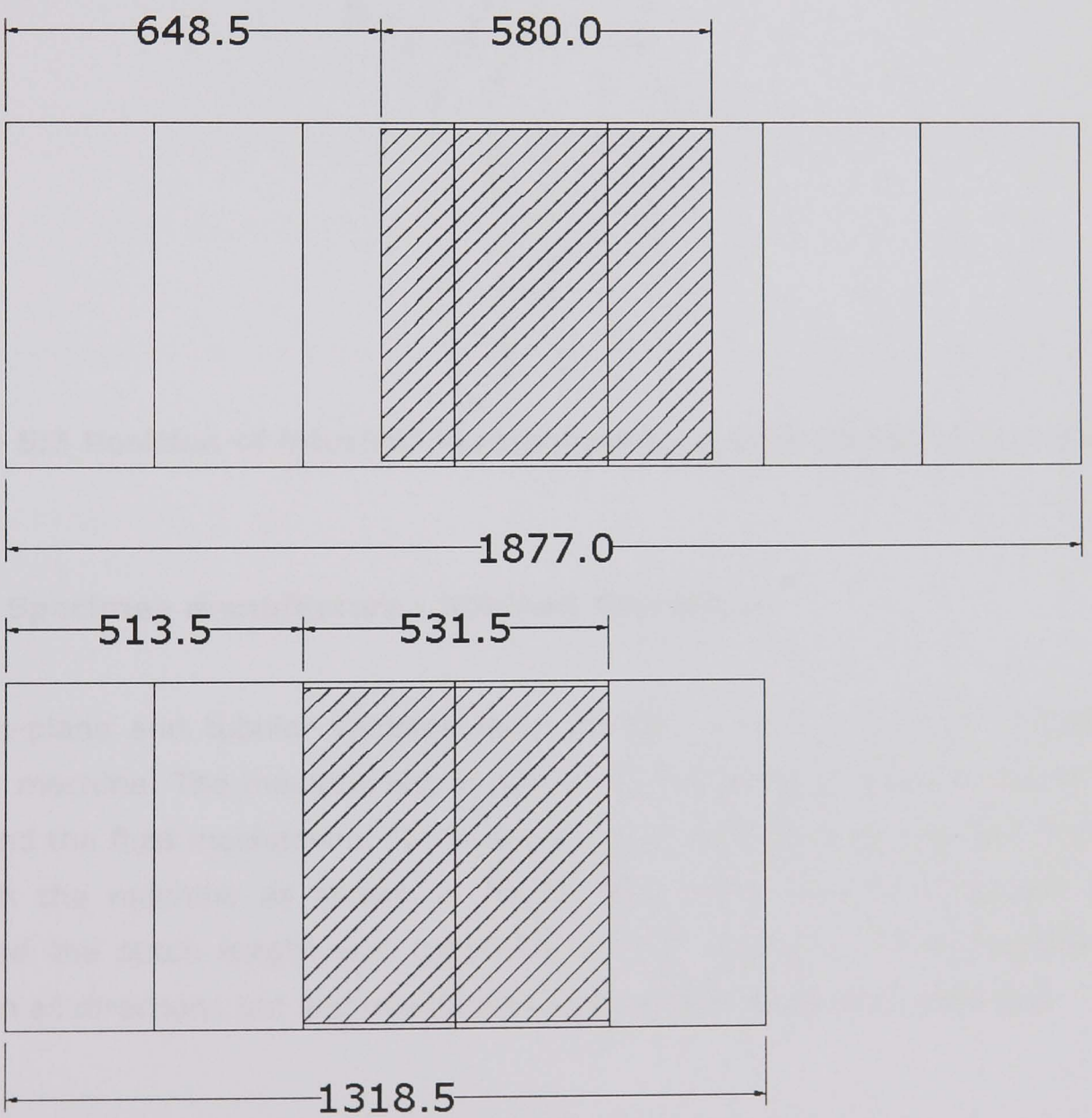

Figure 5:2 Layout of interleaf film on glass preforms – NCF at top (7 layers in final preform) and CoFRM below (5 layers) Shading shows interleaf overlay

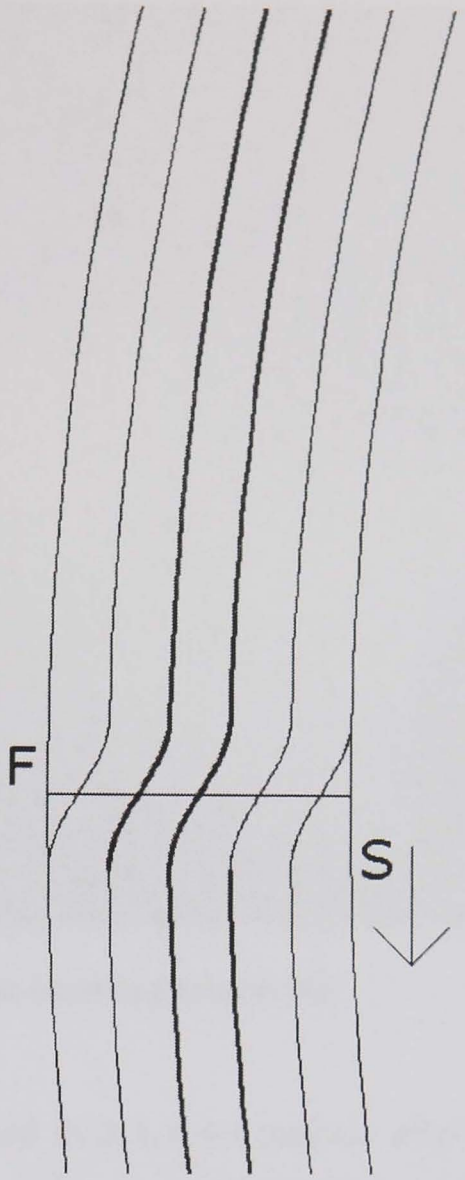

Figure 5:3 Position of interleaf in rolled preform showing start and finish

5.1.2 Specimen manufacture - Stitched Specimens

Both in-plane and tubular samples were stitched on a conventional lockstitch sewing machine. The machine was modified by removing a large portion of the base and the feed mechanism. The reduced size allowed tube preforms to be fed through the machine as shown in Figure 5:4. As the feed mechanism was removed the stitch length was controlled by the operator. It was possible to stitch in all directions but a conventional front-to-back route was preferred.

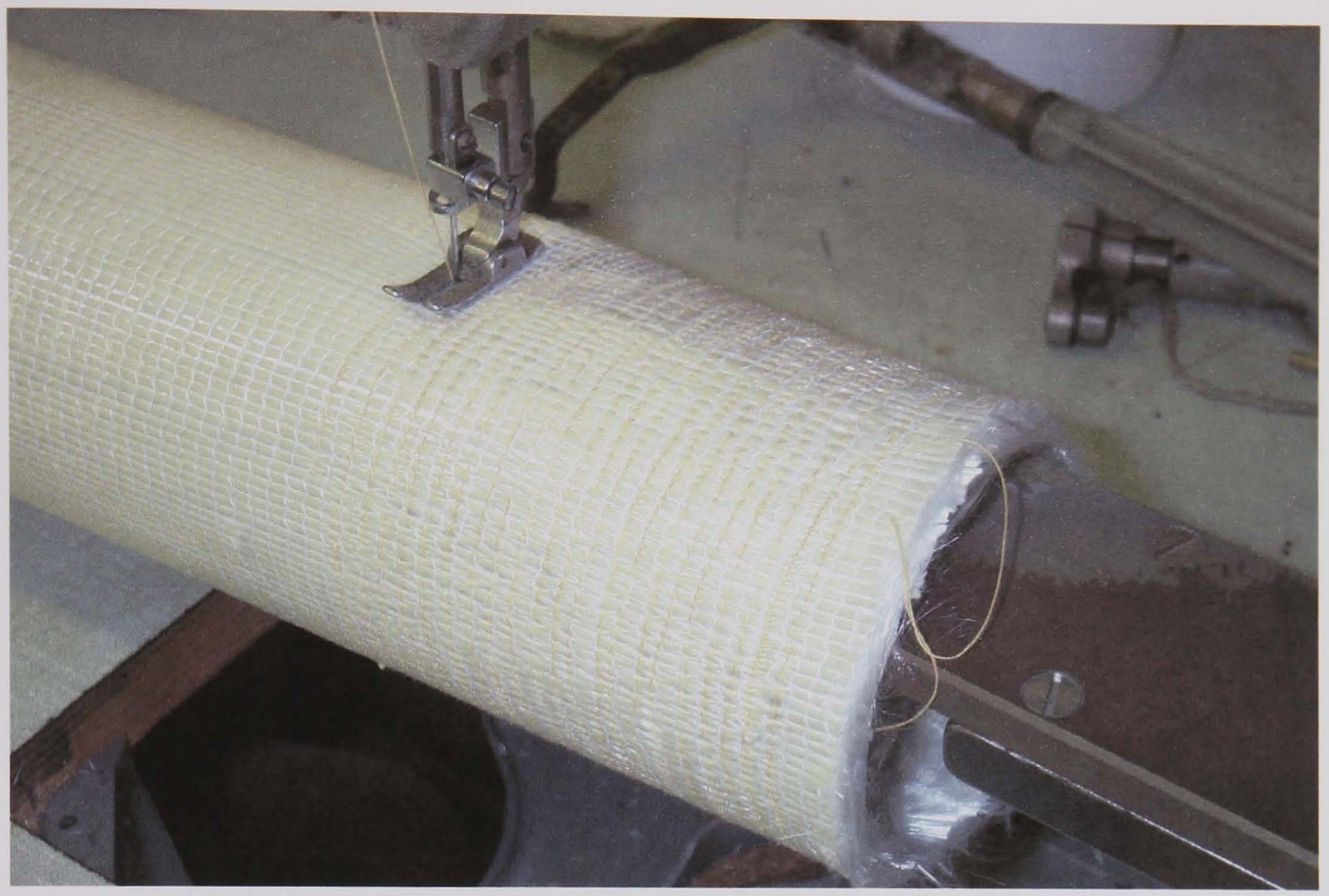

Figure 5:4 Modifications to sewing machine

Stitch materials were as stated in 3.1.4.4 however after preliminary testing of all materials (See section 3.1.4.4), it became apparent that only aramid was useable. Due to the large thread size relatively large needles were used, Needles were denoted 134R in size 120. The machine is a Brother industrial machine type number DB2 B755-3.

5.2 Moulding configurations

Interleaf tube = 4 samples per tube moulding
Stitched tube = 2 stitched samples + 2 control specimens

Due to limitations on throat depth of the lockstitch machine used, the stitched tubes have the end samples (A and D) stitched with the two centres acting as control specimens. As the moulding is the same for interleaved and stitched tubes the control specimens are used as a control for the whole study. This results in there being twice as many stitched tube mouldings as interleaved.

Interleaf – 3 variations

- No interleaf
- Rigid Polypropylene XAF23.401 40gsm (Type 1)
- Flexible Urethane XAF36.304 100gsm (Type 2)

Stitching – 3 levels

- No Stitch
- Low density – 10mm helix with 6mm stitch length
- High density – 3mm helix with 3mm stitch length

Table 5:1 shows the tube crush configurations;

Tube #	Samples	
PI1A	NCF - 4x type 1 interleaf	
PI1B	NCF - 4x type 1 interleaf	
PI1C	NCF - 4x type 1 interleaf	12 repeats
PI2A	NCF - 4x type 2 interleaf	
PI2B	NCF - 4x type 2 interleaf	
PI2C	NCF - 4x type 2 interleaf	12 repeats
PI3A	CoFRM - 4x type 1 interleaf	
PI3B	CoFRM - 4x type 1 interleaf	
PI3C	CoFRM - 4x type 1 interleaf	12 repeats
PI4A	CoFRM - 4x type 2 interleaf	
PI4B	CoFRM - 4x type 2 interleaf	
PI4C	CoFRM - 4x type 2 interleaf	12 repeats
PS1A	NCF – 2 controls , 2 low	
PS1B	NCF – 2 controls , 2 low	
PS1C	NCF – 2 controls , 2 low	
PS1D	NCF – 2 controls , 2 low	
PS1E	NCF – 2 controls , 2 low	
PS1F	NCF – 2 controls , 2 low	12 control, 12 low
PS2A	NCF – 2 controls , 2 high	
PS2B	NCF – 2 controls , 2 high	
PS2C	NCF – 2 controls , 2 high	
PS2D	NCF – 2 controls , 2 high	
PS2E	NCF – 2 controls , 2 high	
PS2F	NCF – 2 controls , 2 high	12 control, 12 high
PS3A	CoFRM – 2 controls , 2 low	
PS3B	CoFRM – 2 controls , 2 low	
PS3C	CoFRM – 2 controls , 2 low	
PS3D	CoFRM – 2 controls , 2 low	
PS3E	CoFRM – 2 controls , 2 low	
PS3F	CoFRM – 2 controls , 2 low	12 control, 12 low
PS4A	CoFRM – 2 controls , 2 high	
PS4B	CoFRM – 2 controls , 2 high	
PS4C	CoFRM – 2 controls , 2 high	
PS4D	CoFRM – 2 controls , 2 high	
PS4E	CoFRM – 2 controls , 2 high	
PS4F	CoFRM – 2 controls , 2 high	12 control, 12 high

Table 5:1 Crush Configurations

Where 'Low' refers to Low density stitching and 'High' to High density.

5.3 Axial tube crush results

Specific energy absorption values for the interleaved parts are shown in the figures and tables below. The two interleaves are shown separately and have 3 moulding repeats each with 4 samples.

Tube ref.	SEA A	SEA B	SEA C	SEA D	Average SEA	St. Dev. (ABS)
PI1A	27.96	26.45	29.57	29.69	**28.4**	**1.5**
PI1B	28.90	27.71	28.16	29.02	**28.5**	**0.6**
PI1C	23.83	24.36	23.90	28.21	**25.1**	**2.1**
				Rep.Av	**27.3**	**2.2**
PI2A	27.45	25.27			**26.36**	**1.5**
PI2B	29.59	25.50	23.09	25.66	**25.96**	**0.6**
PI2C	27.72	22.14	21.61		**23.82**	**3.4**
				Rep.Av	**25.3**	**2.7**

Table 5:2 SEA data for interleaved NCF tubes

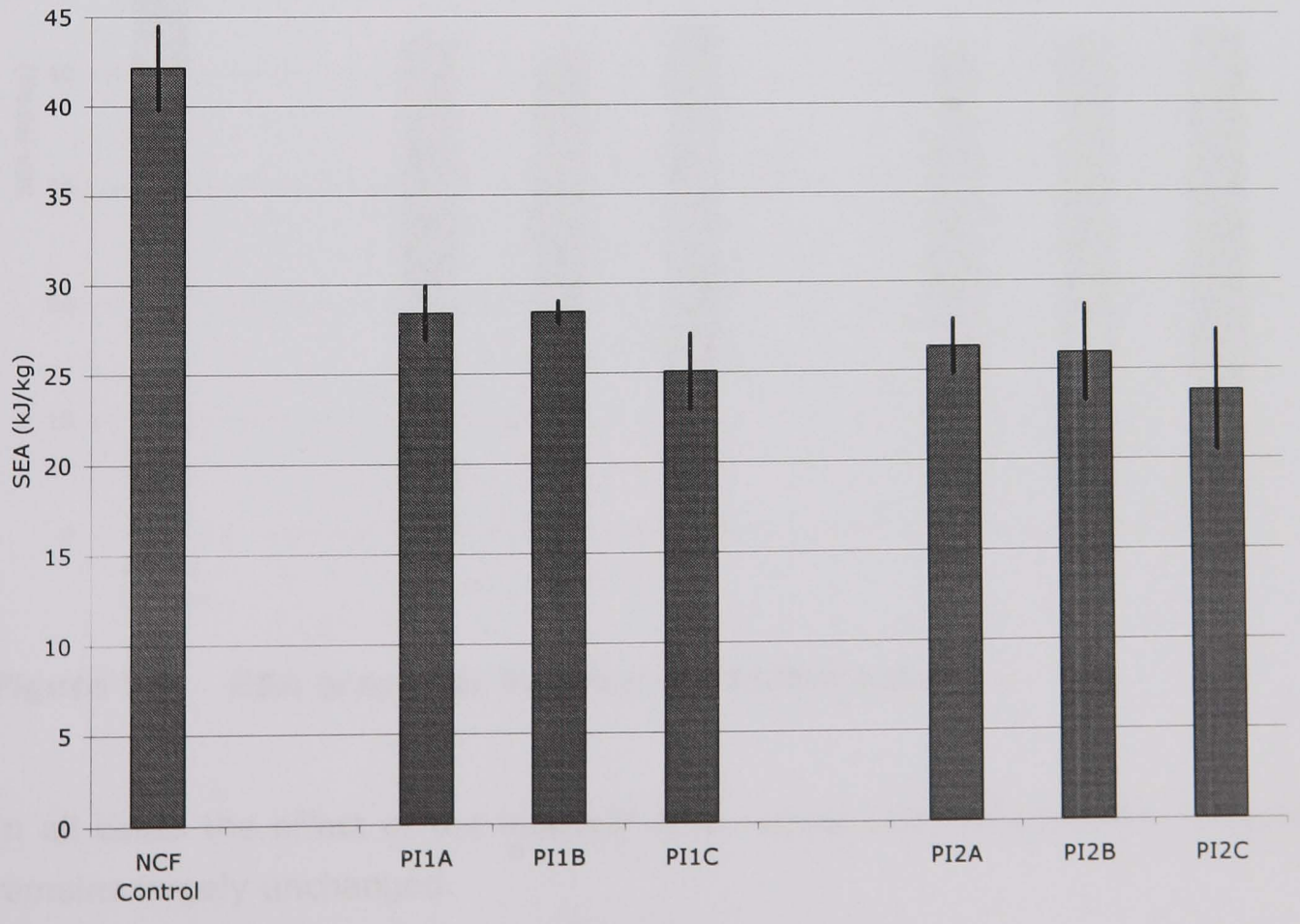

Figure 5:5 SEA graph for interleaved NCF tubes

Tube ref.	SEA A	SEA B	SEA C	SEA D	Average SEA	St. Dev. (ABS)
PI3A	44.71	42.92	44.88	39.20	**42.9**	**2.6**
PI3B	37.29	43.42	43.11	43.88	**41.9**	**3.1**
PI3C	44.61	41.92	43.06	46.46	**44.0**	**2.0**
				Rep.Av	**43.0**	**2.5**
PI4A	45.46	38.84	41.87	41.68	**42.0**	**2.7**
PI4B	42.99	42.20	42.96	41.54	**42.4**	**0.7**
PI4C	44.11	44.91	42.28	41.02	**43.1**	**1.8**
				Rep.Av	**42.5**	**1.8**

Table 5:3 SEA data for interleaved CoFRM tubes

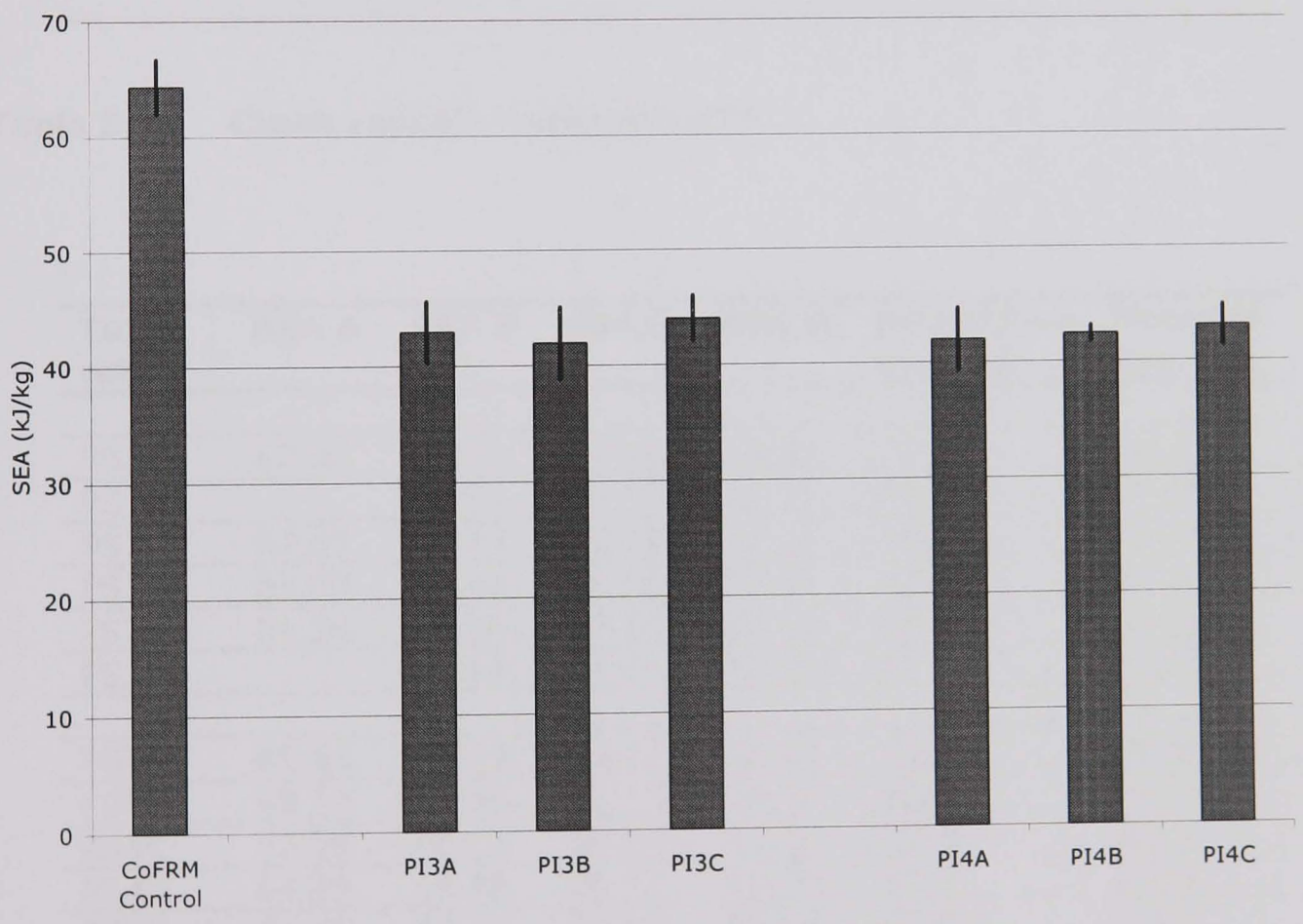

Figure 5:6 SEA graph for interleaved CoFRM tubes

In all cases the effect of the interleaf is to reduce SEA considerably. Variability remains largely unchanged.

Stitching results are shown below, averages are shown for both stitched and unstitched as each moulding consists of two parts of each.

Tube ref.	SEA A	SEA B	SEA C	SEA D	Unstitched average	Stitched average
PS1A	49.36	43.50	44.36	48.81	**43.9**	**48.6**
PS1B	49.00	41.84	43.17	50.97	**42.5**	**50.0**
PS1C	48.59	43.13	41.17	50.11	**42.1**	**49.3**
PS1D	50.91	44.76	44.47	49.98	**44.6**	**50.4**
PS1E	55.22	45.34	46.97	50.14	**46.2**	**52.7**
PS1F	49.37	44.57	42.36	46.78	**43.5**	**48.1**
PS2A	53.35	40.52	39.20	48.65	**39.9**	**51.0**
PS2B	54.06	43.07	41.62	52.89	**42.3**	**53.5**
PS2C	48.42	37.23	37.65	53.06	**37.4**	**50.7**
PS2D	55.11	41.49	40.25	50.23	**41.0**	**52.7**
PS2E	54.11	41.06	40.97	50.27	**41.0**	**52.2**
PS2F	52.30	41.24	41.70	50.24	**41.5**	**51.3**

Table 5:4 Crush results – Stitched NCF

Tube ref.	SEA A	SEA B	SEA C	SEA D	Unstitched average	Stitched average
PS3A	67.92	67.06	67.00	65.52	**67.0**	**66.7**
PS3B		62.85	64.47	65.52	**63.7**	**65.5**
PS3C	67.05	66.24	62.09	52.17	**64.2**	**59.6**
PS3D	61.63	63.40	61.48	55.22	**62.4**	**58.4**
PS3E	61.56	65.63	64.18	55.54	**64.9**	**58.6**
PS3F		68.18	64.94	59.27	**66.6**	**59.3**
PS4A	65.53	65.09	66.12	63.56	**65.6**	**64.5**
PS4B	69.32	65.96	65.75	65.45	**65.9**	**67.4**
PS4C	65.59	66.11	64.88	60.74	**65.5**	**63.2**
PS4D	65.95	64.78	60.72	52.09	**62.7**	**59.0**
PS4E	61.52	57.12	62.97	58.48	**60.0**	**60.0**
PS4F	65.81	63.21	64.12	44.66	**63.7**	**55.2**

Table 5:5 Crush results – Stitched and unstitched CoFRM

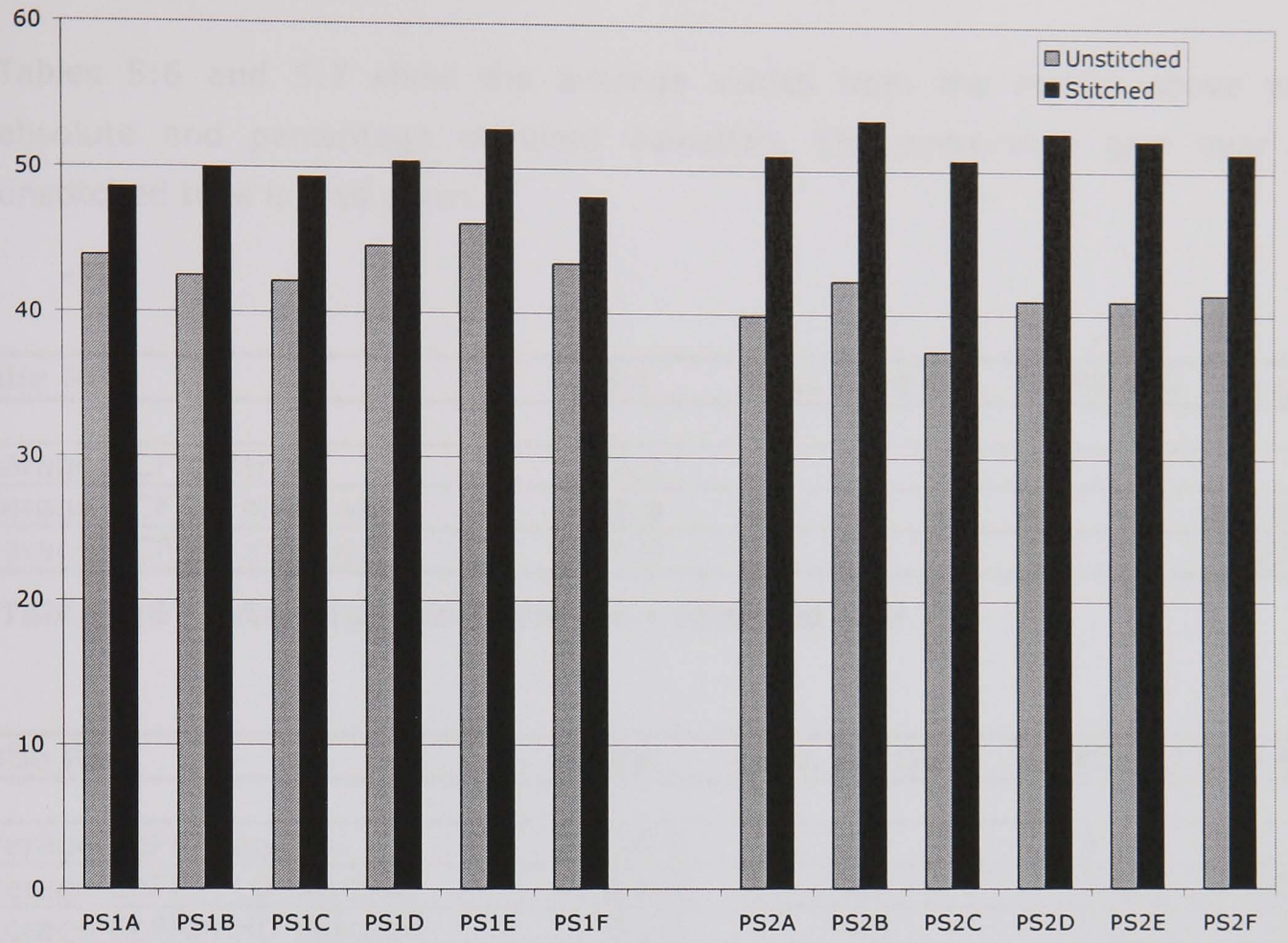

Figure 5:7 Stitched vs. Unstitched SEA – NCF samples

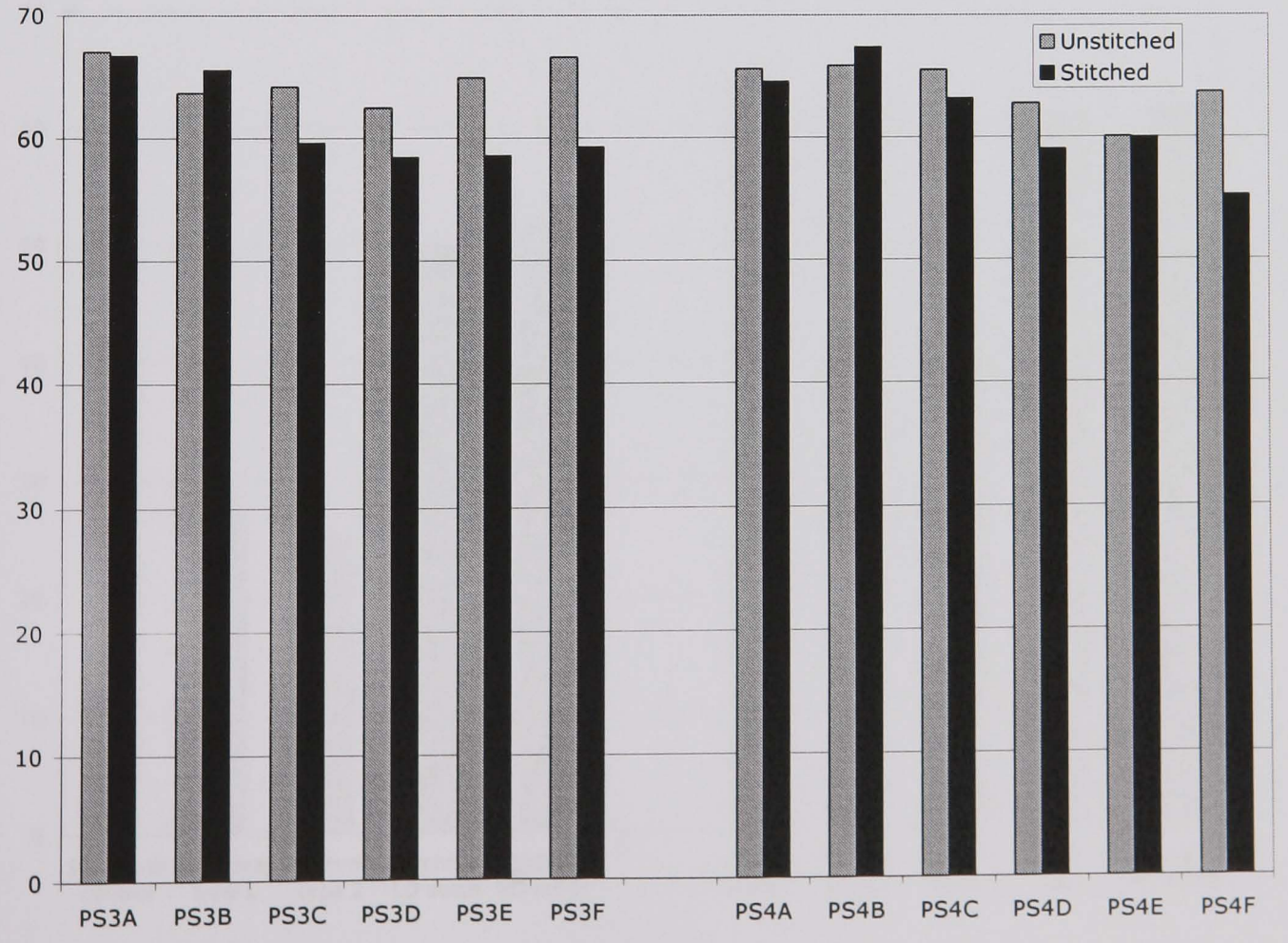

Figure 5:8 Stitched vs. Unstitched SEA – CoFRM samples

Tables 5:6 and 5:7 show the average values from the results above with absolute and percentage standard deviation. The percentage gain over an unstitched tube is also given.

Tube Ref.	SEA	Abs. St. Dev.	% St dev	% gain
Average NCF control	**42.2**	2.3	5.5	
Average NCF LD stitched	**49.9**	2.1	4.2	+18%
Average NCF HD stitched	**51.9**	2.2	4.3	+23%

Table 5:6 Average crush values – Stitched NCF

Tube Ref.	SEA	Abs. St. Dev.	% St dev	% gain
Average CoFRM control	**64.3**	2.0	3.1	
Average CoFRM LD stitched	**61.3**	3.7	6.1	-5%
Average CoFRM HD stitched	**61.6**	4.3	7.1	-5%

Table 5:7 Average crush results for stitched CoFRM

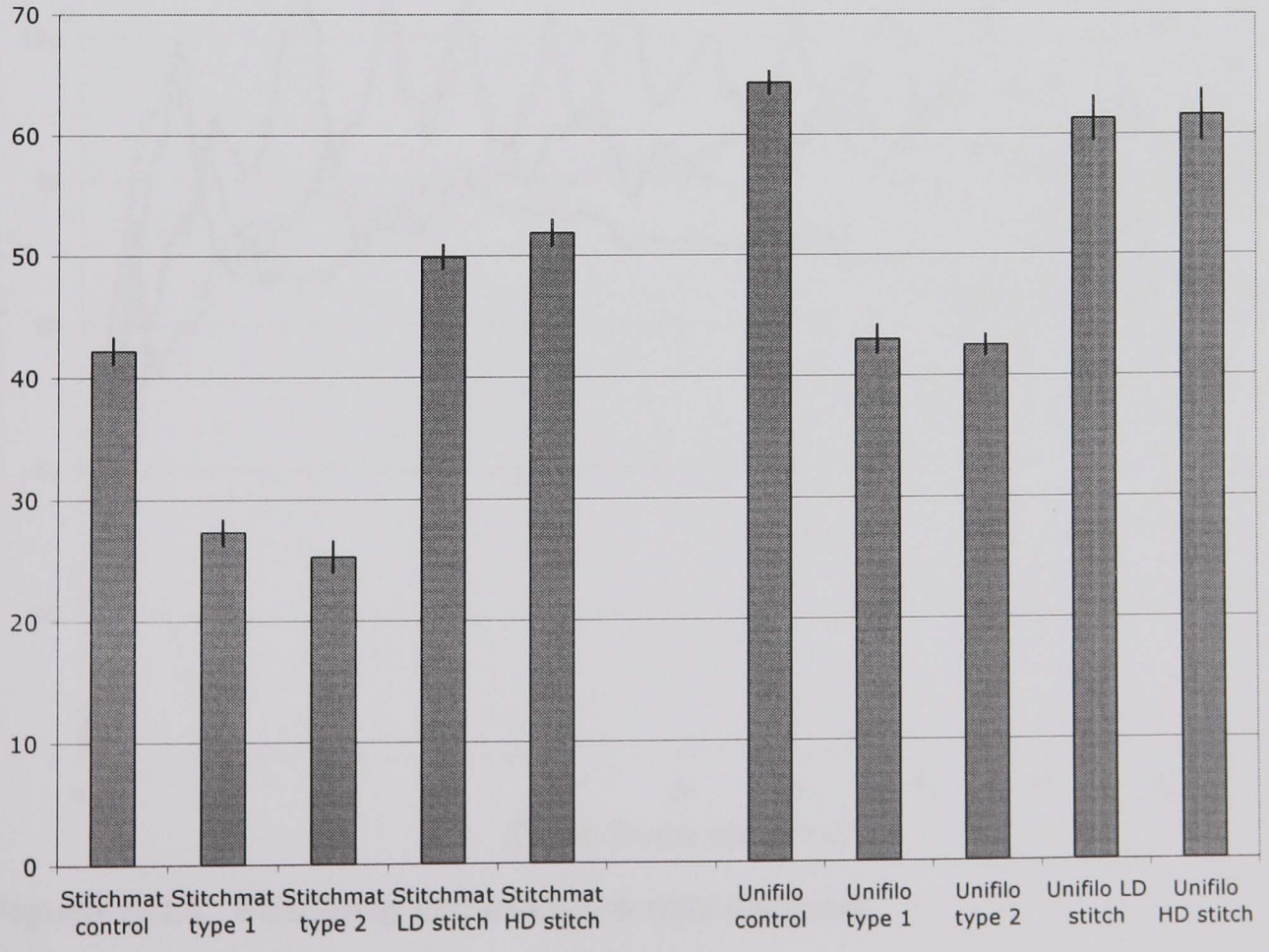

Figure 5:9 Overall results for interleaving and stitching for NCF (left) and CoFRM (right)

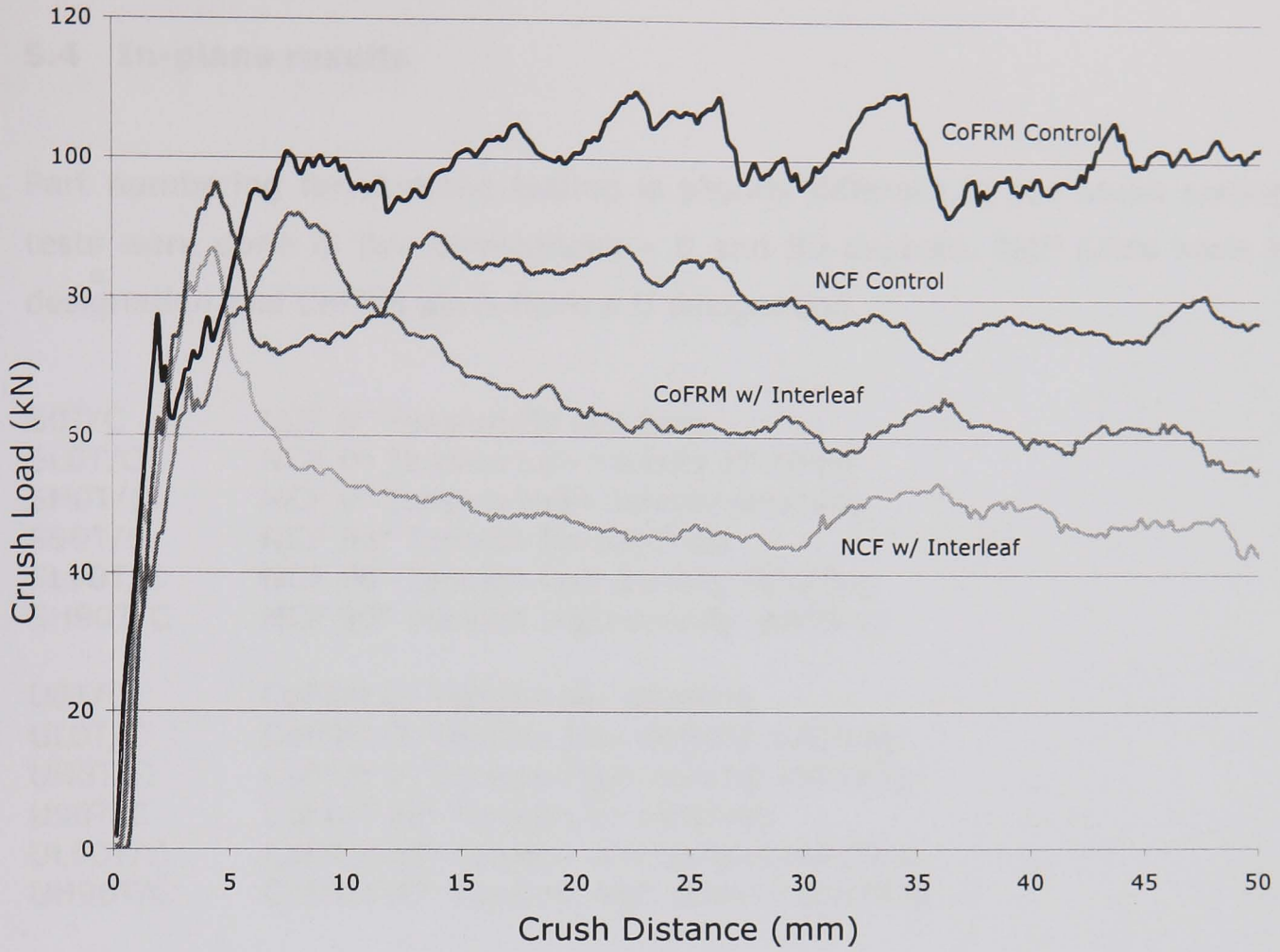

Figure 5:10 Interleaf crush curve comparison

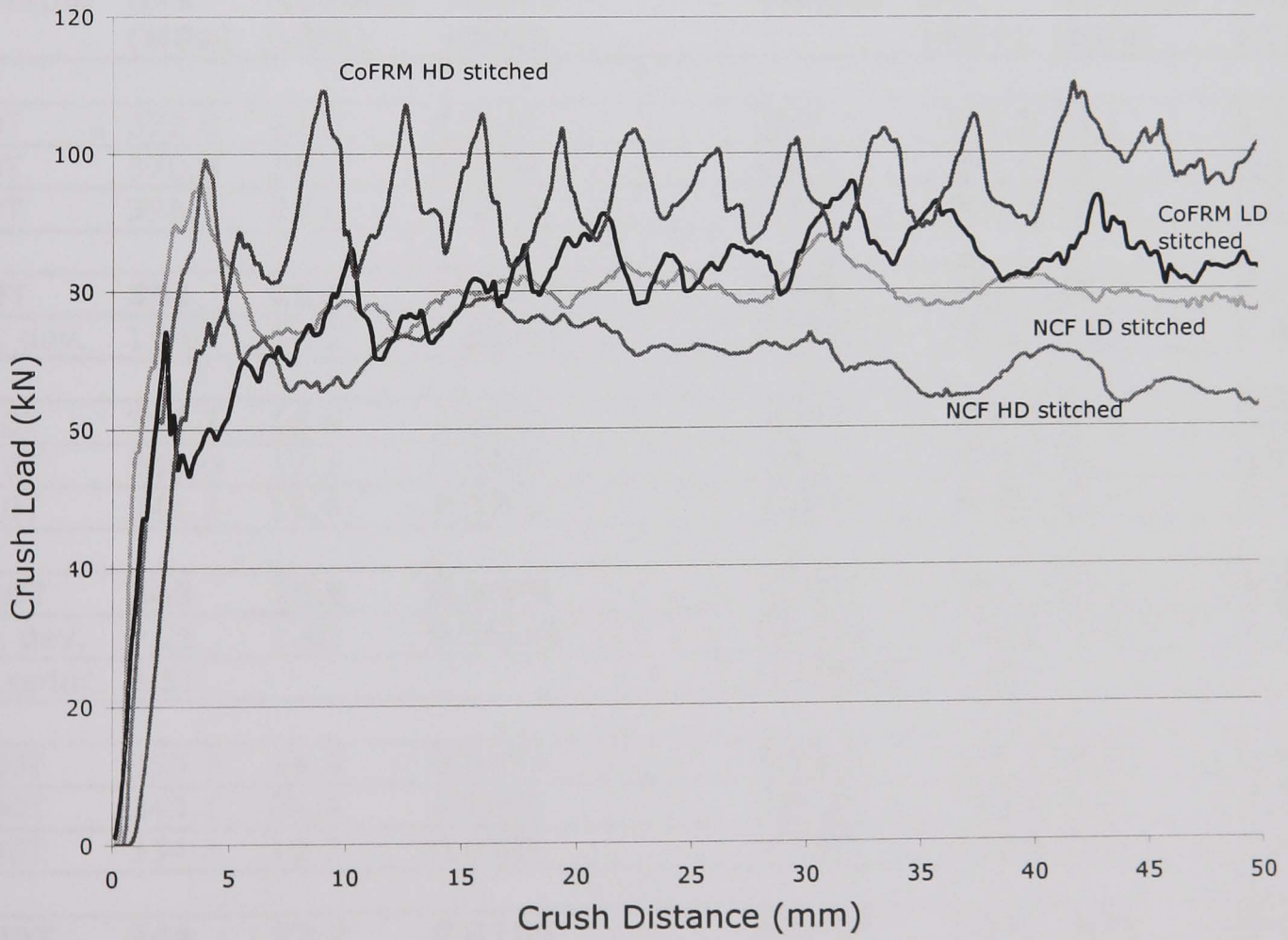

Figure 5:11 Stitching crush curve comparison

5.4 In-plane results

Part numbering for in-plane testing is slightly different to the crush testing as tests were done in two orientations – 0 and 90 degrees. NCF parts have an S designation and CoFRM parts have a U designation.

S0T/C	NCF 0° Tension No stitching
SL0T/C	NCF 0° Tension Low density stitching
SH0T/C	NCF 0° Tension High density stitching
S90T/C	NCF 90° Tension No stitching
SL90T/C	NCF 90° Tension Low density stitching
SH90T/C	NCF 90° Tension High density stitching
U0T/C	CoFRM 0° Tension No stitching
UL0T/C	CoFRM 0° Tension Low density stitching
UH0T/C	CoFRM 0° Tension High density stitching
U90T/C	CoFRM 90° Tension No stitching
UL90T/C	CoFRM 90° Tension Low density stitching
UH90T/C	CoFRM 90° Tension High density stitching

Results are given in Tables 5:8 and 5:9;

Sample	UTS (MPa)	Modulus (GPa)	failure strain	Sample	UTS (MPa)	Modulus (GPa)	failure strain
S0T	372.8	19.7	0.0187	S90T	397.5	23.1	0.0218
S0T	370.5	20.1	0.0188	S90T	381.4	24.7	0.0178
S0T	398.7	23.1	0.0178	S90T	366.2	24.8	0.0178
S0T	**381**	**21.0**	**0.0185**	**S90T**	**382**	**24.2**	**0.0192**
St. dev.	15.65	1.83	0.00056	St. dev.	15.66	0.95	0.00229
SL0T	358.7	18.8	0.0202	SL90T	379.3	24.6	0.0183
SL0T	345.0	17.1	0.0213	SL90T	352.1	22.2	0.0196
SL0T	341.2	19.8	0.0181	SL90T	368.7	22.4	0.0195
SL0T	**348**	**18.6**	**0.0199**	**SL90T**	**367**	**23.1**	**0.0191**
St. dev.	9.21	1.40	0.00165	St. dev.	13.69	1.33	0.00071
% reduc.	8.51			% reduc.	3.93		
SH0T	358.3	24.4	0.0170	SH90T	340.7	22.5	0.0184
SH0T	340.1	22.4	0.0180	SH90T	376.7	21.7	0.0219
SH0T	334.7	19.7	0.0206	SH90T	333.8	21.2	0.0201
SH0T	**344**	**22.2**	**0.0185**	**SH90T**	**350**	**21.8**	**0.0201**
St. dev.	12.34	2.37	0.00184	St. dev.	23.05	0.62	0.00173
% reduc.	9.54			% reduc.	8.19		

Table 5:8 In-plane testing – NCF results 0° and 90° orientation

Sample	UTS	modulus	failure strain	Sample	UTS	modulus	failure strain
U0T	119.0	8.6	0.0204	U90T	149.9	11.9	0.0165
U0T	121.6	10.6	0.0164	U90T	171.2	12.1	0.0193
U0T	115.1	8.8	0.0176	U90T	161.6	11.2	0.0192
U0T	**119**	**9.3**	**0.0181**	**U90T**	**161**	**11.7**	**0.0183**
St Dev	3.26	1.06	0.00205		10.65	0.48	0.00156
UL0T	165.5	12.8	0.0171	UL90T	126.0	10.6	0.0180
UL0T	170.3	12.7	0.0182	UL90T	116.1	9.9	0.0163
UL0T	172.5	12.5	0.0176	UL90T	118.8	9.3	0.0194
UL0T	**169**	**12.6**	**0.0177**	**UL90T**	**120**	**10.0**	**0.0179**
St Dev	3.58	0.17	0.00056		5.11	0.64	0.00155
% reduc.	-42.89			% reduc.	25.24		
UH0T	139.5	11.9	0.0156	UH90T	109.2	9.2	0.0165
UH0T	166.8	12.1	0.0197	UH90T	116.7	9.8	0.0173
UH0T	153.1	12.7	0.0168	UH90T	105.0	10.3	0.0134
UH0T	**153**	**12.2**	**0.0174**	**UH90T**	**110**	**9.8**	**0.0157**
St Dev	13.64	0.38	0.00209		5.94	0.55	0.00204
% reduc.	-29.13			% reduc.	31.44		

Table 5:9 In-plane testing – CoFRM results 0° and 90° orientation

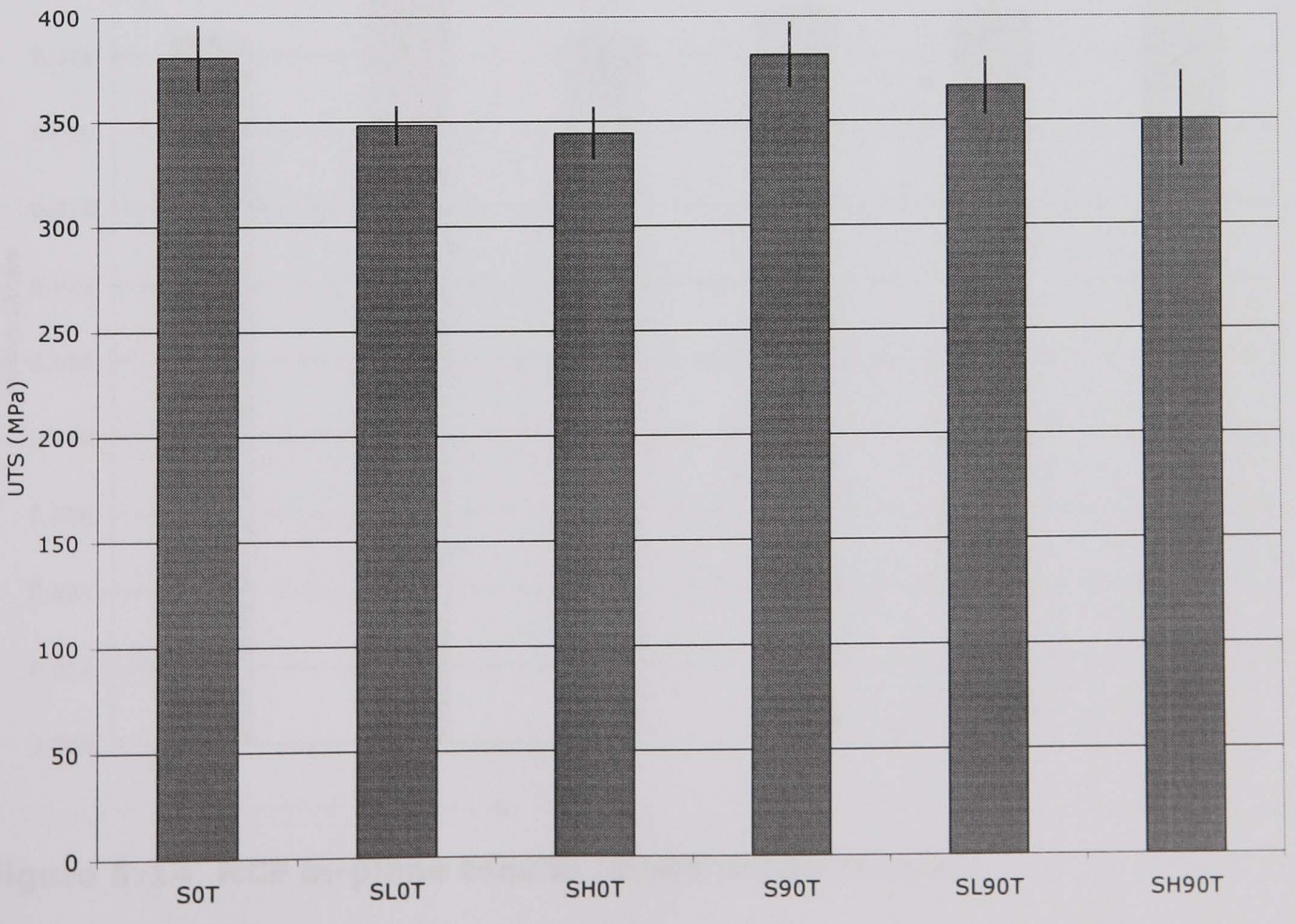

Figure 5:12 NCF in-plane UTS results

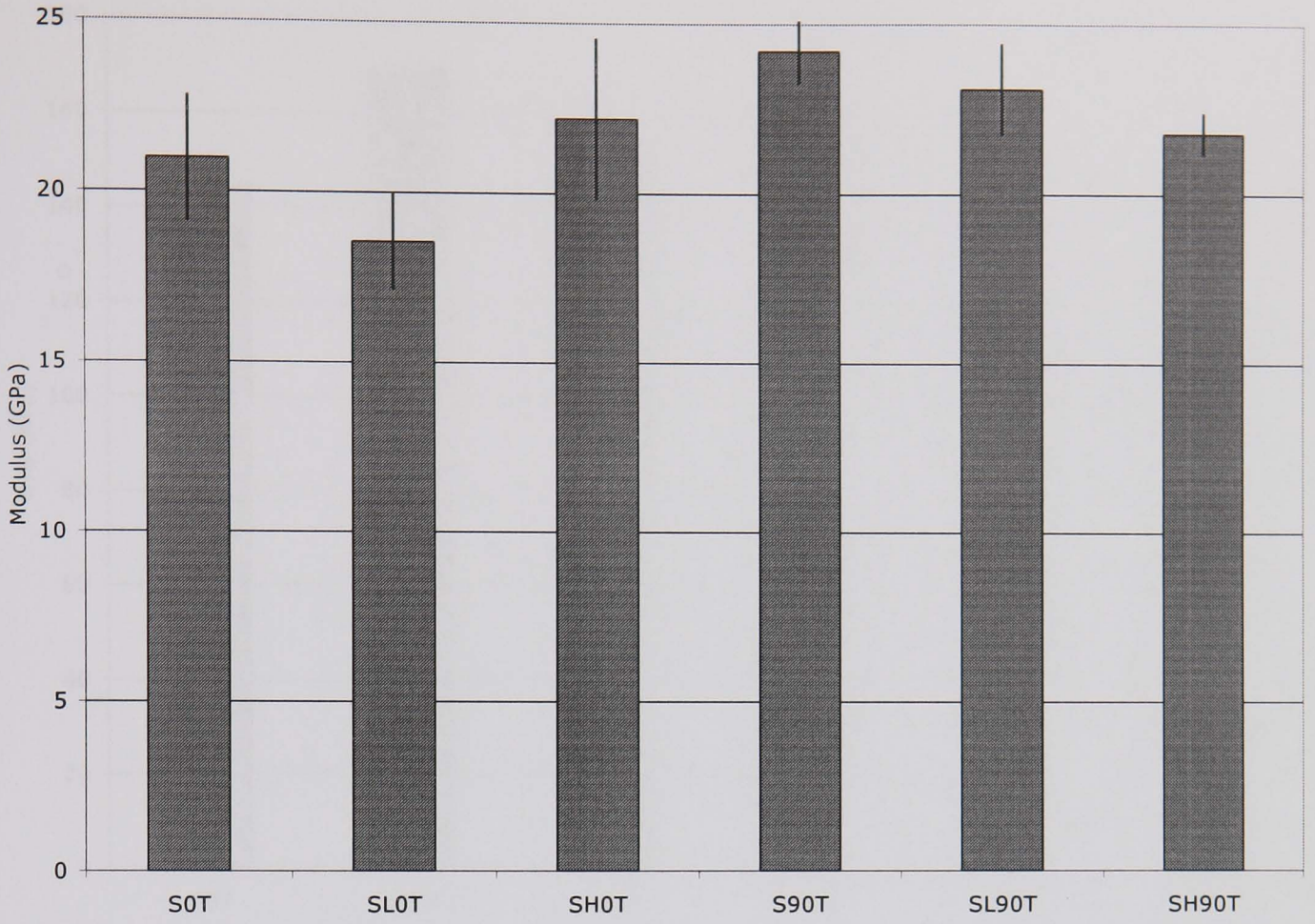

Figure 5:13 NCF in-plane tensile modulus results

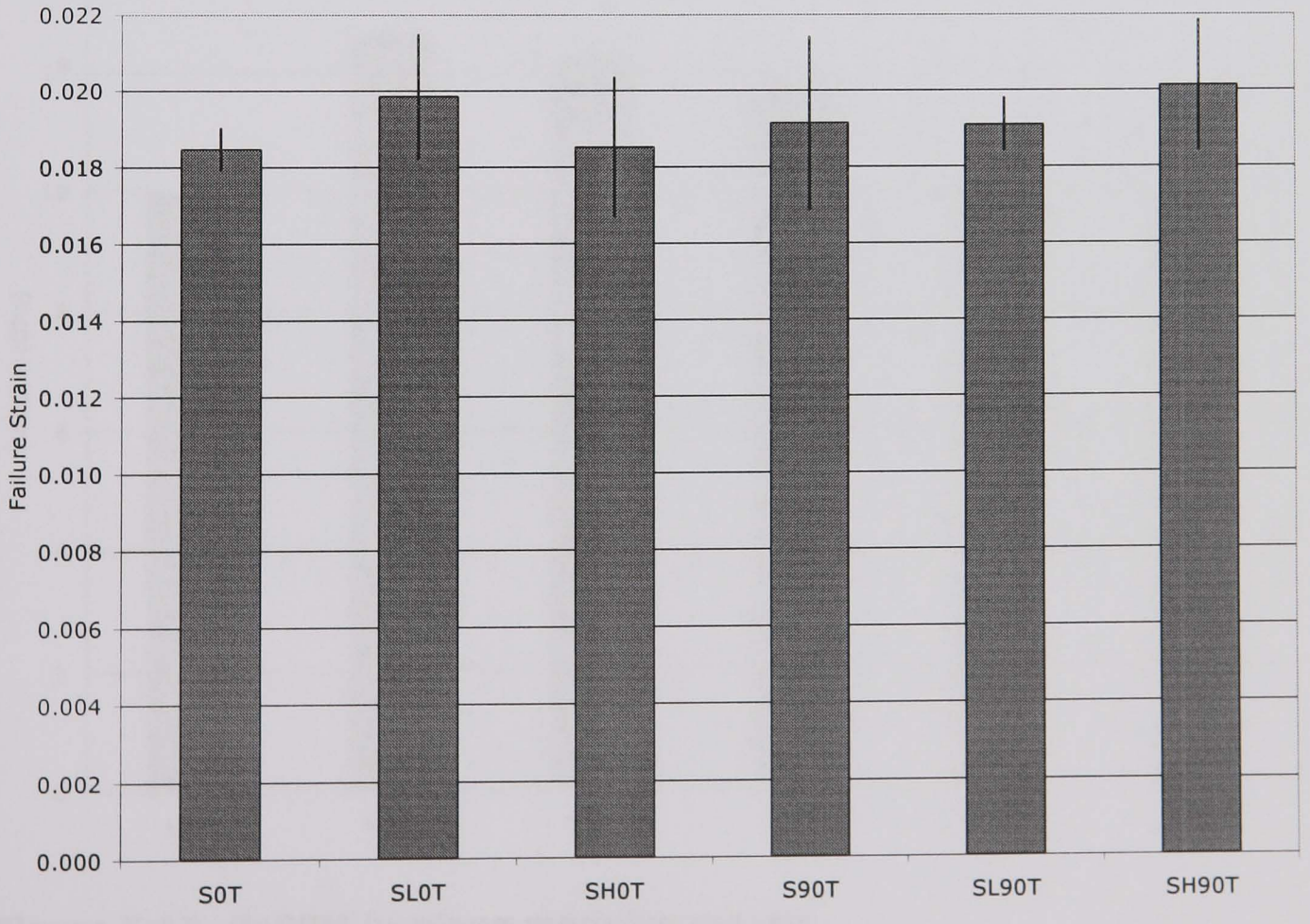

Figure 5:14 NCF in-plane tensile failure strain results

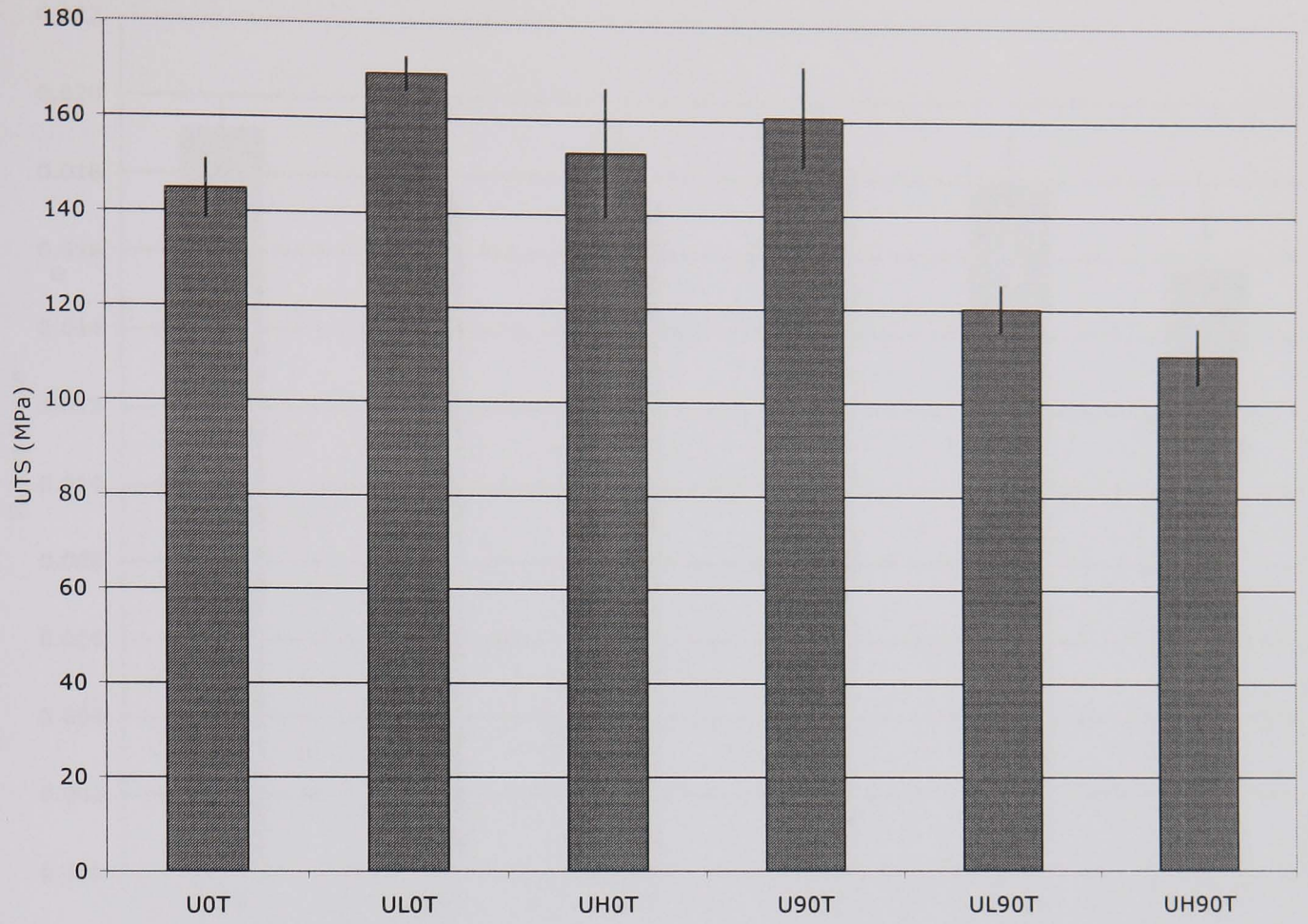

Figure 5:15 CoFRM in-plane UTS results

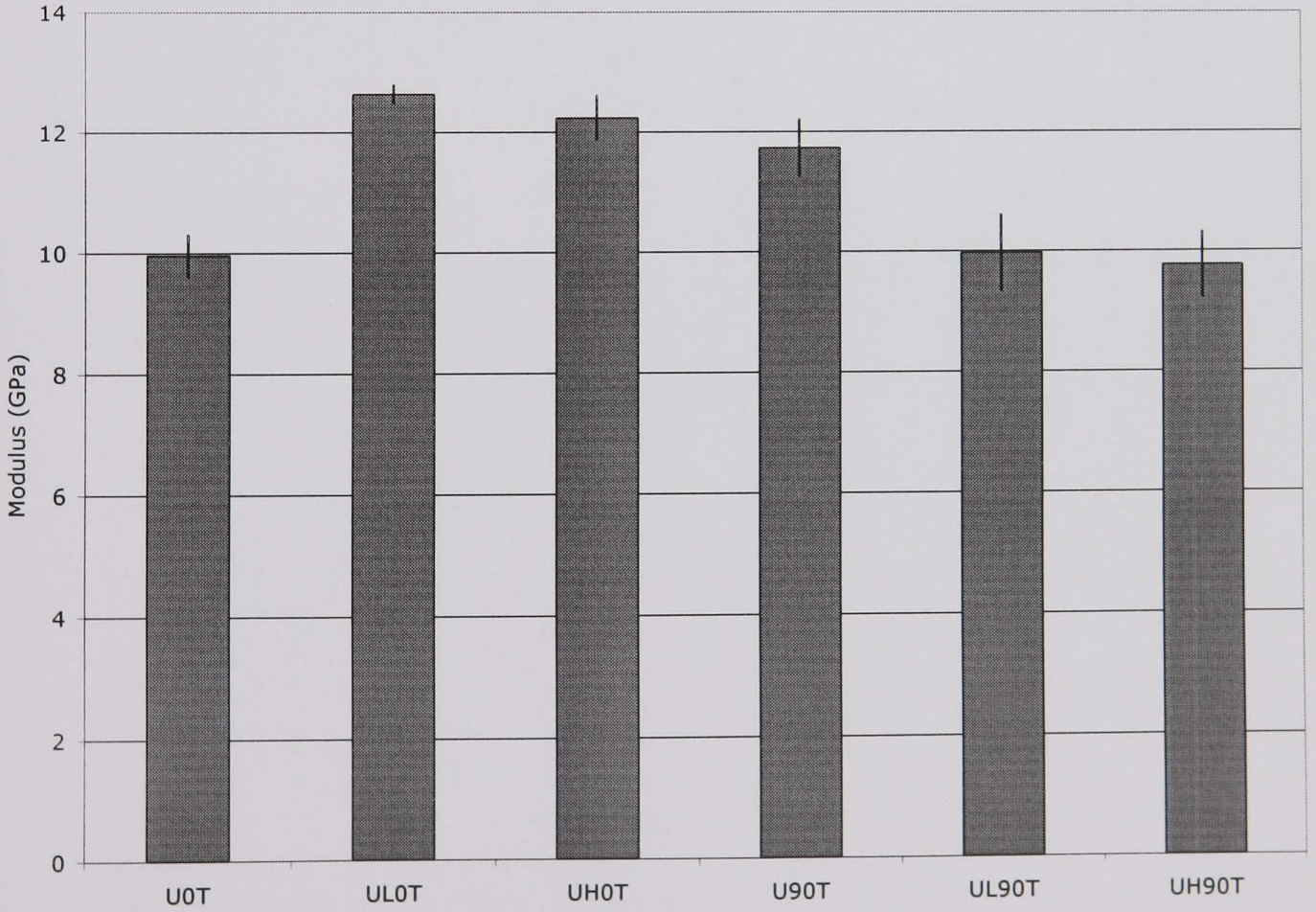

Figure 5:16 CoFRM in-plane modulus results

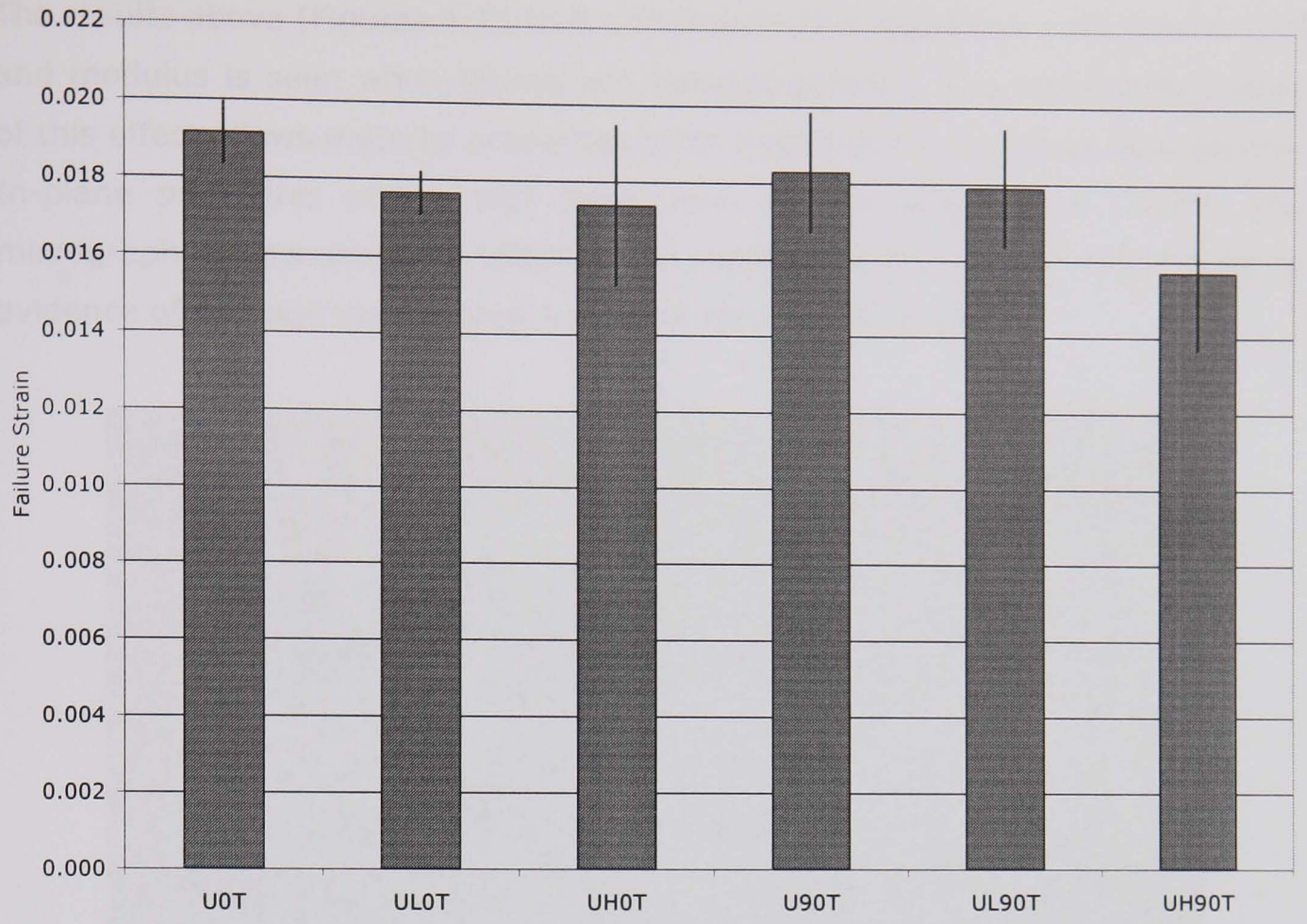

Figure 5:17 CoFRM in-plane tensile strain to failure results

The results above (Figures 5:12 to 5:17) show that a significant reduction in UTS and modulus is seen when fabrics are through-stitched. The predictable nature of this effect allows material properties to be balanced for individual applications. In-plane properties of the NCF fabric are still far superior to CoFRM. The micrographs below show the effect of the stitching on the surrounding fibres, no evidence of damage can be seen (compare with Figure 5:1).

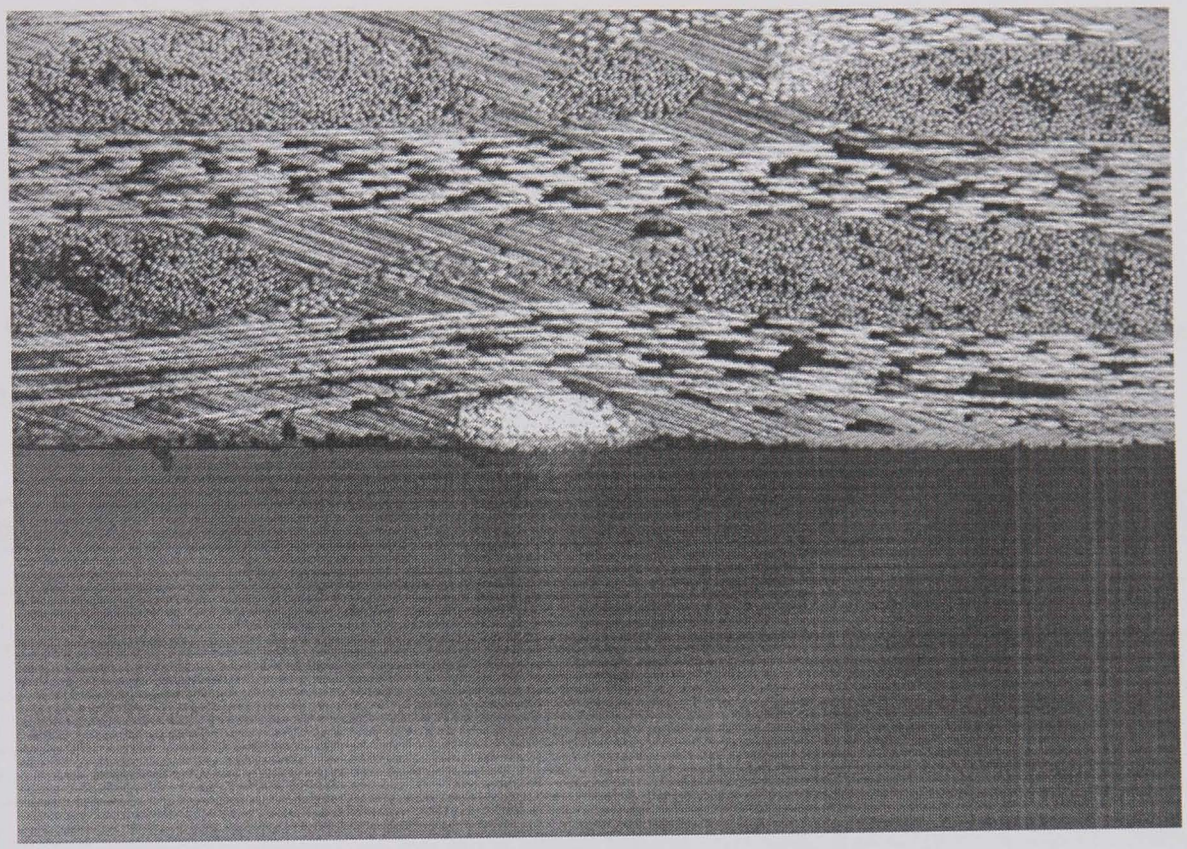

Figure 5:18 Section showing crimping at moulding surface

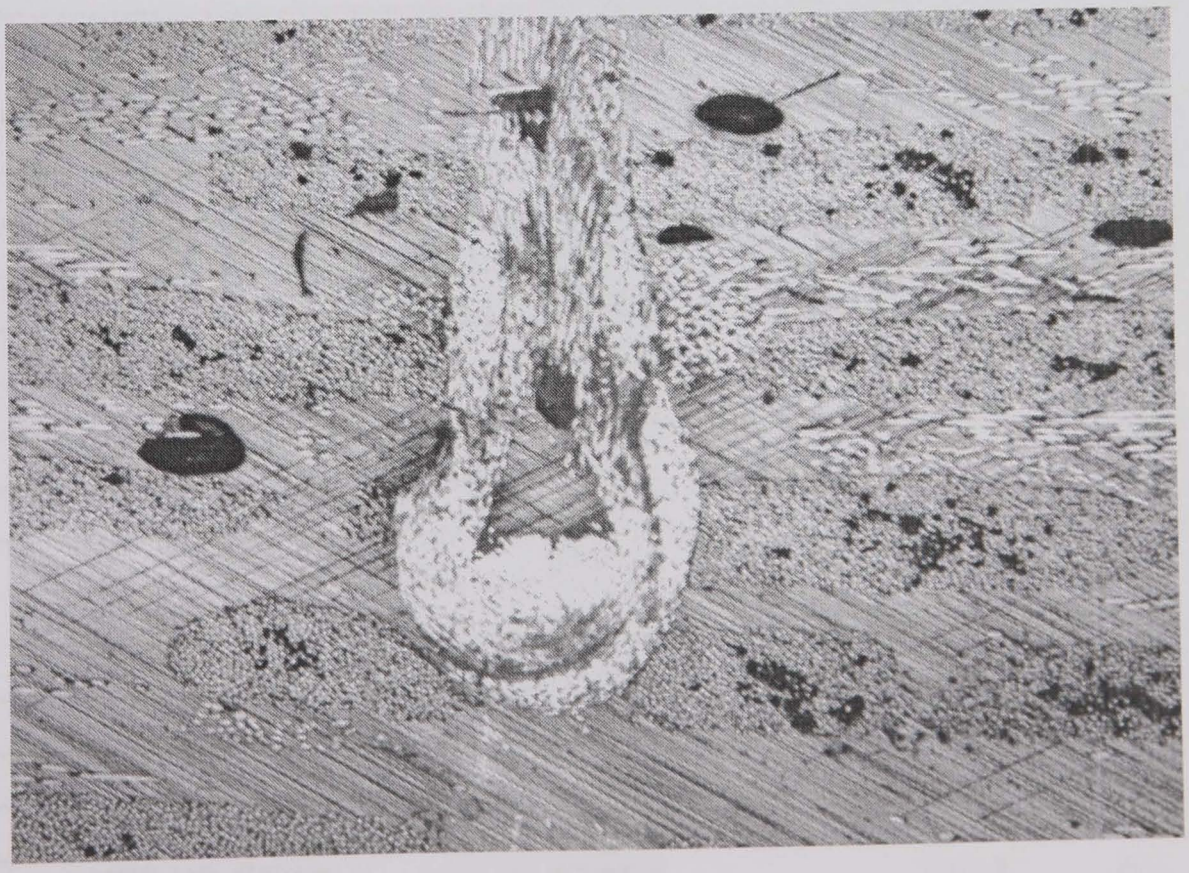

Figure 5:19 Section through DCB plaque showing Kevlar stitch

5.5 Fracture Toughness results

The combinations tested were as follows;

1	DCBP01	CoFRM control
2	DCBP02	NCF control
3	DCBP03	CoFRM LD stitching
4	DCBP04	NCF LD stitching
5	DCBP05	CoFRM HD stitching
6	DCBP06	NCF HD stitching
7	DCBP07	CoFRM Type 1 interleaf
8	DCBP08	NCF Type 1 interleaf
9	DCBP09	CoFRM Type 2 interleaf
10	DCBP10	NCF Type 2 interleaf

Table 5:10 below shows the Mode-I fracture toughness results from this testing. The thick reinforced specimen geometry was used to ensure valid results.

Sample	Definition	G_{IC} (J/m^2)	Average	St Dev %
P01A		1518.5		
P01B		1411.0		
P01C		1326.2		
P01D	CoFRM Control	1424.0	**1420**	5.5
P02A		1057.8		
P02B		1026.8		
P02C		1008.6		
P02D	NCF Control	1117.8	**1053**	4.3
P03A		2178.4		
P03B		2776.4		
P03C		2670.0		
P03D	CoFRM LD Stitch	2200.0	**2456**	12.7
P04A		1752.7		
P04B		1654.6		
P04C		1954.5		
P04D	NCF LD Stitch	2659.7	**2030**	21.6
P05A		3679.0		
P05B		3401.3		
P05C		4411.3		
P05D	CoFRM HD Stitch	4153.6	**3911**	11.6
P06A		2549.2		
P06B		2348.6		
P06C		2402.8		
P06D	NCF HD Stitch	2798.8	**2525**	8.0
P07A		3658.1		
P07B		3564.1		

P07C		3261.9		
P07D	CoFRM Type 1 interleaf	3680.0	**3541**	5.4
P08A		1749.3		
P08B		1028.6		
P08C		1919.8		
P08D	NCF type 1 interleaf	2252.9	**1562**	39.7

Table 5:10 DCB test data

The following table shows the correlation between stitching and SEA.

Ref.	**SEA**	**G_{Ic}**
CoFRM control	64.3	1420
NCF control	42.2	1053
CoFRM LD stitch	61.3	2456
NCF LD stitch	49.9	2030
CoFRM HD stitch	61.6	3911
NCF HD stitch	51.9	2525

Table 5:11 Correlation between energy absorption and fracture toughness

Figure 5:20 below shows these results graphically. For NCF an increase in stitch density gives an increase in SEA which is not seen for CoFRM.

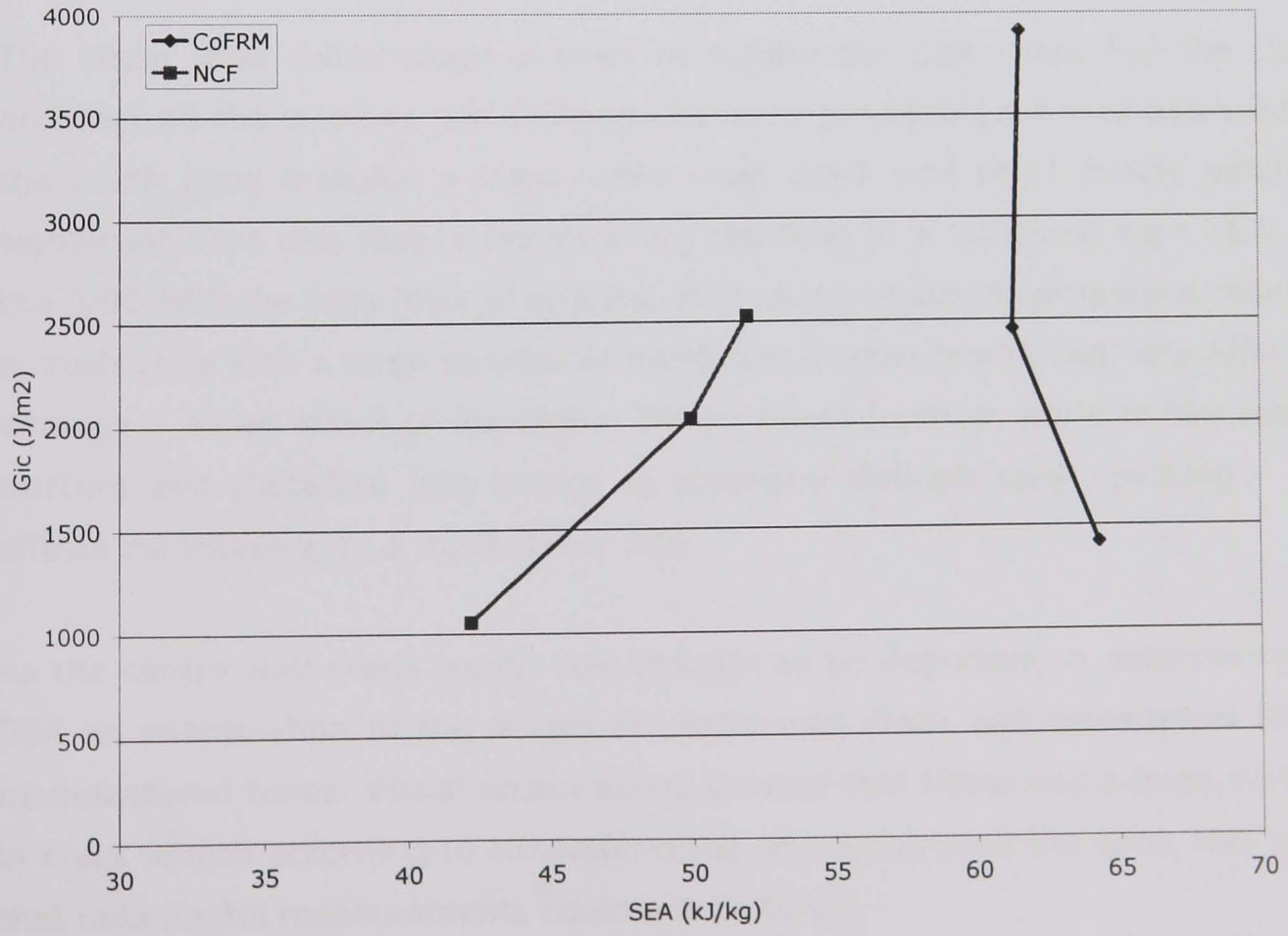

Figure 5:20 Correlation between energy absorption and fracture toughness

5.6 Discussion

5.6.1 Effect of preform stitching

The mechanisms by which through-thickness stitching can greatly increase z-axis volume fraction and interlaminar fracture toughness are well documented. However, the stitching process is generally believed to reduce in-plane properties due to fabric damage and 'quilting' which can misalign the fibre and result in resin-rich pockets. For the CoFRM an increase in G_{IC} reduces the central crack length, but this has little effect as the bending strength of the fronds is reduced by the rows of stitching, resulting in breakage along these rows. A reduction in SEA is seen as the material between each row of stitching remains relatively undamaged. The increase in G_{IC} seen in the stitched NCF tubes results in a significant improvement in SEA (see Figure 5:20). Those fronds which are bent radially inwards towards the central axis of the tube are broken at the rows of stitching. In this case this adds to the accumulation of damage in the fronds. The fronds which are forced radially outwards are seen to be less damaged than in the non-stitched tube (due to the higher interlaminar strengths), but consequently, the axial force required to drive them outwards and the corresponding frictional force are high.

The crush zone morphology is seen to dictate the SEA level. For the CoFRM architecture the in-plane and through-thickness properties are well balanced and the crush zone includes a large centre wall crack and short fronds exhibiting significant fibre and matrix failure sites, resulting in a relatively high SEA. For the 0/90 NCF the high ratio of in-plane to through-thickness properties results in a crush zone with a large number of interlaminar axial cracks and very little fibre damage – as an effect of the higher fibre volume fraction, there is less resin to fracture and therefore less energy is absorbed through resin cracking – both effects contributing to a much lower SEA.

As the centre-wall crack length was thought to be important in determining the SEA an examination of the length of centre-wall crack was undertaken for the manufactured tubes. Visual observations showed that there was a large variation in crack length according to circumferential position around the tube, this meant that meaningful measurements could not be taken.

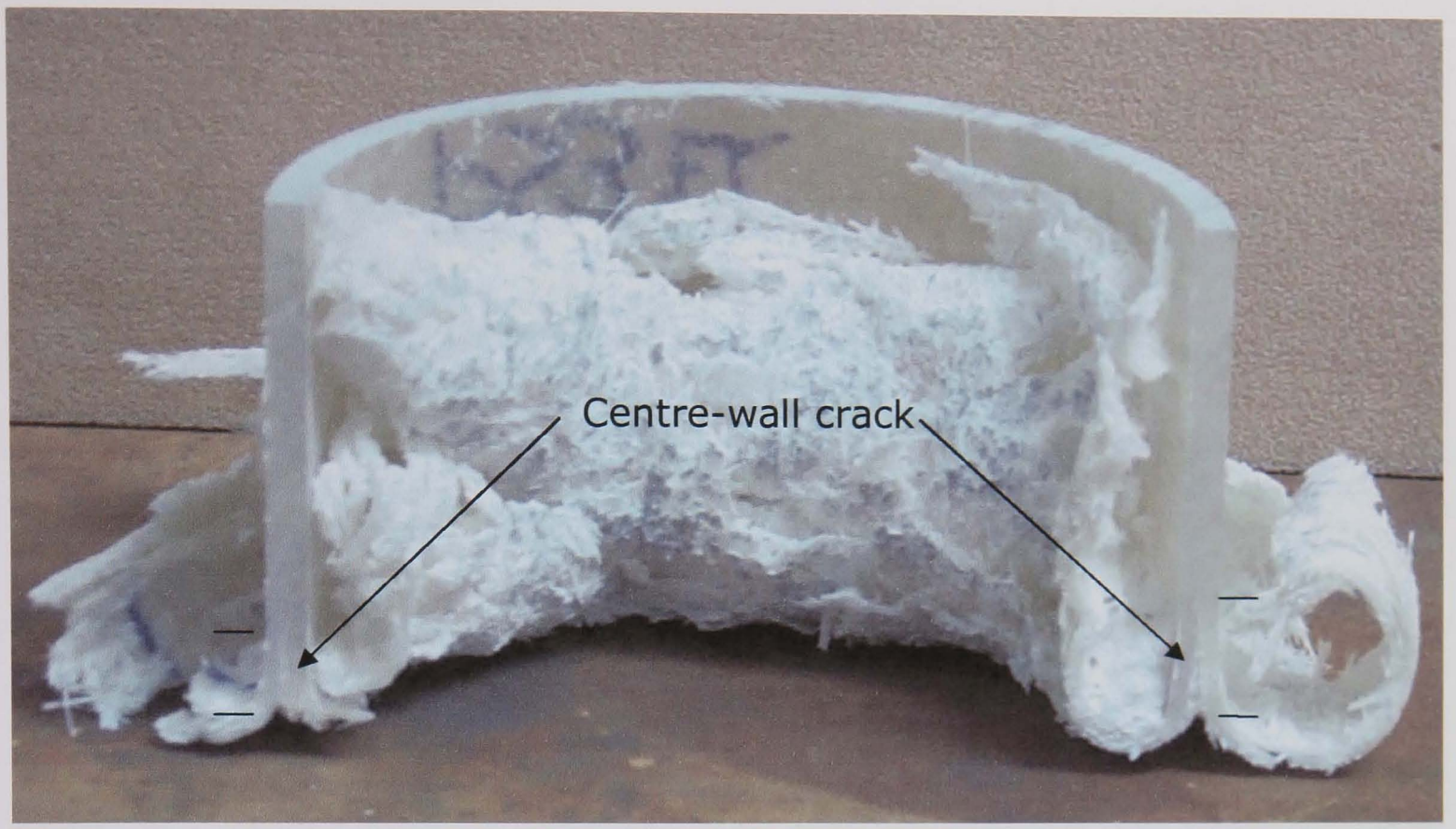

Figure 5:21 Sectioned CoFRM Control specimen showing difference in centre-wall crack length at different circumferential positions

Figure 5:22 Sectioned CoFRM Stitched specimen

Figure 5:21 in particular shows the large variation in crack length from two positions 180 degrees opposed, the crack on the left being much shorter than that visible on the right. The stitched specimen is totally dependent on the position of the next row of stitching. When the last row has just broken the crack

length is very short but increases to a maximum just before the next row breaks.

Figure 5:23 Sectioned NCF control specimen

The NCF tubes fronds are not as tightly curled around with more residual strength. Most of the comments above apply to the NCF tubes; the effect of stitching is even more clearly visible as the tube tilts over. There is much less interlaminar cracking with the NCF tubes as the rows of stitching seem to constrain the plies.

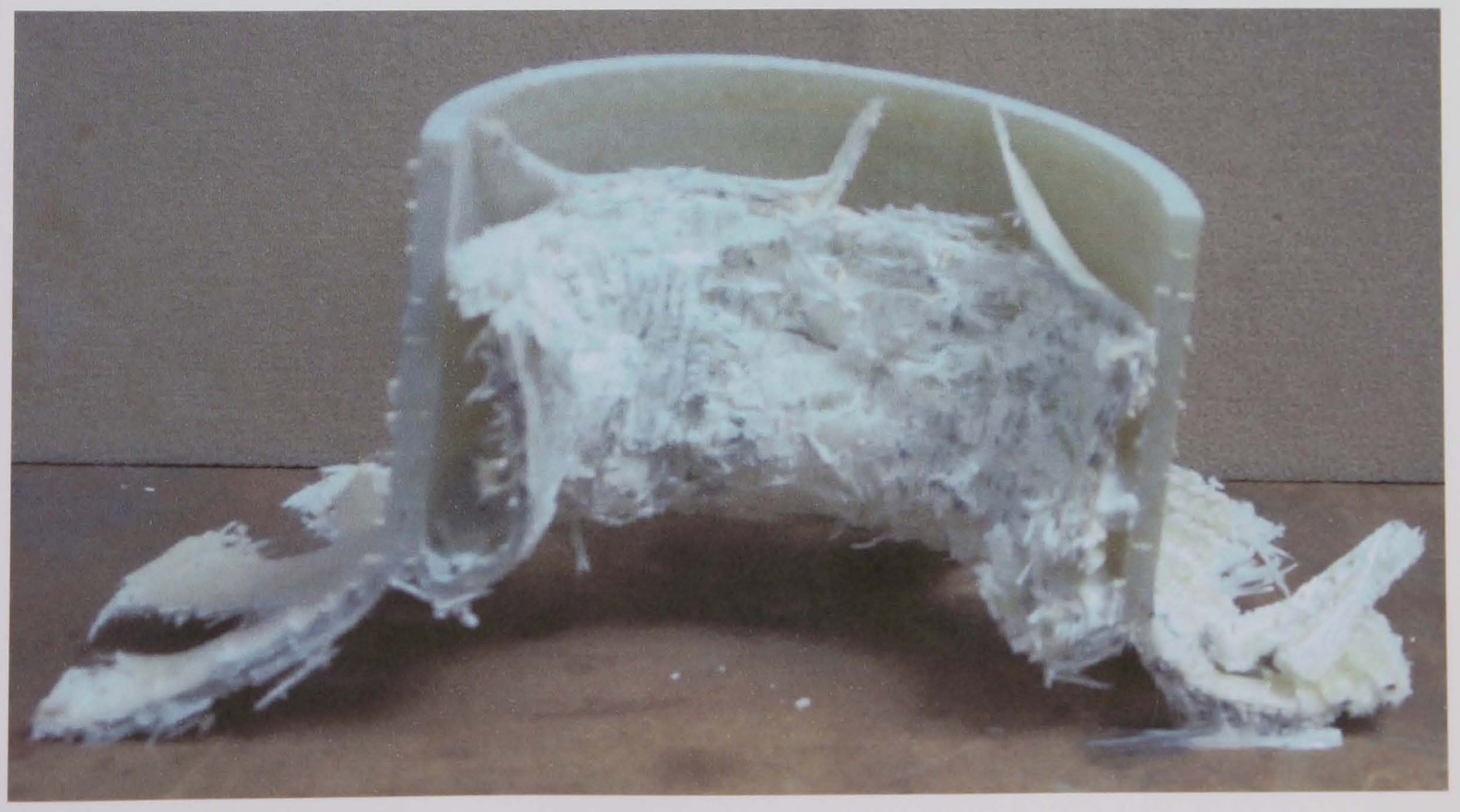

Figure 5:24 Sectioned NCF stitched specimen

Stitching obviously has a high cost and is probably less cost-efficient than improving SEA by the use of a high toughness resin. The original reason for examining the behaviour of NCF was for its potential use in areas that needed high in-plane properties. Stitching therefore offers the potential to combine high in-plane strength with improved energy absorption.

5.6.2 Effect of interleaving

The aim for this part of the work was to apply a relatively common aerospace technique to low-cost high-volume RTM production. In the absence of data from available literature two entirely different interleaves were chosen, the only criteria being high service temperature and compatibility with the glass and resins. The objectives of this work were to consider the effects of increasing interlaminar fracture toughness on SEA for two generic fibre architectures (CoFRM and NCF). Two cases are presented: Refined z-axis properties by through-stitching, where an increased G_{IC} was seen for both architectures, but SEA was seen to improve only for NCF, and refined z-axis properties by thermoplastic interleaf, where an increased G_{IC} was seen for both architectures but SEA decreased (Figures 5:5 and 5:6).

Fracture toughness is known to be improved by interleaving so DCB testing was undertaken in parallel with the crush testing to quantify the improvements. Control specimens for this work were taken from the stitched tubes as the manufacturing and testing was performed concurrently. Interleaving had two main effects for all combinations of materials studied: a reduction in SEA of 33% for CoFRM and 35% for NCF was observed, additionally a much smoother load displacement curve was obtained in most cases. The smooth curve suggests that the stick-slip nature of the crushing process was being altered in some way. As the crush load is so dependent on friction, this appears to be the crucial difference. The composite splits through the interleaf; in the present work the interfacial strength of the interleaf to the composite ply is greater than the through-thickness strength of the interleaf – and the fronds which contact with the platen are coated with the interleaf material.

The thermoplastic interleaf introduces a tough layer between the plies of the reinforcement – this increases the fracture toughness. Where cracking occurred in the interleaf fracture toughness was increased by 52% and 45% for CoFRM and NCF respectively. In some cases as the interleaf is relatively thin the composite was observed to crack beyond the area occupied by the interleaf, in this instance the test load dropped presumably giving G_{IC} values similar to those of the non-interleaved specimens. This effect is relatively common in DCB testing of NCF materials where intralaminar cracking affects the apparent interlaminar fracture toughness [2]

Interleaves obviously have potential for improving composite properties: Provided that a perforated thick/heavy film is used, the improvement in interlaminar fracture toughness and damage resistance is clear. Further testing would be beneficial if specific properties were needed. In this case a heavy urethane material seems appropriate with an open structure allowing through-thickness resin flow. An accurate heating method may increase consistency; particularly where thicker interleaves are employed.

Chapter 5 References

1. Rudd, C.D. and N.A. Warrior, *Embroidered reinforcements - a potentially advantageous process for fabricating strong, net shape structural composites.* Materials Technology, 1997. **12**(1): p. 6-9.

2. de Moura, M.F.S.F., A.B. Pereira, and A.B. de Morais, *Influence of intralaminar cracking on the apparent interlaminar mode I fracture toughness of cross-ply laminates.* Fatigue Fract Engng Mater Struct, 2003.

6 Effect of processing conditions

6.1 Introduction

This investigation comprises two distinct parts, the first of which is concerned with the effect of thermoplastic binder on crush properties and the second of which is related to the effect of processing on void levels and thus crush specific energy absorption.

For the first part of the work binder was dissolved in the resin prior to injection at the following levels: 0%, 2%, 5% and 10%. These levels are based on percentage weight of fibre rather than the actual amount of binder dissolved in the resin. DCB tests are also performed to assess the effect of the binder on toughness properties. The effect of binder is of significant industrial importance as the RTM process is highly dependant on it – particularly for larger preforms.

The second study uses three different processing conditions to manufacture three different voidage levels in the composite tubes. The three processes increase in cost (through increased labour and reduced cycle time) as void level is reduced so crush dependence on void level is an important parameter. High void levels are produced by bubbling air into the resin by aggressive mixing to produce a worst case scenario. The detrimental effect of voids on compressive and interlaminar properties is widely known but no systematic investigation of the effect of voidage on tube crush has yet been undertaken.

6.2 Binder study

6.2.1 Methodology

Binder level was varied in 4 steps; 0%, 2%, 5% and 10% by fibre weight. Binder was dissolved in the resin prior to injection to ensure consistent results. This has the effect of increasing resin viscosity considerably (Figure 6:1) but the situation is analogous to that at the end of injection when the binder placed on the preform has dissolved into the resin. Literature suggests that with a high solubility binder, 95% of the binder is dissolved in 60 seconds [1], such that pre-dissolving binder into the resin does not invalidate the testing. Faster processing or lower binder solubility will decrease the amount of binder dissolved in production mouldings. Binder quantities were calculated from knowledge of finished part volume fractions and material densities. The binder used for this study was DSM Neoxil 940 which is a highly soluble thermoplastic polyester powder.

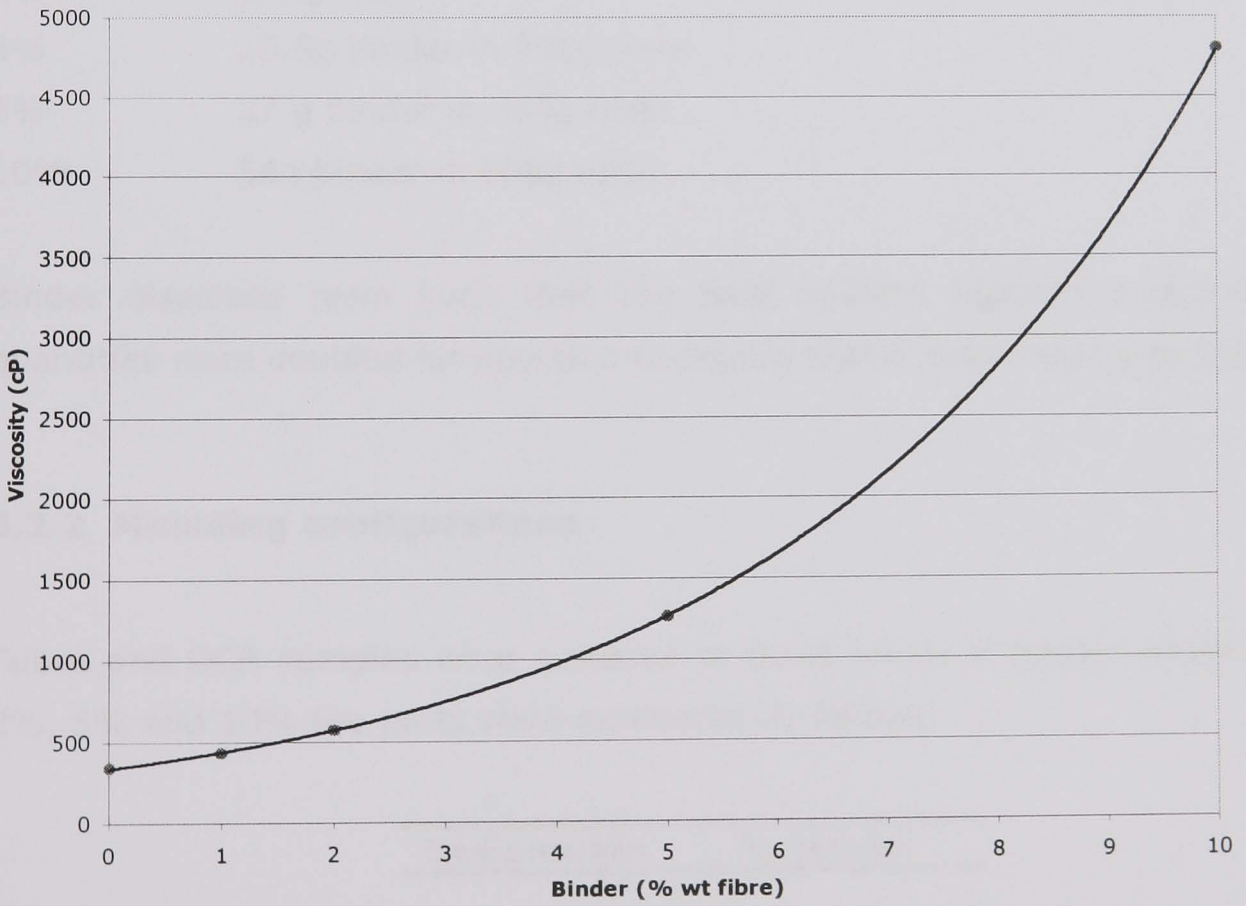

Figure 6:1 Effect of binder level on resin viscosity

Viscosity measurements were performed at 23 °C using a Brookfield DV-II viscometer.

Injection pressure was fixed at 1 bar for all mouldings. Cold resin was injected in to the hot tool (50°C) at 1 bar without vacuum assistance. Cure time was set at 30 minutes in all cases; All parts were post-cured at 80°C for 2 hours.

Binder addition was calculated as follows;

Density of glass $2.56g/cm^3$
Density of resin $1.15g/cm^3$
Density of binder $1.1g/cm^3$

Quantity of glass in a moulding = 1.877m @ $566g/m^2$ = $0.95m^2$
= 537g

Linear density = 1.8kg/m

Quantity of resin (500mm tube) = 900g – 537g = 362g

0% 362g resin
2% 10.8g binder in 351g resin
5% 27 g binder in 335g resin
10% 54g binder in 308g resin

Binder displaces resin such that the total volume remains constant. Resin quantities were doubled for injection to ensure that enough resin was present.

6.2.2 Moulding configurations

Tubes and DCB samples were moulded at three levels of binder addition : 0%, 2%, 5% and 10% the parts were numbered as follows;

Designation	% binder
B1	0
B2	2
B3	5
B4	10

Table 6:1 Binder study moulding configurations

Two repeats were moulded, designated A and B.

Tube Crush

- 4 configurations
- 2 moulding repeats
- 4 crush samples per moulding
- 32 tests

DCB Testing

- 4 Configurations
- 4 plaque mouldings
- 4 samples per plaque
- 16 tests

6.2.3 Binder study crush results

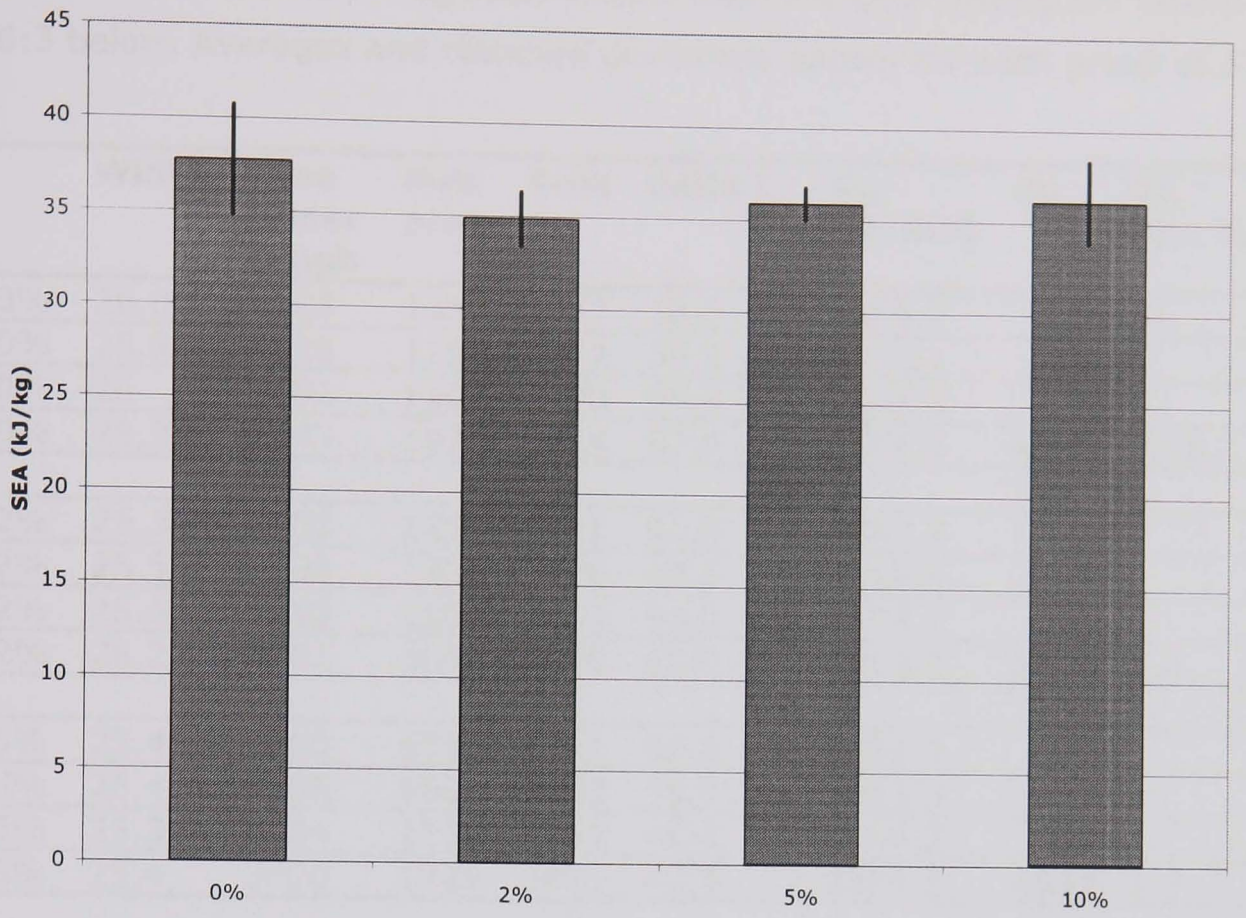

Figure 6:2 SEA vs. binder level

Average SEA at the 0% binder level can be seen in Figure 6:2 to be higher than that normally realised with the NCF parts (chapter 4.5 NCF). The slightly higher standard deviation with the 0% samples may be due to manufacturing inconsistencies inherent in this processing method when used with a minimal amount of binder. Table 6:2 shows data for 4 samples on 2 repeats.

Tube	SEA A	SEA B	SEA C	SEA D	Av. SEA	st.dev	Average	st.dev
B1A	35.4	39.2	38.1	41.8	38.6	2.7		
B1B	32.5	36.2	39.0	40.0	36.9	3.4	37.8	3.0
B2A	35.8	37.2	35.0	34.1	35.5	1.3		
B2B	32.4	35.5	35.3	33.8	34.2	1.4	34.9	1.4
B3A	35.9	35.8	36.2	35.0	35.7	0.5		
B3B	37.3	34.7	35.3	36.9	36.0	1.3	35.9	0.9
B4A	36.8	36.0	37.7	39.8	37.6	1.6		
B4B	35.3	33.0	33.3	36.4	34.5	1.6	36.1	2.2

Table 6:2 SEA vs. binder level

6.2.4 Binder study DCB results

Interlaminar fracture toughness results from the DCB testing are shown in Table 6:3 below. Averages and standard deviations appear for each group of 4 repeats.

	Width	Area under graph	Sub. area	Area	delta L	G_{IC} (J/m2)	Av.	St. dev %	St. dev
0%	26.0	4068	1650	2417	52.0	1785.7		%	
0%	25.9	3126	1254	1872	59.0	1223.1			
0%	26	3086	1108	1978	58.0	1311.5			
0%	25.9	3443	1099	2344	57.0	1585.4	**1373**	13.8	188.9
2%	25.3	3408	1397	2011	50.0	1587.7			
2%	25.5	3196	1320	1876	48.5	1517.6			
2%	25.6	3383	1101	2283	56.0	1594.7			
2%	26.2	3457	1097	2360	60.0	1503.3	**1551**	3.0	47.1
5%	25.4	2400	639	1761	67.0	1036.9			
5%	25.4	2368	965	1403	55.0	1005.3			
5%	25.3	2284	1131	1153	44.0	1034.2			
5%	25.4	3800	1325	2475	62.0	1574.1	**1025**	1.7	17.5
10%	25.3	2931	1120	1812	63.0	1136.7			
10%	25.4	2685	911	1774	63.0	1108.2			
10%	25.6	2462	687	1775	72.0	962.4			
10%	25.7	3000	1490	1510	47.0	1246.8	**1069**	8.7	93.5

Table 6:3 DCB results

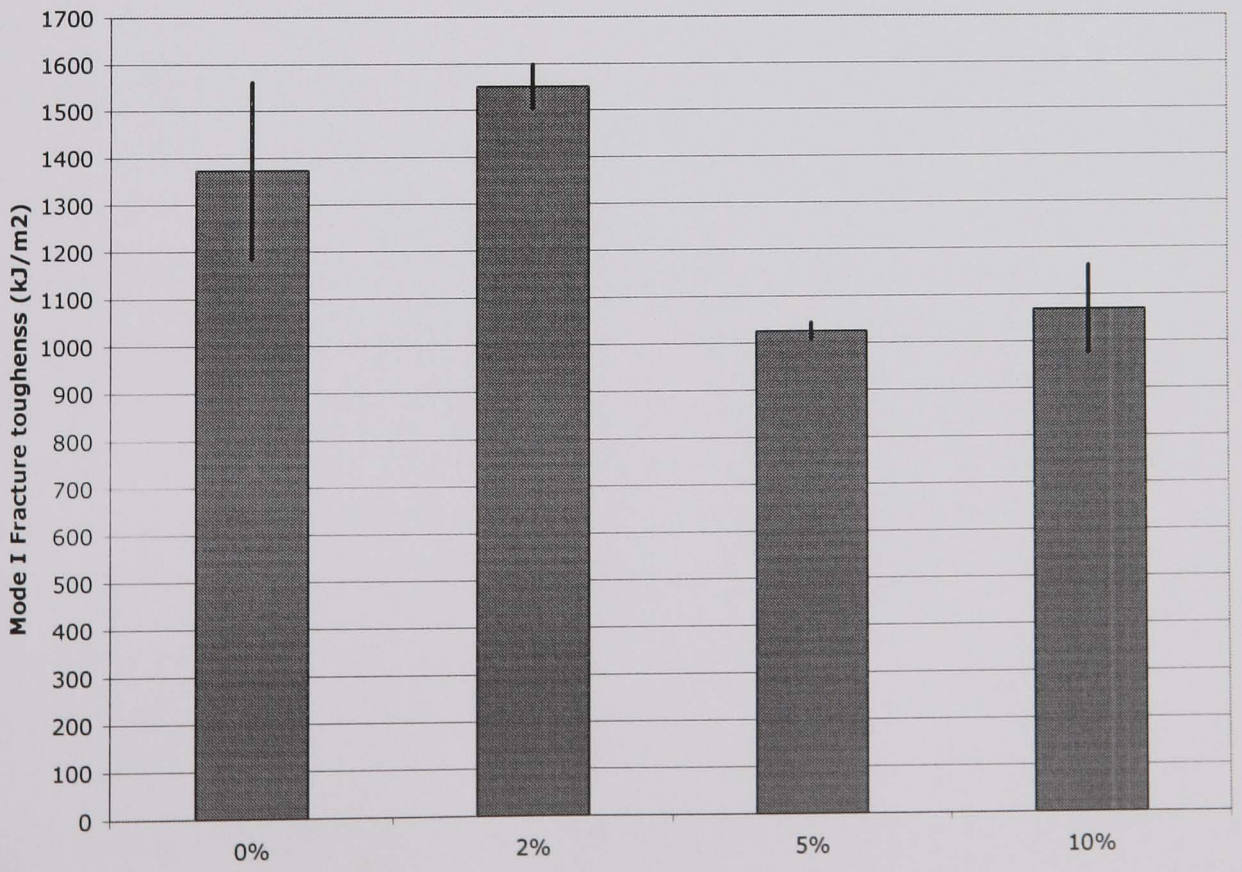

Figure 6:3 Binder study fracture toughness results

The results from the fracture toughness testing again show a fairly high standard deviation for 0% binder with a small rise to 2%, this is due to the toughening effect of the thermoplastic in the resin. At higher levels it is thought that the amount of binder begins to interfere with matrix cohesive strength and fibre-matrix bonding thus inhibiting overall properties.

6.2.5 Discussion - Effect of binder

The processing work aimed to further understanding of how processing conditions affect final part SEA. The level of binder in the part was seen as an important factor, both because of the relatively high proportion occasionally needed to maintain preform integrity and also the potential of improving matrix toughness.

The binder used was seen to dissolve at least partially in the matrix by observation of the resin leaving the tool. Significant matrix colouration and thickening was observed and this was felt to be an unwanted variable as it is affected by temperature and flow rate (which in turn is affected by injection pressure and permeability). In order to remove the effect of varying binder dissolution the binder was dissolved in the matrix prior to injection. This ensures constant material properties through the part but care must be taken to ensure that the injection rate ensures full wetout prior to resin thickening; in practice no problems were encountered. Preform manufacture was difficult due to the lack of binder on the part, consolidation of CoFRM parts would have proved impossible but for NCF little compaction is achieved even with high binder loadings. As the parts have a fairly conservative volume fraction the preforms still fitted the tool.

The SEA results show that any binder has a slight effect on the SEA but that higher proportions (up to 10%) do not degrade properties any further. The average SEA of all the parts with binder is 35.6kJ/kg whereas the parts with no binder have an SEA of 37.8kJ/kg (see Figure 6:2). This represents a decrease of almost 6%. SEA rose slightly at higher values but the higher standard deviation implies that this result is less reliable. The standard deviation is at its highest at the 0% level, it is possible that this is either a manufacturing flaw inherent with preforming with no binder, (e.g. fibre washing) or an interlaminar effect (e.g. variable interlaminar thickness) caused by the lack of binder. Of these the second seems most likely as manufacturing flaws may well have been identified at the preforming stage and fibre washing is unlikely with a tightly stitched fabric at relatively low injection pressures. Overall the SEA is insensitive to binder level.

The fracture toughness values shown in Figure 6:3 are very different. Again a high standard deviation is observed for the 0% and 10% values. Fracture

toughness can be seen to increase by 13% to the 2% level, however it then drops by 34% to the 5% mark where it remains almost constant to 10%. The reason for the initial increase is toughening of the matrix by the introduction of a thermoplastic. This is increase is rapidly offset by the degradation of matrix cohesive strength this giving lower toughness values at higher binder levels. The increase in binder level will also degrade other matrix properties such as chemical and environmental resistance. Overall these findings correspond well with the work of Tanoglu & Seyhan which was discussed in section 2.4.7.

6.3 Void study

6.3.1 Methodology

The three moulding levels are designated low, standard and high. For the low level mouldings the standard moulding scheme was used with the addition of 5 mins. degassing of the resin at 500mbar. After injection the outlet was clamped and the pressure on the inlet raised to 3 bar for the duration of cure. All tubes for the void study used Butanox LPT catalyst at 2% addition. This resulted in a slightly longer moulding time to ensure that the parts could be removed from the tool.

High level tubes were made following the standard moulding scheme with the exception of mixing the resin on an air powered mixer for 5 minutes. The head of the mixer was partially submerged which generated a large number of bubbles. The resin was quickly transferred to the pressure pot and injected.

6.3.2 Determination of volume fraction

Void measurements in this work are performed using optical microscopy techniques. ASTM D1505 documents measurement of void content by comparison of theoretical and measured densities. This method is accurate to ±2.5% by volume. Other void measurement techniques exist but when void fractions must be determined with greater accuracy optical microscopy, although time consuming, can provide greater levels of accuracy (<1%). The accuracy of this method is reliant on taking a sufficiently large number of samples. A method based on computer analysis of the greyscale images produced by a series of micrographs is used in the present work (See [2] for a discussion of the accuracy of various methods).

Annular sections were cut from the tube mouldings coincident with the crush specimens (see Figure 6:4). The specimens were cut into lengths suitable for a 40mm pot.

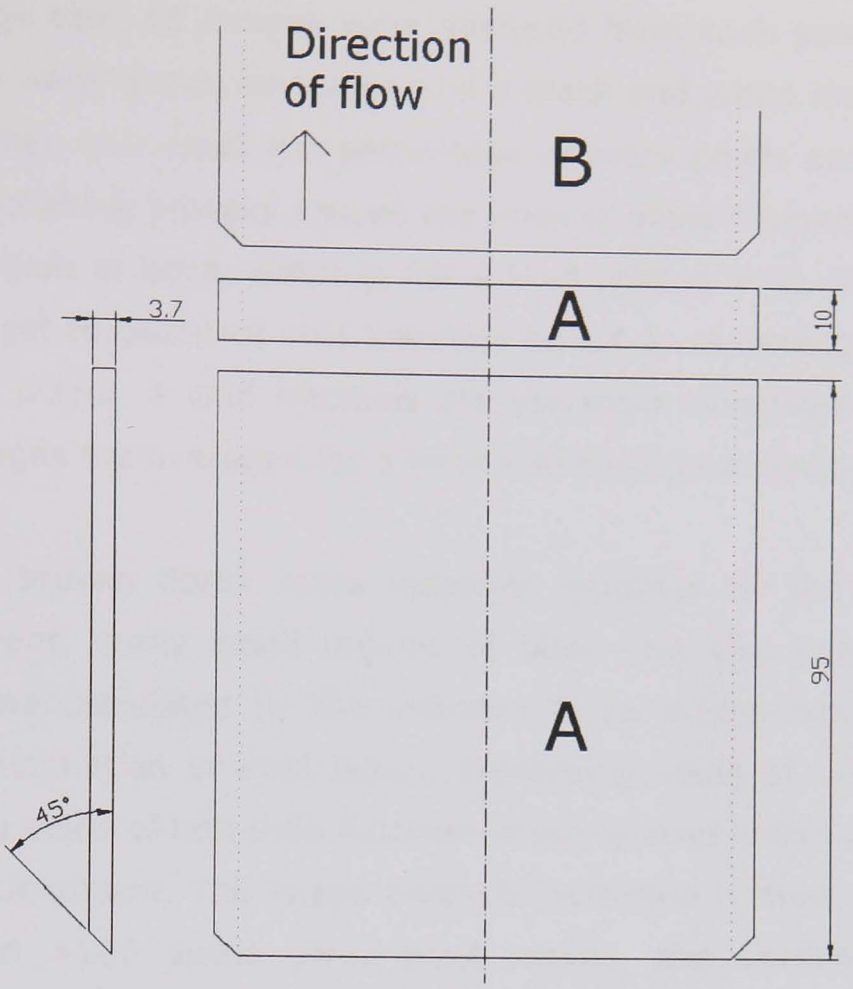

Figure 6:4 Cutting plan for void study specimens

Samples were cast using high clarity polyester resin with 1% Butanox M50 and 0.1% NL49-P. Specimens were polished on a Struers DAP-7 polishing machine with Pedemin-S automatic holder in a complementary motion at 120rpm with the schedule shown in Table 6:4.

Grit	Time (mins)
120	5
400	5
600	5
1200	5
4000	15
1μm Alumina paste	5

Table 6:4 Polishing schedule

After washing and drying specimens were covered in engineers blue ink which was then polished off by hand using a soft cloth. Images were captured using Aphelion image analysis software via a monochrome CCD on a Zeiss microscope. Images were 700 x 500 pixels where 240 pixels = 1mm. 15 images were taken of each sample resulting in a total of 720 images. Images were analysed using

UTHSCSA image tool. 10 images were analysed from each sample. A threshold value is set for each greyscale image and a black and white image is produced. The software then calculates the percentage of black pixels and hence the void fraction. The polishing process causes the ends of glass filaments to fracture off and show a region of black which is not a void (Figure 6:5). The software was therefore also set to calculate void fractions based on excluding voids below 20, 100 and 1000 pixels. 4 void fractions are therefore calculated for each image and the 10 images are averaged for a local void fraction at each position.

Scratches and broken fibres cause incorrect readings for the pure black and white assessment, many small regions of black can also join to form larger region which are calculated by the software to be a large void. These factors result in overestimation of void levels. Discarding voids of under 1000 pixels means ignoring voids of less than 0.15mm which ignores microvoids, the level of which can be significant. The image analysis technique is more accurate for the NCF fabric and >100 pixels gives good results, the CoFRM fabric is more susceptible to image aberrations which means that ignoring voids under 1000 pixels gives intuitively more accurate results (see below).

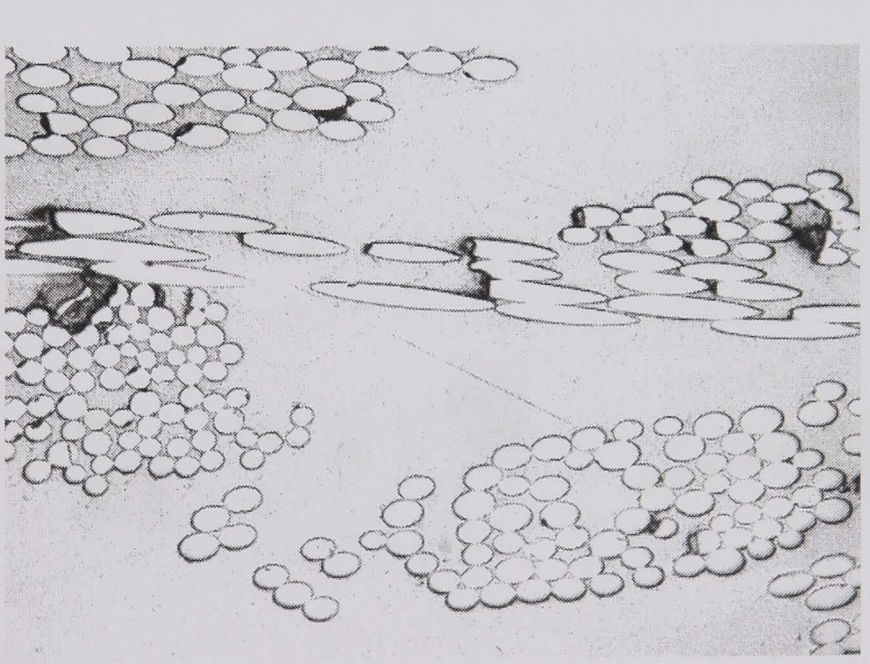

Figure 6:5 CoFRM image showing black sheared areas misinterpreted as voids

Image analysis is performed as follows;

An image is opened in UTHSCSA image tool e.g. V3UAD5 as shown below;

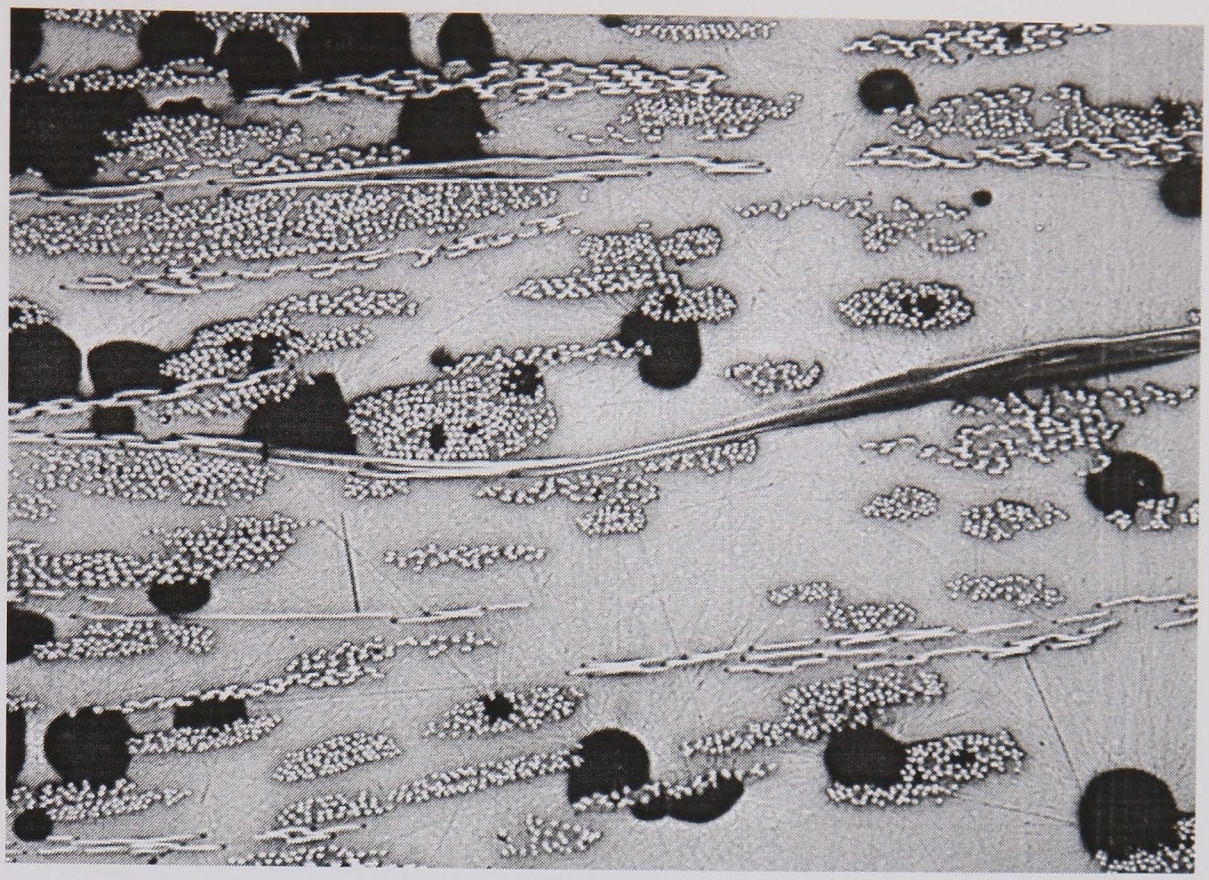

Figure 6:6 Greyscale image opened in Image Tool

The image is then thresholded manually with the following result;

Figure 6:7 Black and White thresholded image

A black and white pixel count can then be performed with the following result;

Black Count	White Count	Black %	White %	
Mean	39939.00	310061.00	11.41	88.59
Std. Dev.	0.00	0.00	0.00	0.00
	39939	310061	11.41	88.59

Table 6:5 Black and white image analysis

The value of 11.41% takes into account all black areas whether they are voids or not. A more advanced method is to classify the voids by size as follows.

Value Range	Count	Mean Value	Std. Dev
Mean	61.33	515.27	132.03
Std. Dev.	107.21	994.42	300.42
- 1.00	370	1.00	0.00
1.00 - 2.00	119	2.00	0.00
2.00 - 5.00	130	3.68	0.75
5.00 - 10.00	55	7.16	1.29
10.00 - 20.00	17	13.24	2.41
20.00 - 50.00	9	31.44	8.52
50.00 - 100.00	4	59.25	6.60
100.00 - 200.00	5	127.20	38.28
200.00 - 500.00	7	339.57	92.23
500.00 - 1000.00	8	700.38	138.89
1000.00 - 2000.00	6	1600.67	239.32
2000.00 -	6	3297.67	1056.09

Table 6:6 Voids classified by size

Figure 6:8 Voids classified by size and coloured (see also Table 6:7)

The following results are then produced using Microsoft Excel:

Value Range	Count	Mean Value	Std. Dev	AREA	Rolling average
Mean	61.33	515.27	132.03		Void fraction
Std. Dev.	107.21	994.42	300.42		
-1	370	1	0	370	**11.49**
1.00 - 2.00	119	2	0	238	**11.39**
2.00 - 5.00	130	3.68	0.75	478	**11.32**
5.00 - 10.00	55	7.16	1.29	394	**11.18**
10.00 - 20.00	17	13.24	2.41	225	**11.07**
20.00 - 50.00	9	31.44	8.52	283	**11.01**
50.00 - 100.00	4	59.25	6.6	237	**10.93**
100.00 - 200.00	5	127.2	38.28	636	**10.86**
200.00 - 500.00	7	339.57	92.23	2377	**10.68**
500.00 - 1000.00	8	700.38	138.89	5603	**10.00**
1000.00 - 2000.00	6	1600.67	239.32	9604	**8.40**
2000.00 -	6	3297.67	1056.09	19786	**5.65**

Total void level	11.41
Greater than 20	11.01
Greater than 100	10.86
Greater than 1000	8.40

Table 6:7 Void results classified by size

Image V1UAA7 is shown below as a typical example of a CoFRM low void image. As the thresholding is manual a number of examples are shown before to enable realistic selection of the correct level (i.e. >20,>100 or >1000). The void levels produced by the automated analysis are as shown in Table 6:8;

Threshold	Black & White	>20	>100	>1000
V1UAA average	2.7%	2.02%	1.27%	0.30%
60	0.80%	0.48%	0.32%	0.00%
70	1.41%	0.72%	0.38%	0.00%
80	2.49%	1.09%	0.56%	0.00%

Table 6:8 Voids results for V1UAA at various threshold levels

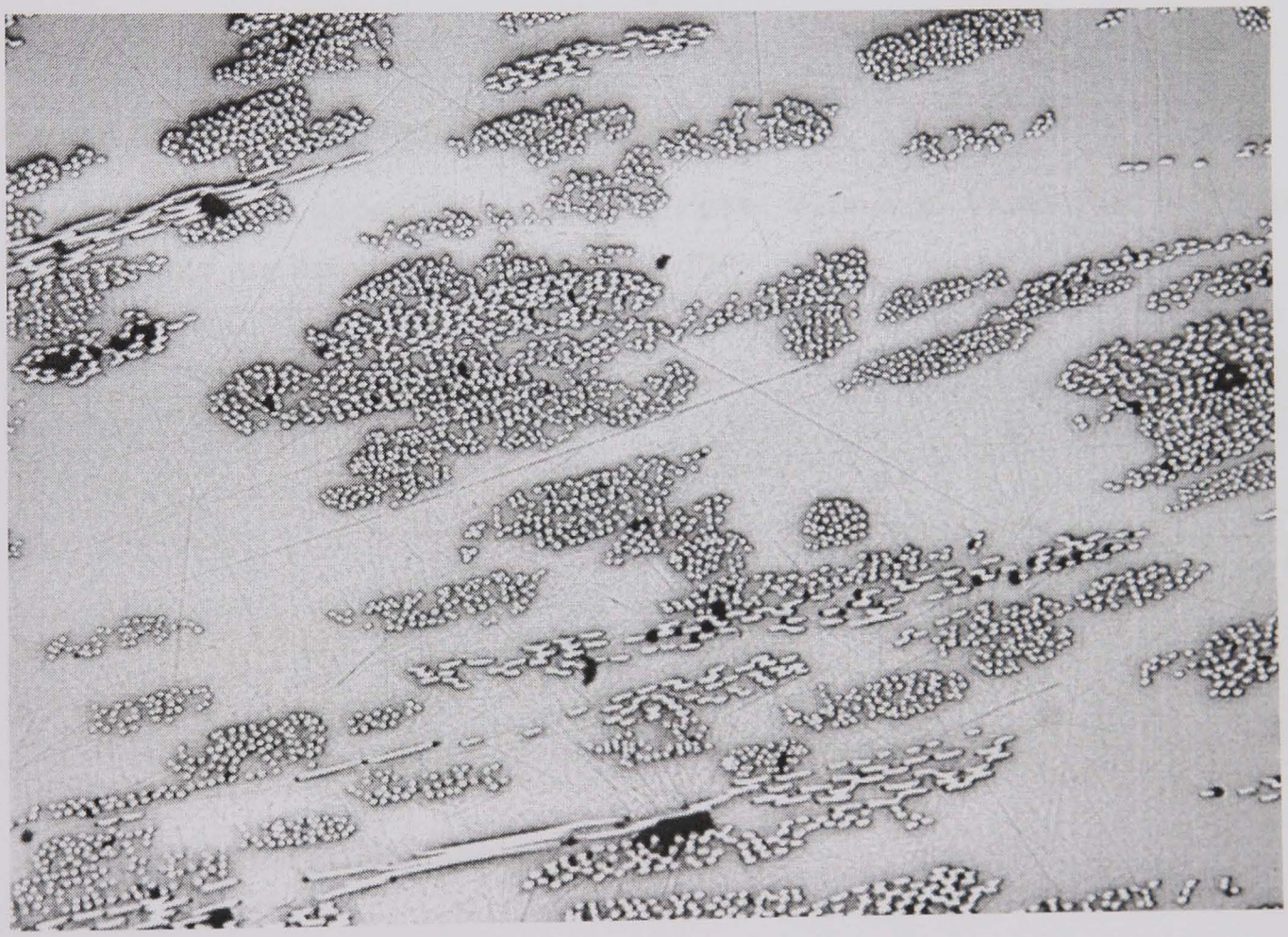

Figure 6:9 Raw image V1UAA7

Figure 6:10 Image thresholded at 60

The image above appears accurate but closer inspection shows that significant areas of void are being ignored (Figure 6:11).

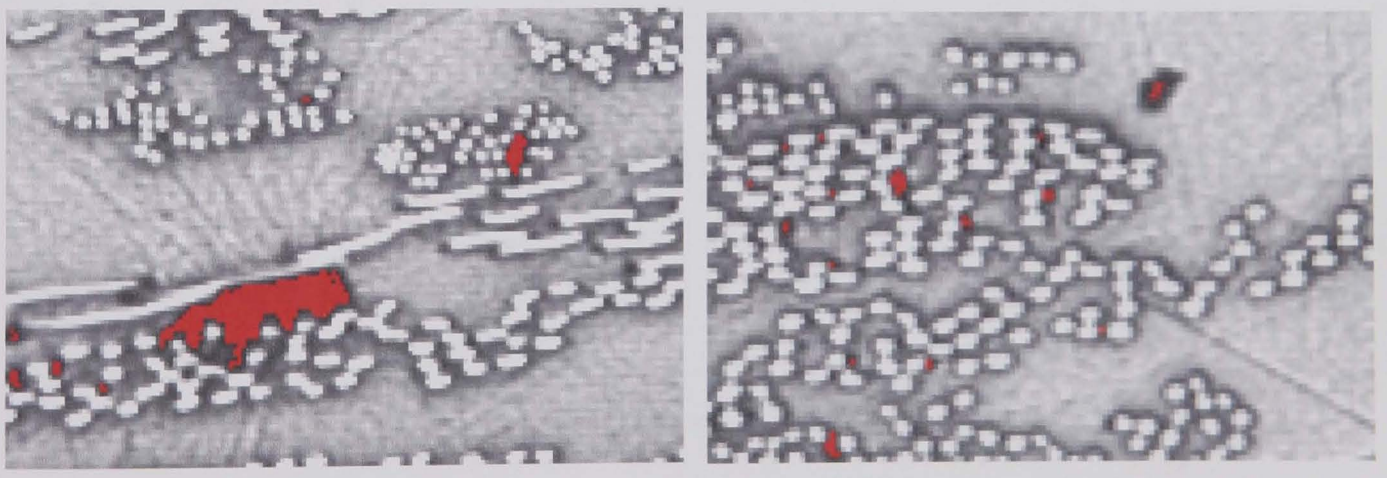

Figure 6:11 Image threshold set too low

Figure 6:12 Image thresholded at 70

Figure 6:13 Image thresholded at 80

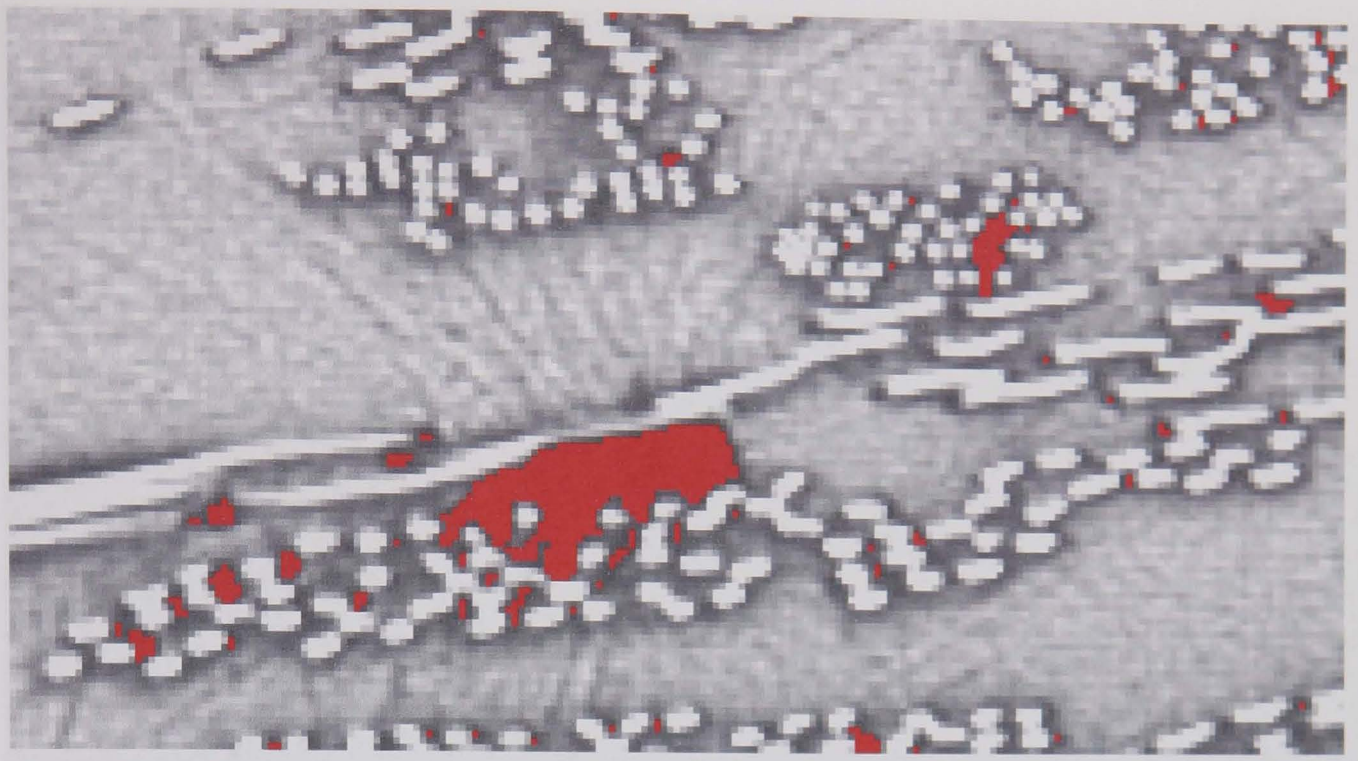

Figure 6:14 Image thresholded at 80 showing excess black areas appearing

Figure 6:14 shows why the threshold limit was taken as 70 for all images as spots of black are beginning to appear in areas where voids are not present. Table 6:8 shows the wide variation in final void results and the sensitivity to the threshold point.

Figure 6:15 Analysis for threshold at 60 (400 objects)

Figure 6:16 Analysis for threshold at 70 (1100 objects)

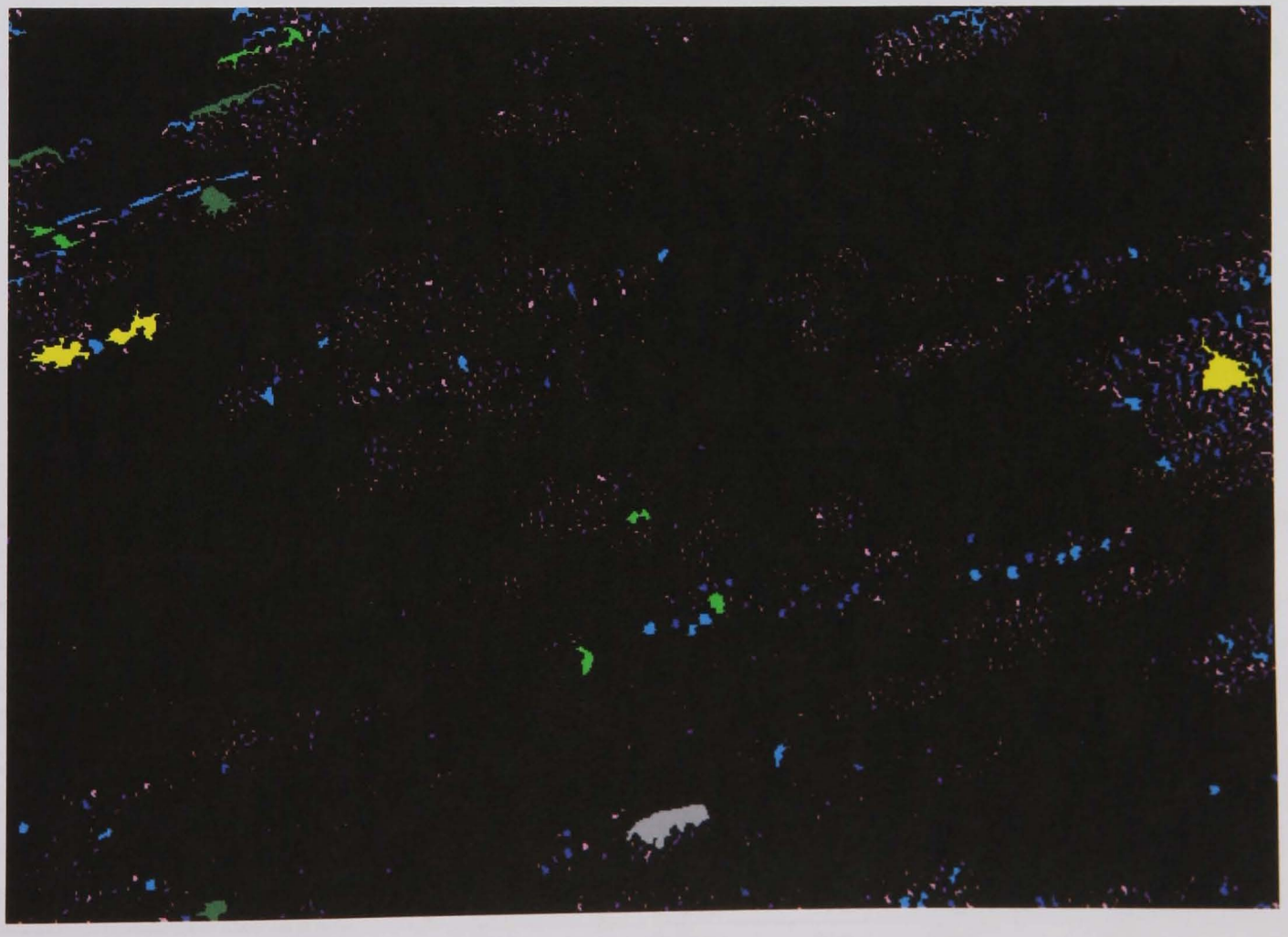

Figure 6:17 Analysis for threshold at 80 (2100 objects)

Pixel area	Objects		
	60	**70**	**80**
-1	234	613	1105
1.00 - 2.00	51	182	394
2.00 - 5.00	52	131	375
5.00 - 10.00	36	61	112
10.00 - 20.00	25	38	67
20.00 - 50.00	14	24	45
50.00 - 100.00	2	6	7
100.00 - 200.00	3	2	4
	2	3	3
500.00 - 1000.00	0	0	1
1000.00 - 2000.00	0	0	0
2000.00 -	0	0	0

Table 6:9 Number of objects for various threshold levels

Table 6:8 above shows that the void fraction doubles in going from under-thresholded to over-thresholded. Additionally the analysis figures show the appearance of many objects in the lower categories (i.e. -1, 1-2). Comparing Figure 6:9 with Figure 6:16 shows that 10-50 pixels area is the region where true voids are counted. This implies that the >20 level is a true representation of the void level in the image shown. At higher levels the black areas join giving a false reading such that for the standard and high void cases the true reading is closer to the >100 value.

6.3.3 Moulding configurations

Void study parts were moulded with both materials at three levels as shown in the following table;

Designation	**Material**	**Void level**	**Inj. Pres.**	**De-gas**	**Packing**	**Bubbles**
V1S	NCF	Low	1 bar	Yes	Yes	No
V1U	CoFRM	Low	½ bar	Yes	Yes	No
V2S	NCF	Standard	2 bar	No	No	No
V2U	CoFRM	Standard	1 bar	No	No	No
V3S	NCF	High	3 bar	No	No	Yes
V3U	CoFRM	High	2 bar	No	No	Yes

Table 6:10 Void study moulding configurations

DCB mouldings for Mode-I fracture toughness testing were manufactured at the same three levels. Microscope samples were taken from the same positions as the crush samples and have the following designation;

V1UAA 1.tif - Void study, level 1, CoFRM, Repeat A, Sample A, image 1

15 images were taken from each potted sample but only 10 were analysed.

Tube Crush

- 3 configurations
- 2 materials
- 2 moulding repeats
- 4 crush samples per moulding
- 48 tests

Microscope images

- 3 configurations
- 2 materials
- 2 moulding repeats
- 48 potted samples
- 720 images

In-plane Testing

- 3 Configurations
- 6 plaque mouldings
- 3 samples per plaque
- 18 tests

DCB Testing

- 3 Configurations
- 4 plaque mouldings
- 4 samples per plaque
- 16 tests

6.3.4 Void study micrograph results

Overall results are shown for the void study first with detailed results for each configuration shown later. Results are shown for 4 different levels of image assessment. As discussed in chapter 3 the >20 value provides the most accurate results for low void fractions with >100 being more accurate for high void fractions. The bold values in the Table 6:11 take this factor into account.

Sample	**>0**		**>20**		**>100**		**>1000**	
	Av.	St. dev.	Av.	St. dev.	Av.	St. dev.	Av.	St. dev.
V1U	4.6	1.4	**3.3**	1.2	2.1	0.8	0.7	0.4
V2U	5.4	1.8	**4.2**	1.4	3.0	1.3	1.4	1.1
V3U	13.0	1.8	11.8	1.7	**10.8**	1.5	9.1	1.2
V1S	3.9	1.2	**1.4**	0.5	0.4	0.2	0.2	0.2
V2S	9.4	3.3	**7.1**	2.9	5.8	2.8	3.8	2.2
V3S	15.3	3.0	13.3	2.7	**11.4**	2.7	6.9	2.2

Table 6:11 Overall void results

Intuitively the CoFRM material would be expected to have lower void levels than the NCF due to volume fraction and permeability and in particular the results for V1U appear very high. This suggests that the methods employed for determination of threshold level and pixel area rejection level are perhaps too general to be accurately applied to all samples.

V1UA					**V1UB**			
	>0	>20	>100	>1000	>0	>20	>100	>1000
A	3.0	2.0	1.3	0.3	4.6	3.2	2.3	1.2
B	3.0	2.1	1.5	0.6	5.4	4.2	2.9	1.1
C	3.9	2.6	1.5	0.4	4.0	2.5	1.4	0.4
D	6.0	4.1	2.5	0.6	6.8	5.3	3.5	1.1
Av.	**4.0**	**2.7**	**1.7**	**0.5**	**5.2**	**3.8**	**2.5**	**1.0**
St dev	1.4	0.9	0.5	0.2	1.2	1.2	0.9	0.4

Table 6:12 V1U void results

V2UA					V2UB			
	>0	>20	>100	>1000	>0	>20	>100	>1000
A								
B					4.7	3.7	2.5	0.8
C	3.2	2.6	1.7	0.7	5.2	4.0	2.8	0.9
D	8.0	6.4	5.2	3.4	5.9	4.2	2.8	1.4
Av.	**5.6**	**4.4**	**3.5**	**2.0**	**5.5**	**4.0**	**2.7**	**1.0**
St dev	3.4	2.8	2.5	1.9	0.6	0.2	0.1	0.3

Table 6:13 V2U void results

V3UA					V3UB			
	>0	>20	>100	>1000	>0	>20	>100	>1000
A	10.1	8.9	8.0	6.9	15.0	13.9	12.4	10.5
B	10.8	9.6	9.0	7.9	12.5	11.7	10.7	9.0
C	14.7	13.1	11.7	9.8	13.7	12.6	11.6	9.8
D	14.3	12.8	11.9	10.2	12.7	12.0	11.3	8.9
Av.	**12.5**	**11.1**	**10.1**	**8.7**	**13.5**	**12.6**	**11.5**	**9.6**
St dev	2.4	2.2	2.0	1.5	1.1	0.9	0.7	0.7

Table 6:14 V3U void results

V1SA					V1SB			
	>0	>20	>100	>1000	>0	>20	>100	>1000
A	1.8	0.5	0.2	0.0	3.8	1.0	0.2	0.0
B	3.2	1.1	0.5	0.2	5.0	1.5	0.3	0.0
C	3.2	1.1	0.5	0.2	4.9	1.7	0.4	0.0
D	4.4	1.6	0.7	0.5	5.3	2.3	0.9	0.5
Av.	**3.1**	**1.1**	**0.5**	**0.2**	**4.7**	**1.6**	**0.4**	**0.1**
St dev	1.1	0.5	0.2	0.2	0.7	0.5	0.3	0.2

Table 6:15 V1S void results

V2SA					V2SB			
	>0	>20	>100	>1000	>0	>20	>100	>1000
A	10.7	7.3	5.2	3.3	6.5	2.8	1.1	0.2
B	6.7	6.3	5.9	4.6	14.2	11.9	10.5	7.4
C	4.8	4.0	3.8	2.7	11.4	8.4	6.7	4.0
D	12.6	9.8	8.0	5.6	8.8	6.6	5.3	2.7
Av.	**8.7**	**6.8**	**5.7**	**4.0**	**10.2**	**7.4**	**5.9**	**3.6**
St dev	3.6	2.4	1.8	1.3	3.3	3.8	3.9	3.0

Table 6:16 V2S void results

V3SA					V3SB			
	>0	>20	>100	>1000	>0	>20	>100	>1000
A	11.9	8.8	6.2	2.8	19.8	17.0	14.2	9.0
B	14.2	12.8	11.4	7.2	19.9	16.9	15.0	9.7
C	13.2	11.5	9.7	5.3	14.1	13.1	11.5	7.5
D	14.3	13.0	11.6	6.7	15.3	13.5	11.6	7.4
Av.	**13.4**	**11.5**	**9.7**	**5.5**	**17.3**	**15.1**	**13.1**	**8.4**
St dev	1.1	1.9	2.5	2.0	3.0	2.1	1.8	1.1

Table 6:17 V3S void results

1mm = 241 pixels on image	
1 pixel =	0.00415 mm
1 pixel squared	0.00002 mm2
20 pixels area	0.00034 mm2
100 pixels area	0.00172 mm2
1000 pixels area	0.01722 mm2
20 pixels diameter	0.02094 mm
100 pixels diameter	0.04682 mm
1000 pixels diameter	0.14806 mm

Table 6:18 Void areas for void image analysis

Typical images are shown below for V1-V3 for both fibre architectures

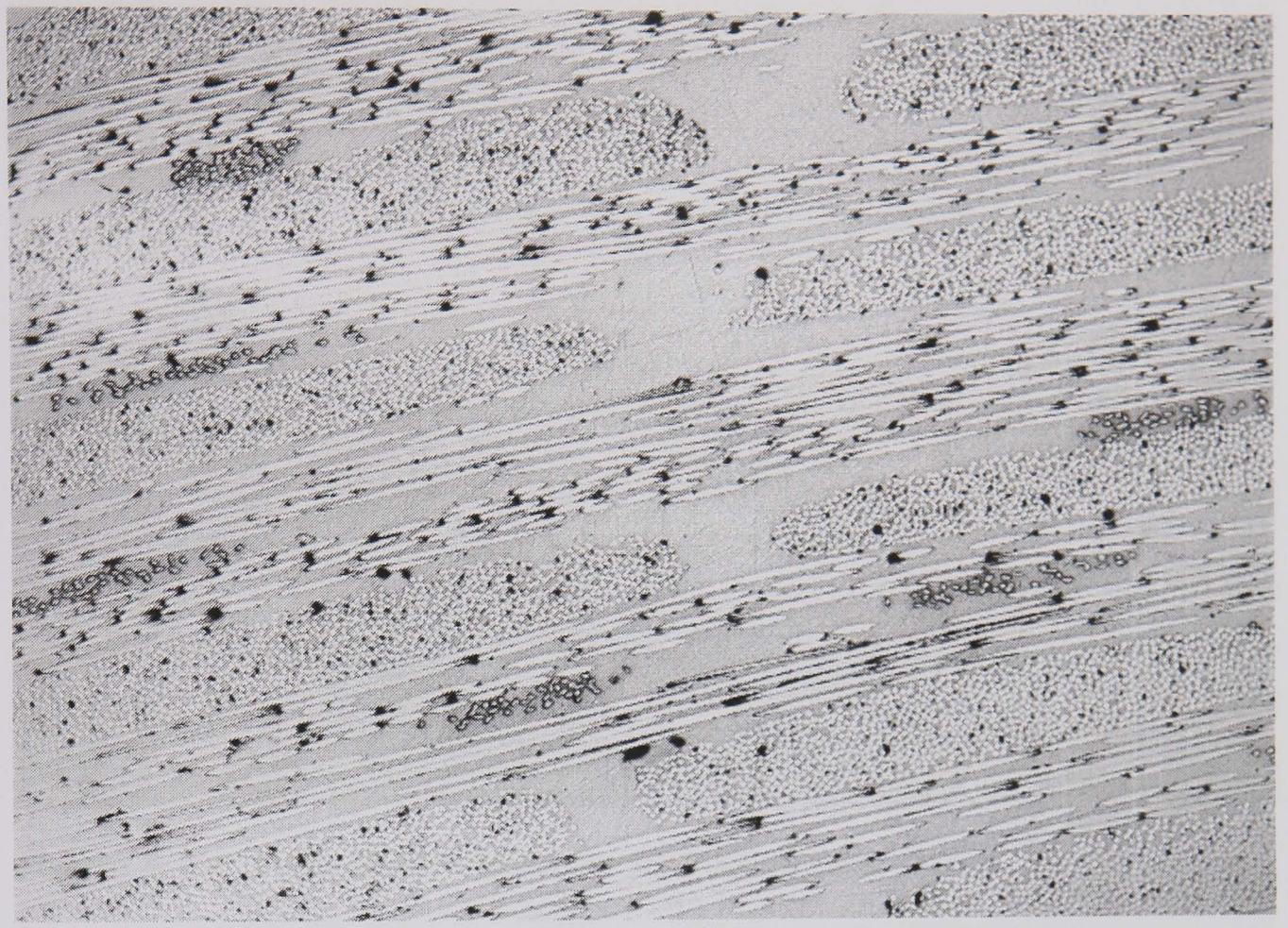

Figure 6:18 Typical void level for V1S specimen

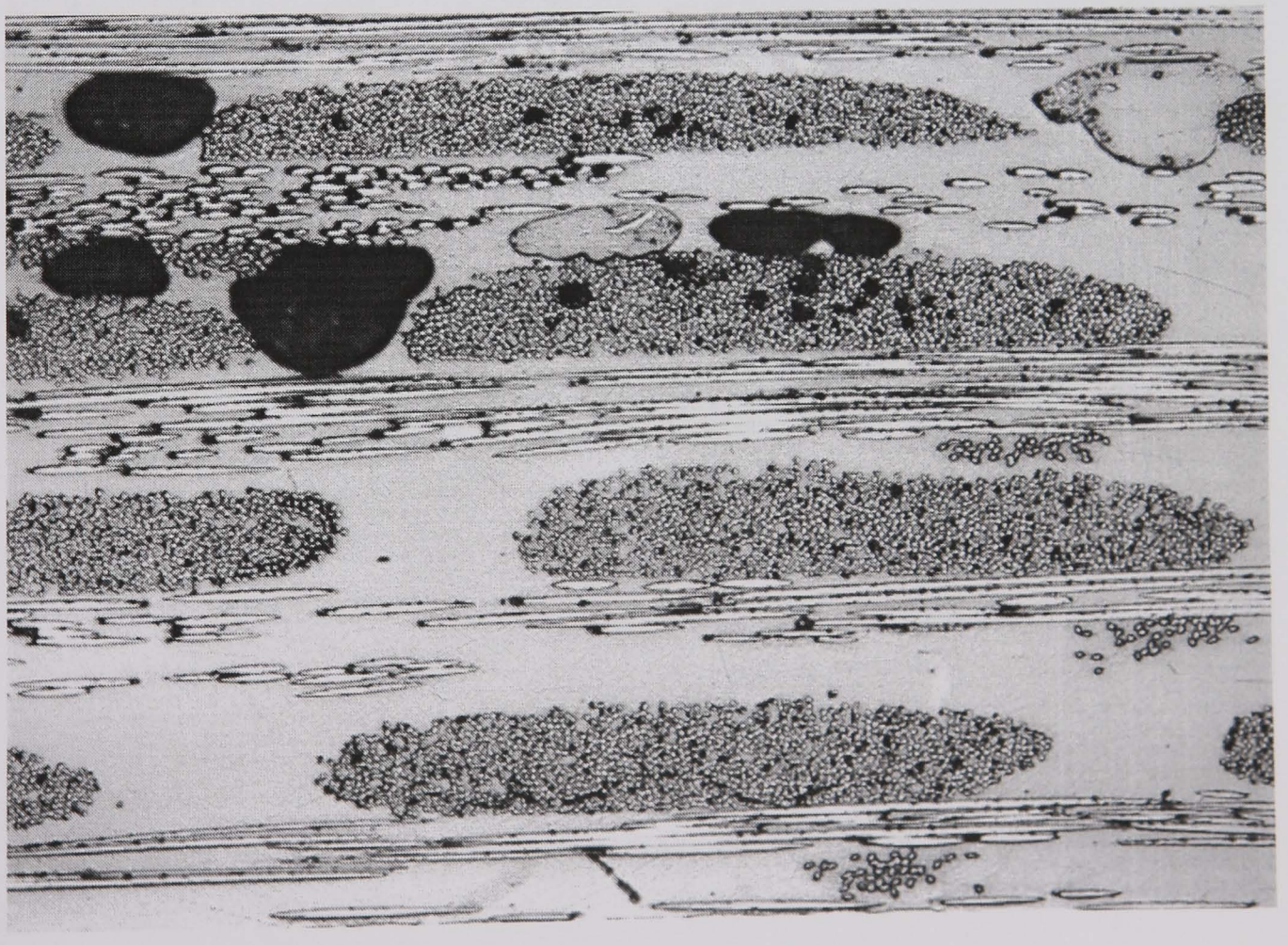

Figure 6:19 Typical void level for V2S specimen

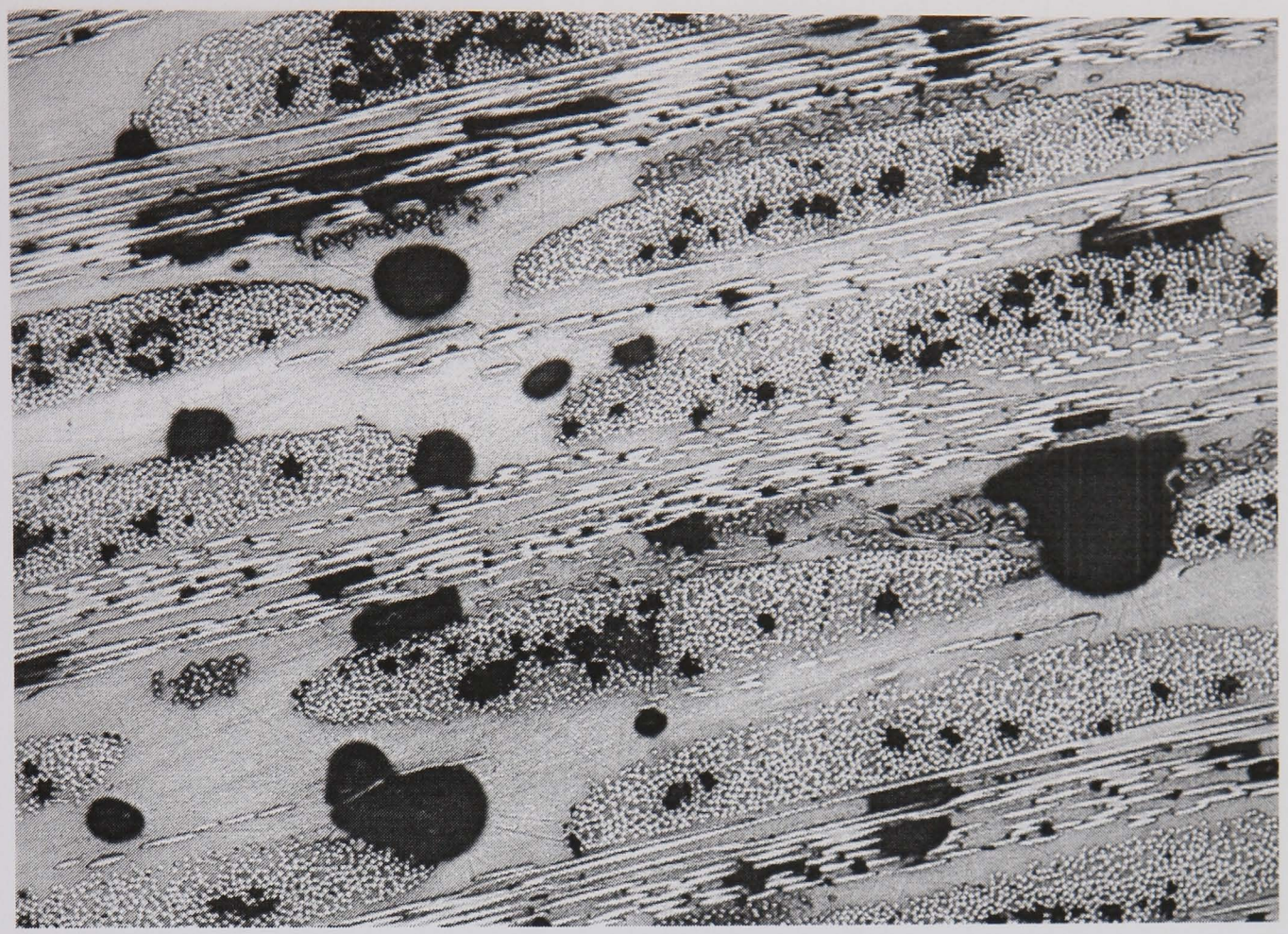

Figure 6:20 Typical void level for V3S specimen

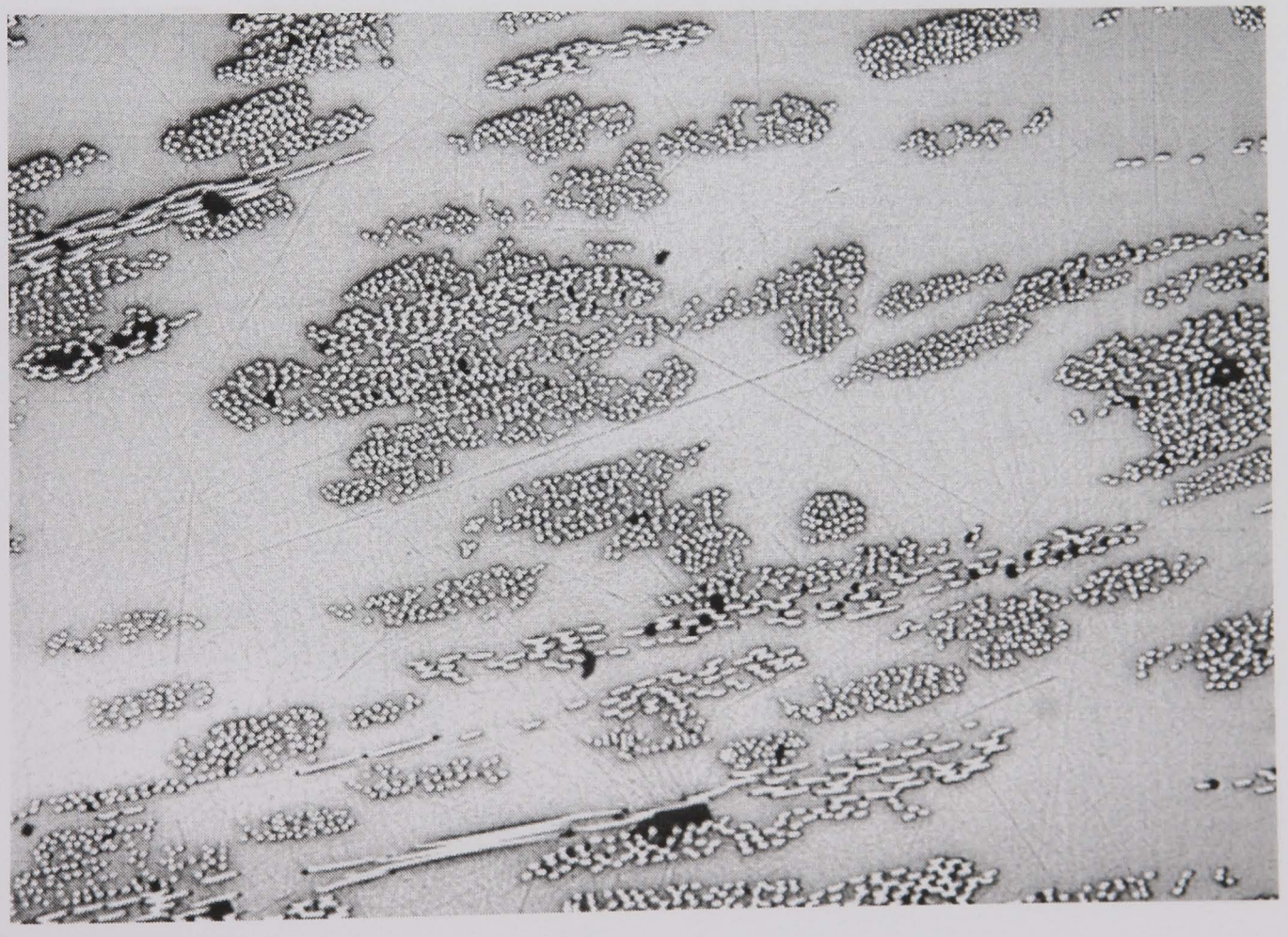

Figure 6:21 Typical void level for V1U specimen

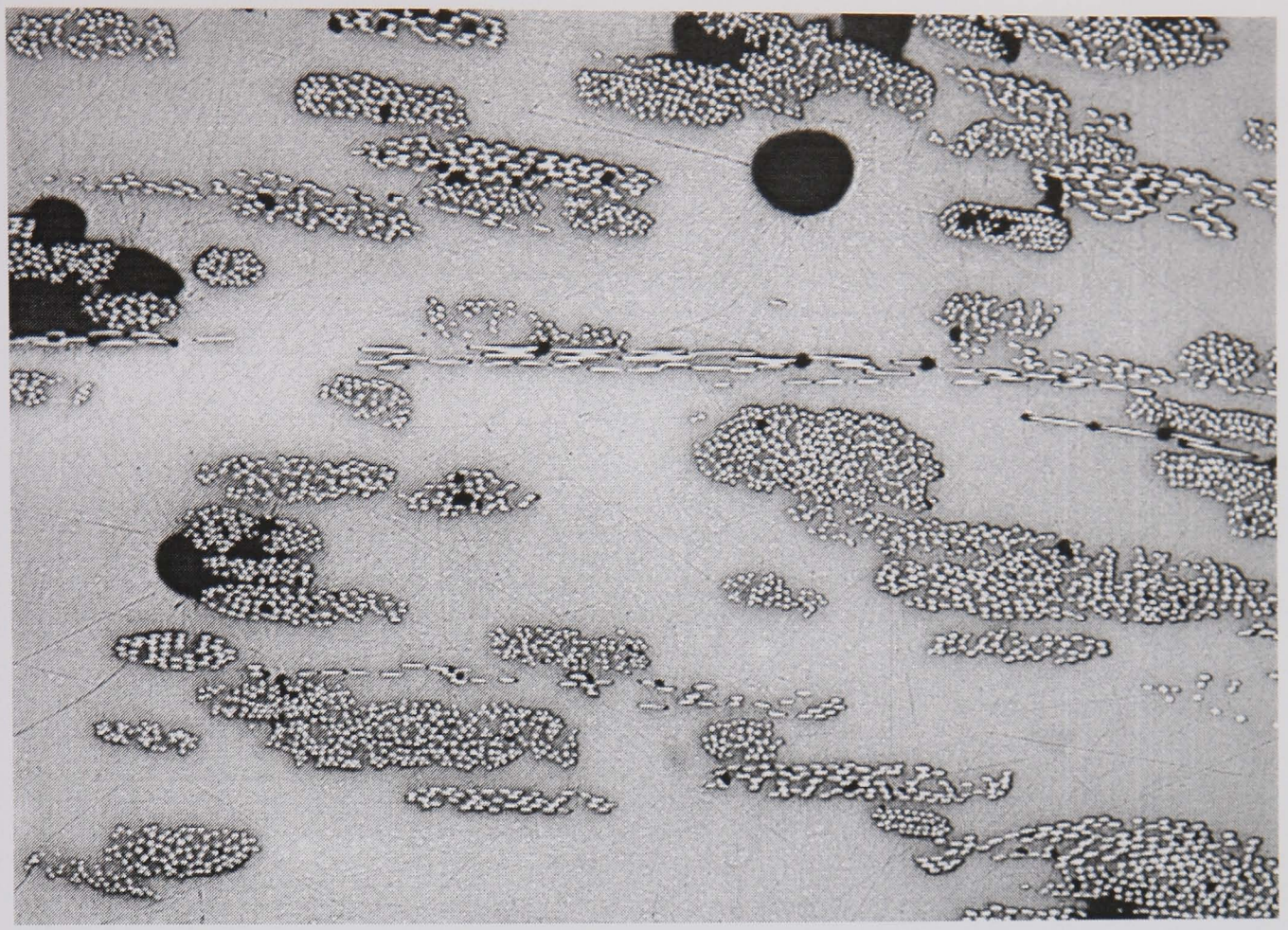

Figure 6:22 Typical void level for V2U sample

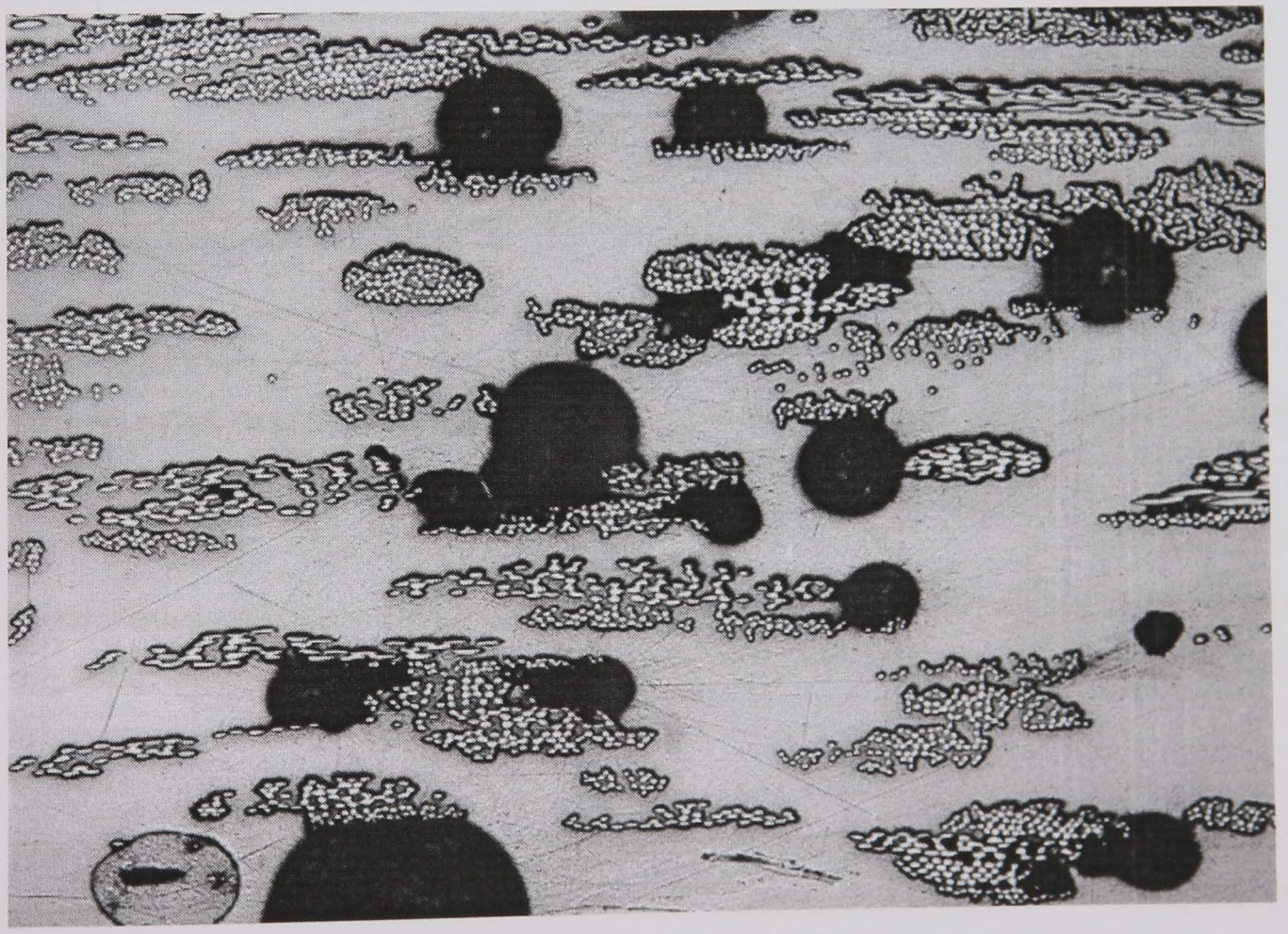

Figure 6:23 Typical void level for V3U sample

The CoFRM specimens show an additional problem with analysis which is that the black areas around the fibres join up resulting in interpretation by the software as larger voids.

Typically void levels increase along the length of the moulding as can be seen in Figure 6:24

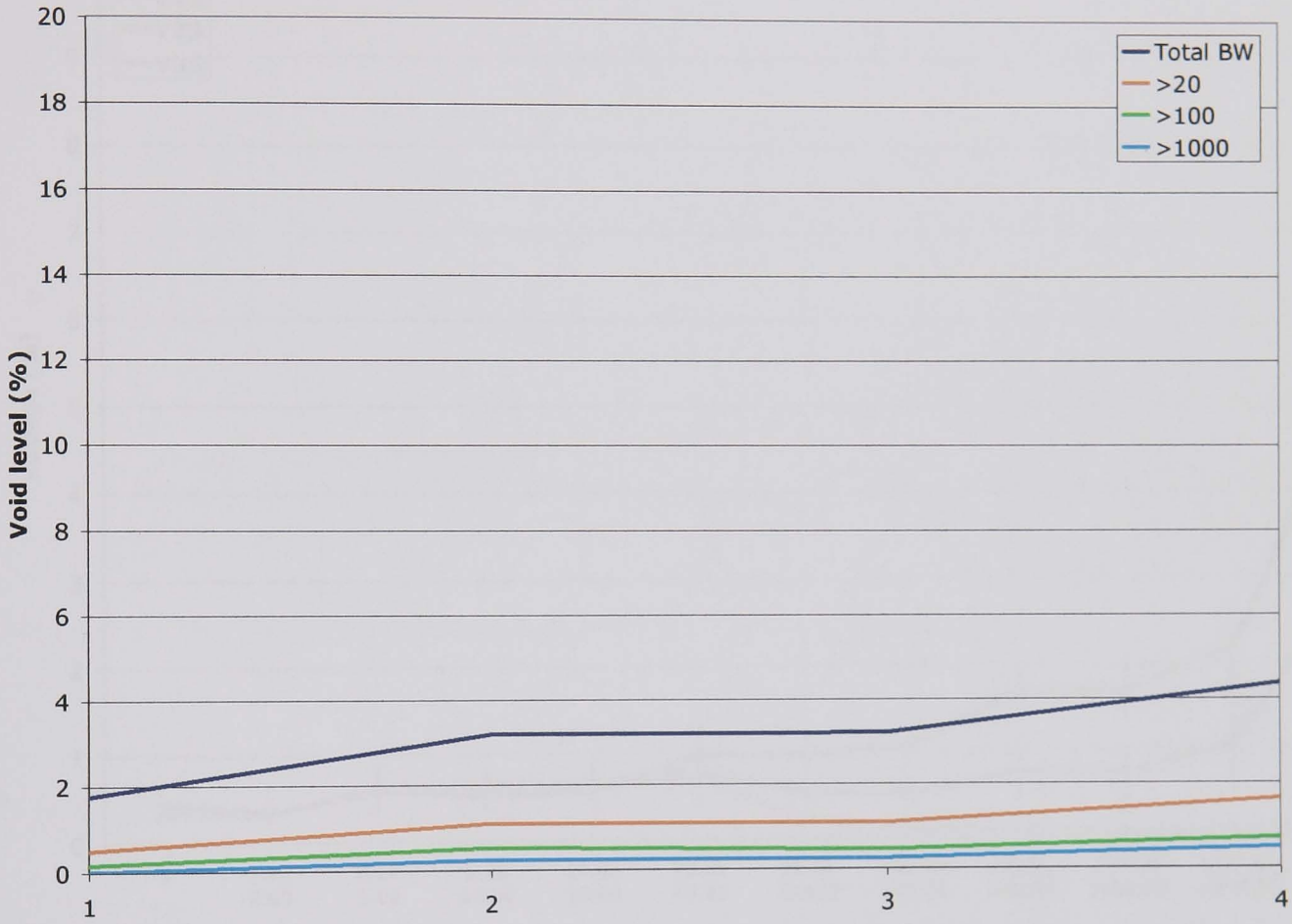

Figure 6:24 Void distribution for V1SA showing void level against position of sample in the mould (sample 1 = inlet end)

In two-thirds of cases void levels are observed to rise slightly along the length of the tube. The mechanism for this effect is unknown but may be a measurement artefact due to coalescence of the voids.

The following figures show average void size distribution within the categories shown in Section 6.3.2. The values are averaged across the 4 samples (40 images) and 2 repeats for each tube.

It can be seen from the Figures 6:25 and 6:26 that the void size distribution is different for the two materials at any given level. For instance the V1S samples have a higher proportion of small areas (2-5 pixels) but a much lower proportion

of real voids (50-100 voids and above). In the case of the V2 specimens the NCF examples have higher large void levels whereas smaller voids are similar in level to the CoFRM examples. V3U specimens show a sharp rise in percentage at the final classification (>2000 voids) whereas NCF samples have more spread into the smaller size ranges.

Figure 6:25 Void size distribution for NCF samples

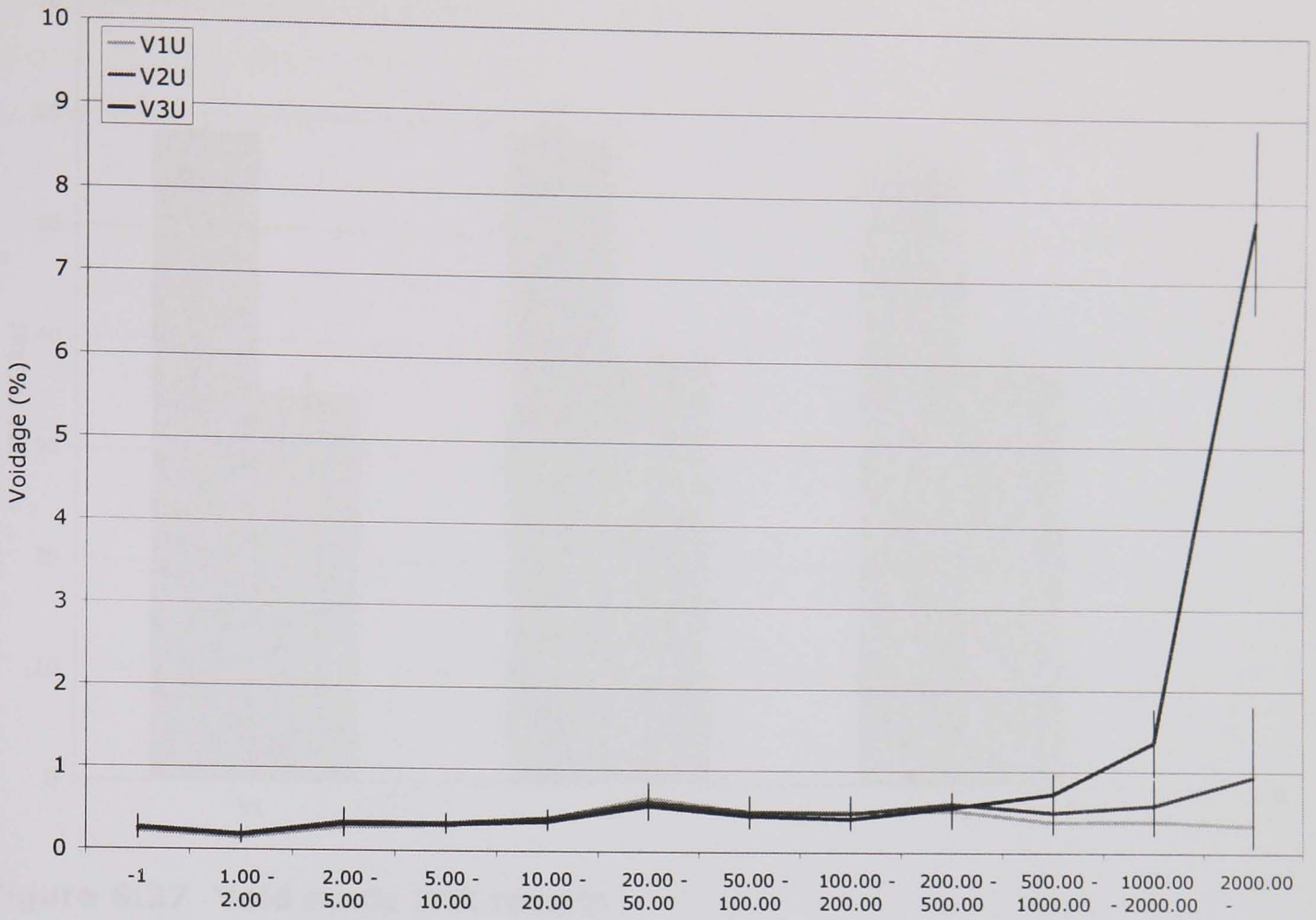

Figure 6:26 Void size distribution for CoFRM samples

6.3.5 Axial tube crush results

Crush results for the two fabric types appear in Figure 6:27. Specific energy absorption is just under 60kJ/kg for the CoFRM material for the three processing conditions, a slight drop can be seen with the V3 samples and an increase in standard deviation for both V2 and V3. The NCF material shows a slight increase in SEA with the V2 and V3 processing conditions. The increase in SEA is a result of a slight increase in mean load and a similar decrease in linear density due to the increased level of voidage. As the density of both materials is reduced by the voidage this implies that the CoFRM load is being reduced more than the NCF load.

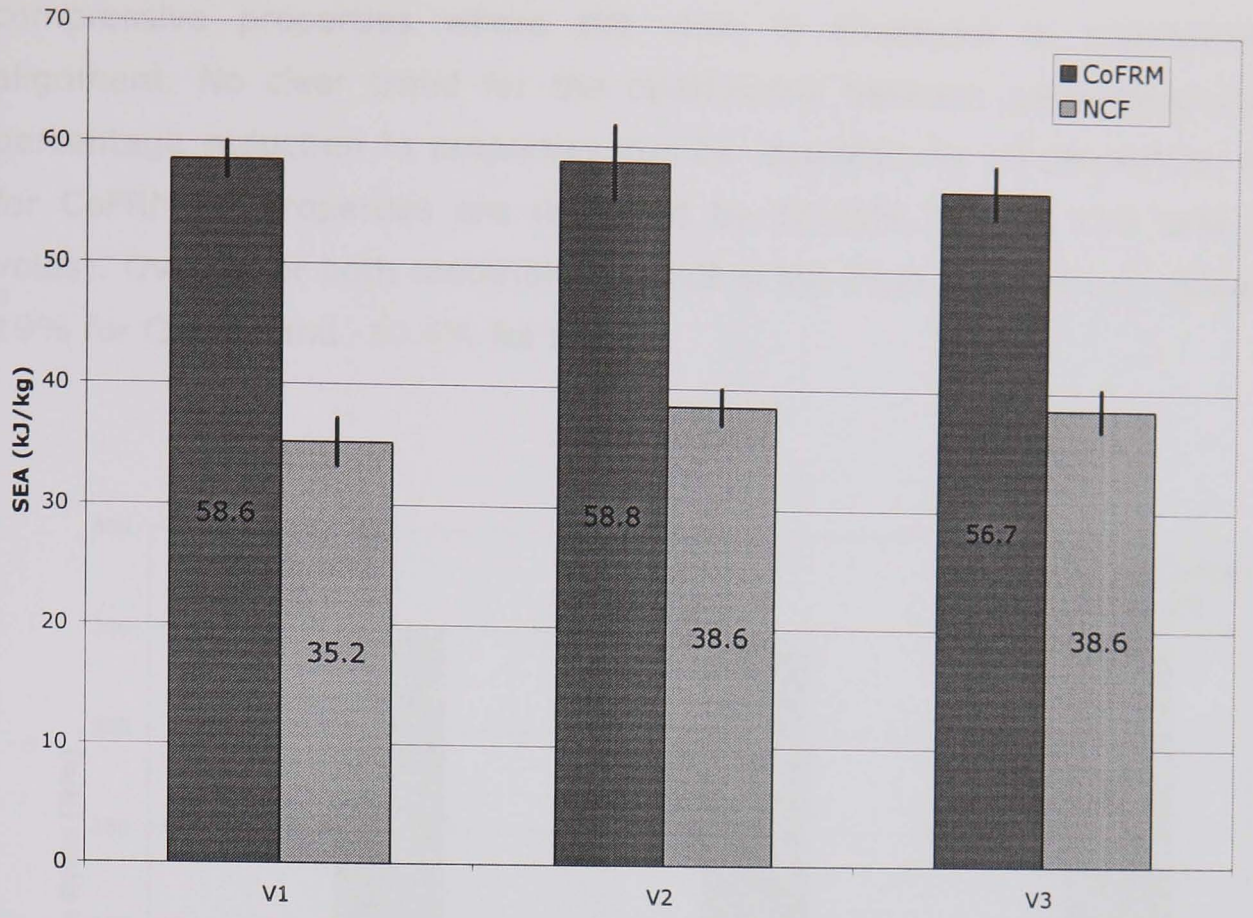

Figure 6:27 Void study SEA results

6.3.6 In-plane testing results

In-plane testing results appear in Figures 6:28 to 6:31. Both fabrics are plotted on one graph for each mechanical property studied. All figures demonstrate the vastly superior mechanical properties of the higher volume fraction non-crimp fabric. In some cases repeatability of the results decreases with increasing void fraction which is thought to be due to the relatively small plaque size and consequent uneven distribution of voids over the three samples. The CoFRM material suffers a greater reduction in ultimate tensile properties of -10.8% and -19.8% (VS1 to VS2 and VS1 to VS3) than the non-crimp fabric (-2.7% and -0.5%) which is to be expected as tensile failure is fibre dominated. Modulus properties are similarly affected, the NCF showing a relatively constant value and the CoFRM displaying a similar reduction to the UTS results.

Figures 6:30 and 6:31 show the compressive data which displays similar trends to the tensile data. The non-crimp fabric displays a more significant reduction in UCS than was seen with the UTS. Overall the CoFRM material shows a greater susceptibility to voidage as the properties of the material are more resin dependent than the NCF; particularly in tension. NCF properties are more fibre dependent although voidage obviously has a significant effect on the

compressive properties where the resin is employed in maintaining fibre alignment. No clear trend for the relationship between percentage voids and percentage reduction in properties can be identified for all properties, however for CoFRM all properties are degraded by 18-20% for the V3U case (9-13% voids). Overall for both materials the UCS is the most affected by voidage with -19% for CoFRM and -10.4% for NCF.

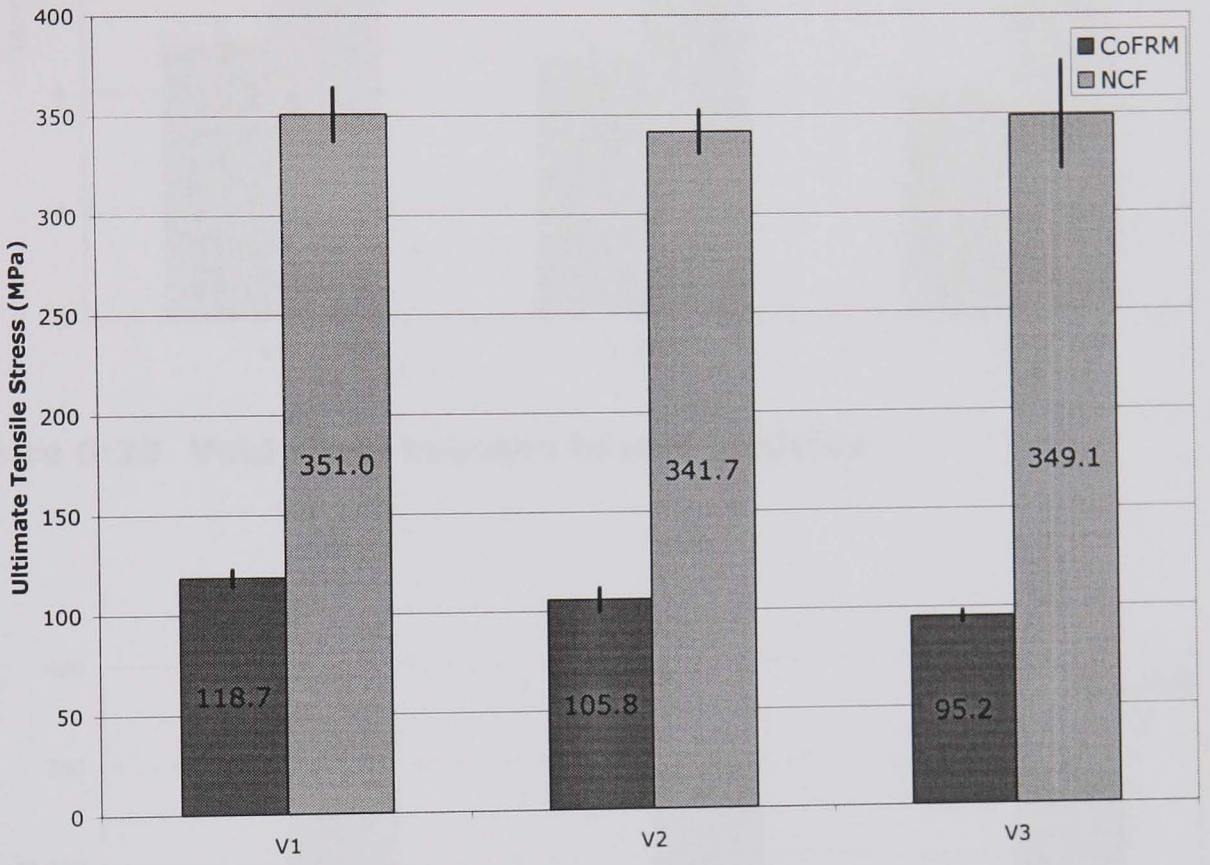

Figure 6:28 Void study in-plane ultimate tensile stress

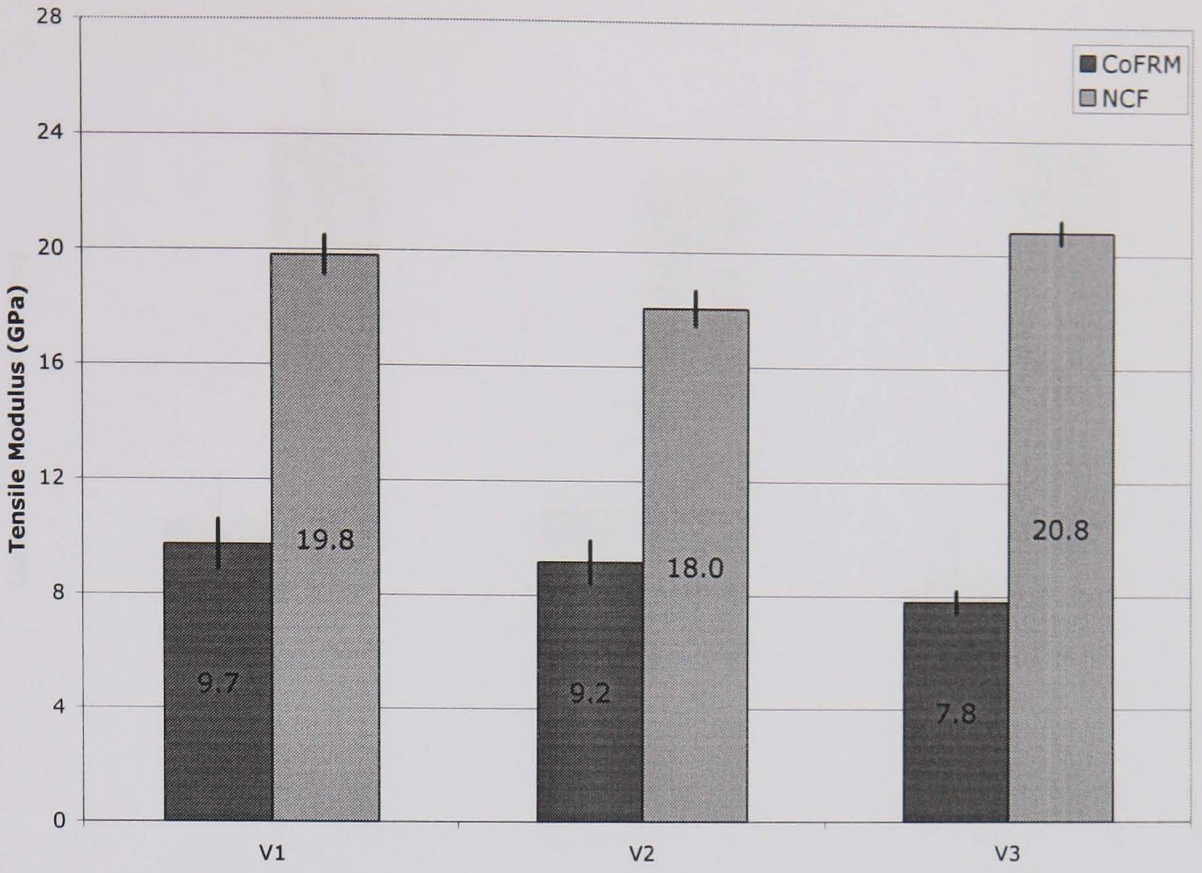

Figure 6:29 Void study in-plane tensile modulus

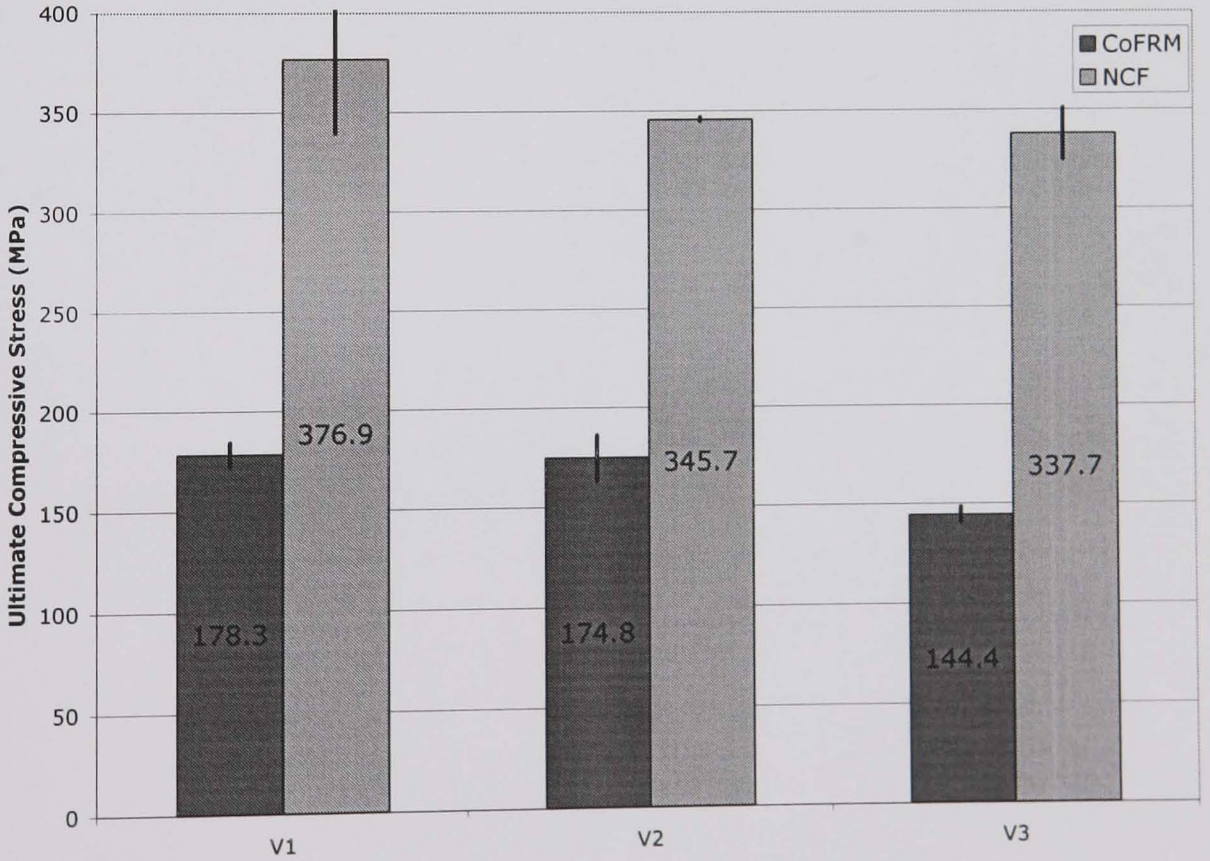

Figure 6:30 Void study in-plane ultimate compressive stress

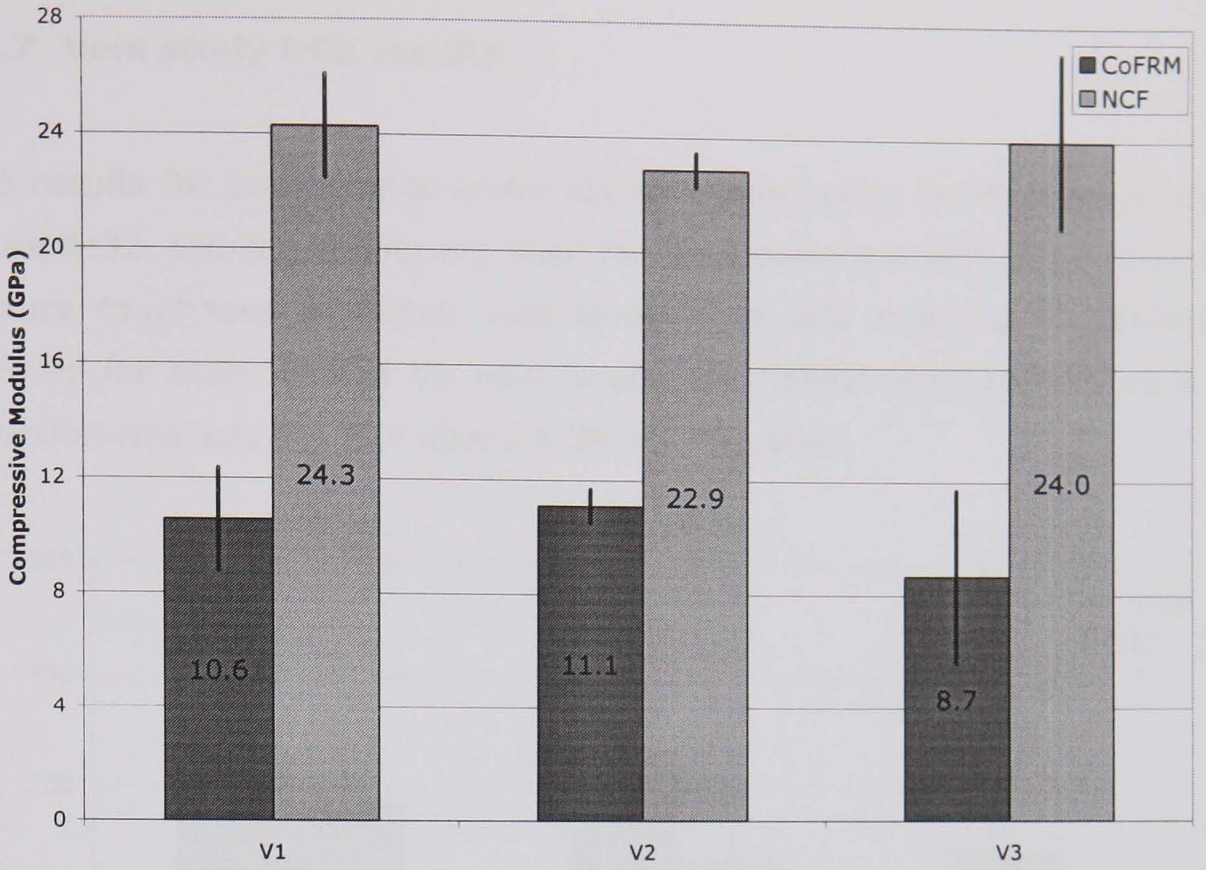

Figure 6:31 Void study in-plane compressive modulus

6.3.7 Void study DCB results

DCB results for both fabrics under identical processing conditions are shown in Figure 6:32. Similar results are seen for both materials with large reductions in fracture toughness at higher void levels. The NCF material is affected more severely for both V2 and V3 void levels, the CoFRM material suffers a 13.7% reduction whereas the NCF shows a 38.4% reduction.

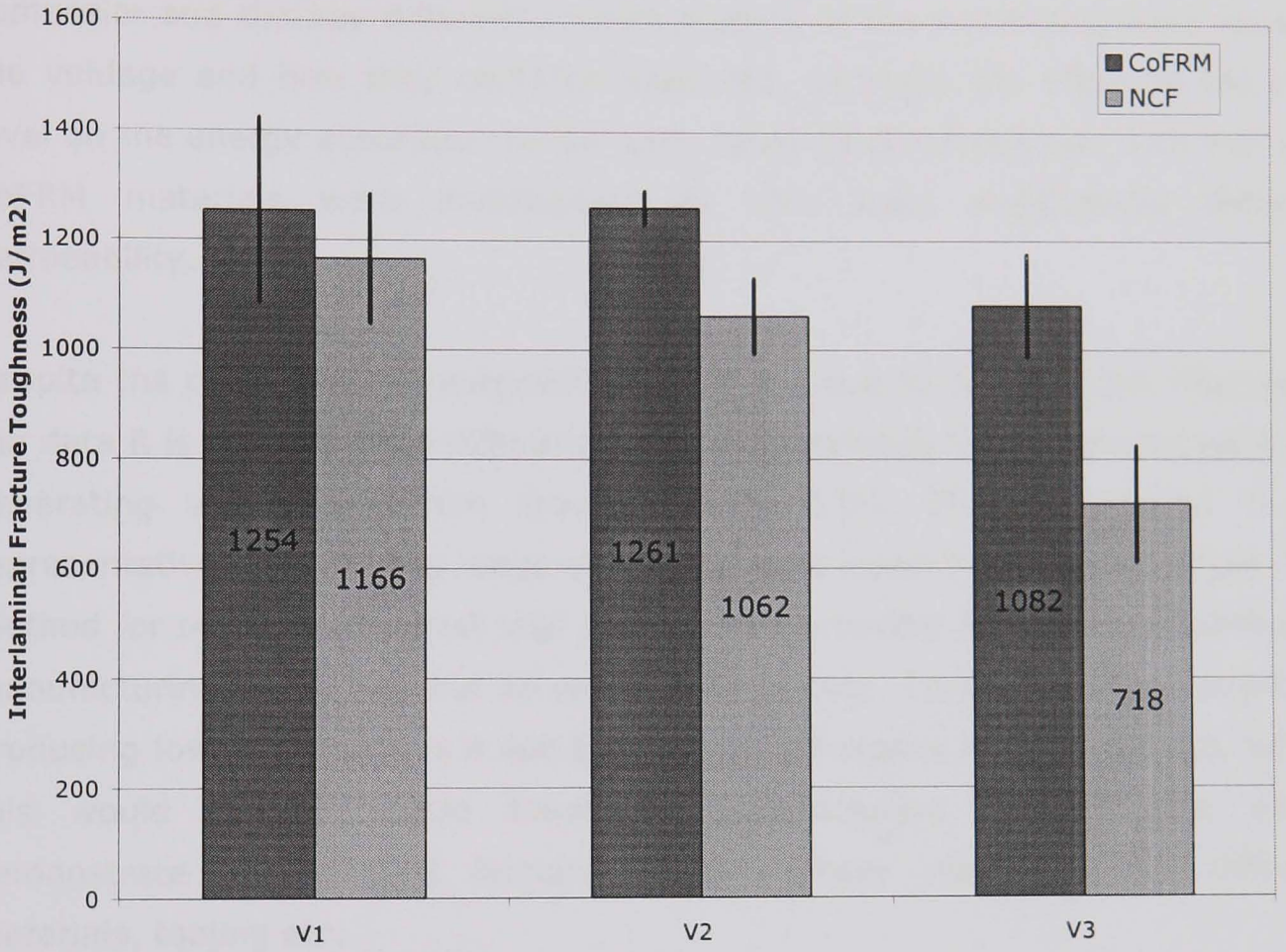

Figure 6:32 Void study DCB results

6.4 Discussion - Effect of voids

As seen in Chapter 2 voidage can have a dramatic effect on mechanical properties at the lowest reliably measurable levels (i.e. well under 1%). Voidage is a concern for any process and RTM is no exception. Typical void levels were initially estimated to be between 2% and 5% for the processing procedure used for this work. The aims of this work were twofold: Firstly it was important to quantify the effect of process-related parameters on the level of voids in the composite and thereby determine which aspects of the processing were causing the voidage and how they could be improved, secondly the effect of the void level on the energy absorption of the parts could be characterised. Both NCF and CoFRM materials were investigated as they have significantly different permeability.

Despite the difficulties in interpreting the results due to the different filtering of the data it is clear that the different processing methods used were successful in generating void levels from around 1% to 11%. This is believed to be representative of the entire range of possible void levels for these materials. The method for producing highest void levels is not intended to be representative of manufacturing in any way but serves as a worst case. Conversely the method for producing lowest voidage is a combination of techniques in common use. Whilst this would increase cycle times in manufacturing further work would demonstrate the efficient factors, however these may vary for different materials, tooling etc.

Voidage values were generally higher for the NCF material which is logical given the higher fibre volume fraction and necessarily faster injection. The grade of CoFRM used is also a high permeability variant intended for use with filled resins. Standard deviations are fairly high but consistent across all the tests. Void sizes are large for the high voidage cases in both fabrics and it is not known how this will affect the results (see figures Figure 6:25 and Figure 6:26). The void distribution results are difficult to interpret but very generally the voidage can be seen to increase along the tube for the low voidage specimens (Figure 6:24). This also applies to the standard processing conditions for the CoFRM but not for the NCF which is inconclusive. The changes along the length of the tube are probably caused by thickening of the resin but may also be due to coalescence of

the voids and consequentially higher readings with the data reduction methods employed.

Crush results are almost constant (Figure 6:27). CoFRM displays a slight downward trend and the NCF a slight upward one. Voidage appears to reduce the SEA of the CoFRM material more than that of the NCF for a given void level, which is logical given the lower volume fraction hence higher matrix dependency. The slight increase in the NCF results is due to the reduction in mass through the reduced density. The in-plane results (see Section 6.3.6) show similar trends as the CoFRM material suffers greater reductions in the measured properties than the NCF. The NCF results in particular are not as consistent as the earlier in-plane work, in particular it was very difficult to replicate the level of voidage in the small plaque tool as the geometry is different from the tube moulds, actual voidage levels in the plaques were not measured.

The fracture toughness results shown in Section 6.3.7 show large reductions in fracture properties at high void levels. This property is less volume fraction dependant; the interface plays a more significant part in determining the results. The NCF material is affected more severely for both V2 and V3 void levels, the CoFRM material suffers a 13.7% reduction whereas the NCF shows a 38.4% reduction. The decrease cannot be entirely due to reduction of area as the fabrics have similar void levels but suffer very different reductions in G_{IC}. The difference may however be due to the distribution in voids between the layers of material, NCF having a much more defined interlaminar structure. This effect was not noted during image analysis where void distribution through the thickness appeared uniform.

Chapter 6 References

1. Chen, J., D. Backes, and K. Jayaraman, *Dynamics of Binder Displacement in Liquid Molding.* Polymer Composites, 1996. **17**(1): p. 23-33.
2. Garcia-Gil, R., *Forming and consolidation of textile composites*. 2002, University of Nottingham: Nottingham.

7 Conclusions

The majority of composite components in automotive applications are non-structural (e.g. engine air intakes and instrument housings) or semi-structural (e.g. body panels and bumpers). Although the use of composites in primary structures is rare it is now increasing as vehicle weight is driven down. The advantages of composites are attractive but in crashworthiness applications their use is limited by a lack of design data and understanding. This leads to inefficient designs which can negate the potential advantages. Reducing mass at the extremities of the vehicle is particularly important and the resultant reduction in polar moment of inertia can provide greater gains than reduction of mass in the centre of the vehicle. The work presented here is timely and relevant as it offers designers and manufacturers of composite crash structures reliable ways to tailor crush performance and reduce cost through efficient use of materials, labour and processing time.

A wide range of factors have been studied in this work and all of the initial aims have been fulfilled. The primary means of assessment has been the axial tube crush. The part is dissimilar to standard coupon tests in its complexity but it is necessary due to the large number of interactions present in the various energy absorbing mechanisms. Reliance on such a part is unsatisfactory and one of the major aims of this work was to increase the understanding of the crush process. Table 7:1 below shows the tests that have been undertaken in each section.

Where possible the sections have built on knowledge gained from the previous work. Therefore results from each section can be easily compared. In all cases a control specimen case was made. The control specimen results from each section compare well, showing that the crush testing and tube moulding was repeatable.

	RESIN	**PREFORM**	**PROCESSING**	
			binder	voids
Tube crush	108	144	36	48
DCB	27	24	16	16
in-plane	198	36	0	36
DSC	162	0	0	0
Image analysis	0	0	0	720

Table 7:1 Experimental matrix

The first part of the work consisted of tests to determine the effect of constituent materials on the crush properties. Two resins were tested, one a high temperature UP resin already in use on automotive front ends and the other a high toughness, rubber modified vinylester. The resin chemistry was compatible and therefore mixes could be reliably tested. The degree of cure was varied to give different resin properties. Degree of cure ranged from 75% to ~100%. This allowed an accurate assessment of the effect of the resin on overall composite properties in the context of axial crushing. Use of the vinylester resin showed an increase in energy absorption of 33%.

The increases observed when changing the resin are the highest achieved in this work and have important economic implications. The change to vinylester resin has a significant effect on the cost of the CoFRM part (+72%) but a lower effect with the higher volume fraction NCF material (37%). Moving from CoFRM to NCF increases raw material cost by 23% for vinylester composites and 54% for polyester (see Section 3.6). Based purely on raw materials there is no economic benefit in selecting the VE resin – a 33% increase in SEA comes at a cost increase of 72%. It is only when considered in conjunction with other factors (material and processing) that the true benefits can be assessed. There is obviously a great benefit in exploiting a low cost UP based resin which provides the properties needed for efficient crushing.

The work on constituent materials suggested that the resin properties were very important. The stress-strain curve shown in Section 4.2.1.1 demonstrates the main differences between the UP and VE matrices. The VE resin only has a slightly higher Young's modulus but the elastic strain limit is higher. The UTS is also significantly higher. Given the importance of fracture properties it is suggested that the total strain energy of the resin is the important factor. In this work it is difficult to isolate the properties of composite compressive strength and interlaminar fracture toughness.

The two fibre architectures tested are both in use in automotive structures. A random fibre architecture at 22% volume fraction was shown to have significantly higher energy absorption properties than a non-crimp 0/90° fabric at 38% volume fraction. The differences in in-plane properties were measured due to the need for higher in-plane properties in certain automotive applications; particularly where crash structures must fulfil other load bearing roles. The NCF material was observed to delaminate as the fronds were forced around the

radius caused by the debris wedge. This delamination both limits intralaminar damage and reduces the compressive load on the sample. CoFRM samples fragment and retain little strength in the fronds after crushing, in this material the constituents are utilised more effectively. The laminar nature of the NCF material is reflected in the fracture toughness values which are typically 20% lower than the CoFRM.

The complex interactions and large number of variables present in composite crushing have limited its acceptance and use. Energy is absorbed through a variety of mechanisms including friction, cracking, bending and fragmentation. As part of the work on resins a variety of in-plane and interlaminar fracture toughness tests including UTS, UCS, E_c and E_t were performed. The large amount of data for different SEA levels allowed a large experimental matrix. No single material property correlated perfectly with crush characteristics, although compressive ultimate stress was the best. Fracture properties were also a poor indicator of crush potential when considered in isolation. A full understanding of the crush state has not been reached and is reliant on a large experimental investigation and subsequent modelling. There may be some scope in using the ILSS test as some authors have demonstrated (see Section 2.3.3) but whilst this test is much simpler it doesn't characterise a single material property. Additionally, as much of the energy absorption takes place through friction this is an important variable which is not characterised via standard coupon tests.

The benefits of interleaving and stitching in terms of increasing interlaminar fracture toughness have been widely reported in the aerospace field. This work has identified the effect of these methods, both on the low and high volume fraction materials. Two different interleaving materials were chosen based on discussions with the supplier. Interleaving in general was shown to have a detrimental effect on specific energy absorption, however there is great potential in the improvement of crush stability, load-displacement curve smoothing and damage tolerance.

Stitching can be seen to improve the Mode I centre-wall crack energy absorption and interlaminar frond delamination energy absorption. It may also contribute slightly to the interlaminar friction between fronds after delamination by prohibiting shear as the threads are very ductile. The primary means by which the stitching improves the properties is by reducing the length of the centre-wall

crack and therefore forcing the fronds around a tighter radius, thus inducing greater intralaminar damage.

Through-thickness stitching with aramid was shown to have a positive effect on the non-crimp fabric and no effect on the random fabric. This effect demonstrates that the random fabric has a synergistic blend of material properties leading to high overall performance. The non-crimp fabric has a deficit of through-thickness properties and therefore benefits from the increase which stitching gives. The non-crimp fabric energy absorption rises to almost the same level as the random fabric on a specific basis with only a small decrease in in-plane properties. Stitching obviously represents an additional manufacturing process but has a niche where high in-plane properties are needed with high energy absorption. In this work no evidence of fibre damage caused by stitching was observed but reductions in in-plane properties were observed.

Both toughening methods have potential as local modifications of the material rather than global material changes. This provides great opportunities in the design of real parts rather than generic structures. Further opportunity exists in the identification of more suitable interleaving materials, the exact mechanism by which interleaving affects energy absorption is thought to be the reduction of friction in the crush zone.

The effect of the other toughening methods on the overall cost is difficult to quantify. Interleaving is a relatively low cost method with the cost being highly dependent on the film type. Extra labour may be required to process the material but in volume production the process could be easily automated. Automating the stitching process is more difficult and would probably mean manual stitching of small areas of the preform. Labour costs are already significant in determining final part cost and a thorough cost analysis would need to be undertaken to quantify the final cost. None of the improvements in SEA presented come at zero cost so it is very difficult to compare the economic benefit of the improvements without part-specific cost modelling.

Identification of the effect of processing conditions was one of the main aims of the work. Thermoplastic binder is an essential aspect of the resin transfer moulding process, however its effect on crush performance had not been ascertained. The binder was shown to significantly affect resin properties, interlaminar fracture toughness was improved at the relatively low binder levels

which are generally employed. At higher binder additions the fracture toughness decreased due to adverse effects on the chemistry of the resin. The net effect on energy absorption was minimal. This is reassuring where large preforms in particular may require levels of binder up to 10% by fabric mass.

A large experimental study was undertaken examining the effect of processing on energy absorption with the focus on voidage levels. Three manufacturing processes were used based on the standard process, one attempting to give very low voidage and one where additional voids were manufactured by the introduction of air into the resin. This allowed the effect of processing on void level to be identified and the concomitant effect of void level on specific energy absorption. The methods employed were successful in producing a wide range of void levels in both fibre architectures. Both fabrics were found to be tolerant of void volume fractions of up to 10%. This has implications for processing and potential reductions in cycle time represent a significant cost saving.

At present, liquid moulding technologies remain the only realistic processing route for structural crash energy absorbing parts at high volume. Sheet moulding compounds are in use at higher volume levels but the material properties are much lower than the parts discussed in this work. However, some of the results in this work are applicable to other preforming routes including automated spray processing (e.g. P4) where the moulding process is the same.

7.1 Future Work

The work undertaken has identified numerous areas for possible future work building on knowledge gained. The following can be studied:

- Development of a low cost polyester resin (or PE/VE blend) suited to crush applications. The resin should be easily processed with low viscosity whilst combining high toughness with good in-plane properties.

- Further development of an interleaf material providing controlled interlaminar properties without disruption of flow. This could involve selection of a compatible material, testing of bond strengths, testing deterioration of bond strength in styrene etc. An open structure may improve processing.

- The effect of locally modified tubular structures. This is of particular interest to the interleaf and stitching work and has great potential for triggering and damage resistance.

- Further work into characterisation of crush response. This work has demonstrated some of the problems associated with crush characterisation. A potential area of interest is the correlation of interlaminar shear strength with SEA.

Whilst the work has focused on generic tubular parts, there is significant opportunity for the implementation of a demonstrator component utilising the above techniques.

Appendix 1 - Publications

The following papers have been produced as a result of this work, some of which are in press or to be submitted at the time of writing.

1. *'The effect of processing parameters on crash energy absorbing composite structures made by RTM',*
   F Robitaille, T A Turner, E Cooper, N A Warrior, C D Rudd,
   Oral presentation at ICMAC 2000, Belfast, September 2001.
2. *'The effect of processing and matrix parameters on specific energy absorption',*
   F Robitaille, N A Warrior, T Turner, E Cooper, C D Rudd,
   Published in special edition of Plastics, Rubber & Composites, vol. 31,2 2002 pp49-57.
3. *'Effect of resin properties and processing parameters on crash energy absorbing composites made by RTM',*
   N A Warrior, T A Turner, F Robitaille, C D Rudd,
   Published in Composites Part A vol. 34, June 2003.
4. *'Effect of Interlaminar Toughening on Energy Absorption of Composite Structures',*
   N A Warrior, T A Turner, F Robitaille, C D Rudd,
   Oral presentation at the 10th US-Japan conference on composite materials, September 2002.
5. *'The effect of interlaminar toughening strategies on the crash energy absorption of composite tubes',*
   N A Warrior, T A Turner, F Robitaille, C D Rudd,
   Published in Composites Part A vol 35, 2004, pp 431-437
6. *'The influence of processing variables on the crash energy absorption of composite tubes'*
   N A Warrior, T A Turner, F Robitaille, C D Rudd,
   In preparation
7. *'The effect of binder level on the crash energy absorption of composite tubes'*
   N A Warrior, T A Turner, F Robitaille, C D Rudd,
   In preparation

8. *'Fabrication methods for crash energy absorbing composite structures'*
   N A Warrior, T A Turner, F Robitaille, C D Rudd,
   Oral presentation at the SAMPE Europe Conference, Paris 2004.
9. *'Fabrication methods for Energy Absorbing Composite Automotive Structures'*
   N A Warrior, T A Turner, F Robitaille, C D Rudd,
   Oral presentation at the 5th international conference on Materials for Lean Weight Vehicles.
10. ECCM-11 Conference, Greece 2004. To be presented
11. I-Crash 2004 Conference, San Francisco USA 2004. To be presented